AFRL-IF-RS-TR-2007-69
Final Technical Report
March 2007

EUKARYOTIC CELL CYCLE AS A TEST CASE FOR MODELING CELLULAR REGULATION IN A COLLABORATIVE PROBLEM-SOLVING ENVIRONMENT

Virginia Polytechnic Institute & State University

Sponsored by
Defense Advanced Research Projects Agency
DARPA Order No: M299/00

APPROVED FOR PUBLIC RELEASE; DISTRIBUTION UNLIMITED.

STINFO COPY

The views and conclusions contained in this document are those of the authors and should not be interpreted as necessarily representing the official policies, either expressed or implied, of the Defense Advanced Research Projects Agency or the U.S. Government.

AIR FORCE RESEARCH LABORATORY
INFORMATION DIRECTORATE
ROME RESEARCH SITE
ROME, NEW YORK

NOTICE AND SIGNATURE PAGE

Using Government drawings, specifications, or other data included in this document for any purpose other than Government procurement does not in any way obligate the U.S. Government. The fact that the Government formulated or supplied the drawings, specifications, or other data does not license the holder or any other person or corporation; or convey any rights or permission to manufacture, use, or sell any patented invention that may relate to them.

This report was cleared for public release by the Air Force Research Laboratory Rome Research Site Public Affairs Office and is available to the general public, including foreign nationals. Copies may be obtained from the Defense Technical Information Center (DTIC) (http://www.dtic.mil).

AFRL-IF-RS-TR-2007-69 HAS BEEN REVIEWED AND IS APPROVED FOR PUBLICATION IN ACCORDANCE WITH ASSIGNED DISTRIBUTION STATEMENT.

FOR THE DIRECTOR:

/s/	/s/
DANIEL J. BURNS Work Unit Manager	JAMES A. COLLINS, Deputy Chief Advanced Computing Division Information Directorate

This report is published in the interest of scientific and technical information exchange, and its publication does not constitute the Government's approval or disapproval of its ideas or findings.

REPORT DOCUMENTATION PAGE

Form Approved
OMB No. 0704-0188

Public reporting burden for this collection of information is estimated to average 1 hour per response, including the time for reviewing instructions, searching data sources, gathering and maintaining the data needed, and completing and reviewing the collection of information. Send comments regarding this burden estimate or any other aspect of this collection of information, including suggestions for reducing this burden to Washington Headquarters Service, Directorate for Information Operations and Reports, 1215 Jefferson Davis Highway, Suite 1204, Arlington, VA 22202-4302, and to the Office of Management and Budget, Paperwork Reduction Project (0704-0188) Washington, DC 20503.
PLEASE DO NOT RETURN YOUR FORM TO THE ABOVE ADDRESS.

1. REPORT DATE *(DD-MM-YYYY)*	2. REPORT TYPE	3. DATES COVERED *(From - To)*
MAR 2007	Final	Sep 01 – Sep 06

4. TITLE AND SUBTITLE

EUKARYOTIC CELL CYCLE AS A TEST CASE FOR MODELING CELLULAR REGULATION IN A COLLABORATIVE PROBLEM-SOLVING ENVIRONMENT

5a. CONTRACT NUMBER

5b. GRANT NUMBER
F30602-01-2-0572

5c. PROGRAM ELEMENT NUMBER
61101E

6. AUTHOR(S)

John J. Tyson, Bela Novak, Kathy Chen, Jill C. Sible, Frederick R. Cross, Layne T. Watson and Clifford A. Shaffer

5d. PROJECT NUMBER
BIOC

5e. TASK NUMBER
M2

5f. WORK UNIT NUMBER
99

7. PERFORMING ORGANIZATION NAME(S) AND ADDRESS(ES)
Virginia Polytechnic Institute & State University
201 Southgate Ctr
Blacksburg VA 24061-5281

8. PERFORMING ORGANIZATION REPORT NUMBER

9. SPONSORING/MONITORING AGENCY NAME(S) AND ADDRESS(ES)

Defense Advanced Research Projects Agency
3701 North Fairfax Dr.
Arlington VA 22203-1714

AFRL/IFTC
525 Brooks Rd
Rome NY 13441-4505

10. SPONSOR/MONITOR'S ACRONYM(S)

11. SPONSORING/MONITORING AGENCY REPORT NUMBER
AFRL-IF-RS-TR-2007-69

12. DISTRIBUTION AVAILABILITY STATEMENT
APPROVED FOR PUBLIC RELEASE; DISTRIBUTION UNLIMITED. PA# 07-109

13. SUPPLEMENTARY NOTES

14. ABSTRACT
The primary objectives of this project were: 1) To develop realistic and accurate mathematical models of t he molecular mechanisms controlling replication and division of yeast cells and frog cells, 2) to test predictions of these models by novel experimental designs, and 3) to create software tools to support computational modeling of cellular regulatory systems at the next level of complexity (100s of interacting genes and proteins). Major advances were made in all three areas. A detailed model of cell cycle controls in budding yeast was published in a molecular biology journal and on a web site that has been receiving 1000 hits per month for 2 years. The model's prediction of 'bistability' of the control system was conclusively demonstrated in both living yeast cells and frog cell extracts. Effective modeling tools were created to build reaction mechanism and kinetic equations, to manage complex sets of simulations, to compare model output to data, to provide optimal estimates of kinetic parameters, and to investigate the bifurcation structure of models.

15. SUBJECT TERMS
Cell Cycle Regulation, Yeast, Xenopus, Dynamical Systems, Stochastic Models, Parameter Estimation, Bifurcation Theory, Problem-Solving Environment

16. SECURITY CLASSIFICATION OF:			17. LIMITATION OF ABSTRACT	18. NUMBER OF PAGES	19a. NAME OF RESPONSIBLE PERSON
a. REPORT	b. ABSTRACT	c. THIS PAGE			Daniel J. Burns
U	U	U	UL	146	19b. TELEPHONE NUMBER (*Include area code*)

Abstract

The purpose of DARPA's BioSPICE Program was to provide a new and useful set of software tools for modeling biochemical pathways and molecular regulatory networks within living cells. Virginia Tech was awarded a contract for model building, model testing, and software development. The project was carried out by an interdisciplinary team of theoretical biologists, cell biologists, molecular geneticists, computer scientists, mathematicians, physicists, and engineers, at Virginia Tech and at two subcontracting institutions: Rockefeller University in New York and the Budapest University of Technology and Economics.

Using nonlinear ordinary differential equations to capture the temporal dynamics of molecular control systems, the modeling team built successful computer models of cell cycle regulation in a variety of organisms, including yeast cells, amphibian embryos, bacterial cells and human cells. These models accurately reproduce the physiological properties of normal cell division, and the bizarre properties of 200+ mutant cells that have been studied. The models predict phenotypes of novel mutants and unintuitive properties of the cell cycle machinery, which have been confirmed by the experimental teams on the project. The theorists used one- and two-parameter bifurcation diagrams to link gene-protein interaction networks to the physiological properties of cells.

The Software Team developed tools for building mathematical models from a chemical reaction network, for associating experimental data with a model, for managing simulations of the data by the model, for evaluating how well the simulation fits the data, and for automatic parameter estimation. In addition a powerful tool for numerical bifurcation analysis was created.

The major accomplishments of the Virginia Tech Consortium are (1) a set of downloadable, open-source computer programs that embody a Problem Solving Environment for dynamic modeling of macromolecular regulatory networks in living cells, and (2) an integrated set of models of cell cycle regulation in bacteria, yeasts, and metazoans that are accurate, predictive and informative. The models are described in the peer-reviewed literature and are freely available from web sites maintained at Virginia Tech. Some of the experimental tests carried out by the group are cited as classic examples of modern molecular systems biology.

Table of Contents

Abstract i
Table of Contents ii
List of Figures iii
List of Tables iv
List of Equations v
Acknowledgements vi
Summary 1
1.0 Project Goals 2
1.1 Network Models 2
1.2 Experimental Tests 2
1.3 Software Tools 3
2.0 Summary of Key Accomplishments 4
2.1 Network Models 4
2.2 Experimental Tests 9
2.3 Software Development 12
3.0 Details of Key Accomplishments in Network Modeling 21
3.1 Budding Yeast Cell Cycle 21
3.2 Fission Yeast Cell Cycle 46
3.3 Frog Embryonic Cell Cycle 51
3.4 Generic Cell Cycle 54
3.5 Fruit Fly Embryonic Cell Cycle 66
3.6 Mammalian Cell Cycle 71
3.7 Caulobacter Cell Cycle 76
3.8 Circadian Rhythm 84
4.0 Details of Key Accomplishments in Experimental Testing 90
4.1 Budding Yeast Cells 90
4.2 Frog Cells and Extracts 103
5.0 Details of Key Accomplishments in Software Development 110
5.1 JigCell 110
5.1.1 The JigCell Model Builder 111
5.1.2 The JigCell Run Manager 113
5.1.3 The JigCell Comparator 116
5.2 Parameter Estimation 120
5.3 Bifurcation Analysis 126
5.4 Modularity, Composition and Fusion 128
6.0 Literature Cited 130
7.0 Publications Resulting from this Project 134
8.0 List of Abbreviations 138

List of Figures

2.1	The modeling cycle	12
3.1	A consensus model of the cell cycle control mechanism in budding yeast	22
3.2	The wild-type cell cycle	29
3.3	The budding yeast cell cycle web page	31
3.4	The logic of cell cycle transitions in budding yeast	32
3.5	The Swe1 box	36
3.6	Time-courses of mass and concentrations during the wild-type cell cycle	37
3.7	Simulation of *cdc24*^{ts} cell cycle	38
3.8	Bifurcation diagrams for the cell cycle engine	40
3.9	Bifurcation diagrams for the packed and unpacked mechanisms	44
3.10	Time evolution of important variables in the unpacked model	45
3.11	Histograms computed from a simulated population of 66 cells	45
3.12	A molecular network for the fission yeast cell cycle	47
3.13	Simulated time courses of cell cycle proteins in wild-type fission yeast cell	48
3.14	Simulated time courses of cell cycle proteins in a *cdc13Δ* cell	49
3.15	Wiring diagram for the unreplicated DNA checkpoint in frog cell extracts	52
3.16	Experimental data and model simulations for MPF activation	52
3.17	Wiring diagram of the generic cell-cycle regulatory network	55
3.18	One-parameter bifurcation diagram and cell cycle trajectory	57
3.19	One-parameter and two-parameter bifurcation diagrams for *wee1* mutants	59
3.20	Attractors and their bifurcations	62
3.21	An illustrative two-parameter bifurcation diagram with one-parameter cuts	64
3.22	Mechanism of MPF oscillations during early embryogenesis of Drosophila	67
3.23	Temporal evolution of protein concentrations	68
3.24	Bifurcation diagrams for the Drosophila model	69
3.25	Molecular network regulating progression through mammalian cell cycle	72
3.26	Effect on cell cycle progression of transient deprivation of growth factor	73
3.27	Effects of transient growth factor deprivation at two different phases	74
3.28	Schematic diagram of some signal transduction pathways in mammals	75
3.29	Physiology and molecular biology of the Caulobacter cell cycle	77
3.30	Wiring diagrams of cell cycle control in Caulobacter and Saccharomyces	78
3.31	Change of protein concentrations during the Caulobacter cell cycle	78
3.32	Master-regulator switch and bifurcation diagram for Caulobacter model	80
3.33	Master-regulator switch and bifurcation diagram for Saccharomyces model	82
3.34	One-parameter bifurcation diagrams for the circadian rhythm model	87
3.35	Time courses of *per* mRNA and protein, and the resetting parameter, v_p	88
4.1	Bistability in a mathematical model of the budding yeast cell cycle	91
4.2	Experimental confirmation of bistability in the budding yeast cell cycle	92
4.3	Two redundant mechanisms for exit from mitosis	94
4.4	Temporal patterns of Clb2, Cdc6 and Sic1	97
4.5	Dosage sensitivity for Clb2 expression	99
4.6	Comparison of trough and peak levels of Clb2 upon Clb2 overexpression	100
4.7	Model predictions	101
4.8	Hysteresis in a model of MPF activation	103
4.9	Bistability of MPF activation in frog cell extracts	104

4.10	Cdc2 activation exhibits critical slowing down near the MPF threshold	105
4.11	The cyclin threshold for MPF activation is raised by unreplicated DNA	106
4.12	The effect of nuclear concentration on time into mitosis in extracts	107
4.13	Effect of nuclear concentration on lag times into mitosis	108
4.14	Effect of nuclear concentration on cyclin thresholds in aphidicolon extracts	109
5.1	Activation of M-phase promoting factor in frog cells	110
5.2	The frog cell model in the JigCell Model Builder	112
5.3	The Run Manager spreadsheet for the frog cell model	113
5.4	The Changes Editor of the JigCell Run Manager	114
5.5	The Basal Initial Conditions Editor of the JigCell Run Manager	114
5.6	The Simulator Settings tab of the JigCell Run Manager	115
5.7	The Plotter Settings tab of the JigCell Run Manager	115
5.8	The JigCell Comparator: experimental data spreadsheet	117
5.9	The JigCell Comparator: transform spreadsheet	117
5.10	The JigCell Comparator: objective spreadsheet	118
5.11	The JigCell Comparator: sample fit of model to data points	118
5.12	An example of rectangle divisions made by DIRECT for a simple problem	121
5.13	The Edit Simulations tab in PET	124
5.14	The Estimator Settings tab in PET	125
5.15	Model fusion, composition, aggregation and flattening	128

List of Tables

3.1	Budding yeast model equations	23
3.2	Basal parameter values and initial conditions for the wild-type cell cycle	26
3.3	Mutants used to derive the model and specify the parameter values	27
3.4	Numbers of molecules (per haploid yeast cell) for several cell cycle genes	41
3.5	Delayed entry into mitosis, as predicted by the model	53
3.6	Protein name conversion table and modules used for each organism	56
3.7	Definitions and examples of codimension-one and –two bifurcations	65
3.8	Differential equations for the Caulobacter cell cycle model	83
4.1	Summary of comparative results fro modeling and genetic experiments	95
4.2	Quantitation of Cdc6-PrA, Clb2-PrA and Sic1-PrA	97
4.3	Average number of Clb2 molecules per budding yeast cell	100

List of Equations

3.1	Langevin equation for Novak-Tyson model	42
3.2	Deterministic equations for the toggle switch	42
3.3	Phenomenological equation for Cdc14 activity	43
3.4	Cell growth equation	44
3.5	Ruoff’s equation	85
5.1	Chemical rate equations	111
5.2	The distance between two compatible bifurcation structures	127

Acknowledgements

The following persons all contributed to the successful completion of this research project.

Lead Investigators	**# Mo**	**Task**	**Title**	**Department**	**Institution**
John J. Tyson, Ph.D.	60	1,3	Professor	Biology	Virginia Tech
Jill C. Sible, Ph.D.	60	2	Assoc. Professor	Biology	Virginia Tech
Layne T. Watson, Ph.D.	60	3	Professor	Computer Sci.	Virginia Tech
Clifford A. Shaffer, Ph.D.	60	3	Assoc. Professor	Computer Sci.	Virginia Tech
Naren Ramakrishnan, Ph.D.	24	3	Assist. Professor	Computer Sci.	Virginia Tech
Katherine C. Chen, Ph.D.	60	1	Sen. Res. Sci.	Biology	Virginia Tech
Frederick R. Cross, Ph.D.	60	2	Professor	Biology	Rockefeller U.
Michael D Mendenhall, Ph.D.	24	2	Assoc. Professor	Biochemistry	U. Kentucky
Bela Novak, Ph.D.	60	1	Professor	Biotechnology	Budapest U.
William Baumann, Ph.D.	6	1	Assoc. Professor	Elec Engin	Virginia Tech
Assistant Scientists					
Andrea Ciliberto	48	1	Postdoc. Res. Sci.	Biology	Virginia Tech
Chung-Seon Yi.	12	1	Postdoc. Res. Sci.	Biology	Virginia Tech
Mohsen Sabouri-Ghomi	36	1	Postdoc. Res. Sci.	Biology	Virginia Tech
Dorjsuren Battogtokh	36	1	Postdoc. Res. Sci.	Biology	Virginia Tech
Laurence Calzone	24	1	Graduate Student	Biology	Virginia Tech
Wei Sha	12	2	Graduate Student	Biology	Virginia Tech
Matthew Petrus	12	2	Graduate Student	Biology	Virginia Tech
Tony Lassaletta	12	2	Undergraduate	Biology	Virginia Tech
Amit Dravid	30	1	Graduate Student	Mathematics	Virginia Tech
Ian Auckland	36	2	Graduate Student	Biology	Virginia Tech
Dayna Wilhelm	24	2	Graduate Student	Biology	Virginia Tech
Bolan Linghu	6	1	Graduate Student	Computer Sci	Virginia Tech
Nicholas Allen	48	3	Graduate Student	Computer Sci.	Virginia Tech
Marc Vass	24	3	Graduate Student	Computer Sci.	Virginia Tech
Jason Zwolak, Ph.D.	60	3	Graduate Student	Computer Sci.	Virginia Tech
Dan Moisa	12	3	Graduate Student	Computer Sci	Virginia Tech
Jian He	12	3	Graduate Student	Computer Sci	Virginia Tech
Tom Panning	24	3	Graduate Student	Computer Sci	Virginia Tech
Robert Ball	12	3	Graduate Student	Computer Sci	Virginia Tech
Sean Shealy	6	3	Undergraduate	Comp Sci Eng	Virginia Tech
Emery Conrad	12	1,3	Graduate Student	Mathematics	Virginia Tech
Jamie Bean	12	2	Graduate Student	Biology	Rockefeller U.
Lea Shroeder	24	2	Research Tech.	Biology	Rockefeller U.
Qinghua Chen	24	2	Postdoc. Res. Sci.	Biochemistry	U. Kentucky
Attila Csikasz-Nagy	60	1	Postdoc. Res. Sci.	Biotechnology	Budapest U.
Bela Gyorffy	48	1	Postdoc. Res. Sci.	Biotechnology	Budapest U.
Zsuzsa Pataki	12	1	Graduate Student	Biotechnology	Budapest U.
Kimberly Heard	6	3	Graduate Student	Bioinfo	Virginia Tech

number of months involved in project (max = 60)

Tasks: 1=modeling, 2=experiment, 3=software

Summary

The living cell is a miniature, membrane-bound, biochemical machine that harvests material and energy from its environment and uses them for maintenance, growth and reproduction. These processes, carried out by macromolecular machines (enzymes, ribosomes, transport proteins, structural proteins, motor proteins, etc.) whose structures are encoded in nucleotide sequences (DNA and mRNA), are controlled and coordinated by regulatory networks of great complexity and exquisite effectiveness. These networks collect information from inside and outside the cell, process the data, and direct cellular responses that foster the survival and reproduction of the cell (Bray, 1995). How these regulatory systems work is no more or less apparent from their network diagrams (representing the components and their biochemical interactions) than is a complex piece of electronics from its schematic wiring diagram. Whereas electrical engineers create accurate mathematical representations of wiring diagrams and use these equations to design new devices, molecular biologists are not accustomed to quantitative modeling as a means to either deeper scientific understanding or more rational engineering of cellular responses.

The goal of DARPA's BioSPICE Program was to change the culture of molecular cell biology by providing useful software tools for modeling biochemical pathways and molecular regulatory networks, by illustrating how these tools might be used on sample problems that are both interesting and challenging, and by testing the predictions of the computational models in laboratory settings. The Virginia Tech Consortium contributed to BioSPICE in all three areas.

The Software Team developed tools for building models of arbitrary complexity from a chemical reaction network (a set of chemical reactions sharing a common set of reactants and products), for associating experimental data with a model, for describing efficiently how to simulate the data from the model, and for evaluating how well the simulation fits the data. In a parallel effort, the team explored methods for automatic parameter estimation and built a toolkit to make these methods readily available to users. A third effort provided users with a powerful tool for numerical bifurcation analysis.

The Modeling Team constructed realistic models of the molecular machinery controlling cell cycle progression in a variety of organisms: budding yeast, fission yeast, frog embryos, fruit fly embryos, mammalian cells, and bacterial cells. The model building efforts provided impetus for designing and developing the software tools, and later provided serious tests of the robustness and utility of the tools. The modelers also interacted with the experimentalists to design experiments that would test consequences of the model and provide data for extending the models.

The Experimental Team carried out two sorts of tests. In budding yeast they characterized the properties of mutant cells, by knocking out and/or overexpressing the genes encoding protein components of the control system. Such genetic tests provide very strong qualitative constraints on the computational model. Using frog cell extracts, the team also made biochemical measurements (enzyme activity assays) of the cell cycle control system, to test quantitative predictions of the models.

1.0 Project Goals

1.1 Network Models

- Budding Yeast Cell Cycle
  - G1-S-G2-M cycle (DNA synthesis and mitosis)
  - Morphogenetic checkpoint (bud initiation)
  - Bifurcation analysis of mutants
  - Stochastic model of G1-S transition
- Fission Yeast Cell Cycle
  - G1-S-G2-M cycle (DNA synthesis and mitosis)
  - Septation initiation network (control of cell division)
  - Bifurcation analysis of mutants
- Frog Cell Cycle
  - Activation and inactivation of MPF (mitosis promoting factor)
  - Oscillations of cyclin E-dependent kinase activity
  - Unreplicated DNA checkpoint
- Other Cell Cycles
  - Generic cell cycle models
  - Fruit fly embryonic division cycles
  - Mammalian cell cycle regulation
  - Bacterial cell cycle regulation
- Circadian Rhythm
  - Temperature compensation
- Education
  - Review articles
  - Lectures

1.2 Experimental Tests

- Budding Yeast Mutant Analysis
  - Experimental confirmation of bistability in mitotic commitment
  - Quantitative measurements of cell cycle regulators
  - Genetic dependencies during exit from mitosis
  - Quantitative determination of cyclin thresholds for exit from mitosis
- Frog Cell Extract Assays
  - Activation and inactivation of MPF (mitosis promoting factor)
  - Oscillations of cyclin E-dependent kinase activity
  - Unreplicated DNA checkpoint

1.3 Software Development

- Model Representation
  - JigCell Model Builder
  - Modularity, Composition, Fusion
- Data Representation
  - JigCell Run Manager
  - JigCell Comparator
- Parameter Exploration
  - Parameter Estimation Toolkit (PET)
  - Bifurcation Analysis Tool (Oscill8)
- Cooperation
  - Software services
  - SEPDTF (System Engineering Product Design Task Force)
  - SBML (Systems Biology Markup Language)

The following chapters contain references in two different formats.

References in the format **[REF00]** appear in Chapter 6: Literature Cited.

References in the format **(Chen et al., 2004)** appear in Chapter 7: Publications Resulting from this Project.

2.0 Summary of Key Accomplishments

2.1 Network Models

- Budding Yeast Cell Cycle

In 2004 we completed and published a comprehensive model of the molecular mechanism that governs progression through the budding yeast cell cycle (G1-S-G2-M). The mechanism keeps track of the dynamical relationships among 19 different gene products, involved in 43 different molecular species. The model consists of 32 nonlinear ordinary differential equations, along with 12 algebraic equations and 4 discontinuous switches. Specification of the equations requires numerical values for 135 parameters (rate constants, binding constants, etc.). The parameter values were estimated by fitting the model to a data set comprising the phenotypes of 130 different mutants. The best parameter set we were able to find by trial-and-error was consistent with the phenotypes of 120 of the 130 mutants.

In addition to the publication (Chen et al. 2004) describing the model, we also opened a web site (http://mpf.biol.vt.edu/research/budding_yeast_model/pp/) that fully describes the model in terms of the reaction mechanism, the experimental basis for all components and reactions, the mathematical equations, basal parameter values (for wild-type cells), modified parameter values (for every mutant), and simulations of every mutant. Since going public in August 2004, the web site has consistently received about 1000 hits per month.

Progression into M phase (mitosis) in budding yeast cells is blocked if the mother cell fails to make a bud properly. This blocking signal is called the morphogenetic checkpoint, and we have built a mathematical model of the molecular mechanism thought to be responsible. The check-point model (Ciliberto et al. 2003) consists of an additional 8 differential equations and 20 new parameters. The parameter values are estimated by fitting the model to the phenotypes of an additional 13 mutant strains.

We have also been successful in computing bifurcation diagrams for the budding yeast cell cycle (wild-type cells and selected mutants) (Battogtokh & Tyson 2004; Csikasz-Nagy et al. 2006). These diagrams are very useful in understanding how genetic mutations lead to specific changes in cell phenotype.

- Fission Yeast Cell Cycle

We have carried out a thorough analysis of the fission yeast cell cycle (in wild-type and mutant cells) by bifurcation diagrams (Tyson et al. 2002; Sveiczer et al. 2004). But we were unable to produce a comprehensive model of the fission yeast cell cycle comparable to the budding yeast model. We have not been able to find a basal set of parameter values that is consistent with the phenotypes of wild-type cells and all the mutants in our fission yeast data set.

When MPF (M phase promoting factor) is destroyed as cells exit mitosis and return to G1 phase, the falling MPF activity triggers the Septation Initiation Network (SIN) which causes medial cell

division in fission yeast. Our model (Csikasz-Nagy et al. 2007) captures the qualitative features of the network.

- Frog Cell Cycle

First of all, we used the classical Novak-Tyson model [NOV93] to support and analyze the experiments carried out by Sha and Sible (below) to measure the thresholds for activation and inactivation of MPF (mitosis promoting factor) in frog cell extracts. The experiments and simulations were published together in PNAS (Sha et al. 2003), in a paper that is widely cited as a classic demonstration of bistability in protein interaction networks.

Secondly, inspired by two interesting papers [HAR96, HAR97] reporting double-frequency oscillations of Cdk2/cyclin E activity during the early cell cycle of a developing frog embryo, we proposed a model that would generate two peaks of cyclin E-dependent kinase activity per cell cycle. Matthew Petrus, in Sible's lab, took up the challenge of testing some of the implications of this model. The model and accompanying experiments were published in *Biophysical Chemistry* (Ciliberto et al. 2003).

(For key to references and literature citations, see p. 3.)

If a cell is prevented from completing the process of DNA synthesis (e.g., by exposure to a drug like aphidicolin), the cell senses the problem and generates a 'checkpoint' signal that blocks entry into M phase. (M phase, or 'mitosis', is the process by which fully replicated DNA molecules are separated to daughter cells just before cell division. If mitosis commences when the DNA molecules are only partially replicated, then the DNA molecules are broken and the daughter cells inherit an incomplete set of genes. Under these circumstances, the daughter cells invariably die.) The classical Novak-Tyson model suggested that the unreplicated DNA checkpoint functions by promoting inhibitory phosphorylation of MPF and thereby raising the threshold for MPF activation. One of the experiments in Sha et al. (2003) supported this prediction. Sible's lab has pursued this idea experimentally (see below), and the modeling group has extended the Novak-Tyson model to account for post-1993 information on the molecular machinery behind the unreplicated-DNA checkpoint. The challenge here is to find an optimal set of parameter values that is consistent with all the experimental data on MPF activation in the absence and presence of the DNA-replication inhibitor, aphidicolin.

- Other Cell Cycles

Our remarkably successful models of cell cycle regulation in budding yeast, fission yeast, and frog cells are all built around the same set of molecular interactions: cyclin synthesis and degradation, Cdk phosphorylation and dephosphorylation, and the regulated synthesis and degradation of a Cdk-inhibitory protein (CKI = cyclin-dependent kinase inhibitor). The seemingly universal nature of the molecular regulatory network led us to propose a 'generic' model of the eukaryotic cell cycle. The generic model is a universal set of differential equations accompanied by a set of to-be-specified kinetic parameters. The values of these parameters (rate constants, binding constants, etc.) are determined ultimately by the genetic sequences that encode the proteins that carry out the functions. Hence, we may think of the wild-type genome of

budding yeast as encoding a set of proteins that maps to a specific point in the multi-dimensional parameter space (p_1^{BY}, p_2^{BY}, …, p_M^{BY}) of the generic cell cycle model. Each of the various mutant strains of budding yeast may be thought of as a perturbation of one or more of these parameters away from the wild-type value. In this view, fission yeast 'lives' at a different point in parameter space (p_1^{FY}, p_2^{FY}, …, p_M^{FY}), frog cells at a third point (p_1^{FC}, p_2^{FC}, …, p_M^{FC}), and so forth. In our paper on the generic model (Csikasz-Nagy et al., 2006) and on the accompanying web site (http://mpf.biol.vt.edu/research/generic_model/main/pp/) we propose a universal set of differential equations and particular parameter sets for BY, FY and FC. To confirm our parameter sets, we show that the models are consistent with a great body of specific experimental details on each of these cell types. The basic modeling tool that we employ is the one- and two-parameter bifurcation diagram.

From the generic model, it is now much easier to develop models of cell cycle regulation in new organisms. For example, we have developed new models of the mammalian cell cycle engine (Novak & Tyson, 2004) and of the early embryonic cycles of the fruit fly (Calzone et al., 2007).

Mammalian cell cycle modeling provides a challenging test bed for the software tools we built for BioSPICE. Unlike yeast cell proliferation, which is controlled only by nutrient availability and mating factors, mammalian cell growth and division is controlled by a very complex signal processing network that decides, on the basis of external and internal signals, whether the cell will remain quiescent (alive but non-proliferating), will grow and divide, or will embark on a pathway of programmed cell death (called 'apoptosis'). Toward the conclusion of the BioSPICE project we embarked on an exploratory program to model the mammalian signal transduction network controlling cell growth, division and death.

Lastly, we initiated a project to model cell cycle regulation in the free-living aquatic bacterium, *Caulobacter crescentus*. The molecular machinery governing DNA synthesis and cell division in bacteria is completely different from the machinery in eukaryotes. The control molecules in bacteria (DnaA, CtrA, GcrA, DivJ, DivK, etc.) bear no functional or evolutionary relationship to the control molecules of yeast cells (Cdk, CycB, Cdc20, Cdh1, Sic1, Cdc14, etc.). Nonetheless, as shown by Brazhnik & Tyson (2006), the wiring diagrams of the two networks are uncannily convergent (topological similarity of the network designs) and the bifurcation diagrams of the differential equations are nearly identical (functional similarity of the network dynamics). In addition to the evolutionary significance of these observations (Brazhnik & Tyson, 2006), these surprising convergences allowed us to make rapid progress in modeling the Caulobacter cell cycle (Li et al., submitted 2007). The detailed molecular mechanism/mathematical model for Caulobacter is provided at http://mpf.biol.vt.edu/secure/caulobacter/pp/. Furthermore, the genetic regulatory network in Caulobacter is known to be closely related to the networks controlling cell division and differentiation in economically important bacteria, such as Sinorhizobium (the nitrogen-fixing bacteria in root nodules of legumes) and Brucella (the pathogenic bacteria that cause brucellosis in cattle). Using the modeling experience gained on the DARPA project and the software developed there, we have embarked on a new project of modeling and experimental characterization (joint with Sobral's group at the Virginia Bioinformatics Institute) of cell cycle control in Sinorhizobium.

- Circadian Rhythm

The circadian rhythm is the innate 24-hour oscillation of physiological properties of myriad organisms from all kingdoms, phyla and divisions of life. The circadian rhythm has three defining characteristics: it is endogenous (i.e., it persists at a period ~24 h in the absence of any external cues), it entrains to periodic external cues over a range of periods close to 24 h, the endogenous rhythm is phase shifted by brief pulses of light, and the period of the endogenous rhythm is temperature compensated (i.e., it does not vary much from 24 h over a large range of temperatures from < 20^{o}C to > 32 ^{o}C). A great deal is known about the underlying molecular machinery of the circadian rhythm in eukaryotes (bread mold, fruit fly, rodent) and in prokaryotes (cyanobacteria). In eukaryotes, there is a distinct negative feedback loop, whereby the *period* protein inhibits transcription of the *period* gene. Many theoretical groups have shown how this negative feedback loop can generate spontaneous limit cycle oscillations with a period close to 24 h. The limit cycle hypothesis is consistent with the defining characteristics of the circadian rhythm except for temperature compensation. Robust temperature compensation of limit cycle oscillators is unexpected and difficult to explain. Our modest contribution to the theory of circadian rhythms is to point out that the molecular control network has positive as well as negative feedback loops, that the positive feedback can generate oscillations by homoclinic bifurcations (as opposed to Hopf bifurcations), and that homoclinic bifurcations can provide a mechanism for more robust temperature compensation of the circadian rhythm [TYS99] (Hong et al., 2007).

Although they have the same defining characteristics, circadian rhythms in cyanobacteria are generated by a molecular mechanism that is much different from that in eukaryotes. The basic oscillatory proteins, KaiA-B-C, in cyanobacteria bear no functional or genetic similarity to the *period* proteins (and their partners) in eukaryotes, and, although the negative feedback loop on *period* transcription is essential to rhythmogenesis in eukaryotes, the negative feedback loop on *kai* transcription is dispensable in cyanobacteria. As the BioSPICE project was winding down, we began a project to model these curious properties of cyanobacterial circadian rhythms (Laomattechit et al., in preparation).

- Education

During the course of the DARPA project, we were invited to prepare a number of review articles to communicate to experimental molecular biologists the power and promise of mathematical modeling of molecular regulatory networks. Our first review article ("Network Dynamics and Cell Physiology," *Nat. Rev. Mol. Cell Biol.*, 2001) laid out the basic notion that a reaction network is governed by a set of dynamical equations (differential equations, usually) that define a flow in state space (the coordinate system spanned by the concentrations of all the time-varying species in the reaction network). The flow leads to stable attractors (steady states and oscillatory solutions) that can be interpreted in terms of the characteristic physiological states of the network. Signals impinging on the network warp the flow and may change the nature of the attractors, i.e., modify the physiological response of the cell. Mathematicians call such changes 'bifurcations of vector fields'; cell physiologists call them the 'signal-response curve' of a cell.

Our second review article ("The dynamics of cell cycle regulation," *BioEssays*, 2002) used these notions to describe cell cycle control in fission yeast in terms of bifurcation diagrams of wild-type and mutant cells. The one-parameter bifurcation diagram shows how cell growth drives progression through the cell cycle (DNA synthesis, mitosis and cell division) by altering the attractors of the Cdk regulatory mechanism. Mutations alter the mechanism, which alters the bifurcation diagram, which alters the physiological responses (the "phenotype") of the mutant cell. This approach was followed up in greater detail in Csikasz-Nagy et al. ("Analysis of a generic model of eukaryotic cell cycle regulation," *Biophys. J.*, 2006), where we studied mutants of budding yeast, using one- and two-parameter bifurcation diagrams.

Our third review article ("Sniffers, buzzers, toggles and blinkers: dynamics of regulatory and signaling pathways in the cell," *Curr. Opin. Cell Biol.*, 2003) showed how to define a set of regulatory modules that can be hooked together to form elaborate control systems. Over the last few years, these three review articles have been cited many times: Nature Review 97, BioEssays 39, and Current Opinions 106.

We also prepared a review article on cell cycle checkpoints for the *Encyclopedia of Life Sciences* (Macmillan Reference Ltd., London, 2002; http://www.els.net/) and a layman's guide to mathematical modeling of the cell cycle for the journal *Methods* (Sible & Tyson, 2007).

Nature Cell Biology invited us to write a commentary on "Irreversible transitions in the cell cycle as consequences of systems-level feedback" (Novak et al. 2007). Progression through the cell cycle is one-way (DNA synthesis, then mitosis, then cell division, then another round of DNA synthesis, etc.). If the events get out of order, the result is usually catastrophic for a cell. What makes the transitions from one event to the next irreversible? The textbook answer is that, at every transition, some protein component is "irreversibly" degraded (broken down into its constituent amino acids). We challenge this accepted wisdom. Protein degradation is, to be sure, thermodynamically irreversible, but it is kinetically reversible. For most proteins, their steady degradation is exactly balanced by de novo protein synthesis. Furthermore, protein degradation at a cell cycle transition can often be blocked without rendering the transition reversible. We argue that irreversibility of cell cycle transitions is not a reductionist property of a unitary molecular event (protein degradation) but rather a systems level property of the global feedback signals in a regulatory network. This is one example of a recurring theme of the BioSPICE program: that crucial aspects of cell physiology (like irreversible progression through the cell cycle, or the temporal organization of circadian rhythms, or pathogenic states of bacteria) are governed not by simple molecular interactions of a few genes or proteins but by complex networks of macromolecules coordinated by feedback and feed forward signals.

Taking every opportunity to get this message across to a broad audience of life scientists, Tyson gladly accepted an invitation by *Nature* to write an opinion piece ("Bringing cartoons to life") to appear in 2007 in a new series of essays called "Making Connections".

2.2 Experimental Tests

- Budding Yeast Mutant Analysis

For some years before the DARPA grant began, Fred Cross and his students at Rockefeller University had been collaborating with Tyson and Chen at Virginia Tech on experimental tests of their mathematical model of the yeast cell cycle. Two important papers appeared in late 2001-early 2002, which laid the foundation for this part of the DARPA project.

(a) In Miller & Cross [MIL01], they tested the idea, foundational to the Chen-Novak-Tyson model, that yeast cells measure their size by accumulating cyclin (Cln3) molecules in the nucleus. Nuclear localization of Cln3 is controlled by specific amino acid sequences on the protein, called NLS's (nuclear localization sequences). By removing Cln3's NLS or by replacing it by an NES (nuclear export sequence), the experimentalist can manipulate the distribution of Cln3 molecules between nucleus and cytoplasm. The results of these experiments are in reasonably good quantitative agreement with the model.

(b) In Cross et al. [CRO02], they confirmed a key qualitative prediction of the Chen-Novak-Tyson model, that activation of Clb-dependent protein kinases (the proteins that initiate DNA synthesis and mitosis in yeast cells) has the properties of a bistable switch. That means, under identical final conditions, the activity of Clb-kinase in a cell can be either high or low, depending on how the cell was put into the final conditions. As predicted, the state of the Clb-kinase switch is fixed by the prior history of Cln-kinase activity (which flips the switch to HIGH) and Cdc14-phosphatase activity (which flips the switch to LOW). In Cross's experiment, the yeast cells' starting conditions were: Cln activity = 0, Cdc14 activity = 0 (neutral) and Clb activity = LOW. The cells were exposed to a fixed level of Cdc14 activity and increasing levels of Cln3 activity, and then shifted back to neutral (Cln = 0, Cdc14 = 0). The final state of Clb-kinase was either HIGH or LOW, depending on the transient stimulation by Cln3. Short stimulation left the switch in LOW, whereas long stimulation flipped the switch to HIGH and the switch stayed HIGH even after Cln3 and Cdc14 conditions were returned to neutral. This experiment from Cross's lab, was the first published indication that a cell cycle transition is governed by a bistable switch.

Under DARPA support, Cross and his collaborators went on to provide further confirming tests and quantitative data relevant to the yeast cell cycle model. In Cross (2003), he studied the destruction of Clb-kinase activity as cells exit mitosis and return to the G1 phase (pre-DNA replication) of the cell cycle. This transition (M-to-G1) flips the switch from Clb = HIGH to Clb = LOW, and it involves the activation of three different 'enemies' of Clb-kinase: Cdc20 (a protein that marks Clb molecules for degradation), Cdh1 (a different protein that also marks Clb for degradation), and Sic1 (a protein that binds to Clb-dependent kinase to form an inactive complex). By genetic manipulation of the amount and/or activity of these three proteins, Cross could study their relative contributions to the M-to-G1 transition (also called mitotic exit). Cross showed that his genetic experiments were in good agreement with predictions of the Chen-Novak-Tyson model (Chen et al., 2000).

In the course of these experiments, a quantitative problem with the model became apparent. The amount of Sic1 protein per cell needed to account for the phenotypes of mutant yeast cells was

much larger than measurements would allow. Either the model was seriously in error, or there was some other protein backing up the role of Sic1. In Archambault et al. (2003), Cross's team showed that the protein Cdc6 plays exactly this role. For many years Cdc6 was known to play an essential role in the initiation of DNA replication, but only in 2001-2002 did it become clear that Cdc6 has a second, non-essential role in binding to and inhibiting Clb-dependent kinase as cells exit from mitosis. By removing the first 47 amino acids of the Cdc6 sequence, the non-essential role of Cdc6 can be eliminated without interfering with its essential role in DNA replication. With this mutant of Cdc6 (called *cdc6Δ47*), Cross and collaborators could study the combined roles of Sic1 and Cdc6 in mitotic exit. These experimental results became part of a major revision of the Chen-Novak-Tyson model that appeared in Chen et al. (2004).

At the same time, Brian Thornton, in David Toczyski's lab at the University of California in San Francisco, was also studying exit from mitosis in yeast strains with lethal mutations in the APC (anaphase promoting complex). 'Anaphase' is the stage of mitosis where the replicated chromosomes are segregated to the incipient daughter nuclei of the dividing cell, and the APC is an essential for the first step of anaphase: the APC destroys the 'sticky' proteins that were holding together the two identical DNA molecules. The APC, in cooperation with Cdc20 and Cdh1 (see above), plays a second role in destroying Clb proteins. Elimination of Clb-kinase activity is necessary to complete cell division and put the daughter cells into G1 phase. Looking for mutant combinations that would rescue the lethal phenotype of apc^- mutations, Thornton and Toczyski found the viable strain: apc^- *pds1Δ clb5Δ* $SIC1^{OP}$. The physiological consequences of such complicated genetic manipulations, knocking out and overexpressing genes at four different loci, is impossible to understand by intuitive reasoning alone. So Thornton and Toczyski asked us to help analyze their experimental data using the revised yeast cell cycle model that was, at the time, under development at Virginia Tech. The published paper describes the success of the model in accounting for the unexpected phenotypes of these bizarre genetic constructs (Thornton et al., 2004).

Finally, Cross et al. (2005) describes a quantitative study of Clb-type cyclins in exit from mitosis. By genetic techniques, Cross was able to manipulate the total concentration of Clb2 cyclin (the most important cyclin protein for mitosis) in genetic backgrounds where mitotic exit is compromised: apc^-, *cdh1Δ*, *sic1Δ*, *cdc6Δ47*, etc. Again, it is impossible to guess in advance the phenotypes of these mutants with any confidence. So Cross asked Chen to predict the results of his experiments, using the new model, before he made the results public. The model predictions were in excellent qualitative and quantitative agreement with the measurements, as explained in the publication.

- Frog Cell Extracts

Jill Sible's research group studies cell cycle regulation in intact embryos of the frog, *Xenopus laevis*, and in cell-free extracts derived from unfertilized eggs. Her methods include microscopic observation, molecular interventions, and biochemical measurements. In her first set of experiments (Sha et al., 2003) she tested three predictions made in the Novak-Tyson model [NOV93] of cyclin-dependent kinase (Cdk) activation in frog cells. Her second set of experiments (Ciliberto et al., 2003b) were done to test and refine a novel model of double-frequency Cdk2/cyclin E oscillations in frog embryos. A third set of experiments (Auckland &

Sible, in preparation) are exploring mechanisms by which unreplicated DNA blocks progression through the cell cycle.

The original paper by Novak and Tyson (1993) made some striking predictions about the activation of MPF (M-phase promoting factor, the active form of Cdk1-cyclin B). Frog cell extracts, as prepared by Solomon et al. [SOL90], have copious amounts of Cdk1 but no cyclin B. By adding fixed amounts of recombinant, non-degradable cyclin B, Solomon observed a distinct threshold below which MPF activity is negligible and above which it is proportional to the total amount of cyclin B in the preparation. The Novak-Tyson model accounts for this threshold in terms of a saddle-node bifurcation in the kinetic equations and makes three predictions about the threshold:

- There should be a different (lower) threshold for MPF inactivation, when cyclin B concentration is decreased in an initially active extract.
- The time delay for MPF activation should increase abruptly as cyclin B concentration approaches the activation threshold from above.
- The threshold value of cyclin B should increase in the presence of inhibitors of DNA synthesis.

In Sha et al. (2003), all three predictions were successfully confirmed.

After fertilization, frog eggs undergo 12 rapid (30 min) synchronous divisions to generate a hollow ball of 4096 cells. During each cell division cycle, MPF (Cdk1-cyclin B) fluctuates from low activity (interphase) to high activity (metaphase). For each cycle of MPF activity, the dimer Cdk2-cyclin E (an initiator of DNA synthesis in metazoans) undergoes two peaks of activity (15 min period), with highs in interphase (when DNA is being synthesized) as well as mitosis [HAR96, HAR97]. Whereas Cdk1-cyclin B oscillations are driven by periodic bursts of cyclin B degradation, Cdk2-cyclin E activity fluctuates in spite of constant levels of both Cdk2 and cyclin E. After cycle 12, the egg's pool of cyclin E is abruptly degraded. We have proposed a molecular mechanism and mathematical model for these curious features of Cdk2-cyclin E activity in early frog embryos (Ciliberto et al., 2003a). We assume that (i) Cdk2-cyclin E oscillations are driven by periodic inhibitory phosphorylations of the Cdk2 subunit by Wee1 kinase, and (ii) cyclin E degradation is dependent on autocatalytic loading of Cdk2-cyclin E onto a nuclear structure. We have tested some predictions of the model. For instance, when the embyro is injected with mRNA for the recombinant protein Xic1Δ34, this specific inhibitor of Cdk2-cyclin E activity blocks the 15 min oscillations, as expected, and delays the degradation of cyclin E until a few hours after Xic1Δ34 itself is degraded. The model predicts that Cdk2-cyclin E and Wee1 are involved in a negative feedback loop, in contrast to Cdk1-cyclin B and Wee1, which are mutual antagonists. Direct experimental evidence for the negative feedback loop has yet to be obtained.

During the last years of the DARPA project, Sible's lab returned to the issue of how, in frog cell extracts, inhibitors of DNA synthesis block activation of MPF (a quite general property of the cell cycle, called the 'unreplicated DNA checkpoint'). The last experiment of Sha et al. (2003) seemed to confirm the prediction of Novak & Tyson [NOV93] that the unreplicated DNA checkpoint works by raising the cyclin threshold for activation of MPF. Sible and her student, Ian Auckland, began a more extensive quantitative study of this effect, while Tyson and his student, Amit Dravid, initiated a revision of the Novak-Tyson model to account for more recent data on the effects of unreplicated DNA in frog cell extracts (see Chapter 3). Because Dravid and

Auckland left the graduate program at VT prematurely, this promising project was delayed. New students have taken up where the old ones left off, under support of an NIH grant, and we hope soon to have the results ready for publication.

2.3 Software Development

The goal of bottom-up modeling in molecular systems biology is to understand how detailed molecular mechanisms, in terms of interacting genes, proteins and metabolites, determine the physiological characteristics of a living cell. The modeling cycle is illustrated in Fig. 1. The modeler starts with curiosity about a certain aspect of cell physiology (say, cell cycle regulation, programmed cell death, circadian rhythm generation, or a developmental transition) and a collection of experimental observations that he or she seeks to understand at a molecular level. The modeler also has some hints about the underlying molecular controls of this process, say a set of genes that are known to influence relevant traits of the organism and properties of the gene- encoded proteins. The modeler sketches out a 'wiring diagram' of the control system, i.e., a network of coupled chemical reactions expressing how the molecules are synthesized and degraded, how they associate and dissociate into transient molecular complexes, how they act on one another in catalyzed chemical reactions, etc. The wiring diagram is a precise hypothesis of how the scientist thinks a certain aspect of cell physiology is controlled at the molecular level. The challenge is to determine to what extent the hypothesis is correct or incorrect.

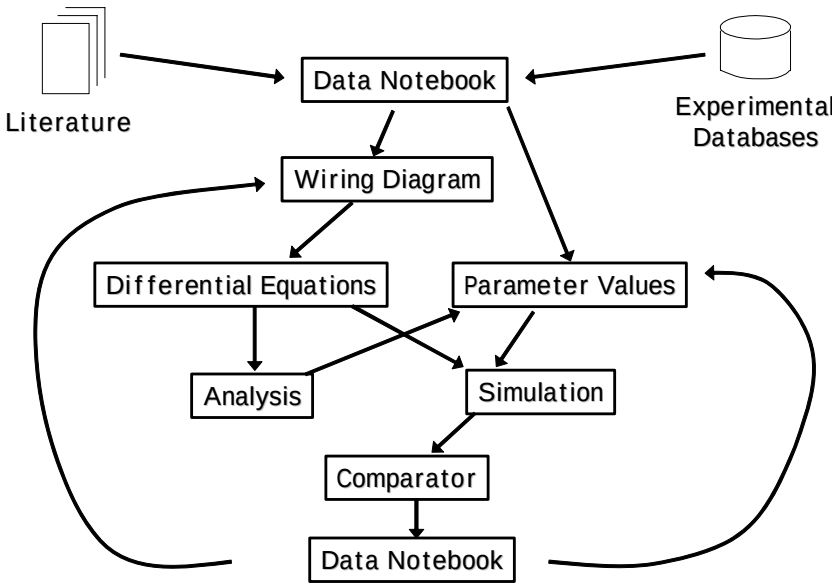

Figure 2.1. The modeling cycle. The modeler starts with a hypothetical wiring diagram that he/she thinks is consistent with a set of experimental observations on a certain aspect of cell physiology. To test this hypothesis, the wiring diagram must be translated into a set of dynamical equations, parameters in the equations must be estimated, simulations run, and the model output compared to the original experimental data. Typically the output looks promising but is not in good quantitative agreement with experiment. Discrepancies trigger the inner loop of parameter adjustments to get a better fit. If no amount of parameter twiddling can bring the model in alignment with the data, then the modeler must consider changes in the wiring diagram itself, which starts the whole process from the top.

Typically, molecular biologists approach this challenge by informal discussions of how they think the mechanism will operate, based on their considerable intuition about the properties of genes and proteins. Their approach is easy, enjoyable, and often adequate for simple mechanisms with a few interacting macromolecules or linear pathways, but as soon as the network gets complex, with interlaced feedback and feed forward control loops, the hand-waving approach flounders in a stormy sea of conflicting signals, endless possibilities and unanticipated results. The intuitive approach is fine for coffee-table discussions and even for thinking about the next experiments to perform. But it is hopeless as a scientific method for connecting molecular interactions to cell behavior under realistic conditions.

Computational biologists approach this challenge by converting the chemical reaction network into a set of dynamical equations (usually nonlinear ordinary or partial differential equations) that describe how the reactions play out in time and space, according to the well-established laws of chemical reaction kinetics, molecular diffusion, directed transport, etc. The dynamical equations capture the myriad interactions in the network and accurately predict the consequences of these couplings under any circumstances. Predictions of the model are precise implications of the hypothetical wiring diagram, regardless of whether they correctly or incorrectly predict the actual behavior of cells observed in experiments. Indeed, early 'predictions' are invariably inconsistent with experiments, because there is an early phase of the modeling process where the fixed parameters in the equations (rate constants, binding constants, time lags, whatever) need to be adjusted to get the best possible agreement of model simulations to the available data.

Even after the parameters are optimized (or, at least, thoroughly explored), the model may be insufficient to explain important aspects of the experimental data set. In that case, the bottom-up modeler goes back to the wiring diagram and considers possible changes in his or her basic hypotheses. The modified hypothesis is then explored in the same way, and the process continues until the modeler is satisfied with the fit of model to data or concludes that there is no satisfactory molecular explanation for the data under consideration.

The modeling cycle is often carried out 'by hand.' The modeler collects relevant experimental data, as a pile of reprints in the corner of the office or, better, as clippings in a notebook organized according to genes, interactions, physiology, etc. With some hypotheses in mind, the modeler then draws a wiring diagram on paper and translates it into differential equations by hand. He or she then picks a suitable computer program to solve the equations numerically and writes the necessary code. This part of the process is not very time consuming, but it is error prone, especially for large networks. Before simulations can be run, the modeler must assign numerical values to the kinetic parameters in the differential equations and provide reasonable initial conditions for each type of experiment to be simulated. Then output from the simulator is compared against the data, typically by visual inspection. Wherever simulations and the data don't fit, suspicion is immediately cast on the parameter values (the most uncertain parts of the model). With a little intuition, the modeler identifies the likely culprits and then 'twiddles' those parameters to see if the fit can be improved. At first this is fun, as the modeler pits his/her intuition against the computer's simulations and refines his/her understanding of how the mechanism works. But after a while, the process of parameter twiddling and curve fitting becomes mighty tedious and unreliable. It would be grand to download the problem to the

computer, but there are no parameter estimation programs available that are flexible and efficient enough to handle the sort of fitting problems faced in computational cell biology.

From this description, it should be obvious that molecular systems biologists desperately need friendly, effective software tools to support key steps of the modeling cycle. Data collection, cataloguing, storing and retrieving is the first area where software can help. Many bioinformatics groups are working on this problem, so the Virginia Tech Team did not attempt to support this aspect of the modeling cycle. 'MONOD,' a product of the BioSPICE program, is a good first try to provide modeler-notebook support (http://monod.molsci.org/).

The next step is digital representation of the model: the chemical reaction network as a list of reactions or as a graphical wiring diagram. Such a facility should guide the modeler in building a chemical reaction network, entering rate laws, checking for completeness and consistency, identifying chemical conservation conditions, and accurately framing a mathematical representation of the network in a variety of formats suitable for computation (FORTRAN, Matlab, C) and communication (SMBL). An integrated software environment (often called a Problem Solving Environment, PSE) should then provide a suite of simulation tools (ODE integrators, PDE solvers, stochastic simulators), seamlessly connected to the model-building tool. Before simulations can be run, the modeler must describe precisely how to simulate each experiment in the collection of experimental data being used to validate the model. This step requires an informatics tool to manage simulation runs: specifying parameter values, initial conditions, simulation conditions, and, possibly, subtle changes to the basic model that are needed to mimic certain experimental conditions. The PSE then executes the simulations and returns the results, suitably displayed, to the user. Next the PSE should support comparison of simulations to experimental data, and some way to assess whether the fit is satisfactory or not. The PSE should then provide a parameter-twiddling facility, whereby the modeler can quickly explore the behavior of the mathematical model as parameters are varied. Finally, it would be very nice if, after the parameter-fitting problem is sufficiently well formulated, the computer could take over, systematically exploring parameter space to find a globally optimal set of parameter values.

At the start of the BioSPICE program, the software Virginia Tech team proposed to build a PSE like that described in the previous paragraph. Our PSE was called 'JigCell' because we think of the modeling process as akin to putting together a 1000-piece jig saw puzzle. The pieces are the genes and proteins thought to underlie the control of some aspect of cell physiology. The interlocking protrusions and indentations of the pieces are the chemical mechanisms by which the macromolecules interact. The picture on the front of the box is the biological behavior we are trying to understand. JigCell creates mathematical representations of the fundamental pieces and permits the modeler to shuffle the pieces around, trying out combinations to see if they fit together to give a coherent view of some part of the whole picture. Computer simulations, in comparison to data, tell us whether we have put the pieces together correctly or not. With some skill, lots of patience, and a modicum of luck, the full picture starts to come together. There may be some missing pieces here or there, some rough edges, some unresolved inconsistencies, but we can see progress as our computational model of the molecular mechanism conforms with more and more experiments and begins to make reliable predictions of new responses of the cells.

Before describing JigCell and other Virginia Tech tools, it is important to place this software development effort in context. At the start of the BioSPICE program, there were only a few PSEs for bottom-up modeling in molecular and cell biology. Virtual Cell (www.vcell.org) is the oldest and most mature resource. It specializes in solving reaction-diffusion equations for small reaction networks on complicated spatial domains derived from microscopic images of cells. It was not intended for simulating complex networks of reactions and comparing the results to many types of experimental data. Another popular PSE at that time, Gepasi (www.gepasi.org), specialized in modeling metabolic control networks. It had some sophisticated tools for curve-fitting and optimization. Jarnac (http://sbw.kgi.edu/software/jarnac.htm) offered similar services. E-Cell (www.e-cell.org) was in a quite primitive and unreliable state at the time. The Kitano Symbiotic Systems Project (http://www.symbio.jst.go.jp/symbio2) was concentrating its efforts on SBML (Systems Biology Markup Language) and just beginning work on CellDesigner (http://celldesigner.org) Berkeley's BioSpice software (http://biospice.lbl.gov) was also a work in progress. This unsatisfactory state of affairs was a major reason for initiating DARPA's BioSPICE program. Between 2001 and 2006, many new software tools and modeling PSEs were developed, through BioSPICE and other efforts. The SBML website (http://sbml.org) now lists over 100 tools that can exchange models using SBML. Of particular relevance to JigCell are: SBW (Systems Biology Workbench, http://sbw.kgi.edu/), especially its reaction diagramming tool, JDesigner; Biomodels (www.biomodels.net), which includes many VT models; a nonlinear-dynamics toolkit, XPPAUT (http://www.math.pitt.edu/~bard/xpp/xpp.html); and two stochastic simulation packages, Dizzy (http://magnet.systemsbiology.net/software/Dizzy/) and BioNetS (http://x.amath.unc.edu:16080/BioNetS/). JigCell is complementary to all these packages and communicates easily with them through SBML.

The following subsections summarize our software achievements under the JigCell umbrella and some related software developments.

- Model Representation

There are at least three ways to help users create a chemical reaction network: with a graphical user interface for drawing wiring diagrams, with a wizard interface for entering the relevant information in a guided fashion, and with a spreadsheet interface that can displays information efficiently and gives the user great flexibility to input and modify the information. GUI's are appealing because a wiring diagram sketched out on a piece of paper is almost always the way a scientist first formulates a mechanistic hypothesis. But graphical diagrams can be very hard to draw when the mechanism gets complicated and very hard to communicate from one computer program/platform to another. Wizard interfaces are great for guiding novices through the modeling process, but they become annoying to experienced users who would prefer faster and more flexible ways to enter data and modify models. Because several groups, within and outside BioSPICE, were developing graphical and wizard interfaces, and because the VT team was convinced that a spreadsheet interface had great advantages and could easily complement other views, we constructed a spreadsheet editor called the JigCell ModelBuilder (JCMB).

The JCMB is described in detail on the JigCell Home Page (http://jigcell.biol.vt.edu/), in some original publications (Vass et al., 2003; …) and later in this technical report. In general terms, the JCMB edits a spreadsheet for which each row represents a reaction in the network. Column 1

specifies reactants, products and stoichiometry. Column 2 specifies the rate law type (mass action, Michaelis-Menten, custom). Column 3 gives unique names to the kinetic parameters that appear in the rate law. In this place, also, are specified any 'modifiers,' which are chemical species (e.g., enzymes or transcription factors) that affect the rate of the reaction but are not produced or consumed by the reaction. Because the information is stored in a spreadsheet, the modeler is able to view on the computer monitor very efficiently the most relevant information about each reaction (columns) for a large number of reactions (rows). Even very large reaction networks can be viewed easily by scrolling up and down through the spreadsheet. Typical editing tools (cut, copy, paste, move, etc.) allow the modeler to control the information readily.

The JCMB assists the modeler by keeping track of chemical species, rate parameters, modifiers, etc. It notices if certain species obey some conservation conditions (linear dependencies in the stoichiometric matrix) and allows the user to determine how these conservation conditions will be employed later in writing the kinetic equations. It checks for consistency and completeness of the network and prompts the user for any problems it spots. When a network is fully entered and checked, the JCMB builds several output files. The network is saved in SBML for easy sharing with other systems biology tools. The network is also expressed as a set of nonlinear differential equations in FORTRAN (for use by VT's BioPack subroutines) and as '.ode' files for use by XPPAUT and related tools (Oscill8). An ode file is also easily comprehended by humans.

At this point, there is a radical divergence of modeling philosophy between JigCell and all other tools, except XPPAUT. SBML, Gepasi, Jarnac, VCell, etc., all store numerical values of the kinetic parameters along with the reaction network, and in many of these tools the only way to get at these values and change them is to edit the entire model and recompile. In JigCell the parameters are given names; their numerical values are meant to be specified outside the model in a file called the 'basal parameter set.' Hence, a JCMB model is not meant to be simulatable as it stands. Parameter values and initial conditions may be specified in the JCMB, but we prefer to leave those jobs to the JigCell Run Manager (JCRM), which sets up and executes simulation(s). To do a simulation, the JCRM needs, in addition to the model (the differential equations), the following information: a specification of the parameter values to be used in the simulation, initial conditions for all the variables, identification of the simulation program to be used, and specification of the numerical tolerances, etc., that control the accuracy and output of the simulator. The additional information is external to the model: it is needed to carry out a specific simulation of a specific experiment, and the specifications typically change from one simulation to another. It is the job of the JCRM to keep track of all this information; i.e., to manage the simulation runs.

The JCRM is also organized as a spreadsheet. For a set of runs, the JCRM takes as input an SBML file specifying the model, and a basal parameter set, giving numerical values to the model parameters. Each row manages a single run. Column 1 names the simulation and associates it with a specific experiment being simulated. Column 2 specifies how the basal parameter set must be modified, if at all, in order to simulate the experiment. For example, because of the way the experiment was carried out, some reaction may be missing from the network, in which case the corresponding rate constants must be changed (e.g., set to 0). Column 3 specifies the appropriate initial conditions for the experiment under consideration. Column 4 specifies the simulator to be used, and column 5 the numerical constants that govern the properties of the simulator.

This organization of runs is very convenient because there are often logical relationships among the parameter settings for a related set of experiments/simulations. For example, we may not be sure, at the start of a modeling project, what is the correct value of rate constant k_5. But we do know that, whatever be the basal value of this rate constant (call it k_5^o), the correct value for simulating experiment #3 should be $2k_5^o$ and the correct value for simulating experiment #7 should be 0. The JCRM keeps track of these logical relationships among the parameters and applies them to a set of simulations, for any specific parameter values given in the basal set. In this way, it is easy for the modeler to 'twiddle' parameter values in the basal parameter set and re-compute a collection of related simulations automatically.

The JCRM is downloadable from our web site, http://jigcell.biol.vt.edu/, along with basic instructions. It is open-source software, as are all our tools developed under the DARPA project.

- Data Representation

The third component of JigCell, called the Comparator, associates simulations with experimental data and assesses whether the fit between theory and experiment is satisfactory or not. Like the other components, the Comparator is a spreadsheet: each row represents a single experiment. The first column names the experiment and points to a location (reference or web link) where the data is reported and described. Column 2 records the data in a flexible format specified by the user. The data format is a 'list of lists'. A list is a set of objects of distinct types: real numbers, integers, Boolean (true/false), or a string. For example, time series data (chemical concentrations as functions of time) can be recorded as a list of lists of real numbers: $\{(t_1, x_1(t_1), x_3(t_1), x_6(t_1)), (t_2, x_1(t_2), x_3(t_2), x_6(t_2)), \ldots\}$. Or we might want to record that a certain mutant is inviable (unable to divide) and arrested in G1 phase of the cell cycle, using the list {false, 0, 0, 'G1'}, where the first element (Boolean) answers the question 'is the mutant viable?', the second and third elements (real numbers) are skipped if the answer is 'false', and the fourth element (string) indicates the cell cycle phase in which an inviable mutant is arrested. Some other mutant might have the list {true, 62, 1.8, ''}, meaning it is viable with a G1 period of 62 minutes and a size at cell division 80% larger than wild-type cells. Almost any type of experimental data can be represented in this way.

Column 3 of the Comparator associates this particular experiment with a row of a RunManager file that specifies how to simulate this experiment (model, basal parameter set, parameter changes, initial conditions, etc.). Column 4 names a 'transform function' that takes as input the results of a simulation $\{(t_1, x_1(t_1), x_2(t_1), \ldots, x_n(t_1)), (t_2, x_1(t_2), x_2(t_2), \ldots, x_n(t_2)), \ldots\}$and produces as output a list-of-lists of exactly the same format as the specification of the data type. To proceed from here, the Comparator must ask the RunManager to execute the simulation and return the time series. Now the simulated data is populated, in the same format as the real data. Column 5 compares the two list-of-lists and computes a penalty function (a real number >= 0). If the lists are identical, the penalty is 0. If there are discrepancies, appropriate penalties are assigned. For example, if the data is a real number x, then the penalty might be $(x_{sim}-x_{obs})^2/v_x$, where v_x is the variance of the observed value x_{obs}. If the penalty value is less than some user-specified threshold, then the fit of the simulation to the experiment is acceptable. Otherwise, the penalty value is highlighted in red, to draw the user's attention to those experiments that are not satisfactorily explained by the model, with its current basal parameter set.

The Comparator is downloadable from our web site, http://jigcell.biol.vt.edu/, and it is described in Allen et al. (2006).

From the summaries provided here, it should be obvious how the JigCell Model Builder, Run Manager and Comparator work together to provide the modeler with a flexible PSE for creating bottom-up models, comparing model behavior with experimental data, assessing successes and failures, and easily exploring parameter space (by making changes to the basal parameter set) to look for better fits of the model to the data.

- Model Fusion and Composition

Towards the end of the DARPA project, the JigCell Team became involved in writing software to support modularity in model building. The basic idea is that models of large networks are built by fusing together smaller models of sub-networks (see, e.g., [TYS01]). If each sub-model is expressed as a separate SBML-Level2 object, how can they be fused together to make a larger model that is properly specified in SBML-Level2? We have outlined the steps through which a modeler must proceed in order to resolve the inconsistencies and/or redundancies among the sub-models, and we have built a Model Fusion tool that guides the user through the process by a series of wizards. The Model Fusion tool is included in the standard JigCell installation.

Model fusion is an irreversible process: the sub-models lose their separate identities and cannot be recovered from the SBML file output by the software tool. It is possible to build a reversible fusion tool (we call the reversible process "composition" to distinguish it from fusion), by keeping track of all the adaptations that must be made to fuse two or more sub-models together. (We call these records the "glue" that binds the sub-models into a full model.) By defining some new language extensions to SBML (to be incorporated in Level3) that describe the glue, we can build a Model Composition Tool that takes several SBML-Level2 models as input and outputs an SBML-Level3 composed model, consisting of the unmodified sub-models (Level2) plus the glue (Level3) that binds them together. Hence, the composed model can be decomposed, if necessary. The Model Composition Tool is expected to be ready in Spring 2007.

Model fusion and composition are described in Shaffer et al. (2006) and Randhawa et al. (2007).

- Parameter Exploration and Optimization

The software development team at Virginia Tech created three other tools for exploring parameter space.

The Parameter Twiddler was a pilot project to provide a flexible and easy way to explore parts of parameter space and view the effects of parameter variations on specific state variables. The user specifies the parameters that he/she wants to twiddle, and they come up on the screen as a list of names and values or as names and sliders. The user also specifies which state variables to monitor and how to plot them, and the appropriate plot windows are created. The user changes a parameter by typing in a new value or by moving the slider. The effects of the change(s) are then quickly reflected in the output windows. The interface can create pdf output on demand, to

maintain a record of interesting parameter sets. There have been various versions of the Parameter Twiddler. A version called 'Param Batch' is available for download from the JigCell web page.

Automatic parameter optimization was always a major goal of the JigCell project. The intention was to build a fourth JigCell component, a Parameter Estimator, that would take information from the Run Manager and Comparator and search automatically through parameter space to find the optimal fit of the model to the data (by minimizing a weighted sum of penalty functions for each experiment in a Comparator file). Technical difficulties prevented accomplishment of this goal. In its place, a stand-alone Parameter Estimation Toolkit (PET) was developed. PET handles simulation runs and data comparisons similar to the philosophy of the Run Manager and Comparator, even using some of the same file formats. But communication demands between the optimizer algorithms and the model and the experiments required data structures that were not easily accommodated within the JigCell framework.

PET offers both local and global optimization algorithms, and it can accommodate penalties that are continuous functions of parameter values or discontinuous functions. If the penalty function is continuous, then local optimization can be carried out very efficiently and informatively by the Levenberg-Marquardt algorithm (ODRPACK) [BOG89], which requires computation of derivatives of the penalty function with respect to the parameters being estimated. Global search is carried out by a dividing-rectangle algorithm (DIRECT) [JON93], for which there is a parallel version (pVTDIRECT) (He et al., 2002). DIRECT can optimize both continuous and discontinuous penalty functions. The usual strategy is to search globally with DIRECT, and then follow up on promising points with a local optimizer. For continuous penalty functions, ODRPACK is recommended. For discontinuous penalty functions, a non-gradient based method is required. PET uses MADS (Mesh-Adaptive Direct Search) [AUD06].

PET can be downloaded from http://mpf.biol.vt.edu. PET routines have been used extensively to optimize cell cycle models, as described in the following publications: Zwolak et al. (2005a, 2005b) and Panning et al. (2007).

Bifurcation theory has also proved to be a powerful tool for exploring parameter space in search of the type of simulation results (multiple steady states, oscillatory solutions) that are expected to be relevant to the cell physiology under consideration. AUTO [DOE86] is a powerful software tool for numerical bifurcation analysis of nonlinear ordinary differential equations. But AUTO is not very user-friendly. The nonlinear dynamics program, XPPAUT, provides a front end for AUTO that helps users explore the bifurcation structures of simple models. A goal of the VT DARPA project was to create a new front end for AUTO that would be easier to use, would automatically track user-guided explorations of parameter space, and would provide algorithms for computer-guided searches for specific types of bifurcation diagrams. These goals were achieved to large extent in the *Oscill8* program, http://sourceforge.net/projects/oscill8. Oscill8 is used heavily by modelers in Tyson's group.

- Cooperation

During the lifetime of DARPA's BioSPICE program, the VT software team (primarily Cliff Shaffer, Nick Allen, Mark Vass and Ranjit Randhawa) played major roles in community software issues, such as SBML development and the SEPDTF (Systems Engineering Product Development Task Force). Much effort on their part was directed to meeting BioSPICE directives on software submissions, updates, compliance, testing, etc.

3.0 Details of Key Accomplishments in Network Modeling

3.1 Budding Yeast Cell Cycle

Integrative analysis of cell cycle control in budding yeast

K.C. Chen, L. Calzone, A. Csikasz-Nagy, F.R. Cross, B. Novak and J.J. Tyson
***Mol. Biol. Cell* 15:3841-3862 (2004)**

The cell cycle regulatory system is most fully worked out for budding yeast (*Saccharomyces cerevisiae*) [MEN98]. A hypothetical molecular mechanism for regulating DNA synthesis, bud emergence, mitosis and cell division in budding yeast is proposed in Fig. 1. How does one determine whether such a hypothesis is correct or not? The classical approach in physical chemistry is to convert the mechanism into a set of kinetic equations (nonlinear ordinary differential equations) and compare the solutions of these equations to the observed behaviour of the chemical reaction system. If a set of rate constants can be found for which the solutions fit the observations, then the mechanism is provisionally confirmed (pending further experimental investigations). If not, inconsistencies identify aspects of the mechanism that require revision and further testing. Although a mechanism can be disproved if it is inconsistent with well-established facts, it can never be proved correct, because new observations may force modifications and additions. Hence, our intention is not to prove that the hypothesis in Fig. 1 is "true" but rather only to show that the mechanism is a reasonable approximation to what is going on inside yeast cells.

According to the general principles of biochemical kinetics, the mechanistic hypothesis in Fig. 1 can be described dynamically by a set of nonlinear ordinary differential equations (Table 1). The kinetic constants that appear in these equations must be assigned values (Table 2) that are consistent with experimental observations, to be described later. Then the equations can be solved numerically and the solutions compared with the physiological properties of 131 mutant strains of budding yeast (Table 3).

Much of the quantitative data on these mutants refers to the timing of bud emergence, onset of DNA synthesis, and cell separation. In order to link the output of the model to these events, some auxiliary variables, called [BUD], [ORI] and [SPN], are introduced. "BUD" represents proteins that are phosphorylated by Cdc28/cyclin and subsequently initiate a new bud when the phosphorylation state reaches a threshold, [BUD] = 1. In a similar fashion, [ORI] = 1 signals the onset of DNA synthesis, and [SPN] = 1 represents alignment of all chromosomes on the metaphase plate. When Clb-dependent kinase activity drops below a threshold value, [BUD], [ORI] and [SPN] are reset to zero.

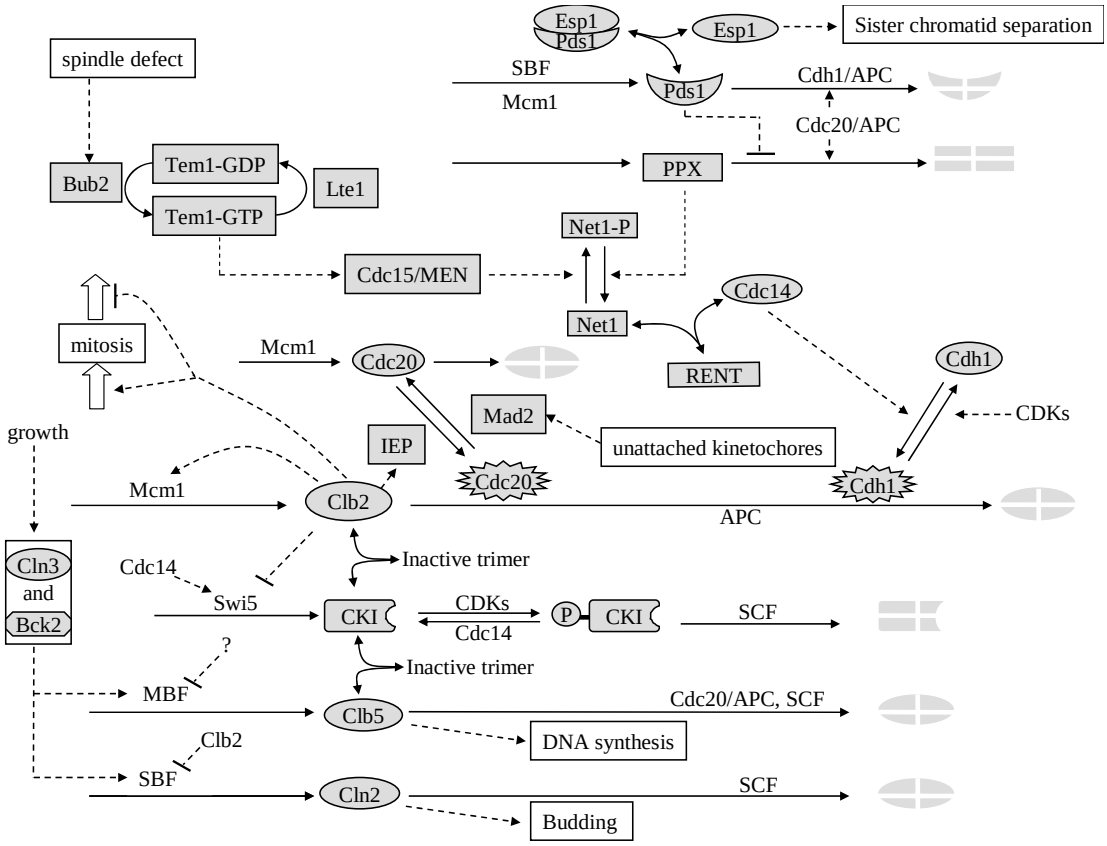

Figure 3.1. A consensus model of the cell cycle control mechanism in budding yeast. The diagram should be read from bottom-left toward top-right. (In the diagram, the kinase partner of the cyclins, Cdc28, is not shown explicitly. There is an excess of Cdc28 and it combines rapidly with cyclins as soon as they are synthesized.) Newborn daughter cells must grow to a critical size to have enough Cln3 and Bck2 to activate the transcript-tion factors, MBF and SBF, which drive synthesis of two classes of cyclins, Cln2 and Clb5. Cln2 is primarily responsible for bud emergence and Clb5 for initiating DNA synthesis. Clb5-dependent kinase activity is not immediately evident because the G1-phase cell is full of cyclin-dependent kinase inhibitors (CKI; namely, Sic1 and Cdc6). After the CKIs are phosphorylated by Cln2/Cdc28, they are rapidly degraded, releasing Clb5/Cdc28 to do its job. A fourth class of cyclins, Clb2, is out of the picture in G1 because the transcription factor, Mcm1, is inactive, the degradation pathway, Cdh1/APC, is active, and the stoichiometric inhibitors, CKI, are abundant. Cln2- and Clb5-dependent kinases remove CKI and inactivate Cdh1, allowing Clb2 to appear, after some delay, as it activates its own transcription factor, Mcm1. Clb2/Cdc28 turns off SBF and MBF. As Clb2/Cdc28 drives the cell into mitosis, it also sets the stage for exit from mitosis by stimulating the synthesis of Cdc20 and by phosphorylating components of the APC. Meanwhile, Cdc20/APC is kept inactive by a checkpoint signal responsive to unattached chromosomes. When the replicated chromosomes are attached, active Cdc20/APC initiates mitotic exit. First, it degrades Pds1, releasing Esp1, a protease involved in sister chromatid separation. It also degrades Clb5 and partially Clb2, lowering their potency on Cdh1 inactivation. Cdc20/APC promotes degradation of a phosphatase (PPX) that has been keeping Net1 in its unphosphorylated form, which binds with Cdc14. As the attached chromosomes are properly aligned on the metaphase spindle, Tem1 is activated, which in turn activates Cdc15. When Net1 gets phosphorylated by Cdc15, it releases its hold on Cdc14. Cdc14 (a phosphatase) then does battle against the cyclin-dependent kinases: activating Cdh1, stabilizing CKIs, and activating Swi5 (the transcription factor for CKIs). In this manner, Cdc14 returns the cell to G1 phase (no cyclins, abundant CKIs, and active Cdh1).

Table 3.1. Budding Yeast Model Equations

$$\frac{\mathrm{d}}{\mathrm{d}t}[\mathrm{mass}] = k_{\mathrm{g}} \cdot [\mathrm{mass}]$$

$$\frac{\mathrm{d}[\mathrm{Cln2}]}{\mathrm{d}t} = (k'_{\mathrm{s,n2}} + k''_{\mathrm{s,n2}} \cdot [\mathrm{SBF}]) \cdot [\mathrm{mass}] - k_{\mathrm{d,n2}} \cdot [\mathrm{Cln2}]$$

$$\frac{\mathrm{d}[\mathrm{Clb5}]}{\mathrm{d}t} = (k'_{\mathrm{s,b5}} + k''_{\mathrm{s,b5}} \cdot [\mathrm{MBF}]) \cdot [\mathrm{mass}] + (k_{\mathrm{d3,c1}} \cdot [\mathrm{C5P}] + k_{\mathrm{di,b5}} \cdot [\mathrm{C5}]) + (k_{\mathrm{d3,f6}} \cdot [\mathrm{F5P}] + k_{\mathrm{di,f5}} \cdot [\mathrm{F5}]) - (V_{\mathrm{d,b5}} + k_{\mathrm{as,b5}} \cdot [\mathrm{Sic1}] + k_{\mathrm{as,f5}} \cdot [\mathrm{Cdc6}]) \cdot [\mathrm{Clb5}]$$

$$\frac{\mathrm{d}[\mathrm{Clb2}]}{\mathrm{d}t} = (k'_{\mathrm{s,b2}} + k''_{\mathrm{s,b2}} \cdot [\mathrm{Mcm1}]) \cdot [\mathrm{mass}] + (k_{\mathrm{d3,c1}} \cdot [\mathrm{C2P}] + k_{\mathrm{di,b2}} \cdot [\mathrm{C2}]) + (k_{\mathrm{d3,f6}} \cdot [\mathrm{F2P}] + k_{\mathrm{di,f2}} \cdot [\mathrm{F2}]) - (V_{\mathrm{d,b2}} + k_{\mathrm{as,b2}} \cdot [\mathrm{Sic1}] + k_{\mathrm{as,f2}} \cdot [\mathrm{Cdc6}]) \cdot [\mathrm{Clb2}]$$

$$\frac{\mathrm{d}[\mathrm{Sic1}]}{\mathrm{d}t} = (k'_{\mathrm{s,c1}} + k''_{\mathrm{s,c1}} \cdot [\mathrm{Swi5}]) + (V_{\mathrm{d,b2}} + k_{\mathrm{di,b2}}) \cdot [\mathrm{C2}] + (V_{\mathrm{d,b5}} + k_{\mathrm{di,b5}}) \cdot [\mathrm{C5}] + k_{\mathrm{pp,c1}} \cdot [\mathrm{Cdc14}] \cdot [\mathrm{Sic1P}] - (k_{\mathrm{as,b2}} \cdot [\mathrm{Clb2}] + k_{\mathrm{as,b5}} \cdot [\mathrm{Clb5}] + V_{\mathrm{kp,c1}}) \cdot [\mathrm{Sic1}]$$

$$\frac{\mathrm{d}[\mathrm{Sic1P}]}{\mathrm{d}t} = V_{\mathrm{kp,c1}} \cdot [\mathrm{Sic1}] - (k_{\mathrm{pp,c1}} \cdot [\mathrm{Cdc14}] + k_{\mathrm{d3,c1}}) \cdot [\mathrm{Sic1P}] + V_{\mathrm{d,b2}} \cdot [\mathrm{C2P}] + V_{\mathrm{d,b5}} \cdot [\mathrm{C5P}]$$

$$\frac{\mathrm{d}[\mathrm{C2}]}{\mathrm{d}t} = k_{\mathrm{as,b2}} \cdot [\mathrm{Clb2}] \cdot [\mathrm{Sic1}] + k_{\mathrm{pp,c1}} \cdot [\mathrm{Cdc14}] \cdot [\mathrm{C2P}] - (k_{\mathrm{di,b2}} + V_{\mathrm{d,b2}} + V_{\mathrm{kp,c1}}) \cdot [\mathrm{C2}]$$

$$\frac{\mathrm{d}[\mathrm{C5}]}{\mathrm{d}t} = k_{\mathrm{as,b5}} \cdot [\mathrm{Clb5}] \cdot [\mathrm{Sic1}] + k_{\mathrm{pp,c1}} \cdot [\mathrm{Cdc14}] \cdot [\mathrm{C5P}] - (k_{\mathrm{di,b5}} + V_{\mathrm{d,b5}} + V_{\mathrm{kp,c1}}) \cdot [\mathrm{C5}]$$

$$\frac{\mathrm{d}[\mathrm{C2P}]}{\mathrm{d}t} = V_{\mathrm{kp,c1}} \cdot [\mathrm{C2}] - (k_{\mathrm{pp,c1}} \cdot [\mathrm{Cdc14}] + k_{\mathrm{d3,c1}} + V_{\mathrm{d,b2}}) \cdot [\mathrm{C2P}]$$

$$\frac{\mathrm{d}[\mathrm{C5P}]}{\mathrm{d}t} = V_{\mathrm{kp,c1}} \cdot [\mathrm{C5}] - (k_{\mathrm{pp,c1}} \cdot [\mathrm{Cdc14}] + k_{\mathrm{d3,c1}} + V_{\mathrm{d,b5}}) \cdot [\mathrm{C5P}]$$

$$\frac{\mathrm{d}[\mathrm{Cdc6}]}{\mathrm{d}t} = (k'_{\mathrm{s,f6}} + k''_{\mathrm{s,f6}} \cdot [\mathrm{Swi5}] + k'''_{\mathrm{s,f6}} \cdot [\mathrm{SBF}]) + (V_{\mathrm{d,b2}} + k_{\mathrm{di,f2}}) \cdot [\mathrm{F2}] + (V_{\mathrm{d,b5}} + k_{\mathrm{di,f5}}) \cdot [\mathrm{F5}] + k_{\mathrm{pp,f6}} \cdot [\mathrm{Cdc14}] \cdot [\mathrm{Cdc6P}] - (k_{\mathrm{as,f2}} \cdot [\mathrm{Clb2}] + k_{\mathrm{as,f5}} \cdot [\mathrm{Clb5}] + V_{\mathrm{kp,f6}}) \cdot [\mathrm{Cdc6}]$$

$$\frac{\mathrm{d}[\mathrm{Cdc6P}]}{\mathrm{d}t} = V_{\mathrm{kp,f6}} \cdot [\mathrm{Cdc6}] - (k_{\mathrm{pp,f6}} \cdot [\mathrm{Cdc14}] + k_{\mathrm{d3,f6}}) \cdot [\mathrm{Cdc6P}] + V_{\mathrm{d,b2}} \cdot [\mathrm{F2P}] + V_{\mathrm{d,b5}} \cdot [\mathrm{F5P}]$$

$$\frac{\mathrm{d}[\mathrm{F2}]}{\mathrm{d}t} = k_{\mathrm{as,f2}} \cdot [\mathrm{Clb2}] \cdot [\mathrm{Cdc6}] + k_{\mathrm{pp,f6}} \cdot [\mathrm{Cdc14}] \cdot [\mathrm{F2P}] - (k_{\mathrm{di,f2}} + V_{\mathrm{d,b2}} + V_{\mathrm{kp,f6}}) \cdot [\mathrm{F2}]$$

$$\frac{\mathrm{d}[\mathrm{F5}]}{\mathrm{d}t} = k_{\mathrm{as,f5}} \cdot [\mathrm{Clb5}] \cdot [\mathrm{Cdc6}] + k_{\mathrm{pp,f6}} \cdot [\mathrm{Cdc14}] \cdot [\mathrm{F5P}] - (k_{\mathrm{di,f5}} + V_{\mathrm{d,b5}} + V_{\mathrm{kp,f6}}) \cdot [\mathrm{F5}]$$

$$\frac{\mathrm{d}[\mathrm{F2P}]}{\mathrm{d}t} = V_{\mathrm{kp,f6}} \cdot [\mathrm{F2}] - (k_{\mathrm{pp,f6}} \cdot [\mathrm{Cdc14}] + k_{\mathrm{d3,f6}} + V_{\mathrm{d,b2}}) \cdot [\mathrm{F2P}]$$

$$\frac{\mathrm{d}[\mathrm{F5P}]}{\mathrm{d}t} = V_{\mathrm{kp,f6}} \cdot [\mathrm{F5}] - (k_{\mathrm{pp,f6}} \cdot [\mathrm{Cdc14}] + k_{\mathrm{d3,f6}} + V_{\mathrm{d,b5}}) \cdot [\mathrm{F5P}]$$

$$\frac{\mathrm{d}[\mathrm{Swi5}]_{\mathrm{T}}}{\mathrm{d}t} = k'_{\mathrm{s,swi}} + k''_{\mathrm{s,swi}} \cdot [\mathrm{Mcm1}] - k_{\mathrm{d,swi}} \cdot [\mathrm{Swi5}]_{\mathrm{T}}$$

$$\frac{\mathrm{d}[\mathrm{Swi5}]}{\mathrm{d}t} = k'_{\mathrm{s,swi}} + k''_{\mathrm{s,swi}} \cdot [\mathrm{Mcm1}] + k_{\mathrm{a,swi}} \cdot [\mathrm{Cdc14}] \cdot ([\mathrm{Swi5}]_{\mathrm{T}} - [\mathrm{Swi5}]) - (k_{\mathrm{d,swi}} + k_{\mathrm{i,swi}} \cdot [\mathrm{Clb2}]) \cdot [\mathrm{Swi5}]$$

$$\frac{\mathrm{d}[\mathrm{APC\text{-}P}]}{\mathrm{d}t} = \frac{k_{\mathrm{a,apc}} \cdot [\mathrm{Clb2}] \cdot (1 - [\mathrm{APC\text{-}P}])}{J_{\mathrm{a,apc}} + 1 - [\mathrm{APC\text{-}P}]} - \frac{k_{\mathrm{i,apc}} \cdot [\mathrm{APC\text{-}P}]}{J_{\mathrm{i,apc}} + [\mathrm{APC\text{-}P}]}$$

$$\frac{\mathrm{d}[\mathrm{Cdc20}]_\mathrm{T}}{\mathrm{d}t} = k_{\mathrm{s},20}^{'} + k_{\mathrm{s},20}^{''} \cdot [\mathrm{Mcm1}] - k_{\mathrm{d},20} \cdot [\mathrm{Cdc20}]_\mathrm{T}$$

$$\frac{\mathrm{d}[\mathrm{Cdc20}]_\mathrm{A}}{\mathrm{d}t} = (k_{\mathrm{a},20}^{'} + k_{\mathrm{a},20}^{''} \cdot [\text{APC-P}]) \cdot ([\mathrm{Cdc20}]_\mathrm{T} - [\mathrm{Cdc20}]_\mathrm{A}) - (k_{\mathrm{mad2}} + k_{\mathrm{d},20}) \cdot [\mathrm{Cdc20}]_\mathrm{A}$$

$$\frac{\mathrm{d}[\mathrm{Cdh1}]_\mathrm{T}}{\mathrm{d}t} = k_{\mathrm{s,cdh}} - k_{\mathrm{d,cdh}} \cdot [\mathrm{Cdh1}]_\mathrm{T}$$

$$\frac{\mathrm{d}[\mathrm{Cdh1}]}{\mathrm{d}t} = k_{\mathrm{s,cdh}} - k_{\mathrm{d,cdh}} \cdot [\mathrm{Cdh1}] + \frac{V_{\mathrm{a,cdh}} \cdot ([\mathrm{Cdh1}]_\mathrm{T} - [\mathrm{Cdh1}])}{J_{\mathrm{a,cdh}} + [\mathrm{Cdh1}]_\mathrm{T} - [\mathrm{Cdh1}]} - \frac{V_{\mathrm{i,cdh}} \cdot [\mathrm{Cdh1}]}{J_{\mathrm{i,cdh}} + [\mathrm{Cdh1}]}$$

$$\frac{\mathrm{d}[\mathrm{Tem1}]}{\mathrm{d}t} = \frac{k_{\mathrm{lte1}} \cdot ([\mathrm{Tem1}]_\mathrm{T} - [\mathrm{Tem1}])}{J_{\mathrm{a,tem}} + [\mathrm{Tem1}]_\mathrm{T} - [\mathrm{Tem1}]} - \frac{k_{\mathrm{bub2}} \cdot [\mathrm{Tem1}]}{J_{\mathrm{i,tem}} + [\mathrm{Tem1}]}$$

$$\frac{\mathrm{d}[\mathrm{Cdc15}]}{\mathrm{d}t} = (k_{\mathrm{a},15}^{'} \cdot ([\mathrm{Tem1}]_\mathrm{T} - [\mathrm{Tem1}]) + k_{\mathrm{a},15}^{''} \cdot [\mathrm{Tem1}] + k_{\mathrm{a},15}^{'''} \cdot [\mathrm{Cdc14}]) \cdot ([\mathrm{Cdc15}]_\mathrm{T} - [\mathrm{Cdc15}])$$
$$- k_{\mathrm{i},15} \cdot [\mathrm{Cdc15}]$$

$$\frac{\mathrm{d}[\mathrm{Cdc14}]_\mathrm{T}}{\mathrm{d}t} = k_{\mathrm{s},14} - k_{\mathrm{d},14} \cdot [\mathrm{Cdc14}]_\mathrm{T}$$

$$\frac{\mathrm{d}[\mathrm{Cdc14}]}{\mathrm{d}t} = k_{\mathrm{s},14} - k_{\mathrm{d},14} \cdot [\mathrm{Cdc14}] + k_{\mathrm{d,net}} \cdot ([\mathrm{RENT}] + [\mathrm{RENTP}])$$
$$+ k_{\mathrm{di,rent}} \cdot [\mathrm{RENT}] + k_{\mathrm{di,rentp}} \cdot [\mathrm{RENTP}] - (k_{\mathrm{as,rent}} \cdot [\mathrm{Net1}] + k_{\mathrm{as,rentp}} \cdot [\mathrm{Net1P}]) \cdot [\mathrm{Cdc14}]$$

$$\frac{\mathrm{d}[\mathrm{Net1}]_\mathrm{T}}{\mathrm{d}t} = k_{\mathrm{s,net}} - k_{\mathrm{d,net}} \cdot [\mathrm{Net1}]_\mathrm{T}$$

$$\frac{\mathrm{d}[\mathrm{Net1}]}{\mathrm{d}t} = k_{\mathrm{s,net}} - k_{\mathrm{d,net}} \cdot [\mathrm{Net1}] + k_{\mathrm{d},14} \cdot [\mathrm{RENT}] + k_{\mathrm{di,rent}} \cdot [\mathrm{RENT}] - k_{\mathrm{as,rent}} \cdot [\mathrm{Cdc14}] \cdot [\mathrm{Net1}]$$
$$+ V_{\mathrm{pp,net}} \cdot [\mathrm{Net1P}] - V_{\mathrm{kp,net}} \cdot [\mathrm{Net1}]$$

$$\frac{\mathrm{d}[\mathrm{RENT}]}{\mathrm{d}t} = -(k_{\mathrm{d},14} + k_{\mathrm{d,net}}) \cdot [\mathrm{RENT}] - k_{\mathrm{di,rent}} \cdot [\mathrm{RENT}] + k_{\mathrm{as,rent}} \cdot [\mathrm{Cdc14}] \cdot [\mathrm{Net1}]$$
$$+ V_{\mathrm{pp,net}} \cdot [\mathrm{RENTP}] - V_{\mathrm{kp,net}} \cdot [\mathrm{RENT}]$$

$$\frac{\mathrm{d}[\mathrm{PPX}]}{\mathrm{d}t} = k_{\mathrm{s,ppx}} - V_{\mathrm{d,ppx}} \cdot [\mathrm{PPX}]$$

$$\frac{\mathrm{d}[\mathrm{Pds1}]}{\mathrm{d}t} = k_{\mathrm{s,pds}}^{'} + k_{\mathrm{s1,pds}}^{''} \cdot [\mathrm{SBF}] + k_{\mathrm{s2,pds}}^{''} \cdot [\mathrm{Mcm1}] + k_{\mathrm{di,esp}} \cdot [\mathrm{PE}]$$
$$- (V_{\mathrm{d,pds}} + k_{\mathrm{as,esp}} \cdot [\mathrm{Esp1}]) \cdot [\mathrm{Pds1}]$$

$$\frac{\mathrm{d}[\mathrm{Esp1}]}{\mathrm{d}t} = -k_{\mathrm{as,esp}} \cdot [\mathrm{Pds1}] \cdot [\mathrm{Esp1}] + (k_{\mathrm{di,esp}} + V_{\mathrm{d,pds}}) \cdot [\mathrm{PE}]$$

$$\frac{\mathrm{d}[\mathrm{ORI}]}{\mathrm{d}t} = k_{\mathrm{s,ori}} \cdot (\varepsilon_{\mathrm{ori,b5}} \cdot [\mathrm{Clb5}] + \varepsilon_{\mathrm{ori,b2}} \cdot [\mathrm{Clb2}]) - k_{\mathrm{d,ori}} \cdot [\mathrm{ORI}]$$

$$\frac{\mathrm{d}[\mathrm{BUD}]}{\mathrm{d}t} = k_{\mathrm{s,bud}} \cdot (\varepsilon_{\mathrm{bud,n2}} \cdot [\mathrm{Cln2}] + \varepsilon_{\mathrm{bud,n3}} \cdot [\mathrm{Cln3}] + \varepsilon_{\mathrm{bud,b5}} \cdot [\mathrm{Clb5}]) - k_{\mathrm{d,bud}} \cdot [\mathrm{BUD}]$$

$$\frac{\mathrm{d}[\mathrm{SPN}]}{\mathrm{d}t} = k_{\mathrm{s,spn}} \cdot \frac{[\mathrm{Clb2}]}{J_{\mathrm{spn}} + [\mathrm{Clb2}]} - k_{\mathrm{d,spn}} \cdot [\mathrm{SPN}]$$

$$G(V_a, V_i, J_a, J_i) = \frac{2 J_i V_a}{V_i - V_a + J_a V_i + J_i V_a + \sqrt{(V_i - V_a + J_a V_i + J_i V_a)^2 - 4 (V_i - V_a) J_i V_a}}$$

[SBF]=[MBF]= $G(V_{\mathrm{a,sbf}}, V_{\mathrm{i,sbf}}, J_{\mathrm{a,sbf}}, J_{\mathrm{i,sbf}})$

[Mcm1]= $G(k_{\mathrm{a,mcm}} \cdot [\mathrm{Clb2}], k_{\mathrm{i,mcm}}, J_{\mathrm{a,mcm}}, J_{\mathrm{i,mcm}})$

$$[\text{Cln3}] = C_0 \cdot D_{\text{n3}} \cdot [\text{mass}]/(J_{\text{n3}} + D_{\text{n3}} \cdot [\text{mass}])$$

$$[\text{Bck2}] = B_0 \cdot [\text{mass}]$$

$$[\text{Clb5}]_{\text{T}} = [\text{Clb5}] + [\text{C5}] + [\text{C5P}] + [\text{F5}] + [\text{F5P}]$$

$$[\text{Clb2}]_{\text{T}} = [\text{Clb2}] + [\text{C2}] + [\text{C2P}] + [\text{F2}] + [\text{F2P}]$$

$$[\text{Sic1}]_{\text{T}} = [\text{Sic1}] + [\text{Sic1P}] + [\text{C2}] + [\text{C2P}] + [\text{C5}] + [\text{C5P}]$$

$$[\text{Cdc6}]_{\text{T}} = [\text{Cdc6}] + [\text{Cdc6P}] + [\text{F2}] + [\text{F2P}] + [\text{F5}] + [\text{F5P}]$$

$$[\text{CKI}]_{\text{T}} = [\text{Sic1}]_{\text{T}} + [\text{Cdc6}]_{\text{T}}$$

$$[\text{RENTP}] = [\text{Cdc14}]_{\text{T}} - [\text{RENT}] - [\text{Cdc14}]$$

$$[\text{Net1P}] = [\text{Net1}]_{\text{T}} - [\text{Net1}] - [\text{Cdc14}]_{\text{T}} + [\text{Cdc14}]$$

$$[\text{PE}] = [\text{Esp1}]_{\text{T}} - [\text{Esp1}]$$

$$V_{\text{d,b5}} = k'_{\text{d,b5}} + k''_{\text{d,b5}} \cdot [\text{Cdc20}]_{\text{A}}$$

$$V_{\text{d,b2}} = k'_{\text{d,b2}} + k''_{\text{d,b2}} \cdot [\text{Cdh1}] + k_{\text{d,b2p}} \cdot [\text{Cdc20}]_{\text{A}}$$

$$V_{\text{a,sbf}} = k_{\text{a,sbf}} \cdot (\varepsilon_{\text{sbf,n2}} \cdot [\text{Cln2}] + \varepsilon_{\text{sbf,n3}} \cdot ([\text{Cln3}] + [\text{Bck2}]) + \varepsilon_{\text{sbf,b5}} \cdot [\text{Clb5}])$$

$$V_{\text{i,sbf}} = k'_{\text{i,sbf}} + k''_{\text{i,sbf}} \cdot [\text{Clb2}]$$

$$V_{\text{kp,c1}} = k_{\text{d1,c1}} + k_{\text{d2,c1}} \cdot (\varepsilon_{\text{c1,n3}} \cdot [\text{Cln3}] + \varepsilon_{\text{c1,k2}} \cdot [\text{Bck2}] + \varepsilon_{\text{c1,n2}} \cdot [\text{Cln2}] + \varepsilon_{\text{c1,b5}} \cdot [\text{Clb5}] + \varepsilon_{\text{c1,b2}} \cdot [\text{Clb2}]) / (J_{\text{d2,c1}} + [\text{Sic1}]_{\text{T}})$$

$$V_{\text{kp,f6}} = k_{\text{d1,f6}} + k_{\text{d2,f6}} \cdot (\varepsilon_{\text{f6,n3}} \cdot [\text{Cln3}] + \varepsilon_{\text{f6,k2}} \cdot [\text{Bck2}] + \varepsilon_{\text{f6,n2}} \cdot [\text{Cln2}] + \varepsilon_{\text{f6,b5}} \cdot [\text{Clb5}] + \varepsilon_{\text{f6,b2}} \cdot [\text{Clb2}]) / (J_{\text{d2,f6}} + [\text{Cdc6}]_{\text{T}})$$

$$V_{\text{a,cdh}} = k'_{\text{a,cdh}} + k''_{\text{a,cdh}} \cdot [\text{Cdc14}]$$

$$V_{\text{i,cdh}} = k'_{\text{i,cdh}} + k''_{\text{i,cdh}} \cdot (\varepsilon_{\text{cdh,n3}} \cdot [\text{Cln3}] + \varepsilon_{\text{cdh,n2}} \cdot [\text{Cln2}] + \varepsilon_{\text{cdh,b2}} \cdot [\text{Clb2}] + \varepsilon_{\text{cdh,b5}} \cdot [\text{Clb5}])$$

$$V_{\text{pp,net}} = k'_{\text{pp,net}} + k''_{\text{pp,net}} \cdot [\text{PPX}]$$

$$V_{\text{kp,net}} = (k'_{\text{kp,net}} + k''_{\text{kp,net}} \cdot [\text{Cdc15}]) \cdot [\text{mass}]$$

$$V_{\text{d,ppx}} = k'_{\text{d,ppx}} + k''_{\text{d,ppx}} \cdot (J_{\text{20,ppx}} + [\text{Cdc20}]_{\text{A}}) \cdot \frac{J_{\text{pds}}}{J_{\text{pds}} + [\text{Pds1}]}$$

$$V_{\text{d,pds}} = k'_{\text{d1,pds}} + k''_{\text{d2,pds}} \cdot [\text{Cdc20}]_{\text{A}} + k''_{\text{d3,pds}} \cdot [\text{Cdh1}]$$

Reset Rules: When [Clb2] drops below K_{ez}, we reset [BUD] and [SPN] to zero, and divide the mass between daughter cell and mother cell as follows:
$\text{mass} \to f \cdot \text{mass}$ for daughter, and $\text{mass} \to (1-f) \cdot \text{mass}$ for mother, with $f = e^{-k_{\text{g}} \cdot D}$, where $D = (1.026/k_{\text{g}}) - 32$ is the observed daughter cell cycle time as a function of growth rate (Lord and Wheals, 1980). When [Clb2]+[Clb5] drops below K_{ez2}, [ORI] is reset to 0.

Flags: Bud emergence when $[\text{BUD}] = 1$, start DNA synthesis when $[\text{ORI}] = 1$, chromosome alignment on spindle completed when $[\text{SPN}] = 1$.

Table 3.2. Basal parameter values and initial conditions for the wild-type cell cycle. All parameters that start with a lower case '*k*' are rate constants (min^{-1}). All other parameters are dimensionless.

$k_g = 0.007702$	$k'_{s,n2} = 0$	$k''_{s,n2} = 0.15$	$k_{d,n2} = 0.12$	$k'_{s,b5} = 0.0008$	$k''_{s,b5} = 0.005$
$k'_{d,b5} = 0.01$	$k''_{d,b5} = 0.16$	$k'_{s,b2} = 0.001$	$k''_{s,b2} = 0.04$	$k'_{d,b2} = 0.003$	$k''_{d,b2} = 0.4$
$k_{d,b2p} = 0.15$	$k'_{s,c1} = 0.012$	$k''_{s,c1} = 0.12$	$k_{d1,c1} = 0.01$	$k_{d2,c1} = 1$	$k_{d3,c1} = 1$
$k_{pp,c1} = 4$	$k'_{s,f6} = 0.024$	$k''_{s,f6} = 0.12$	$k'''_{s,f6} = 0.004$	$k_{d1,f6} = 0.01$	$k_{d2,f6} = 1$
$k_{d3,f6} = 1$	$k_{pp,f6} = 4$	$k_{as,b5} = 50$	$k_{di,b5} = 0.06$	$k_{as,f5} = 0.01$	$k_{di,f5} = 0.01$
$k_{as,b2} = 50$	$k_{di,b2} = 0.05$	$k_{as,f2} = 15$	$k_{di,f2} = 0.5$	$k'_{s,swi} = 0.005$	$k''_{s,swi} = 0.08$
$k_{d,swi} = 0.08$	$k_{a,swi} = 2$	$k_{i,swi} = 0.05$	$k_{a,apc} = 0.1$	$k_{i,apc} = 0.15$	$k'_{s,20} = 0.006$
$k''_{s,20} = 0.6$	$k_{d,20} = 0.3$	$k'_{a,20} = 0.05$	$k''_{a,20} = 0.2$	$k_{s,cdh} = 0.01$	$k_{d,cdh} = 0.01$
$k'_{a,cdh} = 0.01$	$k''_{a,cdh} = 0.8$	$k'_{i,cdh} = 0.001$	$k''_{i,cdh} = 0.08$	$k_{s,14} = 0.2$	$k_{d,14} = 0.1$
$k_{s,net} = 0.084$	$k_{d,net} = 0.03$	$k'_{a,15} = 0.002$	$k''_{a,15} = 1$	$k'''_{a,15} = 0.001$	$k_{i,15} = 0.5$
$k'_{pp,net} = 0.05$	$k''_{pp,net} = 3$	$k'_{kp,net} = 0.01$	$k''_{kp,net} = 0.6$	$k_{as,rent} = 200$	$k_{as,rentp} = 1$
$k_{di,rent} = 1$	$k_{di,rentp} = 2$	$k_{s,ppx} = 0.1$	$k'_{d,ppx} = 0.17$	$k''_{d,ppx} = 2$	$k'_{s,pds} = 0$
$k''_{s1,pds} = 0.03$	$k''_{s2,pds} = 0.055$	$k'_{d1,pds} = 0.01$	$k''_{d2,pds} = 0.2$	$k''_{d3,pds} = 0.04$	$k_{as,esp} = 50$
$k_{di,esp} = 0.5$	$k_{s,ori} = 2$	$k_{d,ori} = 0.06$	$k_{s,bud} = 0.2$	$k_{d,bud} = 0.06$	$k_{s,spn} = 0.1$
$k_{d,spn} = 0.06$	$k_{a,sbf} = 0.38$	$k'_{i,sbf} = 0.6$	$k''_{i,sbf} = 8$	$k_{a,mcm} = 1$	$k_{i,mcm} = 0.15$

$k_{mad2} = 8$ (for [ORI] > 1 and [SPN] < 1) or 0.01 (otherwise)

$k_{bub2} = 1$ (for [ORI] > 1 and [SPN] < 1) or 0.2 (otherwise)

$k_{lte1} = 1$ (for [SPN] > 1 and [Clb2] > K_{ez}) or 0.1 (otherwise)

$\varepsilon_{sbf,n2} = 2$	$\varepsilon_{sbf,n3} = 10$	$\varepsilon_{sbf,b5} = 2$	$\varepsilon_{c1,n3} = 0.3$	$\varepsilon_{c1,n2} = 0.06$	$\varepsilon_{c1,k2} = 0.03$
$\varepsilon_{c1,b5} = 0.1$	$\varepsilon_{c1,b2} = 0.45$	$\varepsilon_{f6,n3} = 0.3$	$\varepsilon_{f6,n2} = 0.06$	$\varepsilon_{f6,k2} = 0.03$	$\varepsilon_{f6,b5} = 0.1$
$\varepsilon_{f6,b2} = 0.55$	$\varepsilon_{cdh,n3} = 0.25$	$\varepsilon_{cdh,n2} = 0.4$	$\varepsilon_{cdh,b5} = 8$	$\varepsilon_{cdh,b2} = 1.2$	$\varepsilon_{ori,b5} = 0.9$
$\varepsilon_{ori,b2} = 0.45$	$\varepsilon_{bud,n3} = 0.05$	$\varepsilon_{bud,n2} = 0.25$	$\varepsilon_{bud,b5} = 1$	$C_0 = 0.4$	$D_{n3} = 1$
$B_0 = 0.054$	$[\text{Tem1}]_T = 1$	$[\text{Cdc15}]_T = 1$	$[\text{Esp1}]_T = 1$		

$J_{d2,c1} = 0.05$	$J_{d2,f6} = 0.05$	$J_{a,apc} = 0.1$	$J_{i,apc} = 0.1$	$J_{a,cdh} = 0.03$	$J_{i,cdh} = 0.03$
$J_{a,tem} = 0.1$	$J_{i,tem} = 0.1$	$J_{a,sbf} = 0.01$	$J_{i,sbf} = 0.01$	$J_{a,mcm} = 0.1$	$J_{i,mcm} = 0.1$
$J_{spn} = 0.14$	$J_{n3} = 6$	$J_{20,ppx} = 0.15$	$J_{pds} = 0.04$	$K_{ez} = 0.3$	$K_{ez2} = 0.2$

Table 3.2. cont'd.

Initial conditions for a newborn, wild-type daughter cell:

[mass]	1.2060	[F5]	7.2e-5	[Cdc14]	0.4683
[Cln2]	0.0652	[F2P]	0.0274	$[Net1]_T$	2.8
[Clb5]	0.0518	[F5P]	7.9e-6	[Net]1	0.0186
[Clb2]	0.1469	$[Swi5_T]$	0.9765	[RENT]	1.0495
[Sic1]	0.0229	[Swi5]	0.9562	[PPX]	0.1232
[Sic1P]	0.0064	[APC-P]	0.1015	[Pds1]	0.0256
[C2]	0.2384	$[Cdc20]_T$	1.9163	[Esp1]	0.3013
[C5]	0.0701	$[Cdc20]_A$	0.4443	[ORI]	0.0009
[C2P]	0.0240	$[Cdh1]_T$	1	[BUD]	0.0085
[C5P]	0.0069	[Cdh1]	0.9305	[SPN]	0.0305
[Cdc6]	0.1076	[Tem1]	0.9039	k_{mad2}	0.01
[Cdc6P]	0.0155	[Cdc15]	0.6565	k_{bub2}	0.2
[F2]	0.2361	$[Cdc14]_T$	2	k_{lte1}	0.1

Table 3.3. Mutants used to derive the model and specify the parameter values **(NEXT PAGE)**

Wild-type
In glucose
In galactose

Cln mutants
cln1Δ cln2Δ
GAL-CLN2 cln1Δ cln2Δ
cln1Δ cln2Δ sic1Δ
cln1Δ cln2Δ cdh1Δ
GAL-CLN2 cln1Δ cln2Δ cdh1Δ
cln3Δ
GAL-CLN3

Bck2 mutants
bck2Δ
Multi-copy *BCK2*
cln1Δ cln2Δ bck2Δ
cln3Δ bck2Δ
cln3Δ bck2Δ GAL-CLN2 cln1Δ cln2Δ
cln3Δ bck2Δ multi-copy *CLN2*
cln3Δ bck2Δ sic1Δ

cln1 cln2 cln3 strain
cln1Δ cln2Δ cln3Δ
cln1Δ cln2Δ cln3Δ GAL-CLN2
cln1Δ cln2Δ cln3Δ GAL-CLN3
cln1Δ cln2Δ cln3Δ sic1Δ
cln1Δ cln2Δ cln3Δ cdh1Δ
cln1Δ cln2Δ cln3Δ multi-copy *CLB5*
cln1Δ cln2Δ cln3Δ GAL-CLB5
cln1Δ cln2Δ cln3Δ multi-copy *BCK2*
cln1Δ cln2Δ cln3Δ GAL-CLB2
cln1Δ cln2Δ cln3Δ apc^{ts}

Cdh1, Sic1 and Cdc6 mutants
sic1Δ
GAL-SIC1
GAL-SIC1-dbΔ
GAL-SIC1 cln1Δ cln2Δ
GAL-SIC1 GAL-CLN2 cln1Δ cln2Δ
GAL-SIC1 cln1Δ cln2Δ cdh1Δ
GAL-SIC1 GAL-CLN2 cln1Δ cln2Δ cdh1Δ
cdh1Δ *(*)*
Cdh1 constitutively active
sic1Δ cdh1Δ *(*)*
sic1Δ cdh1Δ GALL-CDC20
cdc6Δ2-49
cdc6Δ2-49 sic1Δ
cdc6Δ2-49 cdh1Δ *(*)*
cdc6Δ2-49 sic1Δ cdh1Δ *(*)*
cdc6Δ2-49 sic1Δ cdh1Δ GALL-CDC20
swi5Δ
swi5Δ GAL-CLB2
swi5Δ cdh1Δ *(*)*
swi5Δ cdh1Δ GAL-SIC1

Clb1 Clb2 mutants
clb1Δ clb2Δ
clb2Δ CLB1 (*)
GAL-CLB2
Multi-copy *GAL-CLB2*
clb2Δ CLB1 cdh1Δ (*)
clb Δ CLB1 pds1Δ (*)
GAL-CLB2 sic1Δ (*)
GAL-CLB2 cdh1Δ
CLB2-dbΔ
CLB2-dbΔ in gal.
CLB2-dbΔ multi-copy *SIC1*
CLB2-dbΔ GAL-SIC1
CLB2-dbΔ multi-copy *CDC6*
CLB2-dbΔ clb5Δ
CLB2-dbΔ clb5Δ in gal.
GAL-CLB2-dbΔ

Clb5 Clb6 mutants
clb5Δ clb6Δ
clb5Δ clb6Δ cln1Δ cln2Δ
GAL-CLB5
GAL-CLB5 sic1Δ
GAL-CLB5 cdh1Δ
CLB5-dbΔ
CLB5-dbΔ sic1Δ
CLB5-dbΔ pds1Δ
CLB5-dbΔ pds1Δ cdc20Δ
GAL-CLB5-dbΔ

Cdc20 mutants
cdc20^{ts}
cdc20Δ clb5Δ
cdc20Δ pds1Δ
cdc20Δ pds1Δ clb5Δ
GAL-CDC20
cdc20^{ts} mad2Δ
cdc20^{ts} bub2Δ

Pds1/Esp1 interaction
pds1Δ (*)
esp1^{ts}
PDS1-dbΔ
GAL-PDS1-dbΔ
GAL-PDS1-dbΔ esp1^{ts}
GAL-ESP1 cdc20^{ts}

MEN pathway mutants
tem1Δ
GAL-TEM1
tem1^{ts} multi-copy *CDC15*
tem1^{ts} GAL-CDC15
tem1Δ net1^{ts}
tem1Δ multi-copy *CDC14*
cdc15Δ
Multi-copy CDC15
cdc15^{ts} multi-copy *TEM1*
cdc15Δ net1^{ts}
cdc15^{ts} multi-copy *CDC14*

Exit-of-mitosis mutants
net1^{ts}
GAL-NET1
cdc14^{ts}
GAL-CDC14
GAL-CDC14 GAL-NET1
net1^{ts} cdc20^{ts}
cdc14^{ts} GAL-SIC1
cdc14^{ts} then *GAL-SIC1*
cdc14^{ts} sic1Δ at perm. temp.
cdc14^{ts} cdh1Δ at perm. temp.
cdc14^{ts} GAL-CLN2 at perm. temp.
TAB6-1
TAB6-1 cdc15^{ts}
TAB6-1 clb5Δ
TAB6-1 clb2Δ CLB1

Checkpoint mutants
mad2Δ
bub2Δ
mad2Δ bub2Δ
WT I in noc.
mad2Δ in noc.
mad2Δ GAL-TEM1 in noc.
mad2Δ pds1Δ in noc.
bub2Δ in noc. (*)
bub2Δ pds1Δ in noc.
bub2Δ mad2Δ in noc.
pds1Δ in noc.
net1^{ts} in noc.

APC mutants
APC-A
APC-A cdh1Δ
APC-A cdh1Δ in gal.
APC-A cdh1Δ multi-copy *SIC1*
APC-A cdh1Δ GAL-SIC1
APC-A cdh1Δ multi-copy *CDC6*
APC-A cdh1Δ GAL-CDC6
APC-A cdh1Δ multi-copy *CDC20*
APC-A sic1Δ
APC-A GAL-CLB2

l. in gal. = in galactose
2. in noc. = in nocodazole
3. perm. temp = permissive temperature

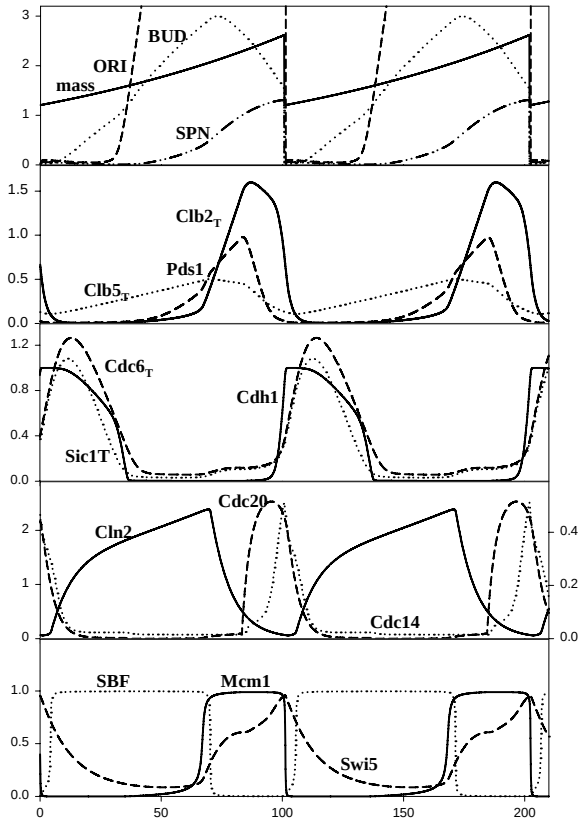

Figure 3.2. The wild-type cell cycle. Numerical solution of the differential equations in Table 1, for the parameter values in Table 2. The mass doubling time (MDT) for an asynchronous culture is 90 min. We show the cycle of a daughter cell (cycle time = 101 min, duration of G1 = 36 min). The cycle time for a mother cell (not shown) is 80 min. Division is slightly asymmetric (daughter size at birth = 0.46 × mother size at division). During G1 phase, Cdh1 is active and there are abundant CKIs. The G1→S transition is driven by accumulation of Cln2. The M→G1 transition is driven by activation of Cdc20. In panel 4, the left ordinate refers to [Cln2] and the right ordinate to [Cdc20] and [Cdc14].

Another commonly observed property of cells is their size at division. An important variable in the model is [mass]. The differential equation for [mass] implies that cells grow exponentially, with mass doubling time (MDT) = $0.693/k_g$, k_g = specific growth rate. (MDT = 90 min on glucose medium, = 160 min on galactose medium.) When a cell exits mitosis, [mass] is divided asymmetrically between mother and daughter cells, according to a rule described in [Chen, 2000]. Notice that [mass] enters the dynamical system as a multiplier of the rates of synthesis of the cyclins; based on the assumption that cyclins are synthesized at a rate proportional to the total number of ribosomes in a cell and then accumulate in a constant-volume compartment of the cell (the nucleus). Hence, [Cln3], [Cln2], [Clb5] and [Clb2] represent the concentrations of the cyclins in the nucleus.

The equations in Table 1, given the parameter values in Table 2 (which are appropriate for a wild-type cell), are solved numerically for the explicit time-dependence of each variable ([Cln2](t), [Clb2](t), …), see Fig. 2, using a computer program, WinPP, freely available from G.

Bard Ermentrout at Department of Mathematics, University of Pittsburgh. To compute a solution numerically, we must also assign initial conditions (at t=0) to all the variables ([Cln2](0), [Clb2](0), …). Initial conditions should reasonably represent an experimental protocol, but their precise values are not important.

To simulate each mutant, exactly the same equations (Table 1) and parameter values (Table 2) are used, except for those parameter changes that are dictated by the nature of the mutation. In the simplest case (gene *X* is deleted), the rate of synthesis of protein X is set to zero. For gene over-expression from multiple integrated copies under control of the natural promoter, the appropriate k_s' and k_s'' parameters are multiplied by an integer, depending on the number of additional copies. For temperature-sensitive (*ts*) mutants in Table 3 it is assumed that the relevant catalytic activity is normal at the permissive temperature and zero at the restrictive temperature.

The model accurately describes the growth and division of wild-type cells

We solve the equations in Table 1, given the parameter values and initial conditions in Table 2 for a wild-type budding yeast cell, and plot (Fig. 2) how cell size, cyclin concentrations and other components vary during repetitive cycling of daughter cells. The computed properties of the model agree reasonably well with observations of wild-type cells growing at MDT=90 min: daughter cell cycle time is 97.5 min (computed value = 101.2 min), G1 length 42 (36) min, S/G2/M length 57 (64) min; mother cell cycle time is 81 (80) min, G1 length 22 (28) min, and S/G2/M 59 (52) min. Furthermore, the relative amounts of certain groups of proteins are in rough quantitative agreement with recent measurements by Cross *et al.* (2002) and Archambault *et al.* (2003). The ratios, for an asynchronous culture with MDT = 90 min, are,

$$([\mathrm{Cln1}]+[\mathrm{Cln2}]):([\mathrm{Clb5}]+[\mathrm{Clb6}]):([\mathrm{Clb1}]+[\mathrm{Clb2}]):[\mathrm{Sic1}]:[\mathrm{Cdc6}]$$

$$= 15:3.8:7.5:1:3 \text{ (in experiments)}$$

$$= 15:3.3:4.7:2.8:3.7 \text{ (in model).}$$

The model conforms to the phenotypes of more than 100 mutant strains

The wiring diagram in Fig. 1 has been composed from evidences provided by the phenotypes of dozens of budding yeast mutants that have been constructed and characterized by deleting or over-expressing each genetic component singly and in multiple combinations. It remains an informal 'cartoon' of the molecular regulatory system until it is converted into a precise mathematical model and demonstrated to be consistent with most of the facts about budding yeast mitotic division. Table 3 lists the 131 mutants that have been used to test the model. For 120 of the mutants in Table 3, the model agrees well with observations; the eleven exceptions are marked with a star in the Table.

At the web site, http://mpf.biol.vt.edu/research/budding_yeast_model/pp/, one can find full details about the model and all simulations (Fig. 3). The web site provides the basic experimental results on which the wiring diagram (Fig. 1) is based and simulations of all mutants in Table 3, including the precise parameter values used in each case.

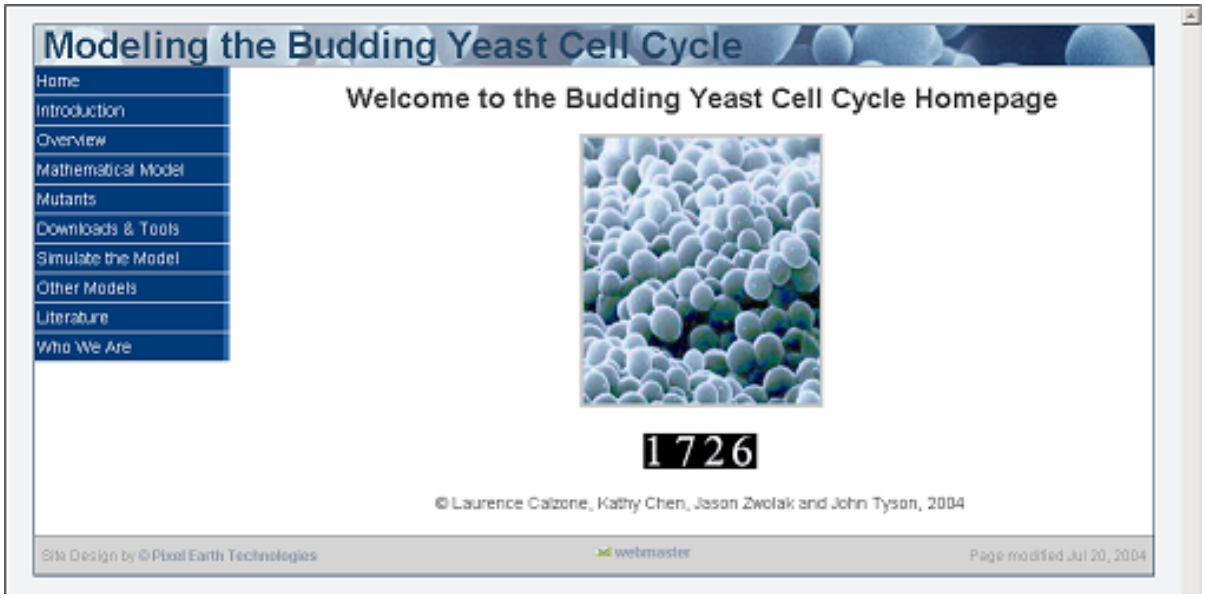

Figure 3.3. The budding yeast cell cycle web page. Between August 2004 and January 2007 (29 months) the web site received 29,000 hits from outside Virginia Tech.

The model has alternative stable steady states corresponding to G1 and S/G2/M phases

Although the rigor and precision of the model are essential attributes in its favor, the sheer magnitude of information that comes out of the computer can overwhelm the user. To make sense of this information, scientists need intuitive ways to understand the model's behavior—an intuition disciplined, of course, by precise numerical simulations of the equations. We rely on the scheme in Fig. 4 (described briefly in Chen *et al.*, 2000). Fundamental to cell cycle control in budding yeast are the antagonistic relations between B-type cyclins (Clb1-6, in association with Cdc28), which promote DNA synthesis and mitosis, and G1 stabilizers (Cdh1, Sic1 and the CKI-role of Cdc6), which oppose cell proliferation by degrading Clbs and stoichiometrically inhibiting Clb/Cdc28 complexes. Sic1 and Cdc6 are lumped together as the CKIs.

Because Clb-dependent kinases can inactivate Cdh1 and destabilize CKIs, these two classes of proteins are mutual antagonists (Fig. 4). The model is designed to have two coexisting, self-maintaining steady states: a G1 state, when Clbs are scarce and their antagonists (Cdh1 and CKIs) are abundant, and an S/G2/M state, when the reverse is true [NAS96, TYS01]. When yeast cells are proliferating, the control system is undergoing periodic transitions from the G1 state to the S/G2/M state and back again. These transitions (called START and FINISH) are irreversible and alternating. Once a cell has executed START, it does not normally slip back into G1 phase and do START again. Rather, it must execute a distinctly different transition (FINISH) to return to G1. Likewise, a cell that has executed FINISH does not slip back into mitosis and try to separate its chromosomes a second time. There are, of course, exceptions to these rules (endoreplication and meiosis), but they do not nullify the central role played by irreversible, alternating START and FINISH transitions in the cell cycle.

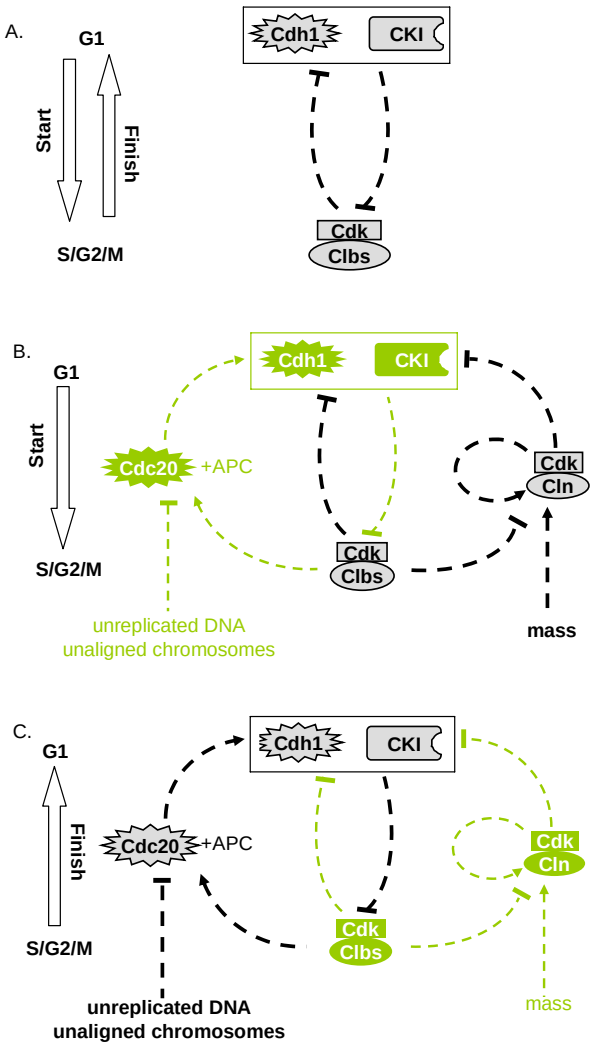

Figure 3.4. The logic of cell cycle transitions in budding yeast. (A) Antagonistic interactions between the G1 stabilizers (Cdh1 and CKI) and the Clb/Cdc28 kinases create two coexisting stable steady states, G1 and S/G2/M. Transitions between these states are called START (G1→S) and FINISH (M→G1). (B) START is facilitated by Cln/Cdc28 kinases. Cell growth ("mass") triggers accumulation of Clns. (C) FINISH is facilitated by Cdc20/APC. Mitotic checkpoint signals restrain the activation of Cdc20.

To a first approximation, the budding yeast cell cycle can be viewed as an alternation between these two stable steady states generated by the antagonism between Clb kinases and G1-stabilizers. From the simulation of the wild type cycle (Fig. 2), one can see how the control mechanism shifts from one state to the other, and how the transitions are carried out.

The START transition is facilitated by Cln1,2/Cdc28 complexes, which can phosphorylate and inactivate Cdh1 and CKIs, but they themselves are unopposed by the G1 stabilizers (for reviews, Schwob *et al.*, 1994; Peters, 1998). This transition occurs when the cell has grown large enough

to accumulate a critical concentration of Cln3-dependent kinase in the nucleus (Miller and Cross, 2000; Cross *et al.*, 2002). Cln3 kinase and a back-up (Bck2) activate SBF and MBF, the transcription factors for Cln1,2 and Clb5,6, so their levels increase. Clb5,6-dependent kinases are inactive due to inhibition by the CKIs, but Cln1,2-dependent kinases are not so inhibited. Cln-dependent kinases depress Cdh1 and CKIs enough to allow the Clb-dependent kinases to assert themselves, switching the control system into the stable S/G2/M state. Once the transition is made, Clb kinases by themselves are able to depress their antagonists without the help of Cln1,2 kinases. Rising activity of Clb1,2/Cdc28 turns off Cln1,2 synthesis, causing Cln-dependent kinase activity to drop. Hence, after doing their job, the START-facilitators disappear.

Cdc20/APC facilitates the FINISH transition. Cdc20 transcription is activated in G2/M phases by the transcription factor complex Mcm1/Fkh2/Ndd1, which is activated in turn by Clb1,2 kinase activity. In addition, APC core proteins (Cdc16, -23 and -27) are phosphorylated by Clb1,2 kinase, which facilitates APC binding with Cdc20 to form an active complex. Cdc20/APC-P depresses Clb kinase activity by labeling Clbs for degradation; it also initiates activation of a phosphatase, Cdc14, which reverses the inhibitory effects of Clb/Cdc28 on Cdh1 and CKIs, so the latter two can overpower the Clb kinases. As the G1 stabilizers extinguish Clb kinase activity, the transcription factor, Mcm1, turns off, and Cdc20 synthesis ceases. Because Cdc20 is an unstable protein, it quickly disappears, preparing the cell for the subsequent START transition.

The theoretical picture is confirmed by experimental tests

Specific aspects of this theoretical picture of the budding yeast cell cycle have been tested. First of all, mutants probe the basic wiring diagram of the model, and the success ratio of the model (120/131 = 92%) indicates that the fundamental antagonistic interactions and negative feedback loops are most likely correct. Secondly, the notion of 'bistability' (alternative stable steady states) has been examined in budding yeast by Cross *et al.* (2002). They constructed a strain (*cln1Δ cln2Δ cln3Δ GAL-CLN3 cdc14*^{ts}) that, when growing on glucose at 37^{o}C, lacks both START-facilitators and FINISH-facilitators. Under these conditions, cells can arrest stably in either a low Clb-kinase state or a high Clb-kinase state, depending on which state the cell is in when it is shifted to glucose at 37^{o}C. (In the 'high' state, Cdc20 is active but Cdc14 is not, so the cell arrests with moderate Clb2 level characteristic of telophase arrested cells.) Bistability has also been confirmed recently for interphase and M-phase states of frog egg extracts (Sha *et al.*, 2003) [POM03]. Thirdly, our crucial assumption that cell size is monitored by Cln3 accumulation in the nucleus has received careful attention. The average size of yeast cells is quite sensitive to changes in *CLN3* dosage (Cross *et al.*, 2002). Results of Miller and Cross [MIL01] using mis-localized Cln3 are in qualitative agreement with the idea that Cln3 nuclear accumulation is important for size regulation, although the quantitative relationship is somewhat unclear.

Parameter identification

With over 100 parameters to be estimated, is it any surprise that the model can be fitted to the phenotypes of lots of mutants? After all, with 4 parameters, one is supposed to be able to fit an elephant. That is true, if the model is elephant-shaped to begin with. But if the model is yeast-shaped, it won't fit any particular elephant and vice versa. Hence, it is essential to prove that the model in Fig. 1 is yeast-shaped by displaying a particular parameter set that brings the model into agreement with the observed properties of yeast cell growth and division. In our experience, many reasonable assumptions about the wiring diagram must be rejected because no amount of

parameter ‘twiddling’ can bring the model into agreement with the phenotypes of all (or nearly all) the mutants in Table 3. Parameter changes that ‘rescue’ a model with respect to one mutant usually have unintended and unanticipated negative effects on other mutants that were fitted just fine by the original parameter set. A mathematical model is the only way to keep track of the subtle interactions among genes and proteins in regulatory mechanisms of such complexity.

Success in simulating most of the mutants in Table 3 indicates that the mechanism in Fig. 1 is a reasonable facsimile of the Cdc28-cyclin control system in budding yeast. But a model of this sort (wiring diagram + equations + parameter values) is not a static, finished product. The model is bound to change as it is extended to new experimental observations.

Summary
The molecular machinery of eukaryotic cell cycle control is known in more detail for budding yeast than for any other organism. Molecular biologists have painstakingly dissected and characterized the genes and protein interactions that underlie the regulatory network. By formulating this network in differential equations and computing their solutions numerically, the Virginia Tech Team, under DARPA support, has shown that a consensus mechanism successfully reproduces the behaviour of wild type and mutant cells in quantitative detail. The model organizes information in a logical, comprehensive and predictive manner, and it is freely available for these purposes at the web site:
http://mpf.biol.vt.edu/research/budding_yeast_model/pp/
.

Mathematical model of the morphogenesis checkpoint in budding yeast

A. Ciliberto, B. Novak and J.J. Tyson
***J. Cell Biology* 163:1243-1254 (2003)**

The main transitions of the cell division process—the onset of DNA replication (Start), entry into mitosis (G2-M transition), and exit from mitosis—are controlled by surveillance mechanisms, also known as checkpoints [HAR89]. The G2-M checkpoint plays a major role in fission yeast (*Schizosaccharomyces pombe*), where it forestalls mitosis until the cell grows to a critical size and properly replicates its DNA. The molecular events which control this transition are the inhibitory phosphorylation of tyrosine-15 of Cdc2 (the fission yeast homolog of Cdc28), executed by the protein kinase Wee1, and the activating dephosphorylation of this site, catalyzed by the phosphatase Cdc25. If DNA is damaged or not properly replicated, the checkpoint is engaged, Cdc2 is phosphorylated on tyrosine-15 and cell cycle progression is halted. The inhibitory phosphorylation is relieved when DNA is fully replicated or the damage repaired.

Budding yeast contains homologs of Wee1 and Cdc25, known respectively as Swe1 kinase and Mih1 phosphatase. But in budding yeast Mih1 and Swe1 are not used to check cell size, nor are they involved in monitoring DNA replication, as evidenced by the fact that cells containing a mutant form of Cdc28 lacking the tyrosine phosphorylation site are still perfectly viable in the presence of inhibitors of DNA synthesis. Recently, Lew and co-workers have shown in an elegant series of papers that these tyrosine phosphorylation/ dephosphorylation reactions in budding yeast are involved in a different kind of checkpoint, called the morphogenesis

checkpoint (see [Lew00] for a review). This surveillance mechanism halts cell cycle progression when bud formation is impaired, which is a plausible event for yeast cells growing in natural conditions, since several external stimuli (such as heat shock and osmotic shock) are able to arrest or delay the formation of a bud (SIA98). By arresting or delaying cell cycle progression, the morphogenesis checkpoint prevents formation of dinucleated cells, which are less viable than mono-nucleated cells (SIA96). The arrest is not complete; after several hours, unbudded cells undergo mitosis (called "adaptation") and become dinucleate (SIA96).

In this paper, the Virginia Tech modeling team proposed a mathematical model for the morphogenesis checkpoint (Fig. 5), based largely on the molecular network suggested by Lew's work (Lew, 2000). The antagonistic relationship between Cdc28/Clb2 and Swe1 is at the core of our model of the morphogenesis checkpoint. When the checkpoint is induced, Swe1 phosphorylates and inhibits Cdc28/Clb2. On the other hand, Cdc28/Clb2 down regulates Swe1 in three ways. By phosphorylating Swe1, it reduces Swe1 activity and prepares Swe1 for degradation. In addition, Cdc28/Clb2 inhibits the transcription factor, SBF, and thereby shuts off synthesis of Swe1. If Cdc28/Clb2 successfully down regulates Swe1, then the cell proceeds into mitosis. If Swe1 successfully inhibits Cdc28/Clb2, then the cell arrests in G2 phase.

The checkpoint mechanism (Fig. 5) was grafted onto a simple model of the budding yeast cell-cycle engine (a simplified version of Fig. 1). The combined wiring diagrams are then converted into a set of differential equations (not shown), and the parameter values in the equations are estimated by comparing simulations to the observed properties of cells under checkpoint-free and checkpoint-induced conditions. The simulation of a checkpoint-free, wild-type cell cycle is illustrated in Fig. 6.

The effect of the morphogenesis checkpoint is commonly measured as a delay of nuclear division (ND) in *cdc24*^{ts} mutants (Fig. 7) relative to *CDC24* control cells (Fig. 6). In most experiments, yeast cells are synchronized by α-factor arrest and release, and then, while the cells are growing at the restrictive temperature, the time of the first ND is measured. The basic mutant, *cdc24*^{ts} at the restrictive temperature, is unable to develop a bud; nevertheless, it undergoes ND 135 - 165 min after release from α-factor (Sia et al., 1996). In other words, the morphogenesis "checkpoint" in this mutant is not very tight; after 2-3 hours the cell "adapts" to it (Sia et al., 1996). The checkpoint depends on Swe1, since *cdc24*^{ts} *swe1*Δ does not show any delay of ND compared to wild type (Sia et al., 1996). Mih1 is necessary for adaptation, since *cdc24*^{ts} *mih1*Δ is irreversibly blocked in G2 (Sia et al., 1996). On the other hand, *cdc24*^{ts} *hsl1*Δ does not show a phenotype more severe than *cdc24*^{ts}, suggesting that Hsl1 is already inactive in *cdc24*^{ts}. The model correctly accounts for the phenotypes of all these mutants (not shown here).

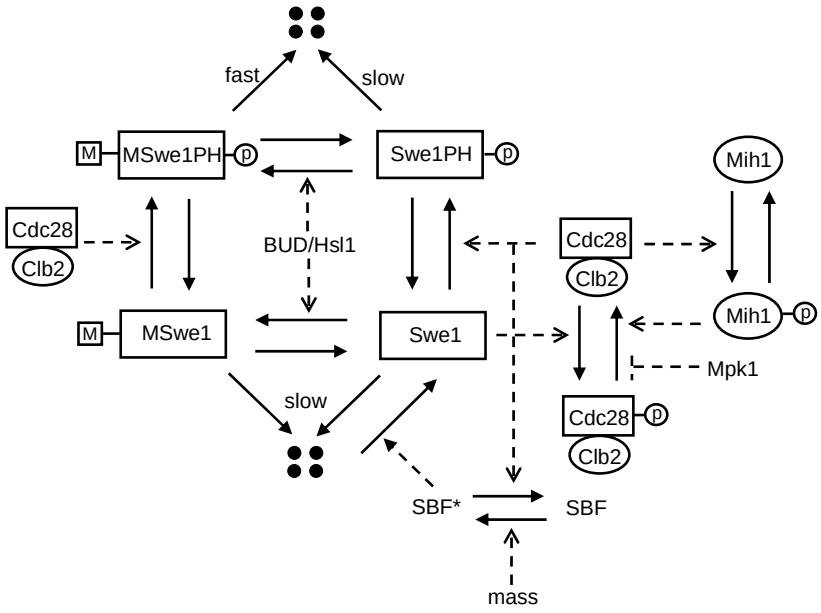

Figure 3.5. The Swe1 box. Swe1 can be present in four different forms during the cell cycle: unchanged (Swe1), phosphorylated by Cdc28/Clb2 (PSwe1), modified by Hsl1 (Swe1M), or both (PSwe1M). The doubly modified form we assume to be less stable than the others. The unphosphorylated, unmodified form of Swe1 is assumed to be most active in phosphorylating Cdc28/Clb2. Cdc28 is dephosphorylated by Mih1. We assume that Cdc28/Clb2 phosphorylates and activates Mih1, and MAP kinase (Mpk1) inactivates Mih1.

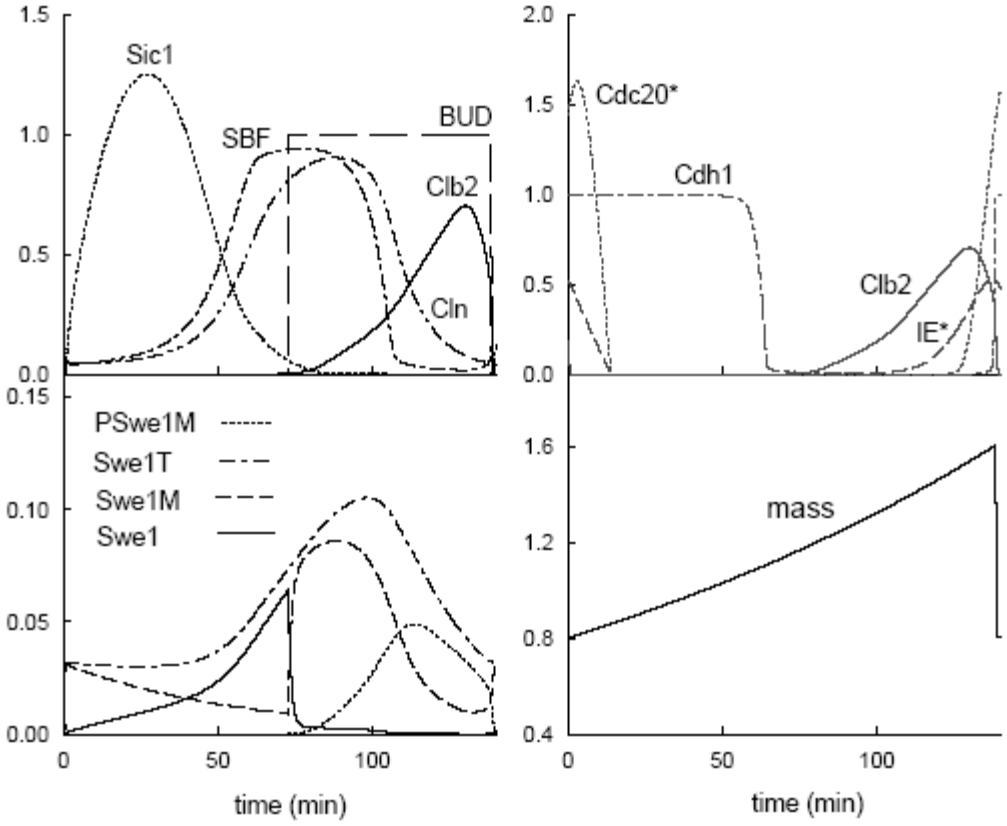

Figure 3.6. Time-courses of mass and concentrations during the wild type cell cycle.

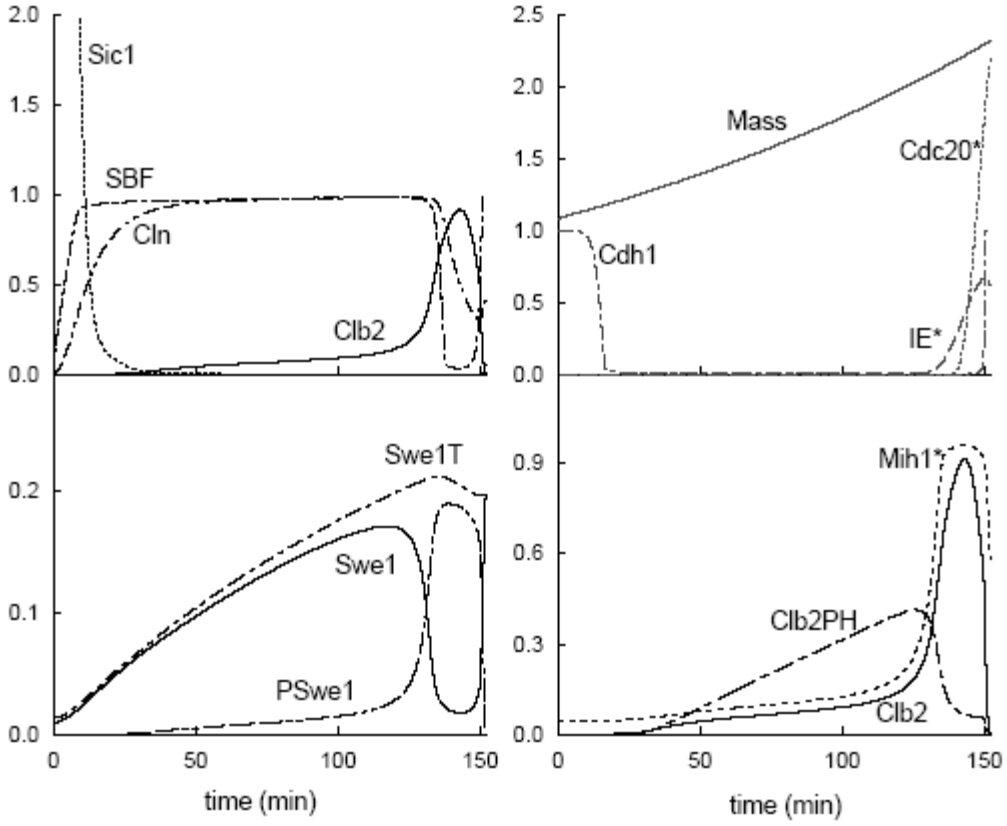

Figure 3.7. Simulation of the *cdc24*^{ts} cell cycle. These cells, at the restrictive temperature cannot make a bud, so the morphogenetic checkpoint is engaged. Division is delayed about 50 min, compared to checkpoint-free cells (Fig. 6).

Bifurcation diagrams

The morphogenesis checkpoint acts like a "governor" to the cell cycle engine, slowing progression through the cell cycle when a particular danger signal (failure to bud) is perceived. To understand the relationship between the engine and its governor, it is useful to introduce the notion of a bifurcation diagram (Fig. 8), in which we plot Cdc28/Clb2 activity—the state of the engine—as a function of cell size—the motive force for cell cycle progression (in yeast). Under normal conditions (Fig. 8A), the Cdc28-control system has two characteristic states: a stable steady state (at small size) and a stable oscillatory state (at large size). A small newborn cell is attracted to the stable steady state of low Cdc28/Clb2 activity; kept low by active Cdh1 and Sic1 (Fig. 1). The cell is trapped in G1 because it is too small to warrant a new round of DNA replication and division. When the cell grows to a critical size (1, in the figure), the stable steady state is lost, and the cell cycle engine begins an oscillation that drives Cdc28/Clb2 to larger activity. The cell replicates its DNA and enters mitosis. The mitotic state is intrinsically unstable, because high levels of Cdc28/Clb2 turn on Cdc20, which destroys Cdc28's cyclin partner. As Cdc28 activity drops, the cell divides and the control system is reset to the domain of the stable steady state. The duration of the budded phase (S-G2-M) is fixed at about 60 min, the time it takes to complete one oscillation. The duration of G1 phase is variable, depending on growth rate and asymmetry of division (how small is the daughter cell at birth).

When the morphogenesis checkpoint is invoked (no bud), active Swe1 creates a second stable steady state of the cell cycle engine at intermediate Cdc28/Clb2 activity (higher than the G1 steady state, lower than the peak of the oscillation; see Fig8). Cdh1 and Sic1 are gone, Cdc28/Cln activity is high, and Cdc28/Clb2 activity is depressed by Swe1-dependent tyrosine-phosphorylation. High activity of Cdc28/Cln drives the cell into DNA synthesis, but low activity of Cdc28/Clb2 is insufficient for mitosis. Hence, the intermediate steady state corresponds to a cell stuck in G2. A newborn daughter cell will grow to size=1 and enter S phase, as usual. But then it arrests in G2 phase until it grows large enough to bypass the G2 arrest and enter mitosis. The delay will be 2-3 hours, depending on growth rate and critical size at the end of the G2-arrested state. When the cell reaches this size, it "adapts" to the checkpoint, undergoes nuclear division, and becomes dinucleate (the cell cannot divide because it never made a bud). At this point the model makes a noteworthy prediction. Because the engine is still in the oscillatory domain, it will pause only briefly in G1, then re-replicate its DNA and enter mitosis, becoming tetraploid (Sia et al., 1996). In order to see the predicted shortening of G1 phase, this experiment is best done at slow growth rates, for which the duration of G1 phase is usually long.

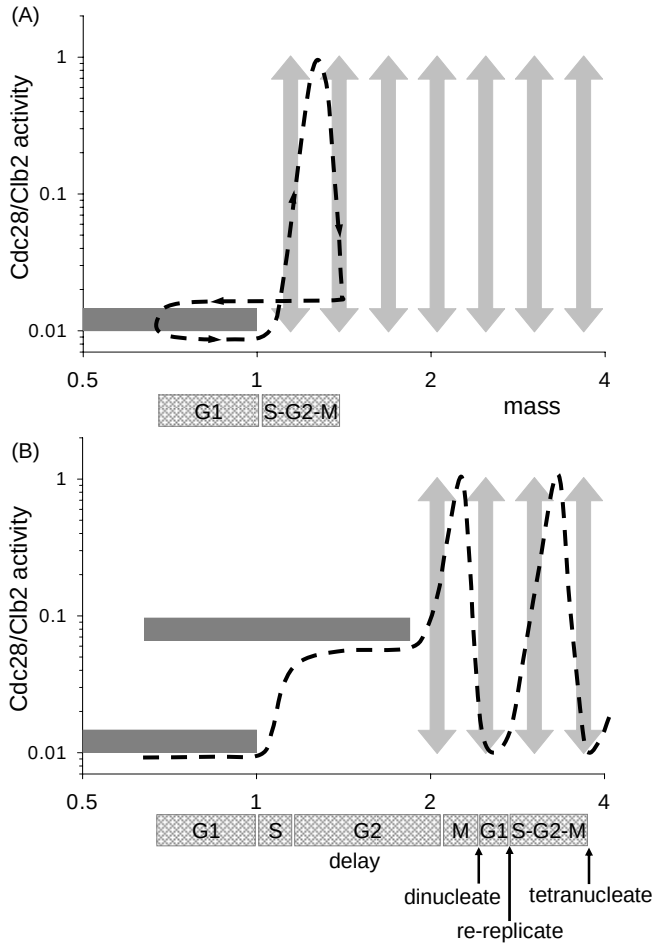

Figure 3.8. Bifurcation diagrams for the cell cycle engine. We plot Cdc28/Clb2 activity, representative of the state of the cell cycle control system, against cell mass, *M*, which is the driving force for progression through the cell cycle. Because we assume cells grow exponentially, equal distances along the log(mass) axis represent equal intervals of time. Horizontal bars are placed at the Cdc28/Clb2 level characteristic of steady states, and vertical arrows represent the range of fluctuations of Cdc28/Clb2 activity in an oscillatory state. Low activity of Cdc28/Clb2 represents G1phase, intermediate activity is S-G2, and high activity is M phase. These diagrams are schematic cartoons; for accurately computed bifurcation diagrams, see the original publication. (A) Checkpoint silent. The bold dashed line is a cell-cycle trajectory: as the cell grows, the Cdc28 control system is attracted to the stable, self-maintaining state at its current cell mass. A small cell persists in the G1-state until that state disappears at M=1. Thereafter, the cell executes an oscillation in Cdc28/Clb2 activity, passing through S, G2 and M phases. When Cdc28 activity falls, as the cell exits mitosis, the cell divides and the newborn progeny are attracted to the stable G1-state. (B) Checkpoint invoked. At the restrictive temperature, a *cdc24*^{ts} cell continues to grow but fails to make a bud. Consequently, Swe1 is stabilized, and a new self-maintaining steady state, with intermediate activity of Cdc28/Clb2, is created. The cell arrests in S-G2 phase for about one mass-doubling time, until it grows to M=2, where the G2-arrested state disappears. At this time, the cell "adapts" to the checkpoint signal, enters mitosis, and becomes dinucleate. Because the cell does not divide, it stays in the oscillatory regime and re-replicates its DNA after a very short G1 phase. The cell re-enters mitosis and becomes tetranucleate. The time between nuclear divisions is the period of the underlying oscillatory state, about 60 min in the model.

Stochastic Modeling of the Budding Yeast Cell Cycle

M. Sabouri-Ghomi, W. Baumann & J.J. Tyson

unpublished

Molecular noise is an unavoidable consequence of chemical reactions in small volumes (like a cell or subcellular organelle), where the total number of molecules involved in a reaction is less than 1000. For the CDK control system in budding yeast, typical numbers of molecules per haploid cell in an asynchronous culture are recorded in Table 4. Clearly, some proteins are present in 1000's of copies per cell and are relatively immune to fluctuations (CV < 2%), whereas other proteins are present in only 100's of copies per cell and are more prone to noise (CV > 6%). mRNAs, on the other hand, are present at very low abundances (0.5 to 2 molecules per cell, on average) [HOL98] and should be subject to large random fluctuations.

Table 3.4. Numbers of molecules (per haploid yeast cell) for several cell cycle genes.

Gene	**# molecules per cell**		**Gene**	**# molecules per cell**	
	mRNA	**Protein**		**mRNA**	**Protein**
cyclins			**CDK**		
CLN1	0.6	320, 500	*CDC28*	2.2	6700, 6000
CLN2	1.2	1300, 1000	**transc. factors**		
CLN3	1.1	–, 110	*SWI4*	0.4	590, –
CLB1	1.6	300, 250	*SWI5*	0.8	690, –
CLB2	1.1	340, 500	*MCM1*	1.6	9000, –
CLB3	1.1	890, 430	**other**		
CLB4	0.6	100, 220	*SIC1*	1.9	770, 100
CLB5	0.9	520, 390	*CDC6*	0.4	–, 310
CLB6	0.4	–, 50	*CDC14*	1.0	8500, –

Protein data (a,b) from a = [GHA03], b = (Cross et al., 2002)
mRNA data from http://web.wi.mit.edu/young/expression/transcriptome.html

For all of these reasons, it seems imperative to develop and study realistic stochastic models of cell cycle progression that include molecular noise in the CDK control system and inevitable variations in the cell division process itself (random distribution of molecules between unequally sized daughter cells at division). Nevertheless, only three published studies have appeared in the literature. Alt & Tyson [ALT87, TYS89], using a primitive model of CDK activation, studied the effects of molecular noise and unequal division, but their model is too simplistic to be relevant to a modern understanding of the cell cycle. Sveiczer et al. [SVE00] used a realistic deterministic

model of the control system and put all the noise into the division process. Steuer [STE04] assumed precise division and added an arbitrary dose of white noise to the right-hand-sides of the Novak-Tyson ODEs;

$$\frac{dx_i}{dt} = f_i(x_i) + \sqrt{2D_i x_i}\,\xi_i(t) \qquad (3.1)$$

where $\xi_i(t)$ is a Gaussian random variable with zero mean and unit variance. Choosing $D_i = 5 \times 10^{-5}$ for all i, Steuer found reasonable agreement between his model and standard properties of yeast cell populations described above, including the curious trimodal distribution of cycle times for the *wee1*$^-$ *cdc25*^{ts} double mutant. Although Steuer's effort is a nice first-try, he gives no justification for the Langevin formalism in Eq. (1) or for his chosen numerical value of D_i. Nor does he take into account the typical asymmetry of division of fission yeast cells (CV ≈ 5%), which can drastically alter the proper choice of D_i.

The deterministic models of Tyson, Novak & Chen were created to guide cell biologists in thinking about the molecular basis of a broad range of experimental observations, mostly phenotypes of mutants defective in cell cycle progression. To this end, they made free and easy use of 'phenomenological' rate laws (Michaelis-Menten kinetics, Hill functions, etc.), which are appropriate for modeling the average behavior of populations of cells but are not appropriate for rigorous stochastic modeling. For that purpose, the molecular mechanisms must be recast in terms of elementary reaction steps. For example, a Michaelis-Menten rate law, $dS/dt = k_2.E_{total}.S/(K_m+S)$, must be 'unpacked' to its elementary steps, explicitly accounting for the enzyme-substrate complex:

$$E + S \underset{k_{-1}}{\overset{k_1}{\rightleftarrows}} C \xrightarrow{k_2} E + P$$

Unpacking must be done in a way that retains the fundamental bifurcations (the bistable switches and oscillators) in the 'packed' model, on which so much of the physiology of the cell cycle depends. Naïve unpacking of the phenomenological equations destroys essential features of the bifurcation diagrams, as we will show shortly. New molecular interactions must be introduced to restore the correct bifurcation structures. On this basis, we will construct a preliminary model of cell cycle regulation, based on elementary reaction steps which are consistent with the desired qualitative behavior of the control system. For this model, the effects of molecular fluctuations in the individual reactions can be simulated by Gillespie's algorithm.

Unpacking reactions of the CDK control system

The simplest and most fundamental regulatory interaction in the yeast cell cycle is the antagonism between Clb2 and Cdh1 [TYS01]. Cdh1 facilitates the degradation of Clb2, and Clb2 (in combination with its kinase partner, Cdc28) phosphorylates and inactivates Cdh1. A phenomenological model of this interaction is given by the following system of nonlinear ODEs:

$$\frac{dX}{dt} = k_1 - (k_2' + k_2''Y)X, \qquad \frac{dY}{dt} = \frac{k_3 A(1-Y)}{J_3 + 1 - Y} - \frac{k_4 m X Y}{J_4 + Y} \qquad (3.2)$$

where X = activity of Clb2-dependent kinase, Y = fraction of Cdh1 in the active (dephosphorylated) form, A = concentration of phosphatase, the k's and J's are rate constants and Michaelis constants (respectively), and m = cell size (considered to be an adjustable parameter). For small values of m, the system of Eqs. (2A,B) has a single stable steady state ($X \approx 0$ and $Y \approx 1$) that we can associate with G1 phase of the cell cycle. For intermediate values of m, the system has three steady states: a stable G1 state ($X \approx 0$ and $Y \approx 1$), a stable S-G2-M state ($X \approx 1$ and $Y \approx 0$), and an

unstable saddle point. For large values of *m*, the G1 state is lost by a saddle-node bifurcation, and the system is forced into S-G2-M. In cell cycle parlance, this is the START transition, driven by growth of daughter cells to a critical cell size.

Let's start by unpacking the two Michaelis-Menten terms in Eq. (2B) (YP = phosphorylated form of Cdh1):

$$A+YP \underset{k_{-a}}{\overset{k_a}{\rightleftarrows}} C_a \xrightarrow{k_3} A+Y, \qquad X+Y \underset{k_{-x}}{\overset{k_x}{\rightleftarrows}} C_x \xrightarrow{k_4} X+YP$$

Naïvely, we might expect that, with $J_3 = (k_{-a}+k_3)/k_a$ and $J_4 = (k_{-x}+k_4)/k_x$, the unpacked system will behave similarly to the packed system given by Eqs. (2). However, the unpacked mechanism cannot exhibit multiple steady state solutions for any values of the rate constants, as can be proved by submitting the mechanism to CRNT (Chemical Reaction Network Toolbox, a wonderful little program that can deduce from the topological structure of a reaction network whether or not it can generate multiple steady states).

Clearly there is a serious discrepancy between the phenomenological model, on which all the deterministic modeling of the yeast cell cycle is based, and the elementary reactions model, on which all stochastic modeling must be based. The inconsistency arises from a subtlety in the phenomenological model: when Clb2 (as an enzyme) is bound to Cdh1 (i.e., the complex C_x in the mechanism), it is not available for degradation by Cdh1. Indeed, most of the Clb2 is hiding in complex C_x and cannot be destroyed by *Y*. Hence, Clb2 always 'wins the battle', and the G1 steady state is impossible. To correct this problem, we must give Cdh1 a chance to degrade Clb2 from the complex C_x:

$$Y+C_x \xrightarrow{k_2''} 2Y + \text{degraded X}$$

Adding this step to the mechanism above, we regain bistability, as demonstrated by CRNT and by simulations.

A preliminary model of the START and FINISH transitions in budding yeast

In the previous subsection we showed how to build an elementary reaction mechanism for the START transition in budding yeast (inactivation of Cdh1, driven by an increase in cell size). At START, Cdh1 is phosphorylated by Clb2-dependent kinase, and the cell switches from G1 phase to S-G2-M phase. At FINISH, the cell switches back to G1 phase by activating Cdh1, and this is the job of a phosphatase, Cdc14 (called 'A' in the mechanism in the previous subsection). Although the actual mechanism is a little more complicated, it is sufficient for our purposes here to imagine that Cdc14 activity rises at the end of the cell cycle due to *de novo* protein synthesis, stimulated by Clb2-dependent kinase. In the phenomenological model [TYS01], Eqs. (2A,B) are supplemented by an ODE for A = [Cdc14],

$$\frac{dA}{dt} = k_5' + k_5'' \frac{(mX/J_5)^n}{1+(mX/J_5)^n} - k_6 A \qquad (3.3)$$

where a Hill function, with $n = 2$, is used to describe the nonlinearity of *de novo* synthesis of A. In Fig. 9A we plot a one-parameter bifurcation diagram (X versus m) for the system of Eqs. (2-3). For $m < 0.33$, there is a single stable G1 steady state; for $0.33 < m < 1$, the system is bistable, and for $m > 1.13$, the system executes limit cycle oscillations.

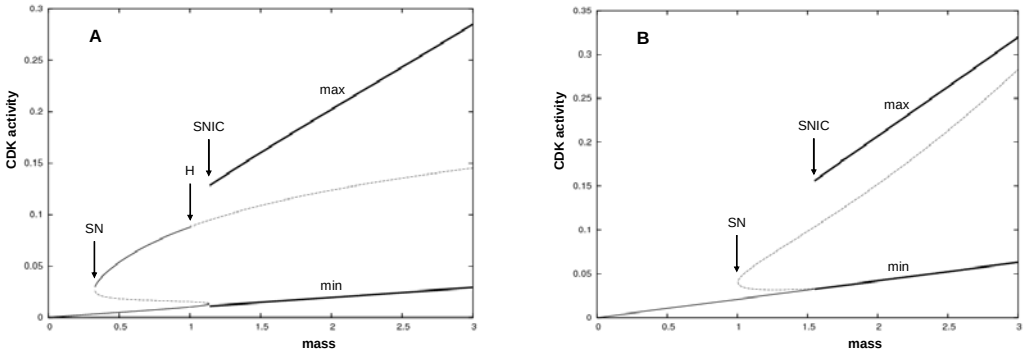

Fig. 3.9. Bifurcation diagrams for the packed and unpacked mechanisms. (A) For the phenomenological model given by Eqs. (2A,B) and (3). (B) For the unpacked system. Solid lines: stable steady states. Dashed lines: unstable steady states. Heavy solid lines: maximum and minimum values of X during limit cycle oscillations. Bifurcation points: SN (saddle-node), H (Hopf) and SNIC (saddle-node invariant-circle).

To model growth and division, the CDK control system in Eqs. (2-3) must be supplemented by equations describing mass increase and partitioning to daughter cells:

$$\frac{\mathrm{d}m}{\mathrm{d}t} = \mu m\ , \qquad m \to \frac{m}{2} \text{ when } X \text{ drops below } 0.05 \tag{3.4}$$

Equations (2-3-4) exhibit periodic cycles of growth and division and of Clb2-dependent kinase activity. The cycles are 'organized' around the SNIC bifurcation in Fig. 3A; i.e., cells are born in the G1 steady state at $m < 1$, must grow large enough to surpass the SNIC bifurcation (START), divide when X drops below 0.05 on the limit cycle oscillation, and then are captured again by the stable G1 steady state. The very elaborate model in Chen et al. (2004), which accounts for so many observed features of the budding yeast cell cycle, is built around the bifurcation diagram in Fig. 3A. Hence, to create a stochastic model of the yeast cell cycle, we should start by unpacking the system of Eqs. (2-3-4).

On pages 42-43, we showed how to unpack the Cdh1-Clb2 switch. There remains to unpack the Hill function in Eq. (3). We do so with the following elementary reactions:

$\mathrm{TF+X} \to \mathrm{TFP+X}$ (phosphorylation & dephosphorylation of transcr. factor)

$\mathrm{G+TFP} \rightleftarrows \mathrm{C_1}$, $\mathrm{C_1+TFP} \rightleftarrows \mathrm{C_2}$ (association & dissociation of transcr. factor to gene)

$\mathrm{C_1} \to \mathrm{A+C_1}$, $\mathrm{C_2} \to \mathrm{A+C_2}$, $\mathrm{G} \to \mathrm{A+G}$ (activated & background transcription of *A* from gene)

The phenomenological model, Eqs. (2-3), tracks three independent protein species, participating in six reactions, characterized by 11 kinetic parameters. The unpacked mechanism tracks eight independent biochemical species, participating in 19 reactions characterized by 19 independent kinetic constants. Hence, the unpacking process, preliminary to stochastic modeling, increases the complexity of the model by 2- to 3-fold.

The next step is to estimate values of the 19 kinetic constants in the unpacked model that will give a bifurcation diagram comparable to the phenomenological model (see Fig. 9). To this end,

we were greatly helped by the bifurcation-searching ability of the software tool Oscill8, developed by Emery Conrad in Tyson's group under support of DARPA's Bio-SPICE program.

Stochastic simulation

The elementary reaction mechanism can now be simulated by Gillespie's direct method [GIL76], and typical results are shown in Fig. 10. In this case we are accounting only for molecular noise in the chemical reactions; division is still assumed to be precisely in half. From 600 simulated cell division cycles, we computed the distributions of age and size at division (Fig. 11). The computed distributions are considerably more variable than typically observed: CV_{age} = 0.3 (computed), 0.15 (observed); CV_{size} = 0.18 (computed), 0.7 (observed). Discrepancies such as these have yet to be resolved.

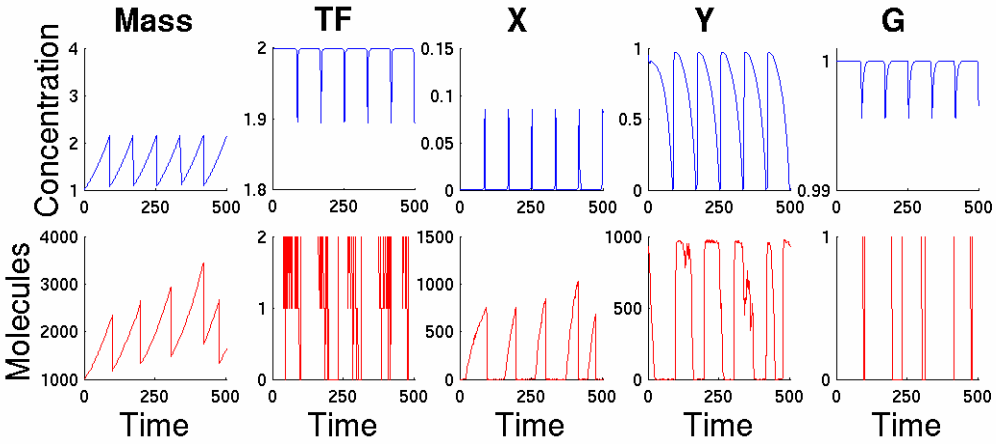

Fig. 3.10. Time evolution of important variables in the unpacked model. (Top panels) Deterministic simulations. Concentrations and time in arbitrary units. (Bottom panels) Exact stochastic simulations.

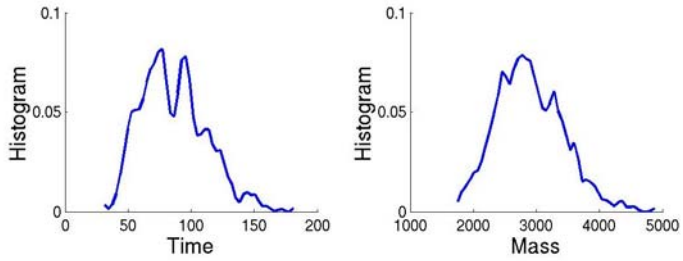

Fig. 3.11. Histograms computed from a simulated population of 600 cells. (Left) Age at division. (Right) Size at division. Age and mass in arbitrary units.

3.2 Fission Yeast Cell Cycle

Modeling the Fission Yeast Cell Cycle

A. Sveiczer, J.J. Tyson and B. Novak

***Briefings in Functional Genomics & Proteomics* 2:298-307 (2004)**

The eukaryotic cell cycle is traditionally divided into four phases: G1, S (DNA synthesis), G2 and M (mitosis). G1 and G2 are "gaps", when the cell presumably prepares for the major events of DNA replication (S) and sister chromatid segregation (M), which must occur in alternation. Nearly all the other constituents of a cell are synthesised continuously. The temporal duration of G1 and G2 ensure that all the main components of a cell (collectively referred to as cell mass) are doubled between two consecutive cell divisions.

The alternation of S and M phases and the co-ordination of growth and division are accomplished by a molecular engine, whose most important components are dimers of cyclins and cyclin-dependent protein kinases (Cdks) (Fig. 12). The catalytic subunit (Cdk) phosphorylates Ser/Thr residues on its substrates. Phosphorylation of specific target proteins is required at the onset of both S and M phases. The regulatory subunit (cyclin) is necessary for Cdk activity and also plays a role in targeting the Cdk to specific substrates.

Unlike higher eukaryotes, fission yeast has only one essential Cdk (namely Cdc2). Although fission yeast cells have four cyclins (Cdc13, Cig1, Cig2 and Puc1), only Cdc13 is essential to progression through the cell cycle (the triple mutant, *cig1Δ cig2Δ puc1Δ*, is viable). This suggests that a single species of Cdk/cyclin dimer can trigger both S and M phases, and it raises the question: how does a fission yeast cell know whether to prepare for DNA replication or mitosis? The answer seems to be that Cdc2/Cdc13 activity is very low in G1 phases, then rises to an intermediate level, sufficient to phosphorylate the substrates necessary for DNA replication. This intermediate level is also sufficient to prevent re-replication of DNA or premature cell division. Later in the cycle, Cdc2/Cdc13 activity rises to a very high value, necessary to trigger entry into mitosis. In order to divide, Cdc2/Cdc13 activity must be reduced to the very low level characteristic of G1 cells.

To create this pattern of activity, Cdc2/Cdc13 is regulated in three ways: cyclin degradation by the anaphase promoting complex (APC); binding to a reversible stoichiometric inhibitor (the Rum1 protein in fission yeast); and reversible inhibitory phosphorylation of the Tyr15 residue of Cdc2 by the Wee1 tyrosine kinase. These three enemies of Cdc2 (APC, Rum1 and Wee1) are regulated by Cdc2/Cdc13 itself.

The molecular interactions just described are used to build a wiring diagram of the control system in Fig. 12. The central component of the cell cycle engine is the Cdc2/Cdc13 dimer, also known as MPF (M-phase promoting factor). Since the Cdc2 subunit is in excess during the cycle and Cdc13 binding to Cdc2 is very fast, the production and destruction of Cdc2/Cdc13 complexes follows that of Cdc13 itself. Cdc13 is continuously synthesised from amino acids (AA) in the cytoplasm, where it binds to Cdc2, and then the dimer moves into the nucleus. The larger the cell, the larger its rate of cyclin synthesis, and the more Cdc2/Cdc13 dimers enter the nucleus per unit time.

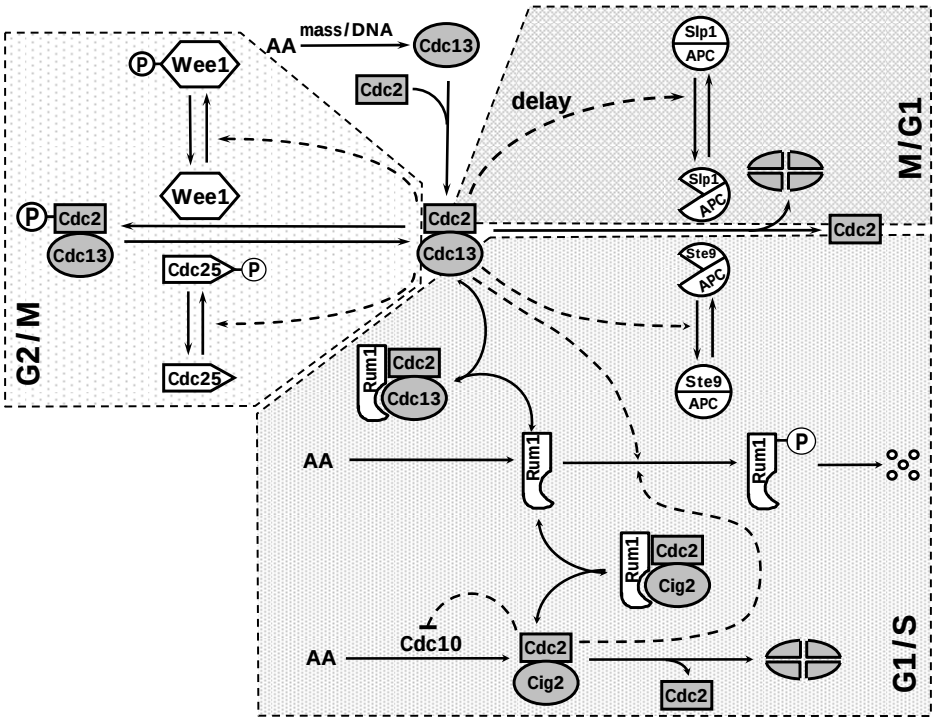

Figure 3.12: A molecular network for the fission yeast cell cycle. Solid lines represent biochemical reactions, and dotted lines represent enzymatic effects of proteins on these reactions. The three transitions of the cell cycle are controlled by separate modules, as the shading indicates. The G1-to-S transition is characterised by antagonistic relationships between Cdc2/Cdc13 and its enemies, Rum1 and Ste9. The cell passes through this transition when Cdc2/Cdc13 (with some help from Cdc2/Cig2) outcompetes Rum1 and Ste9. Negative feedback of Cdc2/Cig2 on Cdc10 activity plays a crucial role in endoreplication cycles in *cdc13Δ* mutants. The G2-to-M module is characterised by the reversible phosphorylation of Cdc2, catalysed by Wee1 kinase and Cdc25 phosphatase. These enzymes are involved in two positive feedback loops with Cdc2/Cdc13. The cell passes from G2 to M when Cdc2/Cdc13 activation by Cdc25 overcomes its inhibition by Wee1. Mitotic exit (M-to-G1) is achieved by a time-delayed negative feedback loop, whereby Cdc2/Cdc13 activates Slp1, which destroys Cdc13. The control system returns to its G1 state.

A mechanism in Fig. 12 can be converted into a set of ordinary differential equations (not shown) by using standard principles of biochemical kinetics. Numerical values of the parameters (rate constants) of the models were chosen so that the concentration profiles of the cell cycle regulators are consistent with experiments on wild type cells and cell cycle mutants. For example, a simulation of wild-type cells (Fig. 13) shows the relative concentrations of some important proteins as functions of time during a cell cycle. Cell mass increases exponentially between two consecutive nuclear divisions, which occur every 140 min. The short (~20 min) G1 phase is characterised by high Ste9/APC and Rum1 and very low MPF levels. When Cdc2/Cdc13 and Cdc2/Cig2 dimers switch off Rum1 and then Ste9/APC as well, the cell passes Start and DNA replication takes place (notice that the mass/DNA ratio is halved in early S phase). Since Wee1 activity is relatively large in mid cycle, it keeps the cell in G2 phase for about 3/4 of the total cycle, until the cell grows to a relatively large mass. During G2 phase, MPF activity can only slowly increase with cell growth, but when the positive feedback loops via Cdc25 and Wee1 turn on, then MPF activity rises abruptly and the cell enters mitosis. Mitosis is short because the negative feedback loop activates Slp1, which destroys Cdc13. When MPF

activity drops below a critical level, the cell completes nuclear division and about 20-30 minutes later undergoes cytokinesis (cell separation). (Notice that these events have no effect on the mass/DNA ratio).

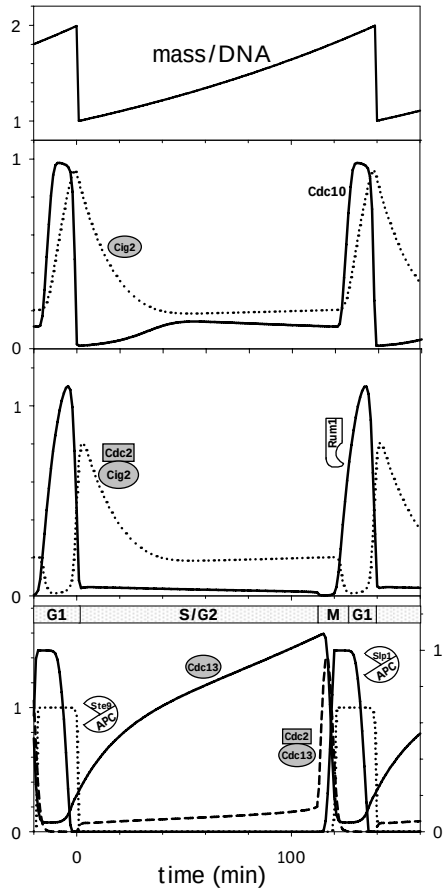

Figure 3.13: Simulated time courses of cell-cycle control proteins in a wild-type fission yeast cell. Mass/DNA is divided by 2 at DNA replication, and grows exponentially between two consecutive S phases. The Cdc13 symbol represents the sum of all the existing forms of Cdc2/Cdc13 complexes, either active or inactive, either free or bound to Rum1. The Cdc2/Cdc13 symbol represents only the active complex. A similar convention is used in the case of Cig2. The short G1 phase is characterised by high activity of Cdc10, Ste9 and Rum1, and the lack of any Cdk/cyclin activity. S/G2 phases are characterised by low activities of Cdc10, Ste9 and Rum1, and a high level of total Cdc2/Cdc13, which is mostly inactive (phosphorylated). M phase is characterised by high activity of Cdc2/Cdc13. M phase is short because Cdc2/Cdc13 activates Slp1, which degrades Cdc13.

To be worthy of consideration, a mathematical model of the fission yeast cell cycle should be able to describe the physiology of a broad set of cell cycle mutants. Laboratory collections maintain many mutant strains in which one or more genes are deleted, over-expressed, or point-mutated, with either loss-of-function or gain-of-function. The phenotypes of all these mutants are known, and our model is able to simulate at least 60 different types of fission yeast mutants. Here we describe only one.

What happens if the gene encoding the main cyclin (Cdc13) is deleted? Since *cdc13Δ* is a lethal mutant, the answer to this question requires a genetic trick, putting a special promoter before the *cdc13* gene that can be switched either on or off by altering the growth medium. After the promoter has been switched off, the cells elongate abnormally and finally die (*cdc* phenotype), because in the absence of Cdc13 they never enter mitosis and cannot divide. However, their nuclei also become extremely large, and the DNA content in the nucleus increases 32-fold or more before they die. In comparison with other *cdc* mutants, the large DNA content of *cdc13Δ* cells is unusual and unexpected, as lack of mitosis should prevent any further rounds of DNA replication by invoking a checkpoint. Apparently, *cdc13Δ* cells abnormally re-enter G1 from G2, leading to endoreplication cycles (consecutive S phases without intervening mitoses). It is worth mentioning that endoreplication often occurs normally during the development of higher eukaryotes, so this fission yeast mutant mimics a fundamental phenomenon.

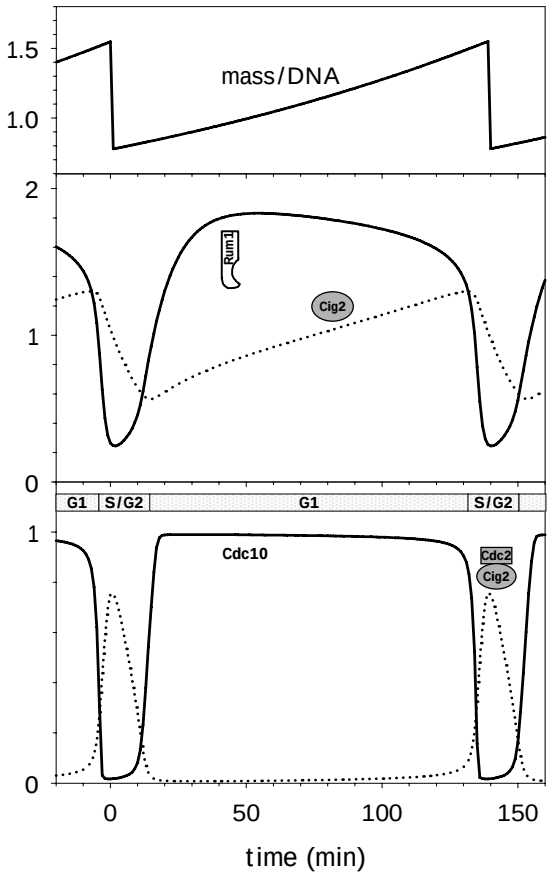

Figure 3.14: Simulated time courses of cell-cycle proteins in a *cdc13Δ* mutant cell. In the absence of Cdc13, the cell never enters mitosis and therefore dies. However, a negative feedback loop in the mechanism (Fig. 12), whereby Cdc2/Cig2 inactivates its own transcription factor (Cdc10), results in an abnormal transition from G2 back to G1, leading to endoreplication (repeated S phases) at intervals close to the mass doubling time. At every S phase the control system is reset (mass/DNA is divided by 2.

This unusual behaviour can be explained by the dynamics of Cig2 in our model (Fig. 12). Since Cdc13 is absent, S phase must be driven by Cdc2/Cig2. Cdc2/Cig2 apparently switches off its

transcription factor, Cdc10, and this negative feedback can return G2 cells back to G1 after successive rounds of DNA replication. Computer simulations show that this might be the case (Fig. 14). After replication, there is a short G2 like state when Cdc10 is off and Cdc2/Cig2 is on. However, Cdc2 activity is dropping because Cig2 is being degraded and not synthesized. Eventually, Rum1 returns, inhibiting the remaining Cdc2/Cig2 and allowing Cdc10 to make a comeback. This G1 state lasts until enough Cdc2/Cig2 accumulates in the nucleus, parallel with cell growth, to initiate a new round of DNA replication. This process is repeated at time intervals very close to the normal mean cycle time, as observed.

3.3 Frog Embryonic Cell Cycle

A Model of the Unreplicated DNA Checkpoint in Frog Cell Extracts

A. Dravid, J.C. Sible and J.J. Tyson

Unpublished

The function of the cell cycle is to turn one cell into two daughter cells with identical copies of the organism's genome (i.e., the DNA molecules in the nucleus). If the cell's DNA becomes damaged in some way (e.g., by ultraviolet or gamma radiation), then progression through the cell division cycle must be abruptly halted until the damage is repaired. This function is provided by cell cycle 'checkpoints'. The cell has molecular mechanisms to sense damage (to its DNA or other essential components of the division cycle, such as the mitotic spindle) and to send a signal to the appropriate checkpoint mechanism, which blocks progression to the next stage of the cell cycle. When these checkpoint mechanisms are not functioning properly, the damaged cell gives rise to genetically mutant progeny. Many of these cells will die, but some may survive with mutant genomes that make the cell into a malignant cancer.

One of these checkpoints (called the 'unreplicated DNA' checkpoint) blocks progression into mitosis if the process of DNA replication becomes stalled for any reason. The unreplicated DNA checkpoint works by preventing activation of M-phase promoting factor (MPF, which is a dimer of Cdk1 and cyclin B). While the cell is in the process of replicating its DNA, MPF is held in an inactive form (called preMPF) by the action of an enzyme called Wee1. When DNA replication is complete and the cell is ready to divide, preMPF is converted into active MPF by an enzyme called Cdc25. The unreplicated DNA checkpoint works by activating the 'checkpoint kinases' (Chk1 and Chk2) that phosphorylate the enzymes Wee1 and Cdc25. These phosphorylation reactions, labeled α and β in our wiring diagram (Fig. 15), serve to activate Wee1 and inactivate Cdc25, thereby delaying the activation of MPF and entry into mitosis.

Under DARPA support, we have been studying this checkpoint pathway in frog cell extracts (see Chapter 4). The extract contains all the proteins illustrated in Fig. 15 plus a certain number of nuclei (typically 500-1000 nuclei/μl) added by the experimentalist. The extract is capable to drive DNA synthesis and mitosis in the added nuclei. The unreplicated DNA checkpoint can be induced by supplementing the extract with a drug (aphidicolin) that blocks DNA replication. In these extracts, the strength of the checkpoint can be manipulated by changing the number of nuclei per μl. The proposed mechanism (Fig. 15) should be consistent with all relevant data and should suggest new experiments to be carried out.

Some typical experimental data are illustrated in Fig. 16. In this experiment, the extract is supplemented with a form of Cdc25 protein that cannot be phosphorylated by the checkpoint kinases, hence $\alpha = 0$ for that fraction of the Cdc25 protein pool. The model equations are simulated under these conditions both without and with aphidicolin (i.e, without and with induction of the checkpoint). Model simulations are compared to the experimental data in the top frames of Fig. 16.

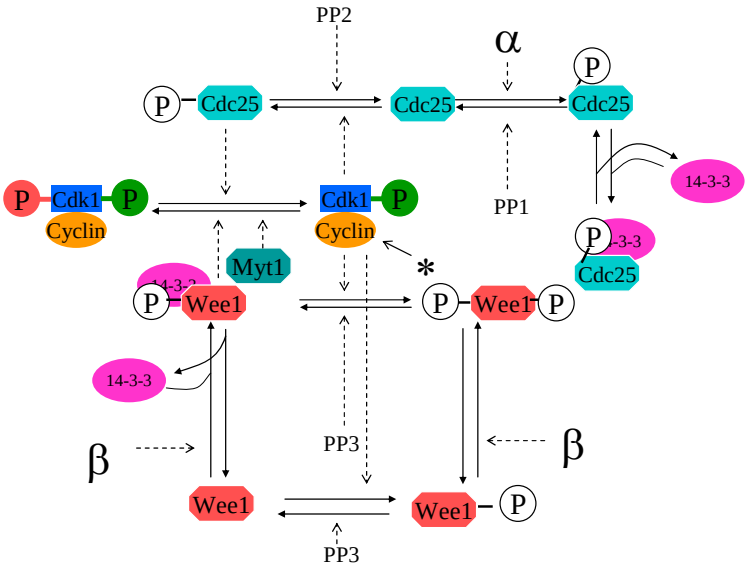

Figure 3.15. Wiring diagram for the unreplicated DNA checkpoint in frog cell extracts. Adapted from Novak & Tyson [NOV93]. The * points to active MPF. MPF is phosphorylated and inactivated by the action of two kinases, Wee1 and Myt1. The unreplicated DNA signal is propagated through parameters α and β, representing the catalytic action of the checkpoint kinases, Chk1 and Chk2.

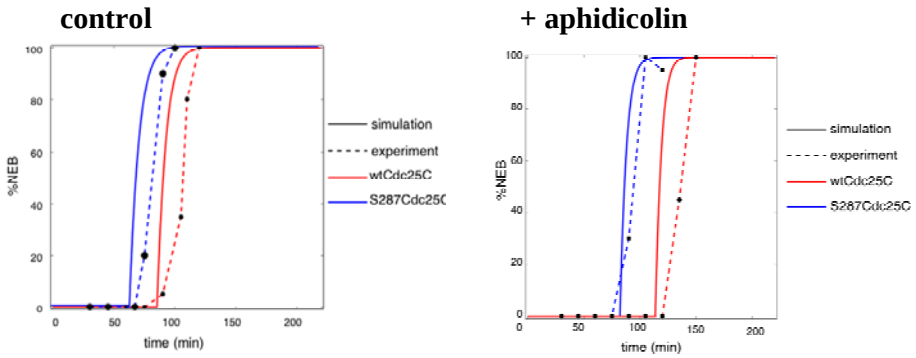

Experimental data
(Kumagai et al. 1998)

Figure 3.16. Experimental data and model simulations for MPF activation. MPF activity is measured as % of nuclear envelope breakdown (NEB).

Once we have some confidence in the model, we can use it to predict the outcome of new experiments, as in Table 5. These predictions served as part of the preliminary studies for an NIH proposal that was funded in 2006. The modeling and experimental studies of this checkpoint in frog cell extracts is continuing past the end of the BioSPICE project.

Table 3.5. Delayed entry into mitosis, as predicted by the model. NEB = nuclear envelope breakdown. 'ΔWee1' means Wee1 protein is removed from the extract by immunodepletion. '2xWee1' means the extract has twice as much Wee1 protein as untreated control. [ΔcyclinB] indicates the amount of non-degradable cyclin B that is added to the extract, relative to the total Cdk1 in the extract.

Treatment	Source of reagent	[Δcyclin B]	Predicted time for 50% NEB	
			Without APH	With APH
untreated	N/A	0.45	98 min	>500 min
		0.6	67 min	145 min
ΔWee1	antibody from Zymed®	0.45	90 min	>500 min
		0.6	61 min	100 min
ΔCdc25C	antibody given by Maller	0.45	>500 min	>500 min
		0.6	>500 min	>500 min
2xWee1	cDNA given by Murakami	0.45	90 min	>500 min
		0.6	61 min	100 min
2x Cdc25C	cDNA given by Maller	0.45	48 min	67 min
		0.6	35 min	42 min

3.4 Generic Cell Cycle

Analysis of a generic model of eukaryotic cell cycle regulation
A. Csikász-Nagy, D. Battogtokh, K. Chen, B. Novák & J.J. Tyson
***Biophysical Journal* 90:4361-4379**

Some years ago Paul Nurse [NUR90] proposed, and since then many experimental studies have confirmed, that the DNA replication-division cycle in all eukaryotic cells is controlled by a common set of proteins interacting with each other by a common set of rules. Nonetheless, each particular organism seems to use its own peculiar mix of these proteins and interactions, generating its own idiosyncrasies of cell growth and division. The 'generic' features of cell cycle control concern these common genes and proteins and the general dynamical principles by which they orchestrate the replication and partitioning of the genome from mother cell to daughter. The peculiarities of the cell cycle concern exactly which parts of the common machinery are functioning in any given cell type, given the genetic background and developmental stage of an organism. We formulate the genericity of cell cycle regulation in terms of an 'underlying' set of nonlinear ordinary differential equations with unspecified kinetic parameters, and we attribute the peculiarities of specific organisms to the precise settings of these parameters. Using bifurcation diagrams, we show how specific physiological features of the cell cycle are determined ultimately by levels of gene expression.

In Fig. 17 we propose a general protein interaction network for regulating cyclin-dependent kinase activities in eukaryotic cells. (Figure 17 uses 'generic' names for each protein; in Table 6 we present the common names of each component in specific cell types: budding yeast, fission yeast, frog eggs, and mammalian cells.) The dynamical properties of the protein interaction network can be described by a set of ordinary differential equations (not shown), given a table of parameter values suitable for specific organisms (see original publication). For each organism we analyze the effects of physiological and genetic changes on the transitions between cell cycle phases, in terms of bifurcations of the vector fields defined by the DEs.

The cell cycle projected onto a one-parameter bifurcation diagram
Figure 18 presents a simulation of the fission yeast cell cycle in two formats. In Fig. 18B are plotted the concentrations of four regulatory proteins as functions of cell mass, but since mass increases exponentially with time, one may think of the lower abscissa as $e^{\mu t}$, i.e. as increasing time. We present the simulation this way so that we can 'lift it up' onto the bifurcation diagram in Fig. 18A: the red curve in Fig. 2A is identical to the green curve (actCycB) in Fig. 18B. In Fig. 18A, a stable, G1-like, steady state exists at very low level of actCycB (active Cdk/CycB dimers). This steady state is lost at a saddle-node bifurcation (SN1) at cell mass = 0.8 au. Between SN1 and SN2 (at cell mass = 2.6 au), the control system has a single, stable, steady state attractor with an intermediate activity (~0.1) of cyclin B (an S/G2-like steady state). The other steady state branches are unstable and physiologically unnoticeable. For mass > 2.6 au, the only stable attractor is a stable limit cycle oscillation. This branch of stable limit cycles is lost by further bifurcations at very large mass (of little physiological significance for wild-type cells).

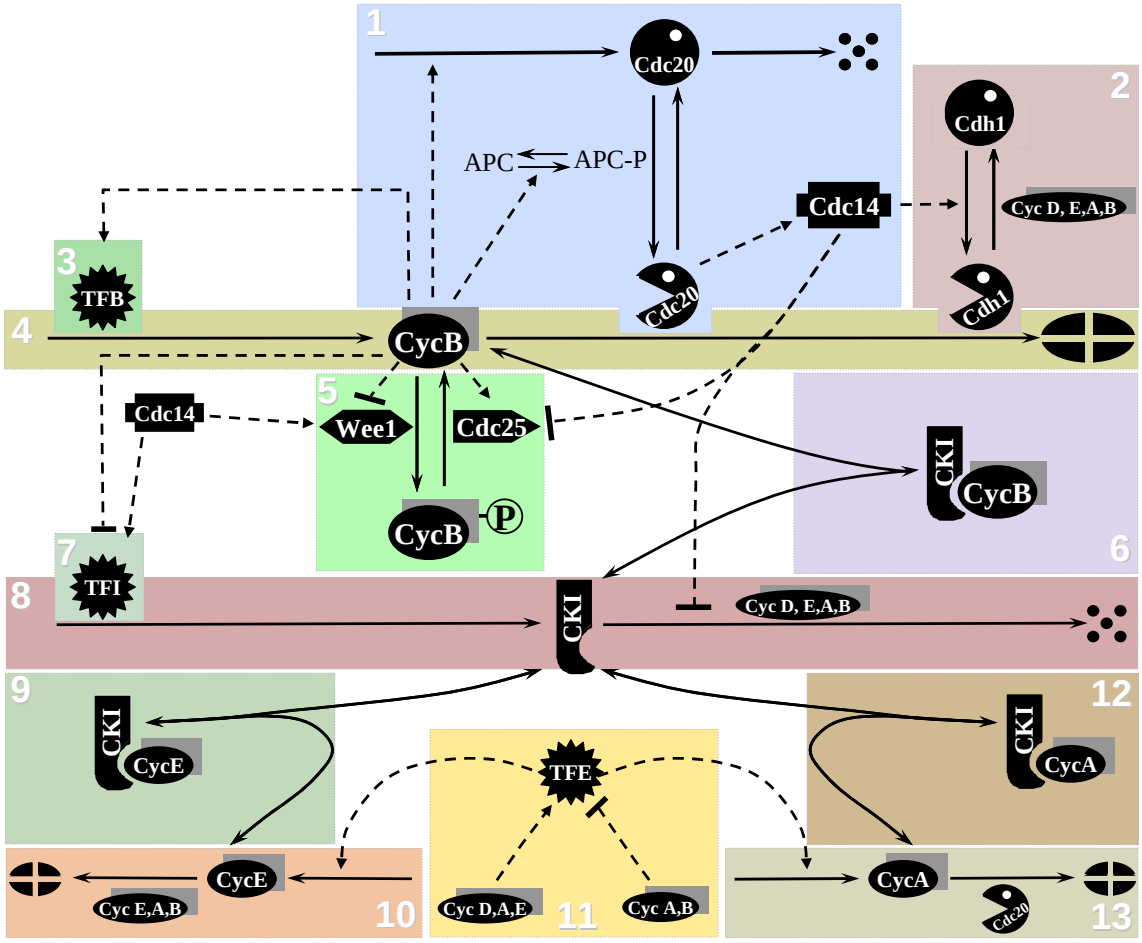

Figure 3.17. Wiring diagram of the generic cell-cycle regulatory network. Solid lines = chemical reactions, dashed lines = regulatory effects, a protein sitting on a reaction arrow represents an enzyme catalyst of the reaction. Regulatory modules of the system are distinguished by colored backgrounds. Open-mouthed PacMan represents active form of regulated protein; gray rectangles behind cyclins represent their Cdk partners. We assume that all Cdk subunits are present in constant, excess amounts.

The red trajectory in Fig. 18A represents the path of a growing-dividing yeast cell projected onto the bifurcation diagram. Let us pick up the trajectory of a growing cell at mass = 2.2 au, where the cell cycle control system has been captured by the stable S/G2-steady state. As the cell continues to grow, it leaves the S/G2 state at SN2 and prepares to enter mitosis. At cell mass > 2.6, the only stable attractor is a limit cycle. This limit cycle, which bifurcates from SN2, has infinite period at the onset of the bifurcation (hence, the onset point is commonly called a SNIPER—Saddle-Node-Infinite-PERiod—bifurcation). Because the limit cycle has a very long period at first, and the cell enters the limit cycle at the place where the saddle-node used to be, the cell is stuck in a semi-stable transient state (where the red trajectory 'overshoots' SN2). As the cell grows, it eventually escapes the semi-stable state (at cell mass ≈ 3), and then actCycB increases dramatically (note the log-scale on the ordinate), driving the cell into mitosis. Because the control system is now captured by the stable limit cycle, actCycB inevitably decreases and the cell is driven out of mitosis. We presume that the cell divides when actCycB falls below 0.1; hence, cell mass is halved (3.4 → 1.7), and the control system is now attracted to the S/G2 steady

state (the only stable attractor at this cell mass). The newly divided cell makes its way to the S/G2 attractor by a circuitous route that looks like a brief G1 state (very low actCycB) but is not a stable and long-lasting G1 state. This transient G1 state is characteristic of wild-type fission yeast cells.

Table 3.6. Protein name conversion table and modules used for each organism.

on Fig 1	Budding yeast	Fission yeast	Xenopus embryo	Mammalian cells	Function
CycB	Cdc28/Clb1,2	Cdc2/Cdc13	Cdc2/CycB	Cdc2/CycB	mitotic Cdk/cyclin complex
CycA	Cdc28/Clb5,6	Cdc2/Cig2	Cdk1,2/CycA	Cdk1,2/CycA	S-phase Cdk/cyclin complex
CycE	Cdc28/Cln1,2	—	Cdk2/CycE	Cdk2/CycE	G1/S transition-inducer Cdk/cyclin
CycD	Cdc28/Cln3	Cdc2/Puc1	Cdk4,6/CycD	Cdk4,6/CycD	starter Cdk/cyclin complex
CKI	Sic1	Rum1	Xic1	p27 ^{Kip1}	Cdk/cyclin stoichometric inhibitor
Cdh1	Cdh1	Ste9	Fzr	hCdh1	CycB degradation-regulator with APC
Wee1	Swe1	Wee1	Xwee1	hWee1	Cdk/CycB inhibitory kinase
Cdc25	Mih1	Cdc25	Xcdc25	Cdc25C	Cdk/CycB activatory phosphatase
Cdc20	Cdc20	Slp1	Fizzy	p55 ^{Cdc}	CycB, CycA degradation-regulator with APC
Cdc14	Cdc14	Clp1/Flp1	Xcdc14	hCdc14	phosphatase working against the Cdk's
TFB	Mcm1	—	—	Mcm	CycB transcription factor
TFE	Swi4/Swi6 Mbp1/Swi6	Cdc10/Res1	XE2F	E2F	CycE/A transcription factor (SBF+MBF in budding yeast)
TFI	Swi5	—	—	—	CKI transcription factor
APC	APC	APC	APC	APC	Anaphase-Promoting-Complex
active modules	1, 2, 3, 4, 6, 7, 8, 10, 11, 12, 13	1, 2, 4, 5, 6, 8, 11, 12, 13	1, 4, 5	1, 2, 3, 4, 6, 8, 9, 10, 11, 12, 13	modules of Fig 1, used for simulation of organism

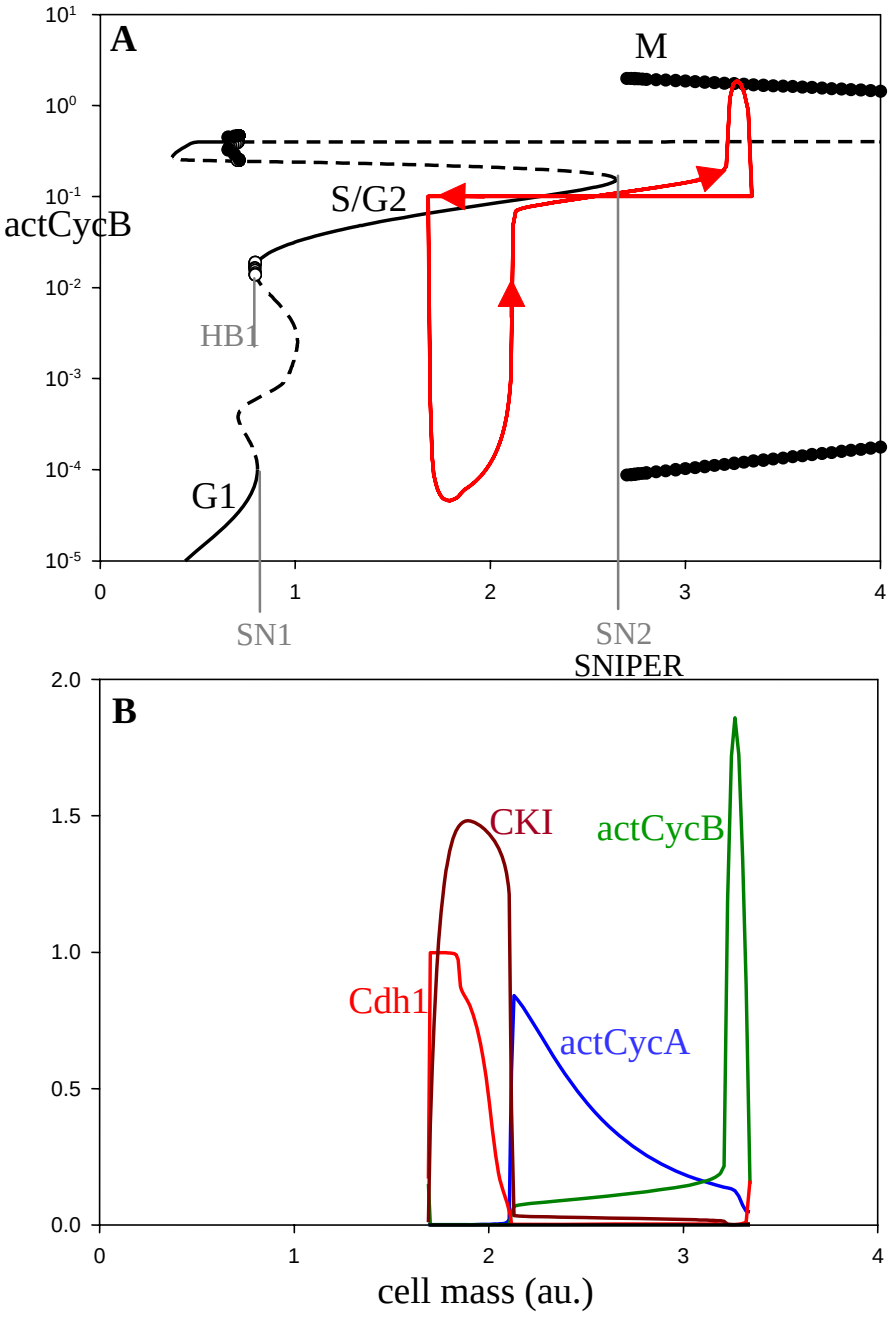

Figure 3.18. One-parameter bifurcation diagram (*A*) and cell cycle trajectory (*B*) of wild-type fission yeast. Both figures share the same abscissa. Notice that cell mass is just the logarithm of age, because we assume that cells grow exponentially between birth (age=0) and division (age=MDT). The red curve in panel A (a 'cell cycle trajectory' for MDT = 120 min) is identical to the green curve in Panel B. Key to panel A: solid line = stable steady state, dashed line = unstable steady state, filled circles = maxima and minima of stable oscillations, open circles = maxima and minima of unstable oscillations, SN1 (saddle-node bifurcation that annihilates the G1 steady state), SN2 (saddle-node bifurcation that annihilates the G2 steady state), and HB1 (Hopf bifurcation on the S/G2 branch of steady states that gives rise to endoreplication cycles). SN2 is a SNIPER bifurcation, i.e., it gives way to stable periodic solutions of infinite period (at the bifurcation point). The other (unmarked) bifurcation points in this diagram are not pertinent to cell cycle regulation.

The one-parameter bifurcation diagram in Fig. 18A is a compact way to display the interplay between the DNA replication-segregation cycle (regulated by Cdk/CycB activity) and the growth-division cycle (represented on the abscissa by the steady increase of cell mass and its abrupt resetting at division). The very strong 'cell size control' in late G2 phase of the fission yeast cell cycle, which has been known to physiologists for 30 year [NUR75], is here represented by growing past the SNIPER bifurcation, which eliminates the stable S/G2 steady state and allows the cell to pass into and out of mitosis (the stable limit cycle oscillation).

A satisfactory model of fission yeast must account not only for the phenotype of wild type cells but also for the unusual properties of the classic *cdc* and *wee* mutants that played such important roles in deducing the cell-cycle control network. Mutations change the values of specific rate constants, which remodel the one-parameter bifurcation diagram and thereby change the way a cell progresses through the DNA replication-division cycle. For example (Fig. 19A), for a $wee1^-$ mutant (reduce Wee1 activity to 10% of its wild-type value) SN2 moves to the left of SN1 and the infinite-period limit cycle now bifurcates from SN1. Hence, the cell cycle in $wee1^-$ cells is now organized by a SNIPER bifurcation at the G1/S transition: $wee1^-$ cells are about half the size of wild type cells, they have a long G1 phase and short G2, and slowly growing cells pause in G1 (unreplicated DNA) rather than in G2 (replicated DNA).

Mutant analysis on the genetics-physiology plane

In our view, genetic mutations are connected to cell phenotypes through bifurcation diagrams. Mutations induce changes in parameter values, which may change the nature of the bifurcations experienced by the control system, which will have observable consequences in the cell's physiology. Mutation-induced changes in parameter values may be large or small: e.g., the rate constant for CycB synthesis = 0 in a *cdc13Δ* cell, but a $wee1^{ts}$ ('temperature sensitive') mutant may cause only a minor change in the catalytic activity of Wee1 kinase. Whether these changed parameter values cause a qualitative change in bifurcation points on the one-parameter diagram (Figs. 18A and 19A), or merely a quantitative shift of their locations, depends on whether the parameter change crosses a bifurcation point or not. In principle, we can imagine a sequence of bifurcation diagrams (and associated phenotypes) connecting the wild type cell to a mutant cell as the relevant kinetic parameter changes continuously (up or down) from its wild type value. This theoretical sequence of morphing phenotypes can be captured on a two-parameter bifurcation diagram, where cell mass continues to stand in for the physiology of the cell cycle (growth and division) and the second parameter is a rate constant that varies continuously between 0 (the deletion mutant) and some large value (the over-expression mutant). Plotted this way, the two-parameter bifurcation diagram spans the entire range of molecular biology from genetics to cell physiology!

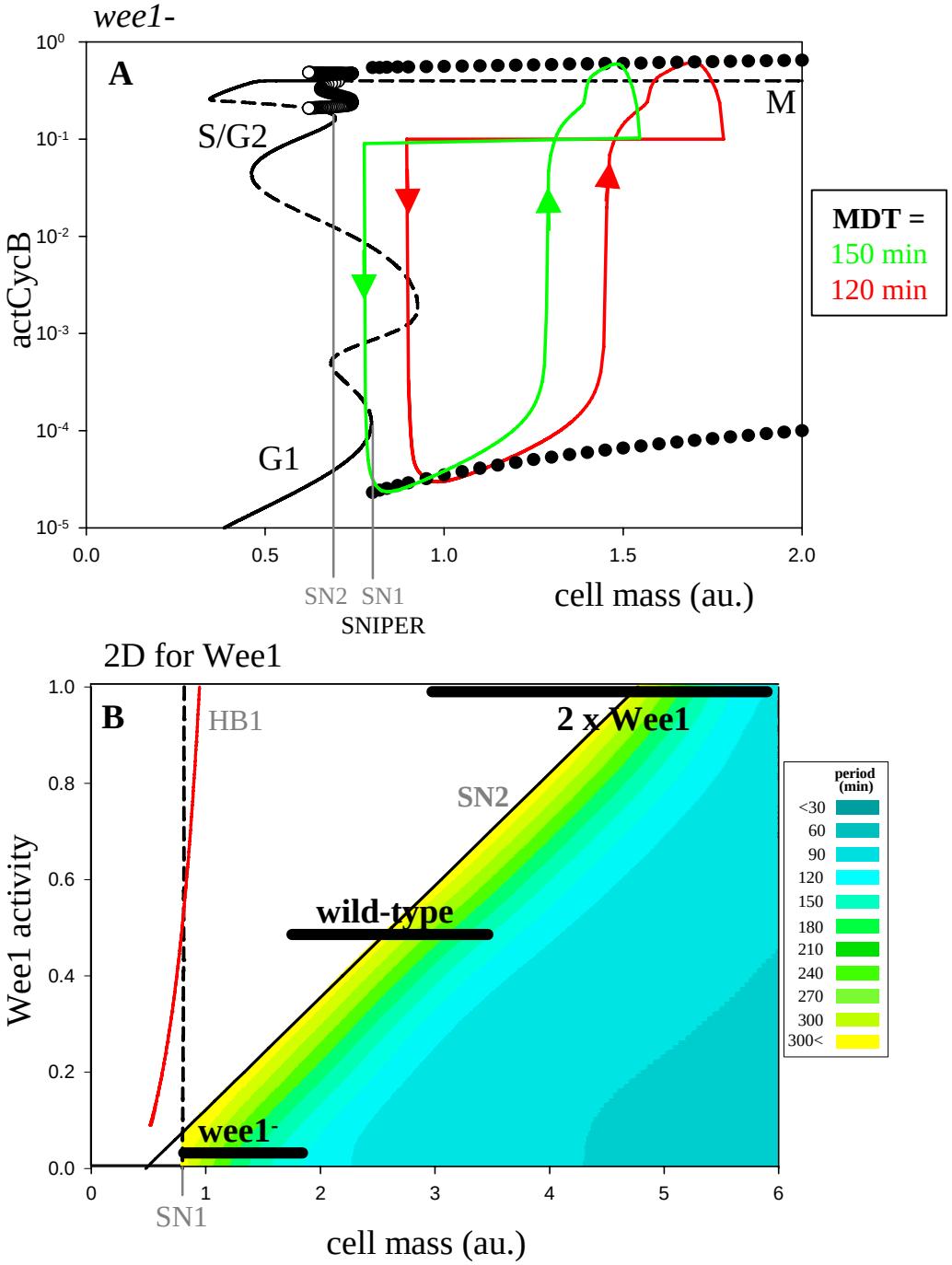

Figure 3.19 One-parameter (*A*) and two-parameter (*B*) bifurcation diagrams for mutations at the *wee1* locus in fission yeast. Panel A should be interpreted as in Fig. 18. MDT = 120 min. Key to panel B: dashed black line = locus of SN1 bifurcation points, solid black line = locus of SN2 bifurcation points, red line = locus of HB1 bifurcation points, black bars = projections of the cell cycle trajectories in Figs. 18A and 19A onto the two-parameter plane. Within regions of stable limit cycles, the color code denotes the period of oscillations. Notice that the period becomes very long as the limit cycles approach the locus of SNIPER bifurcations. The limit cycles switch their allegiance from SN2 to SN1 at Wee1 activity ~ 0.07 (by a complex sequence of codimension-two bifurcations that are not indicated here). Notice that *wee1*$^+$ overexpression leads to large cells, size-controlled at the G2-to-M transition, but *wee1* deletion leads to small cells (half the size of wild type), size-controlled at the G1-to-S transition.

To illustrate this idea, consider *wee1* mutations. On the two-parameter bifurcation diagram in Fig 19B we follow the loci of bifurcation points (SN1, SN2 and HB1) from their position in wild-type cells ("Wee1 activity" = 0.5) in the direction of overexpression (>0.5) or deleterious mutation (<0.5). The one-parameter bifurcation diagrams of wild-type (Fig 18A) and *wee1*$^{-}$ (Fig. 19A) cells are cuts of this plane at the marked levels of Wee1 activity. For over-expression mutations, the SNIPER bifurcation moves toward larger cell mass, and the heavy bar shows where the simulation of 2×*wee1*$^{+}$ cells projects onto the genetics–physiology plane. Clearly, the size of *wee1*^{op} cells increases in direct proportion to gene dosage [NUR76]. As Wee1 activity decreases below 0.5, e.g. in a heterozygote diploid cell (activity = 0.25) or in *wee1*^{ts} mutants, the SNIPER bifurcation moves toward smaller cell mass. Eventually, the SN1 and SN2 loci cross, and the infinite-period oscillations switch from SN2 to SN1 by a short but complicated sequence of codimension-two bifurcations (not shown on the diagram). Since SN1 is not dependent on Wee1 activity, the critical cell size at the SNIPER bifurcation drops no further as Wee1 activity decreases.

Discussion

We propose a protein interaction network for eukaryotic cell cycle regulation that includes most of the important regulatory proteins found in all eukaryotes, and that can be parameterized to yield accurate models of a variety of specific organisms (budding yeast, fission yeast, frog eggs and mammalian cells). The many different control loops in the generic model can be mixed and matched to create explicit models of specific organisms and mutants. Each organism has its own idiosyncratic properties for cell growth and division, depending on which modules are in operation, which depends ultimately on the genetic makeup of the organism. Lethal mutations push the organism into a region of parameter space where the control system is no longer viable.

Our model is freely available at http://mpf.biol.vt.edu/research/generic_model/main/pp/. From the web site one can download .ode and .set files for use with the free software XPP-AUT. From an ode-file one can easily generate FORTRAN or C++ subroutines, or port the model to Matlab or Mathematica. One can also download an SBML version of the model for use with any software that reads this standard format. We have introduced the model and all the mutant scenarios discussed in this paper into JigCell, our problem-solving environment for biological network modeling. The parameter sets in the JigCell version of budding yeast and fission yeast are slightly different from the parameter sets presented in this paper. The revised parameter values give better fits to the phenotypic details of yeast mutants. JigCell is especially suited to this sort of parameter twiddling to optimize the fit of a model to experimental details.

A dynamical perspective on molecular cell biology

A. Csikász-Nagy, D. Battogtokh, K. Chen, B. Novák & J.J. Tyson

***Biophysical Journal* 90:4361-4379 (Appendix)**

A molecular regulatory network, such as Fig. 1, is a set of chemical and physical processes taking place within a living cell. The temporal changes driven by these processes can be described, at least in a first approximation, by a set of ordinary differential equations derived according to the standard principles of biophysical chemistry. Each differential equation describes the rate of change of a single time-varying component of the network (gene, protein or metabolite—the *state variables* of the network) in terms of fundamental processes like transcription, translation, degradation, phosphorylation, dephosphorylation, binding and dissociation. The rate of each step is determined by the current values of the state variables and by numerical values assigned to rate constants, binding constants, Michaelis constants, etc. (collectively referred to as *parameters*).

Given specific values for the parameters and *initial conditions* (state variables at time = 0), the differential equations determine how the regulatory network will evolve in time. The direction and speed of this change can be represented by a *vector field* in a multidimensional *state space* (Fig. 20A). A numerical simulation moves through state space always tangent to the vector field. *Steady states* are points in state space where the vector field is zero. If the vector field close to a steady state points back toward the steady state in all directions (Fig. 20A), then the steady state is (locally) *stable*; if the vector field points away from the steady state in any direction (near the ○ in Fig. 20B), the steady state is *unstable*. If the vector field supports a closed loop (Fig. 20C), then the system oscillates on this *periodic orbit*, also called a *limit cycle*. The stability of a limit cycle is defined analogously to steady states. Stable steady states and stable limit cycles are called *attractors* of the dynamical system. To every attractor is associated a *domain of attraction*, consisting of all points of state space from which the system will go to that attractor.

As parameters of the system are changed, the number and stability of steady states and periodic orbits may change, e.g., going from Fig. 20A to 20B or from 20B to 20C. Parameter values where such changes occur are called *bifurcation points* [KUZ98]. At a bifurcation point, the system can gain or lose a stable attractor, or undergo an exchange of stabilities. In the case of the cell cycle, we associate different cell cycle phases to different attractors of the Cdk-regulatory system, and transitions between cell cycle phases to bifurcations of the dynamical system [TYS01].

To visualize bifurcations graphically, one plots on the ordinate a representative variable of the dynamical system, as an indicator of the system's state, and on the abscissa, a particular parameter whose changes can induce the bifurcation (Fig. 20D). It is fruitful to think of changes to the parameter as a *signal* imposed on the control system, and the stable attractors (steady states and oscillations) as the *response* of the network (Tyson et al. 2003). For the cell cycle control system, the clear choice of dynamic variable is the activity of Cdk1/CycB (the activity of this complex is small in G1, modest in S/G2, and large in M phase). As bifurcation parameter, we choose cell mass because we consider growth to be the primary driving force for progression through the cell cycle. For each fixed value of cell mass, we compute all steady state and

oscillatory solutions (stable and unstable) of the Cdk-regulatory network, and we plot these solutions on a one-parameter bifurcation diagram (Fig. 20D).

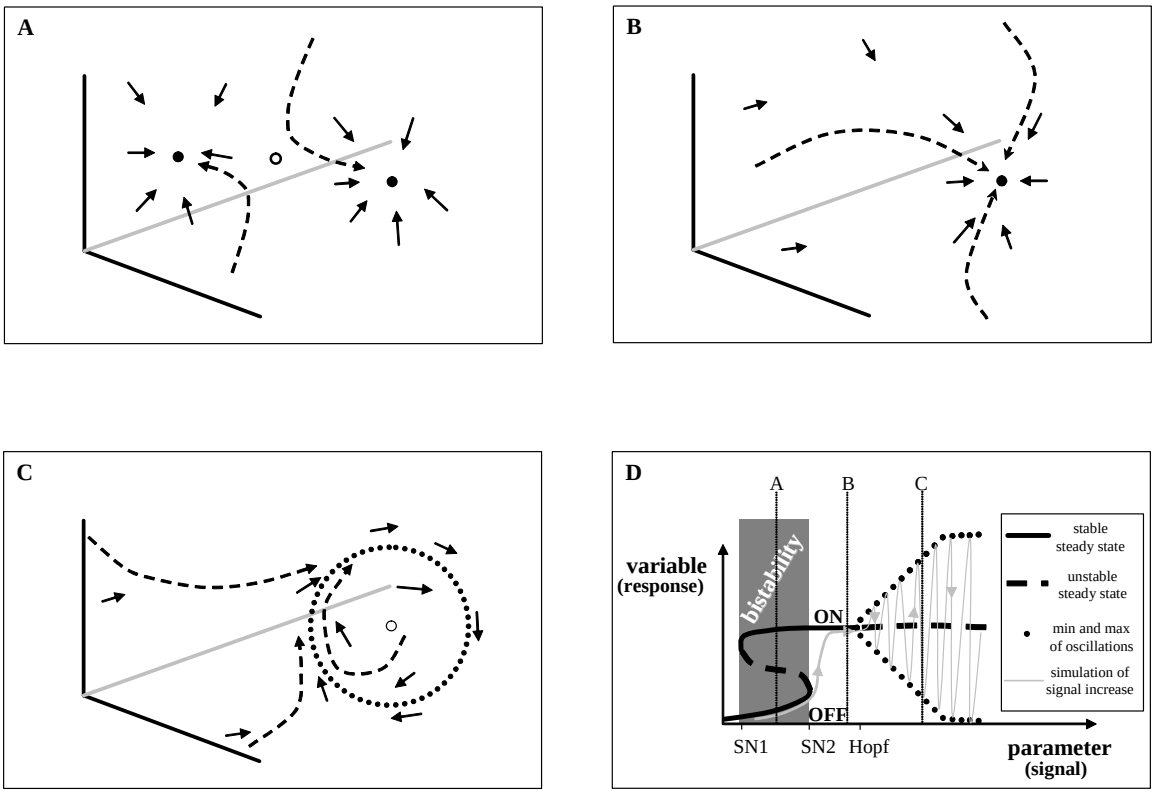

Figure 3.20. Attractors and their bifurcations. (*A*-*C*) Examples of vector fields in a three-dimensional state space. Solid arrows = vector field, dashed arrows = simulation results, filled circles = stable steady state, open circles = unstable steady state, dotted circle = stable limit cycle. (*D*) The transitions (bifurcations) between the vector fields of panels A-C are represented on a one-parameter bifurcation diagram. Solid line = locus of stable steady states, dashed line = locus of unstable steady states, black dots = maximum and minimum values of response variable on a periodic orbit, SN = saddle-node, HB = Hopf bifurcation. The light gray curve indicates a simulation of the response of the control system for a slow increase in signal strength. At SN2, the system jumps from the OFF state to the ON state, and at HB it leaves the steady state and begins to oscillate with increasing amplitude. Within the region of bistability, the control system can persist in either the OFF state or the ON state, depending on how it was prepared (a phenomenon called 'hysteresis').

Following standard conventions, we plot steady state solutions by lines: solid for stable steady states and dashed for unstable. For limit cycles, we plot two loci—one for the maximum and one for the minimum value of Cdk1/CycB activity on the periodic solution—denoting stable limit cycles with ●●● and unstable with ○○○. A locus of steady states can fold back on itself at a *saddle-node* (SN) bifurcation point (where a stable steady state—a node—and an unstable steady state—a saddle—come together and annihilate one another). Between the two SN bifurcation points in Fig. 20D, the control system is bistable (coexistence of two stable steady states, which we might call OFF and ON). To the left and right of SN2 in Fig. 20D, the state space looks like Fig. 20A and 20B, respectively. A locus of steady state solutions can also lose stability at a Hopf bifurcation (HB) point, from which there arises a family of small amplitude, stable limit cycle solutions (Fig. 20D). A Hopf bifurcation converts state space 20B into 20C. For experimental

verification of these dynamical properties of the cell cycle control system in frog eggs, see recent papers by Sha et al. (2003) and Pomerening et al. [POM03, POM05].

Positive feedback is often associated with bistability of a control system. For example, if X activates Y and Y activates X, then the system may persist in a stable OFF state (X low and Y low) or in a stable ON state (X high and Y high). Similarly, if X inhibits Y and Y inhibits X (double-negative feedback), the system may also persist in either of two stable steady states (X high and Y low, or X low and Y high). Typically, bistability is observed over a range of parameter values ($k_{SN1} < k < k_{SN2}$). Negative feedback (X activates Y which activates Z which inhibits X) may lead to sustained oscillations of X, Y and Z, for appropriate choices of reaction kinetics and rate constants. These oscillations typically arise by a Hopf bifurcation, with a stable steady state for $k < k_{HB}$ giving way to stable oscillations for $k > k_{HB}$.

In Table 7 we provide a catalog of common *codimension-one bifurcations* (bifurcations that can be located, in principle, by changing a single parameter of the system). From a one-parameter bifurcation diagram, properly interpreted, one can reconstruct the vector field (see lines A, B and C in Fig. 20D), which is the mathematical equivalent of the molecular wiring diagram. There are only a small number of common codimension-one bifurcations (see Table 7); hence, there are only a few fundamental signal-response relationships from which a cell must accomplish all the complex signal processing it requires. Of special interest to this paper is the SNIPER bifurcation, which is a special type of SN bifurcation point: after annihilation of the saddle and node, the remaining steady state is unstable and surrounded by a stable limit cycle of large amplitude. At the SN bifurcation point, the period of the limit cycle is infinite (SNIPER = *saddle-node infinite-period*). As the bifurcation parameter pulls away from the SNIPER point, the period of the limit cycle decreases precipitously.

To continue this process of abstraction, we go from a one-parameter bifurcation diagram to a two-parameter bifurcation diagram (Fig. 21). As the two parameters change simultaneously, we follow loci of codimension-one bifurcation points in the two-parameter plane. For example, the one-parameter diagram in Fig. 20D corresponds to a value of the second parameter at level 6 in Fig. 21. As the value of the second parameter increases, we track SN1 and SN2 along fold lines in the two-parameter plane. Between these two fold lines the control system is bistable. We also track the HB point in the two-parameter diagram for increasing values of the second parameter. We find that, at characteristic points in the two-parameter plane, called *codimension-two bifurcation* points), there is a change in some qualitative feature of the codimension-one bifurcations. In Fig. 21 (and Table 7) we illustrate the three most common codimension-two bifurcations: degenerate Hopf, saddle-node-loop, and Takens-Bagdanov. From a two-parameter bifurcation diagram, properly interpreted, one can reconstruct a sequence of one-parameter bifurcation diagrams (see lines 1—6 in Fig. 21), which are the qualitatively different signal-response characteristics of the control system. There are only a small number of generic codimension-two bifurcations; hence, there are limited ways by which one signal-response curve can morph into another. These constraints place subtle restrictions on the genetic basis of cell physiology.

In the one-parameter bifurcation diagram, we choose as the primary bifurcation parameter some physiologically relevant quantity (the ‘signal’) that is inducing a change in behavior (the

'response') of the molecular regulatory system. In the two-parameter diagram, we propose to use the second parameter as an indicator of a genetic characteristic of the cell (the level of expression of a particular gene, above and below the wild-type value) with bearing on the signal-response curve. In this format, the two-parameter bifurcation diagram provides a highly condensed summary of the dynamical links from a controlling gene to its physiological outcome (its phenotypes). The two-parameter diagram captures the sequence of dynamically distinct changes that must occur in carrying the phenotype of a wild type cell to the observed phenotypes of deletion mutants (at one extreme) and over-expression mutants (at the other extreme). In between, there may be novel, physiologically distinct phenotypes that could not be anticipated by intuition alone.

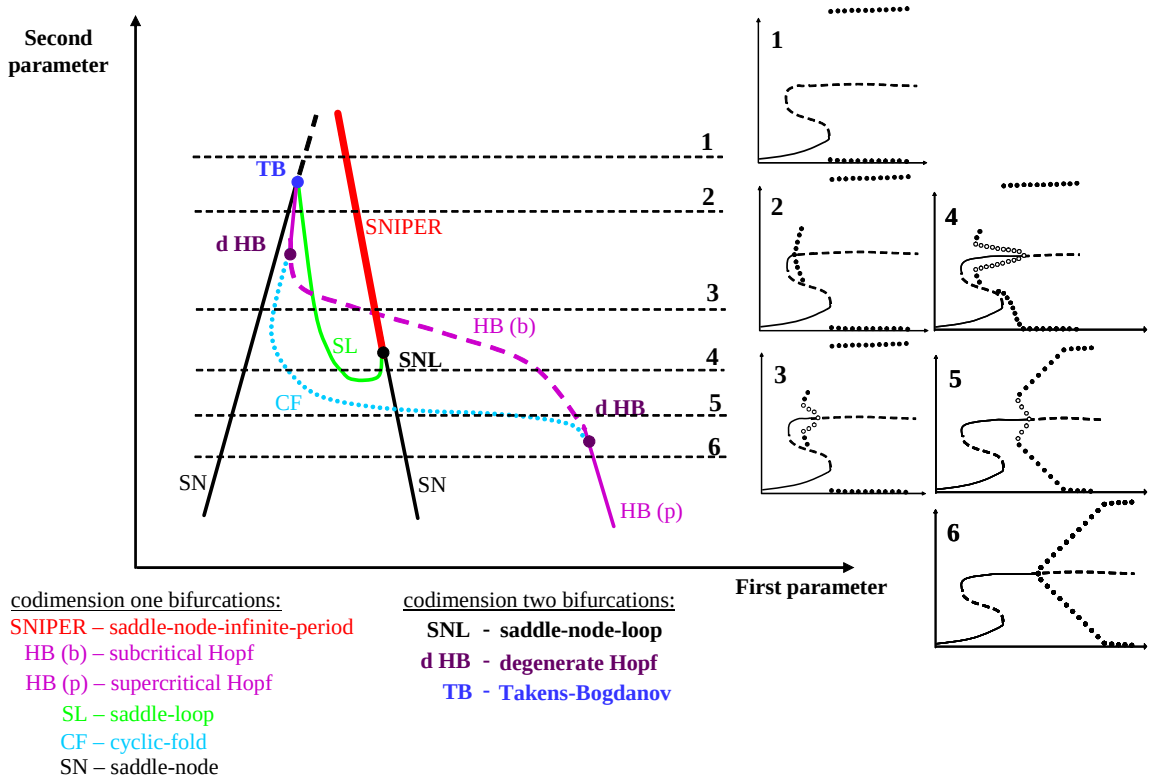

Figure 3.21. An illustrative two-parameter bifurcation diagram with one-parameter cuts (1—6). See Table 3.7 for the nomenclature of codimension–one and –two bifurcation points.

Table 3.7. Definitions and examples of codimension-one and -two bifurcations.

Codimension-one Bifurcations

full name	abbrev	from/to	to/from	1D example
saddle-node	SN	3 steady states	1 steady state	
supercritical Hopf	HBsup	1 stable steady state	unstable s.s. + small amplitude, stable limit cycle	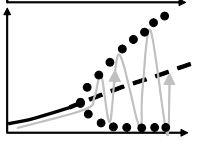
subcritical Hopf	HBsub	1 unstable steady state	stable s.s. + small amplitude, unstable limit cycle	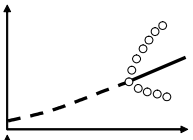
cyclic-fold	CF	no oscillatory solutions	1 stable oscillation + 1 unstable oscillation	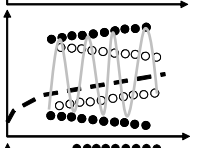
saddle-node-infinite-period	SNIPER	3 steady states	unstable s.s. + large amplitude oscillation	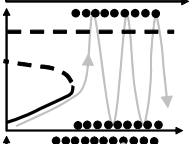
saddle-loop	SL	unstable steady state (saddle)	unstable s.s. + large amplitude oscillation	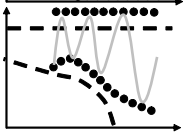

Codimension-two Bifurcations

full name	abbrev.	from/to	to/from	1D example	2D example
saddle-node-loop	SNL	SN + SL	SNIPER	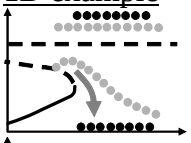	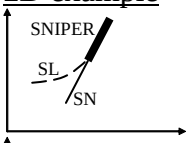
degenerate Hopf	dHB	HBsup	HBsub + CF	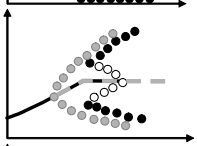	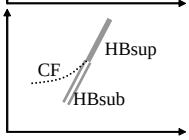
Takens-Bogdanov	TB	SN + HB + SL	SN	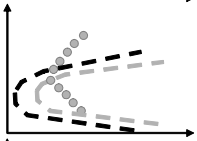	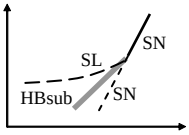
CUSP	CUSP	bistability (2 SN)	mono-stability	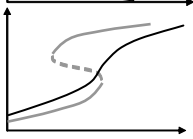	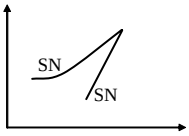

3.5 Fruit Fly Embryonic Cell Cycle

Dynamical Modeling of Syncytial Mitotic Cycles in Drosophila Embryos

L. Calzone, D. Thieffry, J. J. Tyson and B. Novak

***Molecular Systems Biology* (under revision)**

Right after fertilization, the *Drosophila* embryo undergoes a series of thirteen rapid and synchronous nuclear cycles without complete cell division. As a consequence, three hours following fertilization, 6000 nuclei share the same cytoplasm (syncytium). During these rapid nuclear cycles, DNA replication and mitoses are alternating without any observable G1 or G2 phases. The rapidity of these early cycles can be explained by an abundance of maternally supplied cell cycle components. At the end of these mitoses, some cells arrest in G2 while other cells continue to divide.

In sea urchin and frog embryos, the first 12 cell cycles are known to be driven by a cytoplasmic clock that causes periodic degradation of the cyclin B subunit of MPF as cells exit mitosis. The resultant oscillations of MPF activity control both nuclear divisions (M phase) and the characteristic surface contractions that persist even after enucleation. In contrast, in *Drosophila*, Edgar et al [EDG94] observed that total cyclin B level and MPF activity remain high (not oscillating) during the first eight cycles. After cycle eight, small fluctuations appear in both cyclin B level and MPF activity with increasing amplitude. Even though cyclin B degradation might appear negligible during these early cycles, introduction of a non-degradable form of cyclin B into a *Drosophila* embryo blocks mitotic cycles, which underlines the importance of cyclin B degradation at certain stages of the cell cycle [SU98, RAF02].

The apparent paradox surrounding cyclin B degradation during *Drosophila* embryogenesis can be resolved by assuming that cyclin B degradation occurs only locally, in the vicinity of dividing nuclei. Indeed, there is experimental evidence that cyclin B degradation takes place exclusively along the mitotic spindle [RAF02]. If the hypothesis of local cyclin B degradation is correct, then fluctuations in cyclin B level should increase as the number of nuclei increases. In this paper, we use mathematical modeling to explore whether the hypothesis of local cyclin B degradation gives an adequate description of cyclin B patterns during the first thirteen nuclear division cycles of the *Drosophila* embryo. Our model is based on an earlier mathematical description of embryonic cell cycles in *Xenopus* [NOV93]. After introducing compartmentalization and local degradation, we show that it is possible to simulate the key features of early embryonic cell cycles in *Drosophila*. The model also reproduces the effects of alpha-amanitin treatment and loss-of-function mutants.

Our model for cell cycle regulation in the early *Drosophila* embryo is diagrammed in full in Fig. 22. Using the basic principles of biochemical kinetics, we translate the diagram into a set of ordinary differential equations. The equations, which describe the time-rates of change of the fluctuating protein species in the diagram, contain a number of unknown rate constants that must be estimated by fitting the model to the available data (mutant phenotypes, responses to drug treatments, etc.).

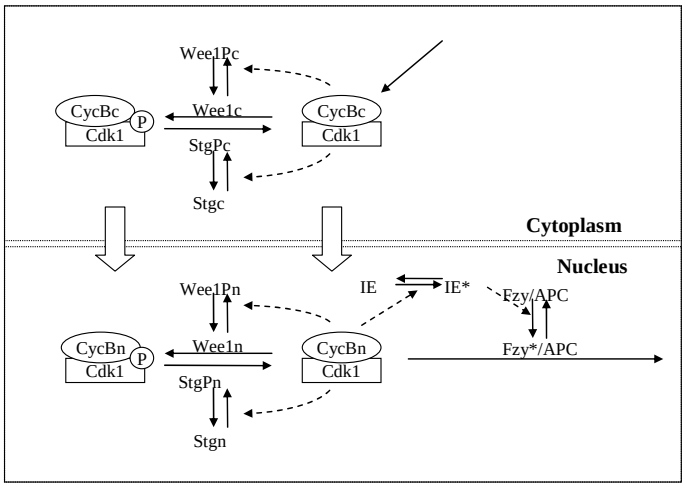

Figure 3.22. Mechanism for MPF oscillations during early embyrogenesis of *Drosophila*. Two compartments are considered: nuclei and cytoplasm. Some cytoplasmic MPF and preMPF are transferred to the nuclei, where they are degraded by Fzy. In the cytoplasm, MPF_c and $preMPF_c$ are degraded at a constant low rate (not shown).

It is known in *Drosophila* embryos that degradation of CycB occurs exclusively in the vicinity of mitotic spindles rather than throughout the whole cytoplasm, as in *Xenopus*. Consequently, we distinguish two compartments in the embryo (Fig. 22): cytoplasm and nuclei. The volume of the nuclear compartment is assumed to be the product of the number of nuclei (N) and the volume of a single nuclear compartment (V_n), *i.e.* $V_N = N \cdot V_n$. Consequently, cytoplasmic volume is $V_C = V_T(1-N\varepsilon)$, where V_T = total egg volume (constant) and $\varepsilon = V_n/V_T << 1$. It is important to point out that what we call the 'nuclear compartment' is not the volume enclosed by the nuclear envelope, because the nuclear envelope breaks down during mitosis. Nonetheless, we assume that CycB degradation during M phase occurs only in a limited region (our 'nuclear compartment') in the vicinity of the mitotic spindle. Hence, the nuclear compartment persists in separation from the cytoplasmic compartment throughout the cell division cycle. At telophase, the number of nuclear compartments doubles.

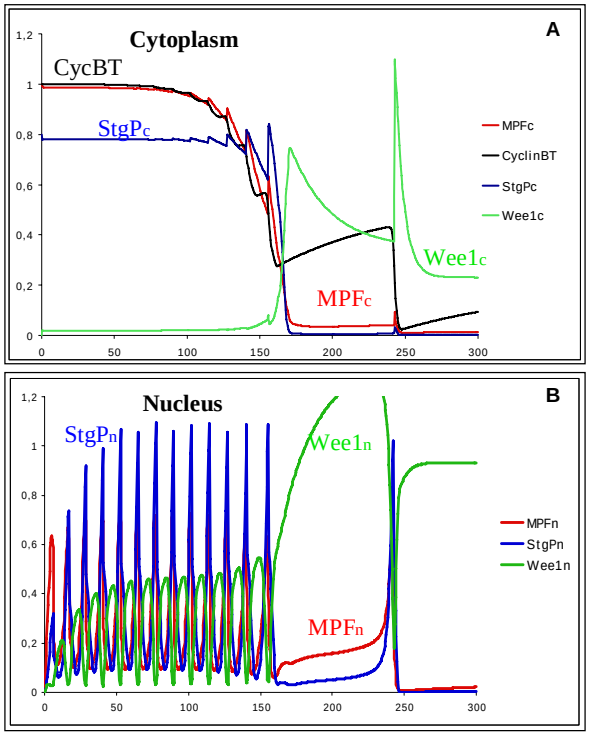

Figure 3.23. Temporal evolution of protein concentrations. MPF denotes the CycB/Cdk1 complex, whereas preMPF denotes the phosphorylated form, CycB/Cdk1-P. The total amount of String and Wee1 is constant. Both proteins are distributed over the two compartments. Fourteen oscillations driven by MPF_n precede the G2 arrest.

Figure 23 shows the results of a numerical simulation of the model with localized cyclin degradation. For this simulation, we assume no synthesis or degradation of String, and the total concentration for String is constant throughout the cycles (StringT=0.8). The initial concentration for MPF in the cytoplasm (MPF_c) is high (one arbitrary unit) and this activity suffices to keep Wee1 inactive and String active in the cytoplasm (at least initially). The first oscillations of the nuclear concentration of MPF (MPF_n) are very rapid. However, in later cycles, they tend to slow down, and finally arrest in G2 phase of the fourteenth cycle with low MPF activity. These initial cycles are so rapid because they are driven not by the synthesis of cyclins, as in *Xenopus*, but rather by nuclear import of pre-formed cytoplasmic cyclins. MPF is pre-synthesized in the cytoplasm and quickly enters into the nucleus. In the early cycles, the rate of MPF entry in the nucleus is so fast that nuclear Wee1 cannot inhibit it and, as a result, the rapid accumulation of MPF_n drives the nucleus into mitosis. These early cycles are driven by the negative feedback circuit involving MPF_n and Fzy/APC. Indeed, MPF_n indirectly (through IE) activates Fzy/APC, which destroys its CycB subunit. Since the number of nuclei and the volume of the nuclear compartment double after each mitosis, the cytoplasmic MPF (and preMPF) concentration decreases. The drop in the cytoplasmic concentration slows down the nuclear transport and thus the oscillations. As Wee1 kinase activity in the nucleus becomes more and more comparable to the nuclear entry rate of MPF, MPF molecules can be inhibited through

tyrosine phosphorylation by Wee1 kinase. MPF_n activity must reach a certain threshold in order to switch Wee1 kinase off and activate String. Since reaching this threshold takes a certain amount of time, the period of the oscillation increases. Finally, during cycle 14, the nuclear MPF concentration is not able to attain the threshold level anymore, and Wee1 remains active while String remains inactive, stopping the oscillations.

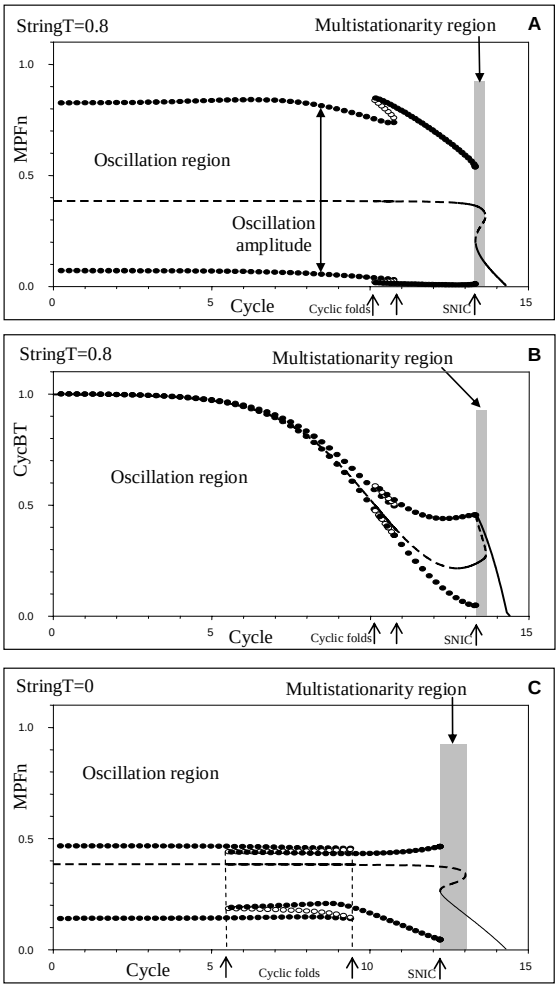

Figure 3.24. Bifurcation diagrams for the Drosophila model. **A**: MPF_n activity is plotted as a function of the cycle numbers for StringT=0.8. MPF_n shows oscillations (*i.e.* a stable limit cycles surrounding an unstable steady states) with varying amplitude for fourteen cycles; the system then arrests on a branch of stable steady states. **B**: CycBT, the total concentration of cyclin in both compartments, is also plotted as a function of the cycle numbers for StringT=0.8. The amplitude in CycBT is very small at first but starts increasing after cycle 10. **C**: MPF_n activity is plotted as a function of the cycle numbers for StringT=0. The bifurcation diagram for StringT=0 is similar to panel A except that the cycles stop earlier. The SNIC bifurcation point is moved from cycle 14 to 13.

Bifurcation diagram for the mechanism

To investigate further the behavior of the cell cycle control system with localized cyclin degradation, we introduce the notion of a one-parameter *bifurcation diagram*. This diagram

describes the stability of the dynamical control system as some key parameter (the *bifurcation* parameter) is changed. As bifurcation parameter, we introduce *C*, defined by $N = 2^C$. Hence, *C*, a real number, represents the number of division cycles (plus fractions thereof) that have transpired.

In Fig. 24, the state of the system is characterized by nuclear MPF for two different values of StringT. Dashed lines represent unstable steady states and solid lines represent stable steady states. The small circles trace the maximum and minimum excursions of the variable during limit cycle oscillations. Filled and empty circles indicate the maximum and minimum of stable and unstable limit cycles, respectively.

For very large numbers of nuclei, the control system has a single, stable steady state with low MPF_n concentration. At this steady state, MPF is tyrosine phosphorylated both in the cytoplasm and in the nuclei. This stable steady state represents a G2 arrest. When the number of nuclei is small, the system is in a region where a branch of unstable steady states is surrounded by limit cycle oscillations. These oscillations have large amplitude in MPF_n, as observed in the simulations in Fig. 23, where limit cycle oscillations can be seen for small number of nuclei. Since after every oscillation, the number of nuclei (and therefore the number of cycles) increases, we move from left to right on the bifurcation diagrams (Fig. 24). Between cycles 10 and 11 (panel A of Fig. 24 with StringT = 0.8), the limit cycle oscillations undergo a pair of 'cyclic fold' bifurcations, which indicate a qualitative change in the oscillation mechanism. For cycle numbers ≤10, the oscillations are driven by the negative feedback loop alone. For cycle numbers ≥ 11, the positive feedback loops involving MPF phosphorylation contribute to the oscillatory mechanism. These positive feedback loops become more and more significant as cycle number increases, eventually creating alternative stable steady states between cycles 13 and 14. The stable steady state with low activity of MPF_n blocks the oscillations at a SNIC bifurcation (Saddle-Node-Invariant-Circle, where the period of oscillation tends toward infinity).

Panel B of Fig. 24 shows the same bifurcation diagram with CycBT as the dynamical variable. When the number of cycles is small ($1 < C < 10$), the system oscillates with negligible fluctuations in CycBT. However, when $C > 11$, oscillations of CycB total level become noticeable as well. As the system approaches the SNIC bifurcation point, the amplitude of CycBT oscillations converges towards that of MPF_n oscillations.

Interestingly, the bifurcation diagram does not change very much in the absence of String (StringT=0, Fig. 24C), which situation corresponds to the extreme case of a maternal *string* loss-of-function mutation. The reason for this behavior is the presence of another protein phosphatase, Twine, which has an overlapping function with String. In the absence of String, the amplitude of MPF_n oscillation is slightly reduced, the overlap of the two stable limit cycles is widened, and the SNIC bifurcation point moves to a slightly smaller cycle number. Consequently, MPF_n oscillations stop in cycle 13, one cycle earlier than for StringT=0.8, in agreement with observations [EDG96]. Of course, in these mutants, the early cycles are maintained because of Twine activity, both in experiments [EDG96] and in the model.

3.6 Mammalian Cell Cycle

A Model for Restriction Point Control of the Mammalian Cell Cycle

B. Novák and J.J. Tyson

***J. Theoretical Biology*, 230:563-579 (2004)**

The molecular controls of cell division are fundamentally similar in all eukaryotes [NUR90]. Major events of the eukaryotic cell cycle are choreographed by periodic activation of several cyclin-dependent kinases (Cdks) and the enzymes and inhibitors that affect their activities. Unicellular organisms, like yeast, grow and divide as rapidly as nutritional conditions permit, but this strategy would be disastrous in multicellular organisms, for which cell growth and division must be highly constrained [HAN00]. These "social constraints" are enforced by a complex network of inhibitions on Cdk activities.

The cells of multicellular organisms proliferate only when permitted by specific growth factors. If growth factors are deprived, cells early in G1 phase leave the cycle and enter a resting state (G0); older cells finish the ongoing cycle and enter the resting state after mitosis. The point in G1, before which cells enter directly into the resting state, is called the **restriction point** [PAR89].

The goal of this paper was to understand the physiological properties of restriction point control in mammalian cells by computer simulations of a mathematical model of the underlying molecular mechanism. Zetterberg and Larsson [ZET95] have located the restriction point quite precisely 3-4 hours after cell birth, whether cell proliferation is stopped by deprivation of growth factor or by partial inhibition of protein synthesis with cycloheximide. They also measured the kinetics of re-entry into the cell cycle, when growth factors are added back or cycloheximide is washed away. They found that cells treated early in the cell cycle (before the restriction point) suffer an immediate delay of 8 hours plus the duration of the treatment; cells treated late in the cycle divide on schedule but are delayed significantly in the next division cycle; and cells treated shortly after the restriction point suffer no delay in either the first or second division cycles.

Our mathematical model explains these observations in quantitative detail by considering the interactions between cell growth and the dynamics of the Cdk regulatory system. The model emphasizes the deep similarities of the Cdk regulatory systems in yeast and mammalian cells, while also accounting for subtle interplays between "sizer" and "timer" functions characteristic of the mammalian cell cycle. In our opinion, the most promising way to understand the molecular basis of mammalian cell cycle control is to build models of social constraints (like growth factor requirements) around a yeast-like core of cyclin-Cdk interactions.

Figure 25 presents our proposed molecular circuitry for control of mammalian cell proliferation.

When proliferating cells are treated with cycloheximide (an inhibitor of protein synthesis), they stop dividing. Cells treated early in G1 stop immediately, whereas cells treated more than a few hours after division complete the current cycle and stop in G1 of the next cycle. The "point of no return" was called the restriction point by Pardee [PAR89]. In our model, the restriction point is about 3 h after division (Fig. 26B). Withdrawing growth factors from the culture medium also

shows a point-of-no-return, which seems to be identical to the restriction point for cycloheximide treatment. If growth factors are added back (or cycloheximide removed), cells re-enter the division cycle after a considerable delay.

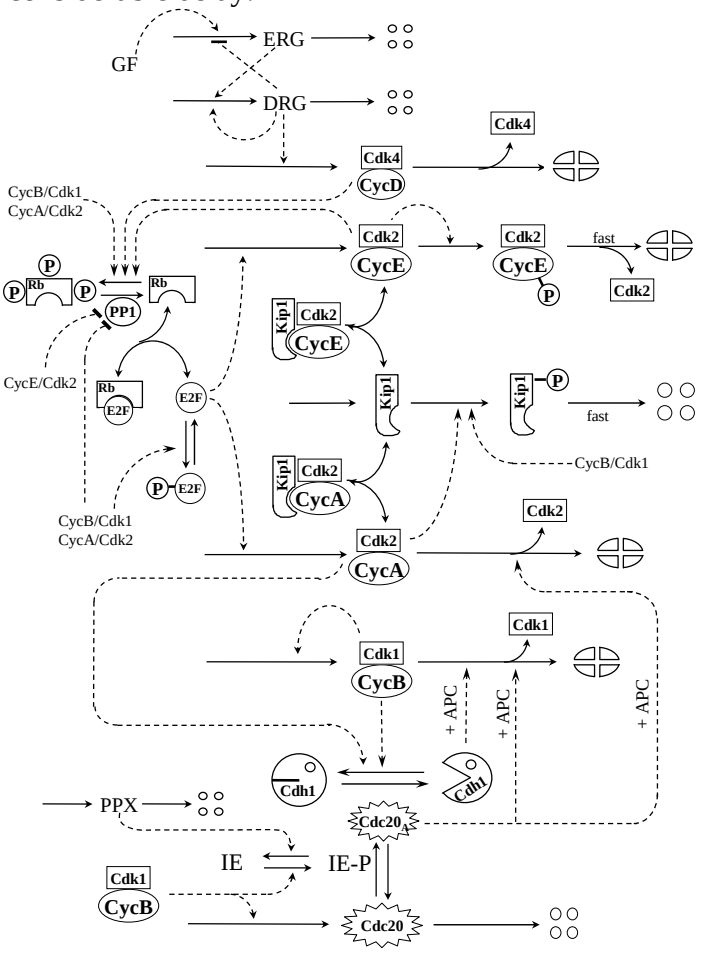

Figure 3.25. Molecular network regulating progression through the mammalian cell cycle. In the center of the diagram we propose a yeast-like cell cycle "engine" composed of Cdk2/CycE, Cdk2/CycA, Cdk1/CycB, and some ancillary proteins (Kip1, Cdh1 and Cdc20). This part of the diagram should be compared to Chen *et al.* (2000). To the engine we attach three components characteristic of mammalian cell cycle controls: (i) the retinoblastoma protein, Rb, which binds to and inhibits E2F, a transcription factor for production of CycA and CycE, (ii) the cyclin-dependent kinase, Cdk4/CycD, which phosphorylates and inactivates Rb, and (iii) the signal transduction pathway, GF-ERG-DRG, which controls CycD synthesis in response to growth factor stimulation. Although not indicated on the wiring diagram, the model includes the fact that Kip1 binds to CycD/Cdk4 but does not inhibit its activity.

To accurately measure the timing of events around the restriction point, Zetterberg and Larsson [ZET95] cultivated mouse fibroblast cells under a photomicroscope, measuring the cycle times of individual cells in response to transient deprivation of growth factor at different stages in the cycle. In continuous presence of GF, the cells divided (on average) every 14 h, spending 7 h in G1 phase and 7 h in S/G2/M. Cells that were deprived transiently of GF in the first 3 h after cell division experienced a long delay of the next cell division (delay = duration of GF deprivation + 8 h), whereas cells deprived after 4 h experienced no delay of the next division. These observations led Zetterberg and Larsson to split G1 into two subphases, G1pm and G1ps ("post mitosis" and "pre S"), with the dividing line being the restriction point at 3-4 h into G1.

Growth factor deprivation causes a general two-fold depression in the rate of protein synthesis, and this depression seems to be responsible for the characteristic cell-cycle response, because the same response is induced by a sublethal dose of cycloheximide (CHX) that causes a 50% decrease in overall rate of protein synthesis [ZET85]. For this reason, the Zetterberg-Larsson experiments are modeled by reducing the rate of translational efficiency on ribosomes to 50%. Because growth factors undoubtedly have more specific roles than general support of protein synthesis, our simulations cannot be expected to reproduce all the subtle responses of cells to GF withdrawal.

When translational efficiency drops below 0.6, the stable steady state of high DRG activity is lost and DRG is rapidly destroyed (half-life = 4 min). With DRG gone, CycD synthesis turns off, and then, because CycD is also unstable (half-life = 8 min), CycD-kinase activity disappears quickly. For cells in G1pm, when CycD/Cdk4 is the only kinase present, the loss of CycD has profound consequences. Rb cannot be inactivated and Kip1 cannot be degraded, so cells in G1pm cannot enter G1ps.

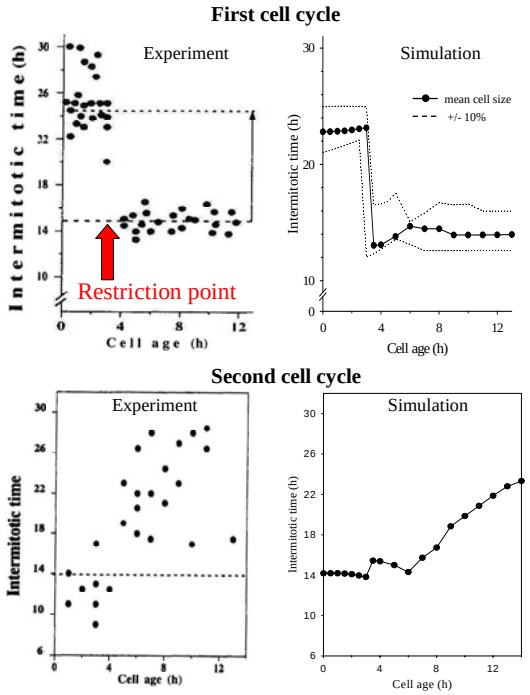

Figure 3.26. The effect on cell cycle progression of transient deprivation of growth factor or transient exposure to cycloheximide. At different time points during the cell cycle, the rate of protein synthesis was temporarily decreased from 1 to 0.5 for one hour. The lengths of the first (A) and the second cycles (B) were determined and plotted as functions of cell age at onset of the treatment, each black circle representing one simulation. These simulations should be compared to the experimental observations in [SET85], Fig. 5, and in [LAR85], Fig. 2.

Figures 27A and B show numerical simulations of one hour treatments (GF deprivation or CHX exposure), in the same format as Fig. 2 of Larsson et al. [LAR85]. Cells treated early in the cycle (age 3 h or less at the onset of treatment), experience an 8.5-9.5 h delay of their first post-treatment mitosis, but their second cycle is normal. By contrast, cells treated later in the cycle (age > 3 h) are not delayed in their first post-treatment division, but some of them experience

significant lengthening of their second mitotic cycle. By comparing Fig. 26 and Fig. 27, we see that passage through the restriction point coincides with phosphorylation of Rb.

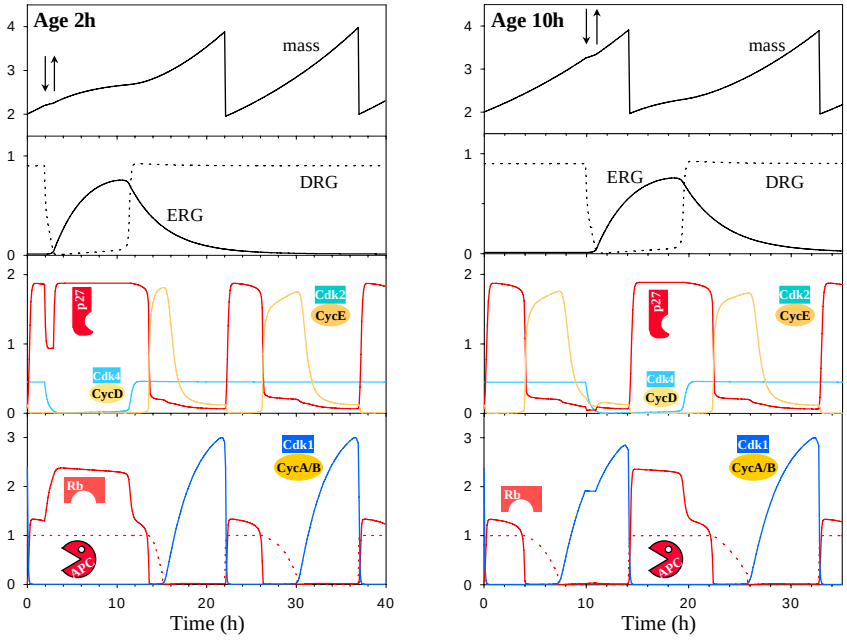

Figure 3.27. Effects of transient (1h) growth-factor deprivation at two different phases of the cell cycle.

The fixed time to reach the restriction point (3 h) is determined by the kinetic constants governing the interactions among CycD, CycE, Rb, E2F, and Kip1. During that interval, as E2F is dephosphorylated and CycD helps to phosphorylate Rb, CycE begins to form. Prior to 3 h, if CycD is lost, there is not yet enough active CycE to carry on the job of phosphorylating Rb, so E2F remains bound to Rb and inactive, and CycE synthesis shuts off. After 3 h, there is enough CycE to keep Rb phosphorylated and to destroy Kip1, even if CycD disappears.

Longer treatments leave the position of the restriction point unchanged, but the delay experienced by G1pm cells is always 7-8 h longer than the duration of treatment (calculations not shown), as observed [ZET85].

The cell-cycle model presented here is grossly simplified from what is currently known about the molecules controlling DNA synthesis, mitosis and division in mammalian cells (Kohn, 1999). However, the full regulatory circuit is much too complex to be modeled computationally at present. Just as experimental characterization of the control system proceeded from simple, incomplete diagrams to increasingly complex and realistic circuitry, so a computational representation of the system must start with a simple "skeleton," capturing the basic topology of the network, on which later can be attached the complicated details that will make realistic models of specific cell types and physiological circumstances.

Our proposal for the skeleton of the mammalian cell cycle control system (Fig. 25) is closely analogous to a model that has proved successful in accounting for most of the complexity of cell proliferation in budding yeast (Chen et al., 2000). In a whimsical sense, we are "getting in touch

with our inner yeast." That is, from the complex machinery regulating mammalian cell proliferation, we are pulling out the underlying yeast-like controls, which presumably were inherited from the earliest ancestors of the eukaryotes. Then we are asking the question: what properties of mammalian cell division can be understood in terms of the basic cell cycle controls that are common to most eukaryotic cells? One cannot expect a model at this beginning level to include everyone's favorite protein, to explain everyone's latest experiment, or even to predict some crucial experimental test of the theory. Rather, its function is to bring together in computer-readable form a reasonable picture of the basic molecular networks underlying cell division in higher vertebrates. If the skeleton is sound, it should serve as a solid framework for building more realistic, comprehensive, predictive, computational models of the future (Fig. 28).

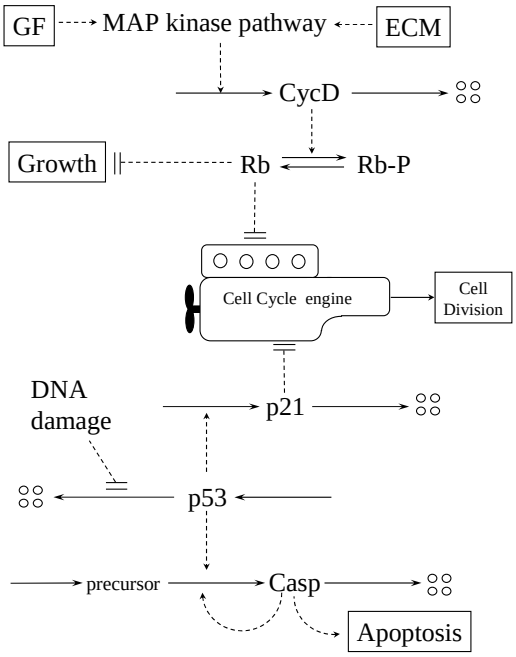

Figure 3.28. Schematic diagram of some signal transduction pathways that control mammalian cell proliferation. The "cell-cycle engine" represents the interactions involving cyclins E, A and B in Fig. 25. Progress through the cell cycle (G1 → S → G2 → M) is repressed by two major negative regulators: Rb (which inhibits the transcription of cyclin genes) and p21 (a stoichiometric inhibitor of cyclin/Cdk complexes). The "default state" is Rb "on" and p21 "off", i.e., no proliferation. In response to permissive signals from growth factor (GF) stimulation and extracellular matrix (ECM) attachments, mediated through MAP kinase pathways, the cell up regulates CycD-dependent kinase activity, which phosphorylates and inactivates Rb. Hence, these signals remove the brake on cell growth and division. Successful completion of the cell cycle depends now on "checkpoint" pathways that monitor DNA integrity (damage, incomplete replication, faulty chromosome alignment at metaphase). For example, DNA damage stabilizes a transcription factor, p53, whose accumulation drives the synthesis of p21. If the damage can be repaired, then p53 disappears, followed by disappearance of p21. If the damage cannot be repaired in a timely fashion, then a sustained high level of p53 seems to drive an irreversible activation of caspases (proteolytic enzymes that execute the cell death program).

3.7 Caulobacter Cell Cycle

Cell Cycle Control in Bacteria and Yeast: A Case of Convergent Evolution?

P. Brazhnik and J.J. Tyson

***Cell Cycle* 5:522-529 (2006)**

Superficially similar traits in phylogenetically unrelated species often result from adaptation to common selection pressures. Examples of convergent evolution are known at the levels of whole organisms, organ systems, gene networks and specific proteins. The phenotypic properties of living things, on the other hand, are determined in large part by complex networks of interacting proteins. Here we present a mathematical model of the network of proteins that controls DNA synthesis and cell division in the alpha-proteobacterium, *Caulobacter crescentus.* By comparing the protein regulatory circuits for cell reproduction in Caulobacter with that in budding yeast (*Saccharomyces cerevisiae*), we suggest that convergent evolution may have created similar molecular reaction networks in order to accomplish the same purpose of coordinating DNA synthesis to cell division. Although the genes and proteins involved in cell cycle regulation in prokaryotes and eukaryotes are very different and (apparently) phylogenetically unrelated, they seem to be wired together in similar regulatory networks, which coordinate cell cycle events by identical dynamical principles.

The aquatic gram-negative bacterium *Caulobacter crescentus* undergoes asymmetrical division producing a sessile stalked cell (ST) and a motile swarmer cell (SW) (Fig. 29a). Chromosome replication is repressed in the swarmer cell. In laboratory culture, the swarmer cell swims around for 30-45 min before it differentiates into a stalked cell and begins the cell replication cycle. A stalked cell, on the other hand, initiates a new round of the DNA replication immediately after each division and, about 90-120 min later, produces a new swarmer cell. In this paper we restrict our attention to the division cycle of a stalked cell.

Of *Caulobacter's* 3760 genes, about 550 are regulated in a cell-cycle-dependent manner [LAU00], in large part by two regulatory proteins, CtrA and GcrA, which together control the expression of 144 cell cycle regulated genes [HOL04]. CtrA upregulates the expression of many genes involved in flagella biogenesis and cell division. In addition, CtrA binds to five DNA sites that overlap with the binding sites of the replication initiation protein, DnaA, and thereby precludes a new round of DNA replication. Furthermore, CtrA inhibits the expression of GcrA, which functions as an activator of components of the replisome and the segregation machinery. Right after cell division, the level of CtrA in a stalked cell is rapidly decreasing due to DivK-promoted proteolysis (Fig. 29b). When CtrA drops sufficiently, the DNA replication origin becomes free to bind DnaA. Also the level of GcrA goes up, promoting assembly of the replication machinery, and a new round of DNA replication starts. Rising GcrA suppresses production of DnaA. Hence, DnaA has a narrow window of opportunity to initiate DNA replication: after CtrA drops but before GcrA increases significantly.

As a first step toward understanding the temporal dynamics of the genes and proteins regulating the cell cycle in *Caulobacter*, we construct a simple mathematical model of the network. From

the molecular interaction network in Fig. 29b, we propose a simpler 'wiring diagram' (Fig. 30a) that covers the major interactions among CtrA, GcrA and DivK.

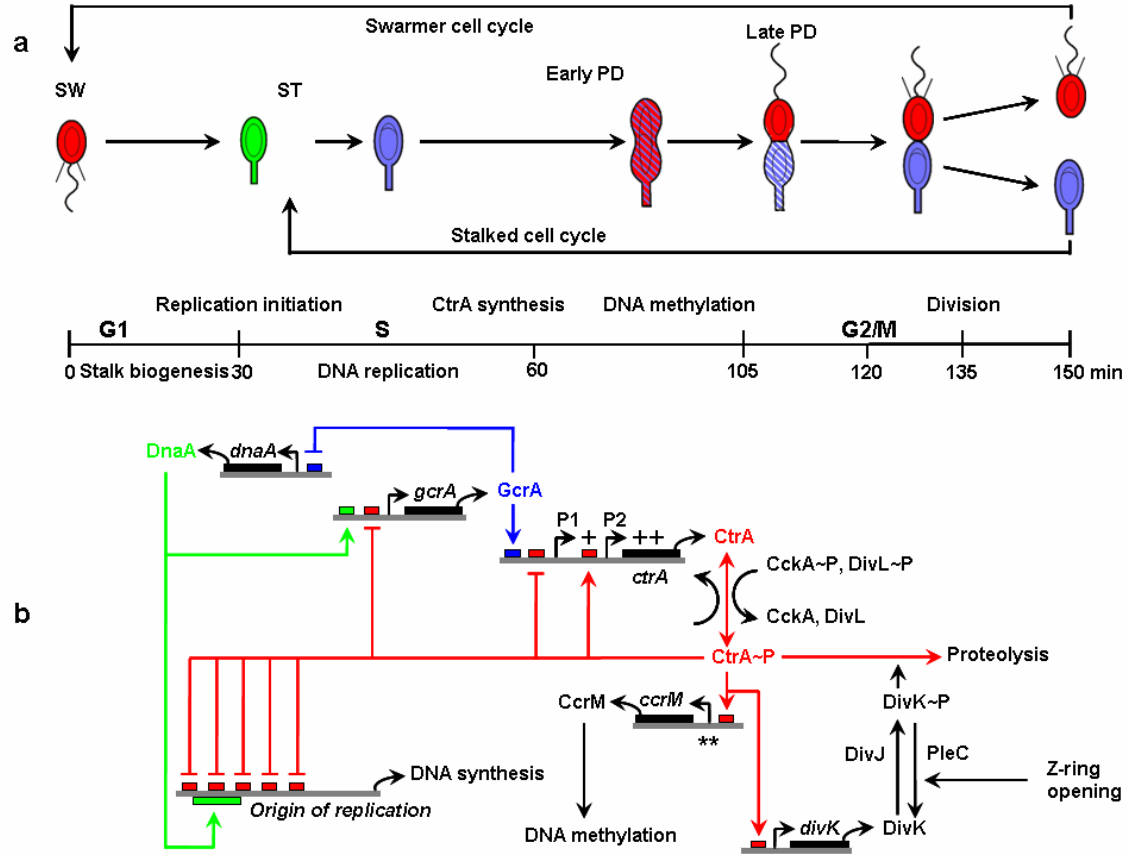

Figure 3.29. Physiology and molecular biology of the *Caulobacter* cell cycle. **a,** Sessile stalked (ST) and motile swamer (SW) cells have distinctive cell cycles. The fill-colours indicate elevated concentrations of CtrA (red), GcrA (blue) and DnaA (green). Theta structures denote replicating DNA. The time scale here is in accord with the one reported in [LAU00, HOL04]. **b,** The *Caulobacter* cell cycle regulatory network. Interactions involving CtrA, GcrA and DnaA are shown in red, blue, and green respectively. The DNA methylation by CcrM implies here that all the genes on the diagram are being methylated, this is not shown on the diagram explicitly.

For our estimated values of the rate constants, the differential equations (Table 8) yield a periodic solution for [CtrA], [GcrA], [DivK~P] , [$DivK_{tot}$] and [Z-ring], as illustrated in Fig. 31a. Figure 31b demonstrates that our simulated concentration curves correctly capture the observed time profiles of CtrA, GcrA and DivK protein concentrations. Also, the production of the CtrA protein from the terms corresponding to activities of the *ctrA* promoters P1 and P2 in the model (first two terms in the right-hand-side of Eq. 1 in Table 8) follows qualitatively the temporal expression pattern of the *ctrA* mRNA from P1 and P2 promoters observed experimentally (not shown).

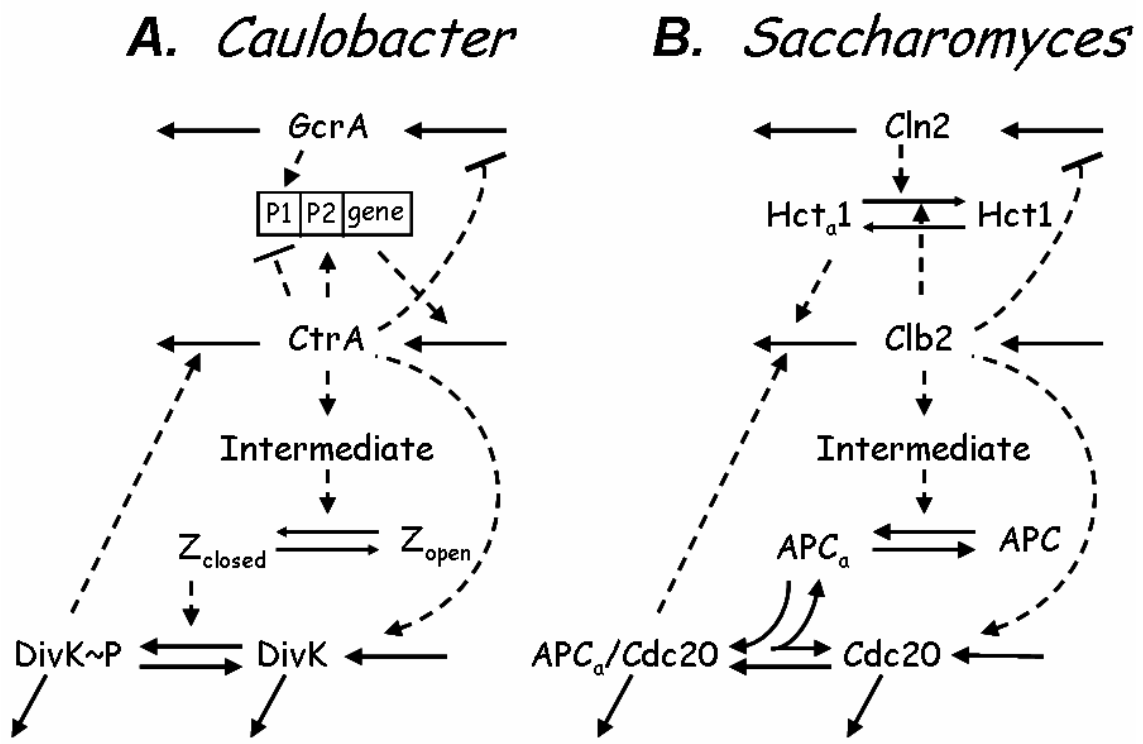

Figure 3.30. Wiring diagrams of the cell cycle control mechanism in (a) *Caulobacter crescentus* and (b) *Saccharomyces cerevisiae*. Solid arrows represent chemical reactions involving mass transfer from reactants to products, while dashed arrows indicate signalling or catalytic interactions. See text for details.

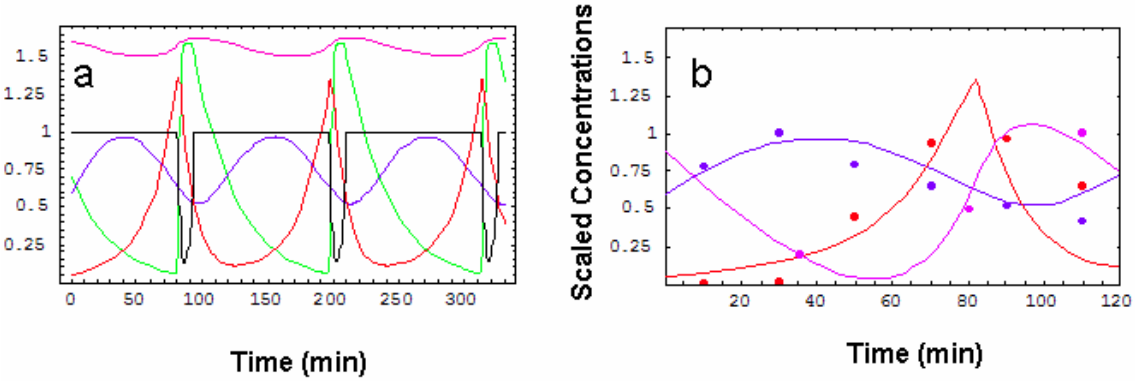

Figure 3.31. Change of the protein concentrations during the *Caulobacter* cell cycle. **a**, Time courses of scaled concentrations of CtrA (red), GcrA (blue), phosphorylated DivK (green) and total DivK (purple) proteins for three cell division cycles; Black curve shows the values of the Z-ring variable at each moment of time. **b**, Comparison of the regulatory protein profiles generated by the model (smooth curves) with experimental data (points). The experimental data for the concentrations of CtrA and GcrA are taken from Ref[3] and for total DivK from Ref[8]. In the latter case, the baseline concentration is subtracted from the model curve and only variations of $DivK_{tot}$ are compared with experimental data.

The core of the model is a master-regulator 'switch' controlling the level of CtrA protein. During the stalked-cell cycle, CtrA alternates between a state of low concentration (at the beginning of the cycle) and a state of high concentration (just before division), see Fig. 31a. These two states

can be thought of as quasi-steady states of CtrA abundance, where the rate of production of CtrA is balanced by its rate of degradation. In Fig. 32a we plot the rates of production and degradation of CtrA (as predicted by the model) as functions of CtrA concentration, for specific values of the concentrations of GcrA and DivK~P. The points of intersection of these two curves correspond to quasi-steady-state concentrations of CtrA (i.e., steady states of [CtrA] as long as [GcrA] and [DivK~P] are kept fixed). Note that the CtrA production curve is sigmoidal because of the regulatory properties of the two *ctrA* promoters. Under the conditions in Fig. 32a ([GcrA] and [DivK~P] both small), the sigmoidal production curve intersects the linear degradation curve in three places, creating two stable steady-state concentrations of CtrA separated by an unstable steady state. At the beginning of the stalked-cell cycle, [CtrA] is small, and we may think of the control system as caught in the lower stable steady state (the black button in Fig. 32a). To enter the cell cycle, [GcrA] must increase to promote DNA replication which ultimately drives CtrA to the upper steady state. In Fig. 32a, the lower steady state is lost at [GcrA] ~ 0.7, and [CtrA] must then switch over to the upper steady state. As [CtrA] rises, GcrA production is turned off and [GcrA] drops. The control system is now caught in the upper steady state in Fig. 32b. To complete the cycle, CtrA must be pushed back to the lower steady state, which is accomplished by increasing [DivK~P], as in Fig. 32b. At [DivK~P] ~ 0.4 the upper steady state is lost and [CtrA] must switch to the lower steady state.

It should be clear from Fig. 32a,b that the number of stable steady states of CtrA depends simultaneously on the concentrations of GcrA and DivK~P. The dependence is captured in Fig. 32c, where we plot a wedge-shaped region in the [GcrA],[DivK~P] plane. Inside the wedge, CtrA exhibits three steady state values (two stable, one unstable). Outside the wedge, there is a unique CtrA steady state (low [CtrA] above the wedge and high [CtrA] below the wedge). As a simulated stalked cell proceeds through the cell division cycle, it crosses back and forth across the wedge, switching first from low- to high [CtrA] to initiate the division process, and then from high- to low [CtrA] when the Z-ring closes at the end of the cycle. This progression of events is illustrated by the green line in Fig. 32c, which is a parametric plot of [GcrA](t) and [DivK~P](t) as time proceeds in the simulation in Fig. 31a. Figure 32c suggests a molecular interpretation of the numerical simulation in Fig. 31a. Start at the arrow, with [CtrA] high, [GcrA] low and [DivK~P] low. CtrA promotes closing of the Z-ring, which causes DivK to be phosphorylated in the stalked compartment. Increasing [DivK~P] pushes the CtrA switch to the 'low' position. As a result, [GcrA] now increases and DivK is steadily dephosphorylated in the young stalked cell. The increase of [GcrA] and decrease of [DivK~P] drives the CtrA control system across the wedge of bistability and eventually brings CtrA back to the high steady state. [GcrA] drops and the cell cycle trajectory returns to the arrow, where we started.

In summary, we conjecture that the CtrA circuit functions as a bistable switch that drives the cell division cycle in *Caulobacter*. The switch is flipped between its 'off' and 'on' positions by coordinated changes in GcrA and DivK. Our model shows that currently available data on the control of cell division in *Caulobacter* can be put in quantitative terms that reproduce experimentally measured time courses of key regulatory proteins and that help to explain the underlying 'logic' of the control system. This simple model provides a foundation on which more complex and realistic models, capable of guiding new experiments, can be built.

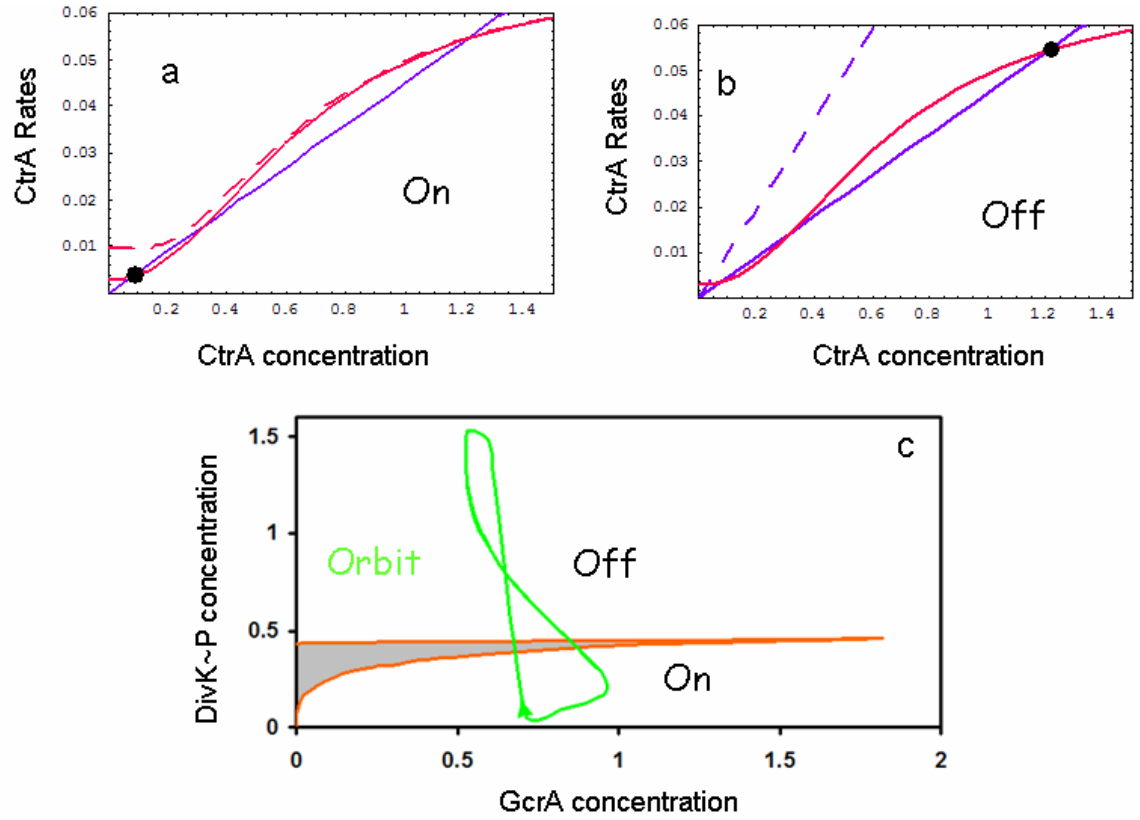

Figure 3.32. Master-regulator switch and corresponding bifurcation diagram for the *Caulobacter* model. **a-b**, Production and degradation rates for the master-regulator protein CtrA. (a) Degradation rate for [DivK~P] = 0.38 (blue solid) and production rates for [GcrA] = 0.3 (red solid) or [GcrA] = 1.0 (red dashed). (b) Production rate for [GcrA] = 0.3 (red solid) and degradation rates for [DivK~P] = 0.38 (blue solid) or [DivK~P] = 0.8 (blue dashed). **c**, Two-parameter bifurcation diagram. Shaded region = domain of bistability; "Off" = domain of low [CtrA]; "On" = domain of high [CtrA]; "Orbit" = projection of [GcrA](*t*) and [DivK~P](*t*) from Fig. 2 onto the bifurcation diagram.

The CtrA/GcrA regulatory circuitry in *Caulobacter* resembles the cyclin/cyclin-dependent-kinase (CDK) system driving cell cycle transitions in eukaryotes. To make this similarity visually apparent, we simplify an existing model of cell cycle regulation in budding yeast (Chen et al., 2000) to a level comparable with the wiring diagram proposed here for *Caulobacter*, Fig. 30b. In budding yeast, cyclins are being synthesised and degraded in each cycle while the CDK subunit is present in constant and excess abundance throughout the cycle. We retain two important cyclins in this simplified model, Cln2 and Clb2. In yeast, they play roles similar to GcrA and CtrA in *Caulobacter*. In nutrient-rich medium, cell growth turns on genes that upregulate Cln2 transcription. Accumulation of Cln2 deactivates (by phosphorylation) the Clb2-antagonist, Hct1, and thereby helps Clb2 to rise (analogous to activation of CtrA synthesis by GcrA in *Caulobacter*). Similar to the inhibitory effect of CtrA on *gcrA* expression, the transcription of *CLN2* is dramatically decreased by Clb2/CDK in S, G2 and M phases. Clb2 also contributes to deactivation of its antagonist, Hct1, which is equivalent to self-activation of CtrA synthesis by the P2 promoter. Clb2 sets the stage for exit from mitosis by activating the APC (the Anaphase Promoting Complex, which initiates separation of sister chromatids) and by upregulating the gene encoding Cdc20. Cdc20 combines with active APC to promote proteolysis of Clb2. The role of APC activation in eukaryotes parallels the action of Z-ring closure in

Caulobacter. The master regulator switch and corresponding bifurcation diagrams for budding yeast are shown in Fig. 33. Not only are the regulatory networks of *Caulobacter* and *Saccharomyces* topologically similar (Fig. 30) but also the dynamical characteristics of the control systems are nearly identical (compare Figs. 32 and 33). Nonetheless, the genes and proteins that constitute these two networks bear no obvious evolutionary relation to one another by common descent. Hence, the similar topologies and dynamics of these control networks appear to be an example of convergent evolution.

Well-known examples of convergent evolution are multiple origins of wings and eyes, and the streamlined bodies of fish, dolphins and penguins. At the molecular level, functionally similar but distinct antifreeze proteins in divergent species of fish are recognized as examples of convergent evolution. In all these cases, it is clear that the phylogenetically unrelated organisms are responding in analogous ways to similar selection pressures. If the regulatory circuits for cell reproduction in *Caulobacter* and *Saccharomyces* provide an example of convergent evolution in network design and function, what might be the common selective pressures on the networks? We suggest that the two lineages are responding to a common constraint on cell cycle regulation, namely that the control system execute a robust and repetitive sequence of irreversible transitions from an uncommitted state (pre-replication, called ‘G1’ in eukaryotes) to a committed state (DNA replication, segregation of replicated DNA molecules) and then back to the uncommitted state (cell division). For both prokaryotes and eukaryotes (as far as *Caulobacter* and *Saccharomyces* are representative), we propose that this pattern is achieved by driving a bistable control system back and forth across the region of bistability.

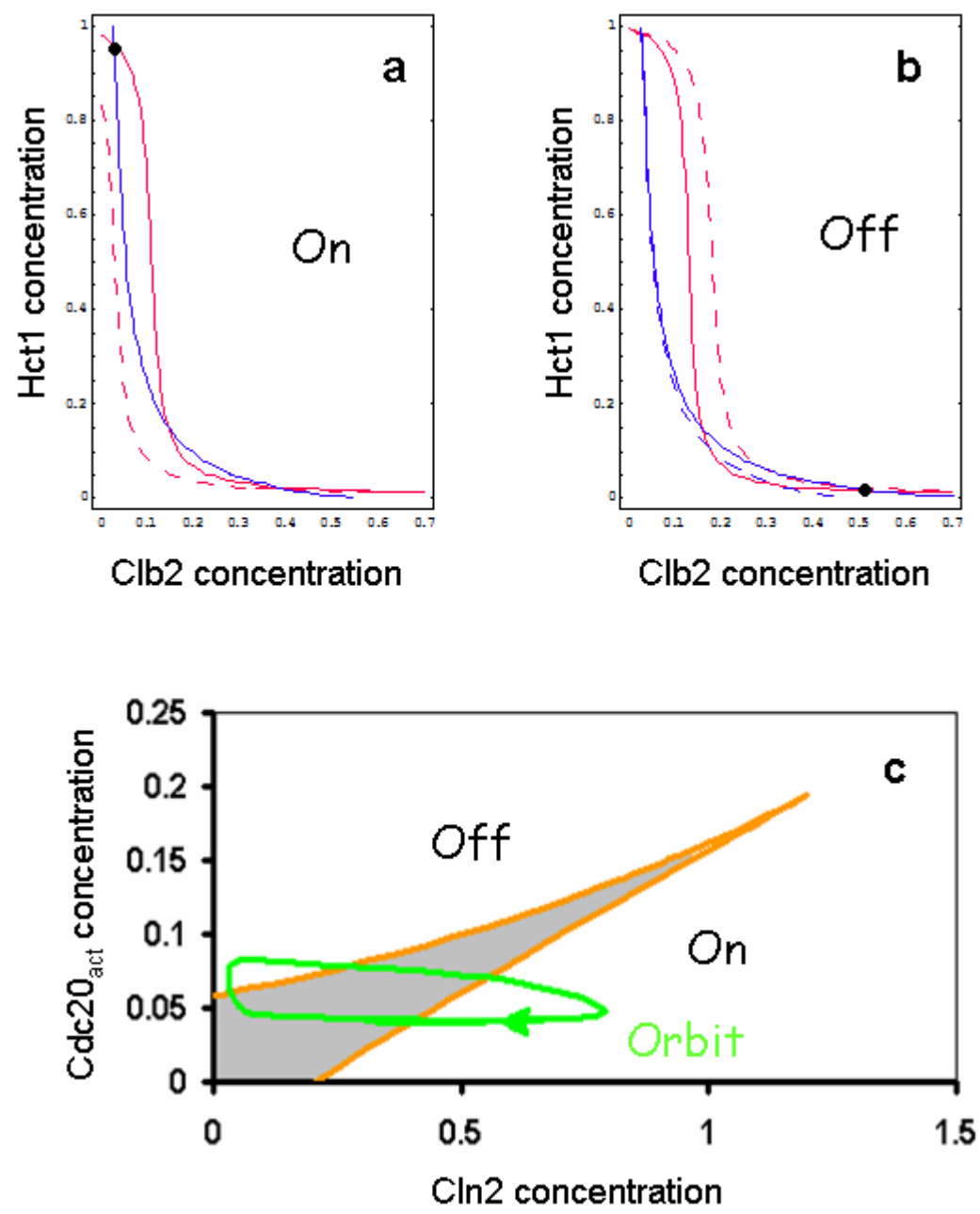

Figure 3.33. Master-regulator switch and corresponding bifurcation diagrams for the *Saccharomyces* model. **a,b** Nullclines in the phase space (Hct1, Clb2) are shown for different values of $Cdc20_{act}$ and Cln2. ('Hct1' and 'Cdh1' are two different names for the same protein.) (a) $[Cdc20]_{act}$ = 0.07, [Cln2] = 0.3 (blue and red solid) and $[Cdc20]_{act}$ = 0.07, [Cln2] = 0.7 (blue solid and red dashed). (b) $[Cdc20]_{act}$ = 0.04, [Cln2] = 0.05 (red and blue solid) and $[Cdc20]_{act}$ = 0.09, [Cln2] = 0.05 (red and blue dashed). **c**, Two-parameter bifurcation diagram. Shaded region = domain of bistability; "Off" = domain of low [Clb2]; "On" = domain of high [Clb2]; "Orbit" = projection of [Cln2](*t*) and $[Cdc20]_{act}(t)$ onto the bifurcation diagram.

Table 3.8. Differential equations for the Caulobacter cell cycle model

$$\frac{d[\mathrm{CtrA}]}{dt} = \frac{k_1^{'} \cdot J_1^2 \cdot [\mathrm{GcrA}]}{J_1^2 + [\mathrm{CtrA}]^2} + \frac{k_1^{''} \cdot [\mathrm{CtrA}]^2}{L_1^2 + [\mathrm{CtrA}]^2} - \left(k_2^{'} + \frac{k_2^{''} \cdot [\mathrm{DivK{\sim}P}]^2}{J_2^2 + [\mathrm{DivK{\sim}P}]^2} \right) \cdot [\mathrm{CtrA}], \quad (1)$$

$$\frac{d[\mathrm{GcrA}]}{dt} = \frac{k_3 \cdot J_3^2}{J_3^2 + [\mathrm{CtrA}]^2} - k_4 \cdot [\mathrm{GcrA}], \quad (2)$$

$$\frac{d[\mathrm{I}]}{dt} = k_5 \cdot [\mathrm{CtrA}] - k_6 \cdot [\mathrm{I}], \quad (3)$$

$$\frac{d[\mathrm{Zring}]}{dt} = \frac{k_7 \cdot (1 - [\mathrm{Zring}])}{J_7 + (1 - [\mathrm{Zring}])} - \left(k_8^{'} + k_8^{''} \cdot \left(\frac{\mathrm{I}}{L_8} \right)^4 \right) \cdot \frac{[\mathrm{Zring}]}{J_8 + [\mathrm{Zring}]}, \quad (4)$$

$$\frac{d[\mathrm{DivK}]}{dt} = k_9 \cdot [\mathrm{CtrA}] + k_{10} \cdot [\mathrm{DivK{\sim}P}] - k_{11} \cdot (1 - [\mathrm{Zring}]) \cdot [\mathrm{DivK}] - k_{12} \cdot [\mathrm{DivK}], \quad (5)$$

$$\frac{d[\mathrm{DivK{\sim}P}]}{dt} = -k_{10} \cdot [\mathrm{DivK{\sim}P}] + k_{11} \cdot (1 - [\mathrm{Zring}]) \cdot [\mathrm{DivK}] - k_{12} \cdot [\mathrm{DivK{\sim}P}]. \quad (6)$$

3.8 Circadian Rhythm

A Proposal for Robust Temperature Compensation of Circadian Rhythms

C.I. Hong, E.D. Conrad & J.J. Tyson
***Proc. Natl. Acad. Sci. U.S.A.* (in press)**

The internal circadian rhythms of cells and organisms coordinate their physiological properties to the prevailing 24-hour cycle of light and dark on earth. The mechanisms generating circadian rhythms have four defining characteristics: they oscillate endogenously with period close to 24 h, entrain to external signals, suffer phase shifts by aberrant pulses of light or temperature, and compensate for changes in temperature over a range of 10^{o}C or more. Most theoretical descriptions of circadian rhythms propose that the underlying mechanism generates a stable limit cycle oscillation (in constant darkness or dim light), because limit cycles quite naturally possess the first three defining properties of circadian rhythms. On the other hand, the period of a limit cycle oscillator is typically very sensitive to kinetic rate constants, which increase markedly with temperature. Temperature compensation is therefore not a general property of limit cycle oscillations but must be imposed by some delicate balance of temperature dependent effects. 'Delicate balances', however, are unlikely to be robust to mutations. On the other hand, if circadian rhythms arise from a mechanism that concentrates sensitivity into a few rate constants, then the 'balancing act' is likely to be more robust and evolvable. We propose a switch-like mechanism for circadian rhythms that concentrates period-sensitivity in just two parameters, by forcing the system to alternate between a stable steady state and a stable limit cycle.

Since the breakthrough discovery of the *period* (*per*) gene by Konopka and Benzer in 1971 [KON71], molecular biologists have identified many new circadian rhythm genes and have uncovered a complex network of interacting feedback loops which comprise the control system. In the consensus view, an endogenous daily rhythm is created by a negative feedback loop whereby the PERIOD (PER) protein inhibits its own expression by interfering with transcription factors [GOL95]. The time-delayed negative feedback loop generates limit cycle oscillations with many properties characteristic of physiological daily rhythms, except for one: the autonomous circadian period (T) is quite insensitive to variations of the kinetic constants, a property that is not characteristic of generic limit cycle oscillators. This insensitivity shows up in two ways: T varies little among individual organisms even though individuals show considerable genetic and/or proteomic variability that translates into variations of kinetic parameters, and T is temperature compensated, even though kinetic constants are strongly temperature dependent. Physiologically, this robustness of the period ($T \approx 24$ h despite genetic variability and environmental fluctuations) is essential to circadian physiology. If the autonomous period of the clock drifts too far from 24 h, then the circadian would not reliably entrain to the external 24 h light/dark zeitgeber.

Rate constants depend on temperature (θ) according to Arrhenius' law, $k_i = \alpha_i e^{-E_i/R\theta}$, where R is the universal gas constant, α_i determines the value of k_i at θ = 298 K, and E_i is the activation

energy of the i^{th} reaction. Ruoff et al. [RUO97] pointed out some years ago that a limit cycle oscillator would be temperature compensated if, according to the chain rule,

$$\frac{\mathrm{d}T}{\mathrm{d}\theta} = \sum_i \left(\frac{\partial T}{\partial k_i} \cdot \frac{\partial k_i}{\partial \theta} \right) = \frac{1}{R\theta^2} \sum_i \left(\frac{\partial T}{\partial k_i} \cdot k_i E_i \right) \cong 0, \qquad (3.5)$$

This sum is a balance of positive and negative terms (because $\partial T / \partial k_i$ is + for some *i* and – for others), and it can always be set close to zero by choosing a suitable set of activation energies. If Ruoff's balance-hypothesis is correct, we would expect that most mutations of circadian rhythm genes (which change kinetic constants and activation energies in the underlying control system) are likely to disrupt this balance and, therefore, to exhibit failures in temperature compensation of the circadian rhythm. As expected, there are mutants with defective temperature compensation in both *Neurospora crassa* and *Drosophila melanogaster*. But more intriguingly, 60-70% of all circadian rhythm mutations in these organisms leave temperature compensation intact. In order for temperature compensation to survive in the face of a variety of mutations at many different places in the mechanism, many terms in the balance equation must be negligible, i.e. $\partial T / \partial k_i \cdot k_i E_i \cong 0$ for many *i*. It is unlikely that $E_i \cong 0$ for many kinetic constants, leading us to the conclusion that $\partial T / \partial k_i \cong 0$ for many k_i's. Hence, the mechanism of circadian rhythms must somehow generate a 24 h period independently of the precise values of many of the rate constants in the mechanism. We suggest that temperature compensation is not the result of a delicate balance of opposing influences of all the rate constants in the mechanism, but rather that temperature compensation is embedded directly in the molecular machinery.

Consider the simple model in Box 1, which supplements the basic negative feedback loop (PER protein inhibits its own production by interfering with factors that promote *per* gene transcription) with a positive feedback loop (PER protein inhibits its own degradation by forming homodimers that are less susceptible to proteolysis). The interplay between these feedback loops creates the potential for the control system to switch between a stable steady state of low PER abundance and a limit-cycle oscillation during which PER protein reaches very high abundance. To see this switching potential, we plot in Fig. 34 a one-parameter bifurcation diagram for the differential equations (Box 1) describing *per* mRNA and protein dynamics. As a function of translational efficiency, v_p, we plot $[PER]_{ss}$, the steady state concentration of total PER protein (the S-shaped curve), and $[PER]_{max}$ and $[PER]_{min}$ during limit cycle oscillations. Limit cycles are found for v_p values between 3.28 and 72. At $v_p = 72$, limit cycles arise by a Hopf bifurcation (small amplitude, finite frequency); at $v_p = 3.28$, they arise by a SNIC bifurcation (Saddle-Node on an Invariant Circle: small frequency, finite amplitude). For a small range of translational efficiencies, $2.98 < v_p < 3.28$, the control system has three steady state solutions (one stable and two unstable).

Box 1: A simple model of PER dynamics

To illustrate the resetting hypothesis, we use a two-variable model of the dynamics of *per* mRNA (M) and total PER protein (P_T) described in an earlier publication [TYS99]. We assume that PER molecules exist in monomeric and dimeric states, in equilibrium,

$$P_T = [\mathrm{PER}_{\mathrm{total}}] = [\mathrm{PER}_{\mathrm{monomer}}] + 2\,[\mathrm{PER}_{\mathrm{dimer}}],\ \frac{[\mathrm{PER}_{\mathrm{monomer}}]}{[\mathrm{PER}_{\mathrm{total}}]} = q = \frac{2}{1+\sqrt{1+8K_{eq}P_T}}\,.$$

The dimeric form enters the nucleus and inhibits transcription of the *per* gene

$$\frac{\mathrm{d}M}{\mathrm{d}t} = \frac{v_m}{1+\left(\frac{P_T(1-q)}{2P_{crit}}\right)^2} - k_m M$$

$$\frac{\mathrm{d}P_T}{\mathrm{d}t} = v_p M - \frac{k_{p1}P_T q + k_{p2}P_T}{J_p + P_T} - k_{p3}P_T$$

In addition to 'background' degradation of PER (the term $-k_{p3}P_T$), there is additional degradation associated with phosphorylation of PER by a kinase called DBT (*doubletime*). We assume that DBT phosphorylates PER monomers faster than PER dimers.

The resetting hypothesis.
At this point, the usual approach would be to choose v_p in the oscillatory region, say $v_p = 30$, and model circadian rhythms as a limit cycle oscillation. The resetting hypothesis is more subtle: it posits (in this case) that *per* mRNA translation rate is not constant but a regulated variable of the mechanism (more on this assumption later). That is, v_p is re-interpreted as a time-dependent variable rather than a rate constant. Suppose that $v_p(t)$ starts at a value < 3.28 and increases exponentially, i.e., $\mathrm{d}v_p/\mathrm{d}t = \mu \cdot v_p$, for some constant value of μ. As long as $v_p < 3.28$, the control system is attracted to the stable steady state with low [PER]. But when v_p passes through the SNIC bifurcation point, the stable steady state is lost and the control system begins an oscillation in [PER]. We assume that when [PER] drops below a threshold level, v_p is reset by a factor $\sigma <$ 1, which brings v_p back below 3.28 (see that dash-dot curve in Fig. 34). In Fig. 35 we display endogenous oscillations of the resetting mechanism, plotting *per* mRNA, protein and v_p as functions of time.

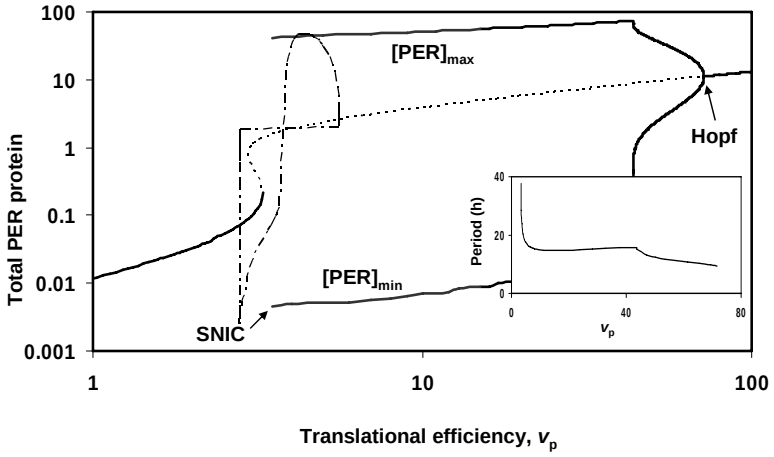

Figure 3.34. One-parameter bifurcation diagrams for the circadian rhythm model. Differential equations given in Box 1. Parameter values: v_m=2, k_m=0.2, k_{p1}=53.36, k_{p2}=0.06, k_{p3}=0.2, K_{eq}=1, P_{crit}=0.6, J_p=0.05. For each value of the bifurcation parameter, v_p, we plot the value of [PER] on recurrent solutions of the differential equations (steady states and limit cycle oscillations). Solid curve = stable steady state; dashed curve = unstable steady state. Curves labeled $[PER]_{max}$ and $[PER]_{min}$ indicate the range of an oscillatory solution at fixed value of v_p. At the Hopf bifurcation, the steady state changes stability and small amplitude, stable limit cycle oscillations arise. At the SNIC bifurcation, two steady states (a stable node and an unstable saddle) annihilate each other and are replaced by a large amplitude limit cycle. As the inset in panel A shows, the period of oscillation at the SNIC bifurcation is infinite, but drops quickly to a value of about 15 h. Superimposed on the bifurcation diagrams are the trajectories (— • —) generated by the resetting hypothesis (see text). Although the locations of the bifurcation points depend strongly on parameter values, as do the shapes of the resetting trajectories (— • —), the period of the two trajectories is precisely 24 h.

In the resetting model, the period of the oscillation is given exactly by $T = \mu^{-1} \cdot \ln \sigma^{-1}$. Temperature compensation requires only that we balance the effects of μ and σ, $\frac{dT}{d\theta} = \frac{1}{\mu} \cdot \left[\ln \sigma \cdot \frac{d \ln \mu}{d\theta} - \frac{d \ln \sigma}{d\theta} \right] \cong 0$; the other rate constants in the mechanism may change considerably as a consequence of mutation without disturbing this balance. For instance, the period of oscillation (T = 24.07 h) is unchanged by a two-fold increase or decrease of any rate constant in the mechanism, except μ and σ (naturally) and k_m. (If k_m is decreased below 0.17, then [PER] never drops below the threshold value, so v_p is never reset; v_p increases to some large value and the control system settles onto a stable steady state.)

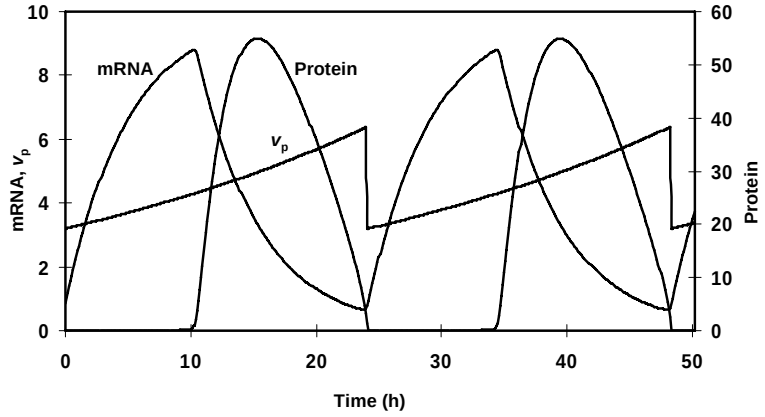

Figure 3.35. Time courses of *per* mRNA and protein, and the resetting parameter, v_p, for the mechanism described in the text. Parameter values as in Fig. 34, plus P_{thresh}=2, μ=0.0288, σ=0.5.

General requirements for resetting.
The resetting mechanism does not depend on the specific assumptions we introduced to compute Fig. 34 or to make v_p (the translational efficiency of *per* mRNA) increase and decrease. It relies instead on having a regulatory network of sufficient richness to generate a bifurcation that carries the system from a stable steady state to a large amplitude oscillation, and on having a re-settable parameter that can carry the control system back and forth across the bifurcation. Both SNIC bifurcations and subcritical Hopf bifurcations [KUZ98] are suitable for this purpose, and they are both commonly observed in regulatory networks with positive and negative feedback.

For resetting to be consistent with a 24 h clock, the period of oscillation close to the bifurcation point must be less than 24 h, because the control system needs to spend some part of the 24 h cycle on the branch of stable steady states and the rest of the cycle traversing (part of) the limit cycle. This would seem to be a problem for a SNIC bifurcation because the period of the limit cycle oscillation diverges to infinity as the bifurcation parameter approaches the bifurcation point. However, it is often the case that the period of oscillation decreases rapidly as the bifurcation parameter moves away from a SNIC bifurcation, and so it is possible to satisfy the timing requirement. In our case, for v_p increasing beyond 3.28, the period drops precipitously to a value of about 15 h (Fig. 34, inset). Hence, the amount of time necessary for [PER] to increase to its maximum value and then drop again below the threshold, when v_p increases above 3.28, is about 12 h. The control system spends about half the day in the stable steady state region and the other half in the oscillatory region (Fig. 35). If the minimum period of oscillations in this region is larger than about 20 h, then the resetting mechanism will not maintain simple periodic repetitions of 24 h.

These bifurcations are generic (their existence does not depend on delicate mechanistic assumptions), and many different parameters in the mechanism are candidates for the resetting role.

In summary, we have found that Ruoff's equation is not robust to mutation if it requires delicate balancing of many rate constants in a limit cycle model for the circadian rhythm mechanism. We propose that temperature compensation and other indicators of the robustness of circadian period to genetic variation are more likely the results of a molecular mechanism for which only a few control parameters significantly affect the period of oscillation, and we suggest a resetting hypothesis as a candidate mechanism. Resetting works by moving an effective rate constant back and forth across a SNIC bifurcation. SNIC bifurcations are common features of regulatory networks with both positive and negative feedback loops, of which the circadian machinery is richly endowed. In general, many different rate constants in the mechanism can serve the resetting role.

4.0 Details of Key Accomplishments in Experimental Testing

4.1 Budding Yeast Cells

The molecular machinery of eukaryotic cell cycle control is known in more detail for budding yeast, *Saccharomyces cerevisiae*, than for any other organism [MEN98], (Chen et al., 2000). Molecular biologists have painstakingly dissected and characterized individual components and their interactions to derive a consensus picture of the regulatory network (Fig. 3.1). Some years ago, Chen et al. (2000) published a thorough computational exploration of this model. The model, developed in collaboration with Fred Cross, consists of about 35 differential and algebraic equations for the regulatory protein species and their complexes (some of which are indicated in Fig. 3.1). The governing equations contain more than 100 parameters (kinetic constants) that must be estimated.

The model has been verified in three specific ways. First of all, it must be consistent with the phenotypes of over 100 mutants that have been constructed and characterized by deleting or over-expressing the genes that code for all the components of the mechanism singly and in myriad combinations. To test for consistency, we define a "basal" parameter set, presumed to describe wild-type budding yeast cells. The solution of the governing equations with this parameter set must be consistent with the physiology of wild-type cells: for example, durations of the unbudded and budded phases of the cell cycle, size of the cell at the onset of DNA synthesis and at division, and the relative amounts of key regulators in the cell at different stages in the cycle. Next, for each mutant, we are allowed to change only certain parameters in specific directions. For instance, if the gene for Cln2 is deleted, then we must set the rate constant for Cln2 synthesis to zero. If the Clb2-gene is engineered to remove the amino acid sequence in Clb2-protein recognized by Cdc20 and Cdh1, then we must set to zero the rate constants characterizing Cdc20- and Cdh1-dependent degradation of Clb2. All other parameters in the basal set must remain as is. When the governing equations are solved with a "mutant" parameter set, the model must be consistent with the observed phenotype of that particular mutant. For example, the Cln2-deletion mutant is perfectly viable, but it is large and bud emergence is significantly delayed. Over-expression of the Clb2-degradation deficient gene renders cells inviable, blocked in late anaphase (chromosomes separated but cell undivided). Phenotypic details of the 125 mutants in our data set provide considerable constraints on the 100-dimensional parameter space, allowing us to estimate all the parameters in the model and to test the accuracy and sufficiency of the wiring diagram. These estimated values are predictions of the model, yet to be tested. In addition, the model can be used to predict the phenotypes of specific mutants that have not yet been constructed.

Progress through the yeast cell cycle is closely linked to cell size [JOH76]. In the model, this link is forged by an assumption that Cdk1-cyclin dimers accumulate in the nucleus of the cell, achieving intra-nuclear concentrations that are proportional to total cell size (total number of ribosomes). Miller and Cross [MIL01] have tested this crucial assumption of the model by manipulating the "nuclear localization signals" on Cln proteins. By increasing or decreasing the targeting of Clns to the nucleus, Miller and Cross made cells smaller or larger, respectively, as predicted.

The third test concerns bistability in the budding yeast cell cycle control system. As Chen et al. (2000) pointed out, the antagonism between the Clb-dependent kinases (Cdk1-Clb2 and Cdk1-Clb5) and their enemies (Sic1 and Cdh1) creates two, coexisting, stable steady states (see Fig. 1): a "G1" state (low activities of the Clb-dependent kinases and high activities of their enemies) and a "S-G2-M" state (vice versa). Transitions between these two states are driven by "helper" proteins, Cln2 and Cdc20-Cdc14 (Fig. 1). Early in the cell cycle, rising activity of Cdk1-Cln2 destabilizes the G1 state and forces the transition to the S-G2-M state. Physiologists call this transition "Start". At the end of the cycle, activation of Cdc20 and Cdc14 destabilize the S-G2-M state and force the transition back to G1 (called "Finish" or "exit from mitosis"). Cross et al. (2002) tested this prediction of the model with an engineered strain of budding yeast that allowed them to control precisely the relative activities of Cln-dependent kinases and of Cdc14. They showed that, with both activities = 0, the control system could stably arrest in either G1 or M phase of the cell cycle, depending on which transition was last induced (Fig. 2).

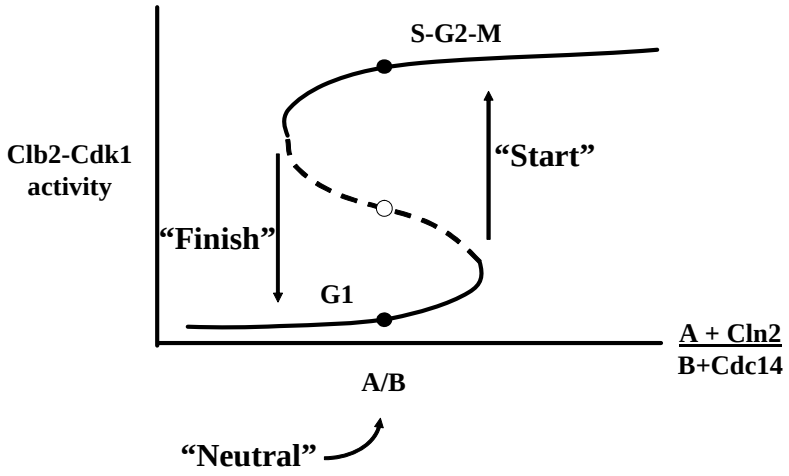

Figure 4.1. Bistability in a mathematical model of the budding yeast cell cycle. Chen et al. (2000) predicted that the activity of Cdk1-Clb2 should show an S-shaped dependence on the combined activities of the Start-promoters (Cln2- and Cln3-dependent kinases) and the Finish-promoters (Cdc20 and Cdc14). When the promoters are absent, the control system is in the "neutral" position (A/B in the figure) and may persist indefinitely in either G1 phase (low Clb2-dependent kinase activity) or M phase (high Clb2 activity). This hand-drawn bifurcation diagram was confirmed by numerical computations in Battogtokh & Tyson (2004).

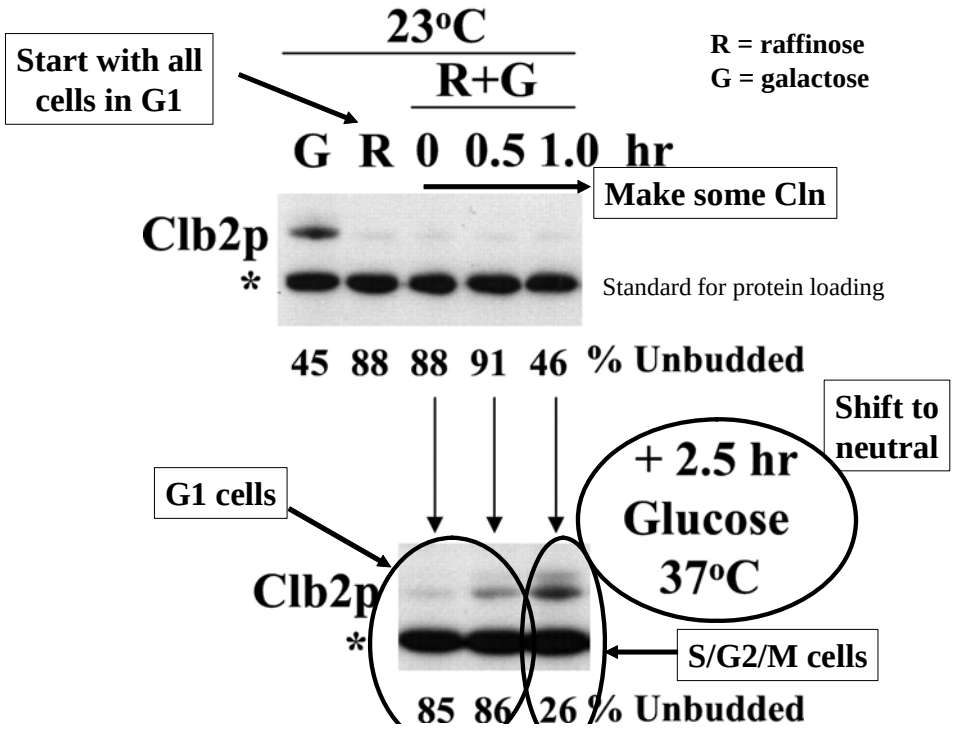

Figure 4.2. Experimental confirmation of bistability in the budding yeast cell cycle. Cross et al. [CRO02] tested the prediction in a yeast strain allowing them to control Cln3 expression by galactose induction and Cdc14 activity by temperature. "Neutral" corresponds to cells growing on glucose (Cln3 synthesis off) at 37 C (Cdc14 inactive). Cell cycle phase is monitored by budding index and Clb2 level (G1 = low budding index and Clb2 absent, M = high budding index and Clb2 present). The figure shows that cells in neutral can arrest stably in either G1 or M phase, depending on which transition (Start or Finish) was the last event experienced.

The experimental work in [MIL01] and [CRO02] provided the basis for further studies in Dr. Cross's lab, supported by a subcontract of the DARPA BioSPICE grant to Virginia Tech.

Two Redundant Oscillatory Mechanisms in the Yeast Cell Cycle
F.R. Cross
***Developmental Cell* 4:741-752 (2003)**

Oscillations of Clb-Cdk kinase activity are due to periodic cyclin degradation by the anaphase-promoting complex (APC) activated by Cdc20 or Cdh1, and to cyclical accumulation of the Sic1 inhibitor. The results reported here are based on the proposal that two distinct oscillatory mechanisms control Clb-kinase oscillations: a "relaxation oscillator," involving Clb kinase and its inhibitors (Sic1, APC-Cdh1), and a "negative feedback oscillator," involving Clb-kinase and APC-Cdc20. Genetic analysis suggests that these two mechanisms function independently, and inactivation of both mechanisms is required to prevent mitosis. Computational modeling confirms that two such mechanisms can be linked to yield a robust cell cycle control system.

The two redundant mechanisms for mitotic exit are illustrated in Fig. 3A. Mitotic entry is initiated by a rise in Clb2-dependent kinase activity, which also inhibits exit from mitosis. For a

cell to exit mitosis and return to G1 phase, Clb-kinase activity must be destroyed or neutralized. Removal of Clb2 at the end of mitosis is accomplished partly by Cdc20 (Fig. 3A, left box) in association with the APC. Cdc20-APC complexes label Clb2 molecules for degradation. Cdc20 association with the APC requires that the APC be phosphorylated by Clb2-dependent kinase, so Clb2, APC and Cdc20 are involved in a three-component negative feedback loop (oscillator). The other pathway for removing Clb2 at the end of mitosis (Fig. 4.3A, right box) relies on Cdh1 and Sic1. Cdh1, in association with the APC (either phosphorylated or not), labels Clb2 for degradation, and Sic1 binds to Clb2-Cdk dimers to form inactive trimers. Phosphorylation of Cdh1 and Sic1 by Clb-dependent kinases inactivates Cdh1 and labels Sic1 for degradation. Hence, Clb2-Cdk is in a state of mutual antagonism with the Cdh1, Sic1 pair (Fig. 3A). This antagonism creates alternative steady states: one with Cdh1 and Sic1 ascendant and Clb2-kinase activity low, the other with active Clb2-kinase and depressed Cdh1 and Sic1. Alternation between these meta-stable states is called a relaxation oscillator.

To explore the relations between these two mechanisms for mitotic exit, the phenotypes of a number of mutants were determined (Table 1). The *APC-A* gene encodes a non-phosphorylable version of the APC; hence, Cdc20 cannot form an active complex with APC-A proteins, but Cdh1 can. The observed viability of *APC-A* mutant cells (they grow and divide) means that the negative feedback loop is not essential for progression through the cell cycle. The relaxation oscillator by itself can coordinate all essential events of the cell cycle. Budding yeast cells can tolerate crippling the relaxation oscillator (the single deletion mutants, *cdh1Δ* or *sic1Δ*, are viable), but not removing it altogether (the double mutant, *cdh1Δ sic1Δ*, is inviable). If the negative feedback oscillator is knocked out, then Cdh1 becomes essential (*APC-A cdh1Δ* is inviable). These inviable cells can be rescued by increasing the level of Sic1 (*APC-A cdh1Δ GAL-SIC1* is viable) or by overexpressing Cdc20 (*APC-A cdh1Δ GAL-CDC20* is viable). Genetic interactions of these sorts provide many constraints on the underlying molecular mechanism and on the effective values of the rate constants characterizing these reactions.

We proposed to model these genetic interactions with a modified version of the Chen (2000) model. In Fig. 3B, we show simulations of the mutant cells described in the previous paragraph. These simulations were done before the experiments were preformed. The model correctly predicted the viability/inviability of the strains. The model studied in this paper ultimately evolved into the Chen et al. (2004) publication.

Robustness—insensitivity to moderate variations in parameter values—is a necessary property of wild-type control networks, but it might be compromised considerably in viable mutant strains. To assess this proposal, we measured the robustness of four models: wild-type, *cdh1Δ*, *APC-A*, and *sic1Δ*. Robustness was measured as the maximum increase or decrease of each parameter in the model that can be tolerated before cyclical behavior is lost. The wild-type model is quite robust, continuing to cycle even with significant (frequently very large) changes of most of the parameters (Fig. 3C). The *sic1Δ* model was almost as robust as wild-type. By contrast, the *cdh1Δ* and *APC-A* models were highly sensitive to changes in many parameters (Fig. 3C). For example, overexpression of Clb2 causes a mitotic block in the *APC-A* background, according to the model, and this prediction was specifically tested and confirmed.

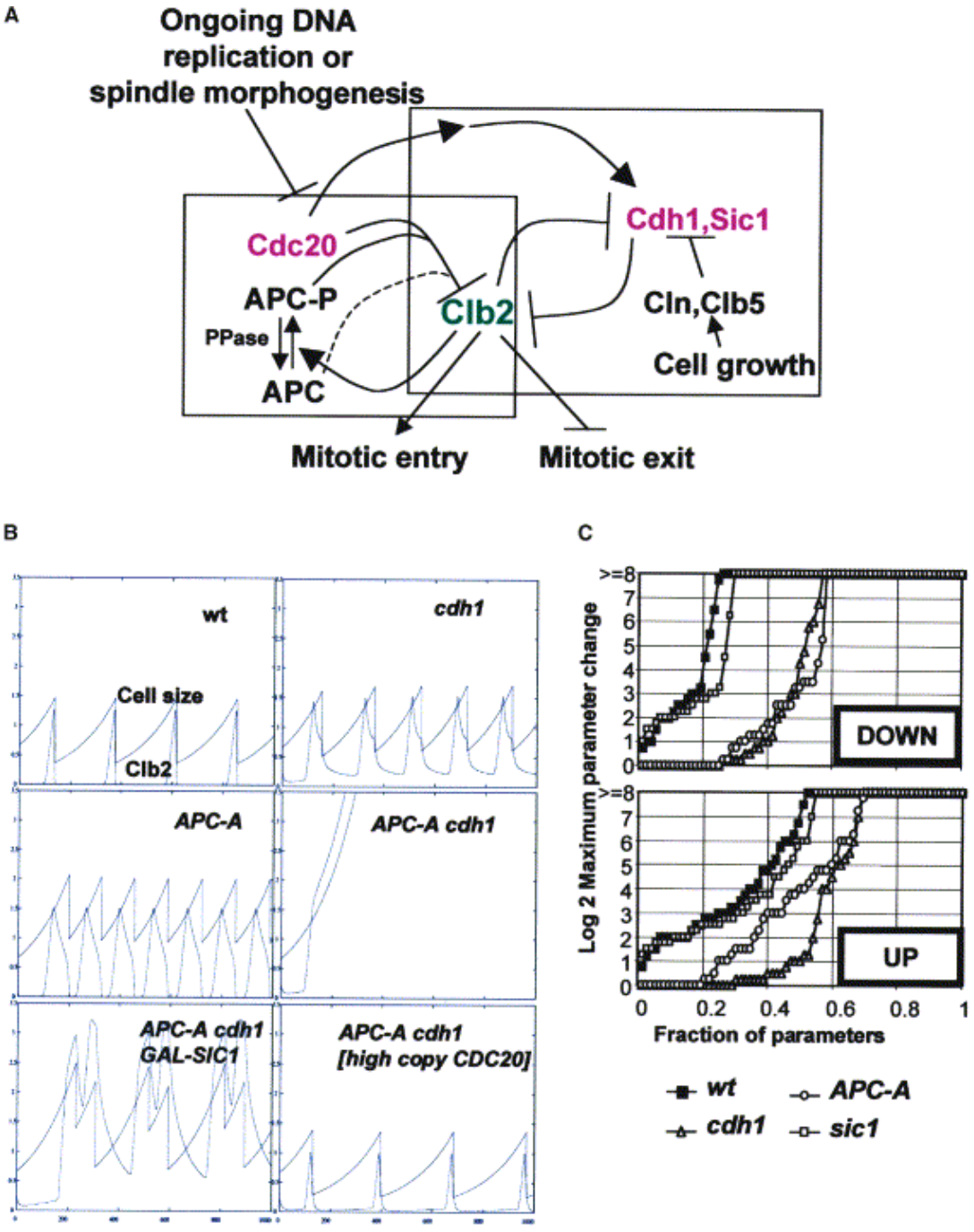

Figure 4.3. Two redundant mechanisms for exit from mitosis. (A) Wiring diagram. For details, see Fig. 3.1 and Chen et al. (2000, 2004). The box at left outlines the main elements of the negative feedback oscillator, and the box at right outlines the main elements of the relaxation oscillator. (B) Simulations of the indicated mutants (see Table 1). The simulated cell mass and Clb2 levels are indicated. (C) Quantitative analysis of sensitivity of different models to parameter variations. Wild-type and mutant simulations were run with systematic variation of all the free parameters in the model, to determine the maximum increase or decrease that the model could tolerate and still cycle effectively (up to 256-fold tested). The cumulative distribution of parameters exhibiting a given level of tolerance is plotted for each model.

Table 4.1. Summary of Comparative Results from Modeling and Genetic Experiments

Modeled Genotype	Parameter Changes	Model Result	Genetic Result
cdh1Δ (or *CLB2-kan*)	kdb2″: 2 → 0	Viable	Viable
APC-A	kaAPC: 1 → 0	Viable; checkpoint super-sensitive	Viable; checkpoint super-sensitive
APC-A cdh1Δ	kdb2″: 2 → 0 kaAPC: 1 → 0	Inviable (mitotic arrest)	Inviable (mixed arrest)
APC-A cdh1Δ [high-copy CDC20]	kdb2″: 2 → 0 kaAPC: 1 → 0 ks20′: 0.005 → 0.05 ks20″: 0.06 → 0.6	Viable	Viable
APC-A cdh1Δ GAL-SIC1	kdb2″: 2 → 0 kaAPC: 1 → 0 ksc1′: 0.02 → 0.15	Viable	Viable
sic1Δ cdh1Δ	ksc1′: 0.02 → 0 ksc1″: 0.1 → 0 kdb2″: 2 → 0	Inviable (mitotic arrest)	Inviable (not mitotic arrest; replication defect?)
CLB2Δdb	kdb2″: 2 → 0.1 kdp2p: 0.2 → 0	Inviable (mitotic arrest)	Inviable (mitotic arrest)
CLB2Δdb [high-copy SIC1]	kdb2″: 2 → 0.1 kdp2p: 0.2 → 0 ksc1′: 0.02 → 0.2 ksc1″: 0.1 → 1	Inviable	Viable

The model was run with the standard parameters or with the indicated additional parameter changes. "Viability" is scored as the ability to undergo repeated rounds of "cell division" at similar cell mass values.

Genetic and Biochemical Evaluation of the Importance of Cdc6 in Regulating Mitotic Exit
V. Archambault, C.X. Li, A.J. Tackett, R. Waeschh, B.T. Chait, M.P. Rout & F.R. Cross
***Molecular Biology of the Cell* 14:4592-4604 (2003)**

Exit from mitosis is a critical cell cycle transition. Although DNA replication and mitotic entry are under positive control by cyclin-dependent kinase (Cdk), exit from mitosis requires at least partial Cdk inactivation. Thus, an oscillation in Cdk activity is obligatory for a complete cell division cycle, because DNA replication and initiation of mitotic division are tied to high Cdk activity, but the replicated chromosomes assembled on the mitotic spindle will not complete division into two daughter cells until Cdk activity is reduced to a sufficiently low level. Buildup of Cdk activity in the next cell cycle is then required before DNA replication can reoccur. This simple mechanism, combined with an oscillatory mechanism for Cdk activation and inactivation, will thus reproduce much of the essential biology of the cell cycle. Therefore, it is important to understand the mechanisms of Cdk inactivation.

A critical conserved mechanism for Cdk inactivation at exit from mitosis is cyclin B proteolysis, under the control of the anaphase-promoting complex (APC) activated by Cdc20 and Cdh1. In budding yeast, two additional regulators have been proposed to inactivate Cdk to allow exit from mitosis: the Sic1 stoichiometric inhibitor, activated by the Cdc14 phosphatase, and the N terminus of the Cdc6 replication protein. This region of Cdc6 was identified as a Cdk-binding domain. Calzada et al. [CAL01] reported that deletion of this region in the chromosomal copy of *CDC6* (*cdc6Δ2-47*) caused a delay in mitotic exit, and remarkably, combination of the *cdc6Δ2-47* mutation with deletion of *SIC1* absolutely blocked mitotic exit. Cyclin proteolysis is known to be essential for mitotic exit, but the *cdc6Δ2-47 sic1Δ* mitotic exit block was shown to occur even

in the presence of all cyclin proteolytic machinery. Thus, this result suggested coequal control of Cdk inactivation by cyclin proteolytic machinery and inhibition by stoichiometric binding proteins.

We evaluated the hypothesis that the N-terminal region of the replication control protein Cdc6 acts as an inhibitor of cyclin-dependent kinase (Cdk) activity, promoting mitotic exit. During late mitosis, Cdc6 is present at levels comparable with Sic1 and binds specifically to the mitotic cyclin Clb2. Moderate overexpression of Cdc6 promotes viability of a mutant strain (*CLB2Δdb*) in which the mitotic cyclin is resistant to proteolytic degradation and which otherwise arrests in late mitosis (before nuclear or cell division). Rescue of *CLB2Δdb* cells by Cdc6 overexpression is dependent on the N-terminal putative Cdk-inhibitory domain. These observations support the potential for Cdc6 to inhibit Clb2-Cdk, thus promoting mitotic exit. Consistent with this idea, we observed a cell-division defect in *cdh1Δ sic1Δ cdc6Δ2–49* triple mutants. However, we were able to construct viable strains that contain neither *SIC1* nor the Cdk-inhibitory domain of Cdc6, in contradiction to previous work. We conclude, therefore, that although both Cdc6 and Sic1 have the potential to facilitate mitotic exit by inhibiting Clb2-Cdk, mitotic exit does not require any identified stoichiometric inhibitor of Cdk activity.

In addition, we showed that *cdh1Δ cdc6Δ2-49* and *sic1Δ cdc6Δ2-49* double mutants have no significant proliferation defect, and the *sic1Δ cdh1Δ* strain proliferates slowly. Hence, the strong inviability of the triple mutant *cdh1Δ sic1Δ cdc6Δ2–49* represents functional overlap among all three genes. The apparent overlap in function between *SIC1*, *CDH1*, and *CDC6* led us to test whether increased *CDC6* gene dosage could bypass the requirement for either *CDH1* or *SIC1* for viability. We found that extra *CDC6* rescued the reduced viability of *sic1Δ cdh1Δ* cells. The phenotypes of these mutants provided additional, important constraints on the mathematical model being constructed simultaneously by Chen, Calzone and Tyson at Virginia Tech.

For modeling purposes, it is important to know the abundances Sic1 and Cdc6 relative to Clb2, and the timing of expression of these proteins during the cell cycle. Timing is displayed in Fig. 3 and quantitation is reported in Table 2. Importantly, at endogenous expression levels, our timing and quantitation measurements clearly imply that the level of Cdc6 will exceed the level of Clb2 as Clb2 level falls due to APC activation during anaphase, allowing for the possibility that Clb2 inhibition by Cdc6 contributes effectively to mitotic exit. In contrast, Sic1 may not accumulate to significant levels until Clb2 degradation is almost complete (see Fig. 4), so the primary biological role of Sic1 may be in Clb inhibition in G1.

Table 4.2. Quantitation of Cdc6-PrA, C1b2-PrA, and Sic1-PrA. Numbers are in estimated copies per cell in asynchronous diploid cells. Published numbers are provided for comparison. The numbers of independent cultures tested are in parentheses.

		Copies/diploid cell (asynchronous)	
Strain	Protein A-tagged protein	This study	Cross *et al.* (2002)
AL4	Cdc6	624 ± 7 (3)	NA
AL4	Sic1	195 ± 29 (3)	NA
MK3	Clb2	1,006 ± 125 (3)	1,128 ± 231 (4)
MK3	Sic1	265 ± 29 (3)	214 ± 42 (5)

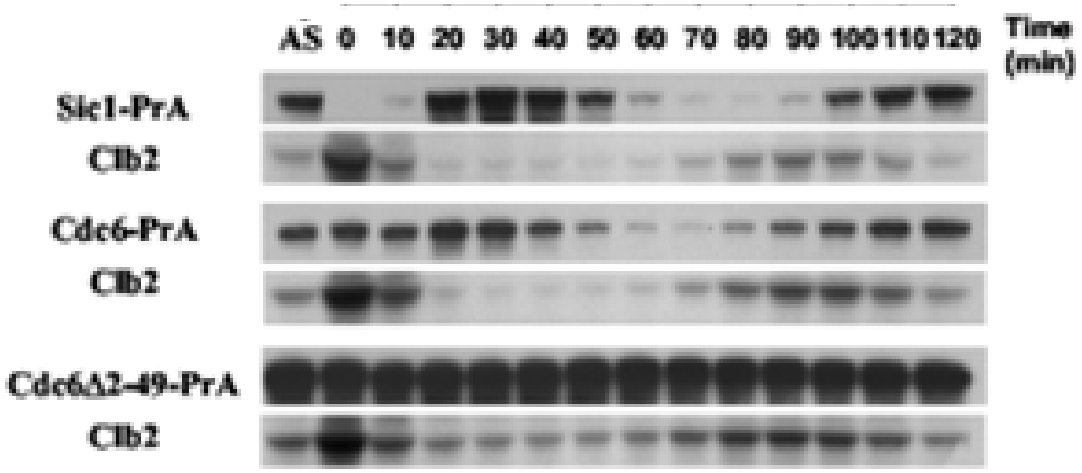

Figure 4.4. Temporal patterns of Cdc6, Sic1 and Cdc2. Cdc6 temporally overlaps with Clb2 during mitosis, but Sic1 is abundant primarily in G1 cells when Clb2 level is very low

Quantitative Characterization of a Mitotic Cyclin Threshold Regulating Exit from Mitosis
F.R. Cross, L. Schroeder, M. Kruse & K.C. Chen
***Molecular Biology of the Cell* 16:2129-2138 (2005)**

Regulation of cyclin abundance is central to eukaryotic cell cycle control. Strong overexpression of mitotic cyclins is known to lock the system in mitosis, but the quantitative behavior of the control system as this threshold is approached has only been characterized in frog cell extracts. Here, we quantitate the threshold for mitotic block in budding yeast cells caused by constitutive overexpression of the mitotic cyclin Clb2. We use a quantitative kinetic model of the budding yeast cell cycle to generate biochemical predictions for Clb2 levels in Clb2-overexpressing mutatnts. Model predictions compare well with biochemical data, even though no data of this type were available during model generation. Loss of robustness of the Clb2-overexpressing cells is also predicted by the model. These results provide strong confirmation of the model's predictive ability.

Clb2 mitotic cyclin must oscillate from a low level in a G1- and early S phase cell to a high level as the cell enters mitosis, and back to a low level as the cell exits mitosis and returns to G1. A complex web of interlocking controls involving proteolysis, regulated transcription, and inhibitor accumulation controls Clb2 activity, and Clb2 reciprocally affects all of these regulators (see Fig. 3.1), making the final result of Clb2 overexpression difficult to predict intuitively. It is known that strong overexpression of *CLB2* RNA from the *GAL1* promoter (unregulated through the cell cycle) from multiple copies of *GAL-CLB2* causes mitotic arrest. We determined that in diploid cells, our *GAL-CLB2* construct resulted in viable cells with close to wild-type proliferation rate when present at single copy ("1x"), but this construct efficiently blocked proliferation when present at two copies ("2x"; a tandem duplicated array of *GAL-CLB2*) (Fig. 5). The 1x *GAL-CLB2* construct blocked proliferation in haploids almost as well as the 2x *GAL-CLB2* construct did in diploids in the same assay (our unpublished data). These results indicate that proliferation is inhibited at a dosage of two copies of the *GAL-CLB2* construct per diploid genome but not by one copy.

The precipitous decline in proliferation capacity with a simple doubling of gene dosage suggests the crossing of a threshold. Consistent with this, we found that 1x *GAL-CLB2* diploid strains had an absolute requirement for *CDH1* and *SIC1* for viability, unlike wild type, suggesting that the 1x *GAL-CLB2* cells were only viable conditional on the full activation of the normally dispensable Cdh1-Sic1 control system. Indeed, 1x *GAL-CLB2* diploid strains exhibited significant slowing of proliferation just upon a halving of *CDH1* gene dosage (Fig. 5), and a weaker but detectable effect was observed upon halving of *SIC1* gene dosage, which was significantly enhanced on removal of the Cdk-inhibitory N-terminal domain of Cdc6 (Fig. 5).

In addition, viability of 1x *GAL-CLB2* diploids is completely dependent on the phosphorylation of APC subunits, phosphorylations that are required for Cdc20-APC to degrade Clb2 at anaphase. Even heterozygosity for the unphosphorylatable APC mutations has a slight effect on proliferation of these cells (Fig. 5). Therefore, we conclude that the 1x *GAL-CLB2* diploids are just under a threshold for inviability due to Clb2 overexpression, whereas the 2x *GAL-CLB2* diploids are just over this threshold. The level of this threshold is set by the combined activities of APC-Cdc20, APC-Cdh1, and Sic1.

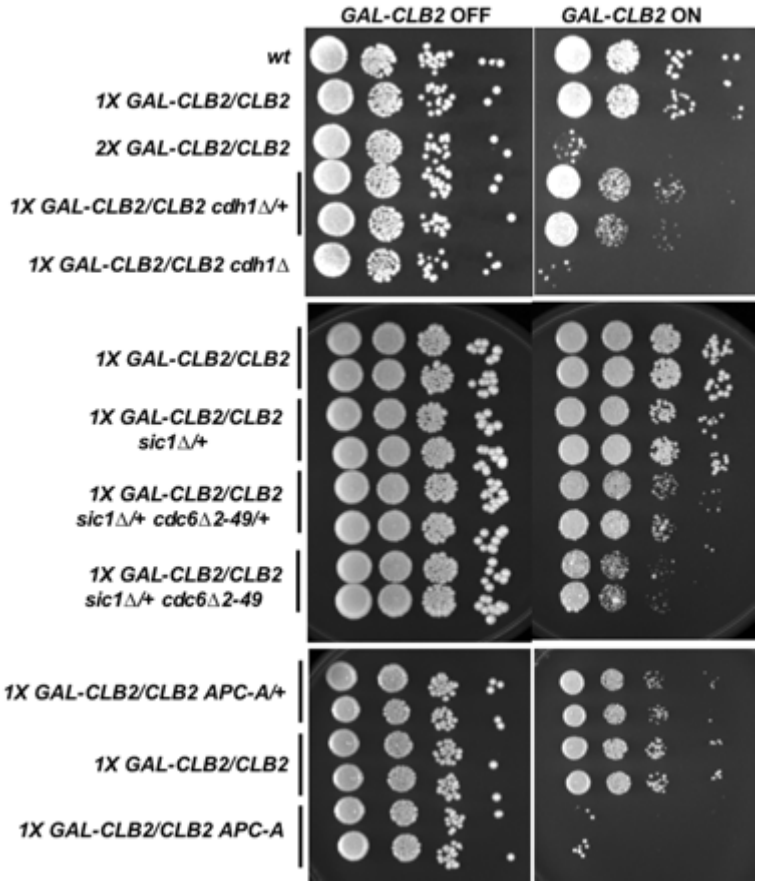

Figure 4.5. Dosage sensitivity for *CLB2* overexpression. Tenfold serial dilutions of fresh stationary phase cultures of diploids of the indicated genotypes were plated on glucose medium (left, "GAL-CLB2 OFF") or on galactose medium (right, "GAL-CLB2 ON"). Genotype nomenclature: *1*x *GAL-CLB2/CLB2* means one copy of *GAL-CLB2* integrated at the *CLB2* locus, heterozygous with a normal *CLB2* locus; 2x is the same but with two tandem copies of *GAL-CLB2*. *cdh1*Δ/+ means heterozygosity for a *cdh1* deletion; *cdh1*Δ means homozygosity for the deletion. *APC-A/+* refers to the presence of mutations blocking Cdk phosphorylation of APC subunits, heterozygous with a wild-type allele of each; *APC-A* is homozygous for these mutations. Top, dosage sensitivity for *GAL-CLB2* and interaction with *CDH1* dosage. Middle, interaction with *SIC1* dosage. Bottom, interaction with *APC-A* mutations.

We used quantitative Western blotting to measure the number of Clb2 proteins per cell in diploid cells that were wild type, 1x *GAL-CLB2*, or 2x *GAL-CLB2* (Table 3). Because Clb2 level varies strongly over the cell cycle, these measurements are averages over a considerable amount of variation. To determine the dynamic behavior of Clb2, we used centrifugal elutriation to isolate small newborn cells known to contain the minimum level of Clb2 and large cells from mid-cycle that contain the peak level of Clb2 (Fig. 6). We carried out this experiment with wild-type diploid cells and with diploid cells containing one or two copies of *GAL-CLB2*.

Next, we compared these biochemical results with predictions from the quantitative model of Chen et al. (2004) (Fig. 7). This model contains two parameters governing *CLB2* transcription. One (ksb2', 0.001 au/min) is unregulated, basal expression. The other (ksb2", 0.04 au/min) represents peak of regulated *CLB2* transcription rate from its endogenous promoter. The concentration of Clb2 protein is expressed in "arbitrary units" (au). As discussed in Chen et al.

(2004), the au for Clb2 can be calibrated from quantitations of asynchronous Clb2 levels (Cross et al., 2002) to yield an estimate of 1 au = 40 nM or 2400 molecules per diploid cell; ksb2" = 0.04 would then correspond to ≈100 molecules per minute per diploid cell.

Table 4.3. Average number of Clb2 molecules per budding yeast cell, as measured (column2) and as predicted by the mathematical model (column 4). Measurements are made by serial-dilution Western blotting in an asynchronous culture of diploid strains containing zero, one, or two integrated copies of a *GAL-CLB2* gene, in addition to two copies of the wild-type *CLB2* gene. Simulations of Clb2 concentration (in arbitrary units/cell mass, averaged over the computed cell cycle) are shown for the wild type and 1x GAL-CLB2 cells. For 2x GAL-CLB2, cells arrest in late mitosis, so the Clb2 concentration is calculated at 240 min, rather than averaged over the cell cycle. The results are not very sensitive to this time choice. For the last three rows, we reduced the rate constants for degradation of Clb2, as described in the publication.

Experiment	Copies/cell, mean ± SEM (fold increase over wt)	Model ksb2-gal (Clb2 au/min)	Model Clb2 concen. (Clb2 au/cell mass)
Wt	1500 ± 461	0.001	1
1x GAL-CLB2	7400 ± 1081 (5x wt)	0.32-0.48	5-7 x wt
2x GAL-CLB2	19,000 ± 2985 (13x wt)	0.64-0.96	7-34 x wt
GAL-CLB2-db	49,000 ± 12,606 (33x wt)	0.32-0.48	39-57 x wt
GAL-CLB2-ken	18,000 ± 2019 (12x wt)	0.32-0.48	12-18 x wt
GAL-CLB2-ken,db	91,000 ± 19,557 (61x wt)	0.32-0.48	39-57 x wt

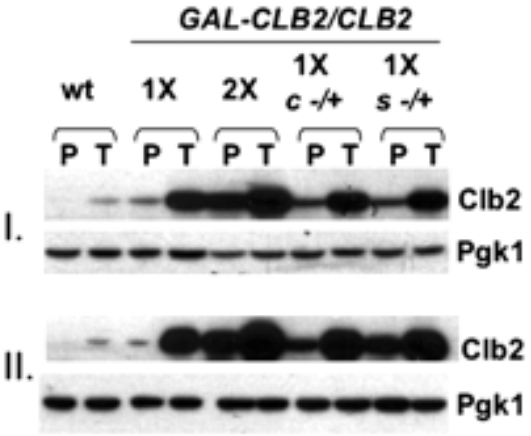

Figure 4.6. Comparison of trough and peak levels of Clb2 upon Clb2 overexpression. The lowest (trough, T) and highest (peak, P) Clb2 samples from elutriation experiments were run on the same gel. Equal loading was established by anti-Pgk1 Western blot, and the relative levels of Clb2 at peak and trough were determined by anti-Clb2 Western blot. Strains tested were wild-type *CLB2/CLB2*, 1x *GAL-CLB2/CLB2*, 2x *GAL-CLB2/CLB2*, 1x *GAL-CLB2/CLB2 cdh1/+*, and 1x *GAL-CLB2/CLB2 sic1/+*. Two replicates of the experiment are shown (I and II), with independent elutriations for all samples.

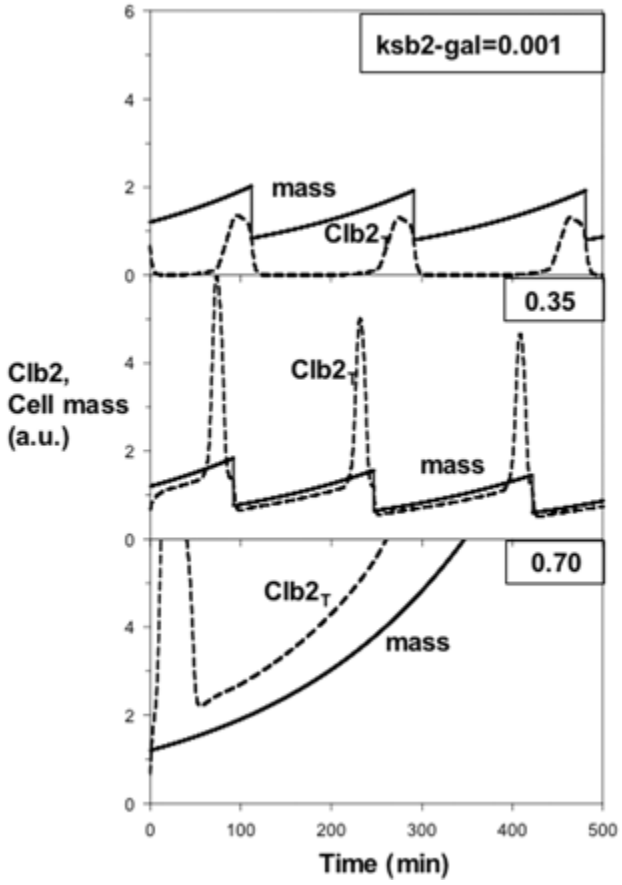

Figure 4.7. Model predictions. Clb2 levels and cell mass plots from the model for ksb2-gal = 0.001 (modeling wild-type; ksb2-gal substitutes for ksb2' = 0.001 in the original model), ksb2-gal = 0.35 (in the estimated range for 1x *GAL-CLB2*), and ksb2-gal = 0.7 (in the estimated range for 2x *GAL-CLB2*). Clb2, cell mass units are arbitrary.

Expression of *CLB2* from the *GAL* promoter is modeled by increasing ksb2', because the *GAL* promoter is not cell cycle regulated. For clarity, we will name this modified ksb2' parameter used to model *GAL-CLB2* "ksb2-gal." We asked whether there was a theoretical level of ksb2-gal that would allow mitotic exit, whereas a twofold increase in this value would block mitotic exit. To make this determination, the standard parameter set of Chen *et al*. (2004) was modified. First, mass-doubling-time was changed to 150 min (from 90 min) to reflect that cell growth is slower on galactose medium. The ksb2' (=ksb2-gal) parameter was then systematically increased, and the ability of both mother and daughter cells to cycle repetitively was tested. At a value of ksb2-gal<= 0.48, both mother and daughter can cycle indefinitely. Values of ksb2-gal from 0.49 to 0.63 cause mother cells but not daughter cells to arrest in mitosis. Still higher values (ksb2-gal ≥ 0.64) cause both mother and daughter cells to arrest. Therefore, ksb2-gal = 0.48 is the maximum level for 1x *GAL-CLB2* to yield viable mothers and daughters, and ksb2-gal = 0.64 is the minimum level for 2x *GAL-CLB2* to yield inviable mothers and daughters. Thus, the predicted allowable range of ksb2-gal for the 1x *GAL-CLB2* strain is 0.32–0.48. Model runs are shown in (Fig. 7). With ksb2-gal = 0.35 (modeling 1x *GAL-CLB2*), cycling occurred normally although

with very high Clb2 levels, whereas with ksb2-gal = 0.70 (2-fold higher, modeling 2x *GAL-CLB2*) the system arrested in the first cell cycle.

Reduced viability of 1x *GAL-CLB2 sic1/+*, *cdh1/+* and *APC-A/+* heterozygous strains (Fig. 5) allows an independent test of the parameter estimation of ksb2-gal. Reducing the activity of Cdh1 toward Clb2 (kdb2") by twofold resulted in predicted mitotic arrest with ksb2-gal ≥0.38 Reducing the ability of Clb2 to phosphorylate and activate the APC (ka20") by twofold resulted in predicted mitotic arrest with ksb2-gal ≥0.46. Reducing the synthesis rate of *SIC1* in the model (ksc1', ksc1") by twofold resulted in predicted mitotic arrest with ksb2-gal ≥0.49. These thresholds for the heterozygous backgrounds are approximately within the 0.32–0.48 range for the ksb2-gal parameter. Thus, the model predicts a transition from viability to inviability in these heterozygous backgrounds somewhere within this range of constitutive Clb2 expression. The reduced viability of these heterozygous backgrounds containing one copy of *GAL-CLB2* thus confirms by an independent set of genetic assays that this parameter range for the *GAL-CLB2* construct gives a reasonable fit between model and experiment. Modeling *GAL-CLB2* expression with ksb2-gal anywhere in the 0.32–0.48 range predicts complete block to mitotic exit in homozygous *cdh1*, homozygous *APC-A* or *sic1/+ CDC6Δ2-49/CDC6Δ2-49* backgrounds, also consistent with experiment (Fig. 3).

To determine whether the above-mentioned estimate for *GAL-CLB2* expression is biochemically accurate, we examined cells blocked for mitotic exit by undegradable Clb2, with the destruction box and KEN boxes mutated (Clb2-ken,db). We used either *CLB2-ken,db* expressed from the endogenous promoter or from the *GAL* promoter at single copy. Because Clb2-ken,db is immune to proteolytic regulation, the Clb2-ken,db levels can be used as a direct readout of transcriptional activity. The Clb2 level in *CLB2-ken,db* should be proportional to ksb2" (peak mitotic expression of *CLB2*), and the Clb2 level in *GAL-CLB2-ken,db* cells should be proportional to ksb2-gal (rate of expression from the *GAL* promoter). From these biochemical measurements (Table 3) we determined that ksb2-gal = 11 x ksb2" = 11 x 0.04 = 0.44. This estimate is within the 0.32–0.48 range derived in the previous paragraph.

Figure 7 presents model runs demonstrating the difference in predicted dynamic behavior as basal *CLB2* RNA expression is increased through the threshold for blocking mitotic exit. A semi-quantitative prediction can be made from these runs that in 1x *GAL-CLB2* cells, near the maximum tolerable level of *CLB2* overexpression, the trough level of Clb2 in G1 corresponds to the peak level of wild-type, whereas the peak level in the 1x *GAL-CLB2* cells approximately corresponds to the trough level in the 2x *GAL-CLB2* cells. These expectations are met by the experimental data (compare Figs. 6 and 7).

4.2 Frog Cells and Extracts

Hysteresis Drives Cell-Cycle Transitions in Xenopus laevis egg extracts
W. Sha, J. Moore, K. Chen, A. Lassaletta, C.S. Yi, J.J. Tyson & J.C. Sible
***Proc. Natl. Acad. Sci. U.S.A.* 100:975-980 (2003)**

Cells progressing through the cell cycle must commit irreversibly to mitosis without slipping back to interphase before properly segregating their chromosomes. A mathematical model of cell-cycle progression in cell-free extracts made from frog eggs predicts that irreversible transitions into and out of mitosis are driven by hysteresis in the molecular control system. Hysteresis refers to toggle-like switching behavior in a dynamical system (Fig. 8). In the mathematical model, the toggle switch is created by positive feedback in the phosphorylation reactions controlling the activity of Mitosis-Promoting Factor (MPF, a dimer of Cdk1 kinase and its regulatory subunit, cyclin B). To determine whether hysteresis underlies entry into and exit from mitosis in cell-free egg extracts, we tested three predictions of the Novak-Tyson model. (*i*) The minimal concentration of cyclin B necessary to drive an interphase extract into mitosis is distinctly higher than the minimal concentration necessary to hold a mitotic extract in mitosis. (*ii*) Unreplicated DNA elevates the cyclin threshold for MPF activation, indication that checkpoints operate by enlarging the hysteresis loop. (*iii*) A dramatic "slowing down" in the rate of MPF activation is detected at concentrations of cyclin B marginally above the activation threshold. All three predictions were validated. These observations confirm hysteresis as the driving force for cell-cycle transitions into and out of mitosis.

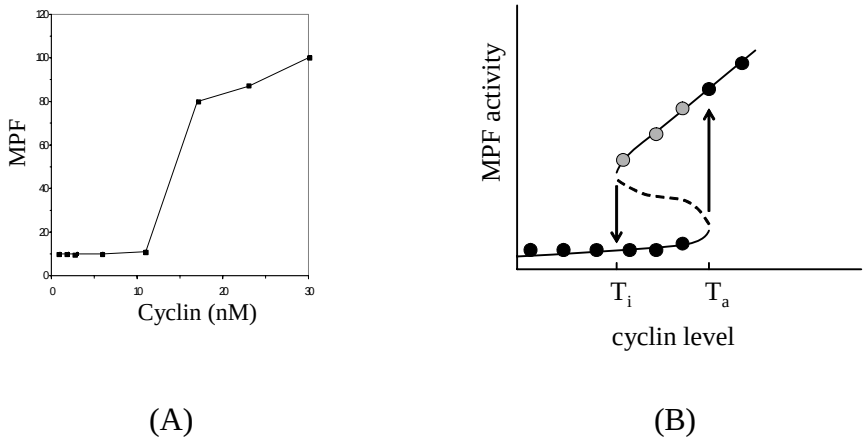

Figure 4.8. Hysteresis in a model of MPF activation. (A) Solomon et al. [SOL90] measured MPF activity in frog egg extracts supplemented with a fixed amount of non-degradable cyclin B, observing a characteristic cyclin threshold for MPF activation. (B) Novak and Tyson [NOV93] predicted that Solomon's threshold is indicative of an S-shaped dependence of MPF activity on cyclin level. For cyclin concentrations between the two thresholds, the control system has two stable steady states (interphase and M phase) separated by an unstable steady state (---).

The threshold for MPF inactivation is smaller than the activation threshold

To measure the MPF-activation and -inactivation thresholds during the same M phase, cycling extracts that autonomously enter and exit mitosis I were prepared. Sperm nuclei were added to extracts to monitor cell-cycle progression (see insets to Fig. 9A: M = mitosis = condensed chromatin, no nuclear envelope; I = interphase = decondensed chromatin, distinct nuclear envelope). While the extracts were in the first interphase (low MPF activity), a measured amount of non-degradable cyclin B (Δcyclin B) was added (t = 0). To measure the activation threshold, the extract was also supplemented with cycloheximide (an inhibitor of protein synthesis) at t = 0. Figure 9A shows that the cyclin threshold for activation of MPF (entry into mitosis I) lies between 30 and 60 nM cyclin; repeats of this experiment place the threshold between 30 and 40 nM. To measure the inactivation threshold, cycloheximide was left out of the extract. The extract makes its own cyclin (the normal, degradable form of cyclin B) and enters mitosis I. At that time (t = 60 min), cycloheximide is added to the extract so that it can no longer synthesize new cyclin molecules. Meanwhile, the degradable cyclin molecules are destroyed, because high MPF activity turns on the cyclin degradation machinery in the extract. The non-degradable cyclin left behind may or may not be sufficient to keep the extract in mitosis. Figure 9B shows that the cyclin threshold for MPF inactivation lies between 16 and 24 nM. Intermediate concentrations of 24 and 32 nM Δcyclin B could support either interphase or mitosis, depending on starting conditions, confirming bistability and hysteresis.

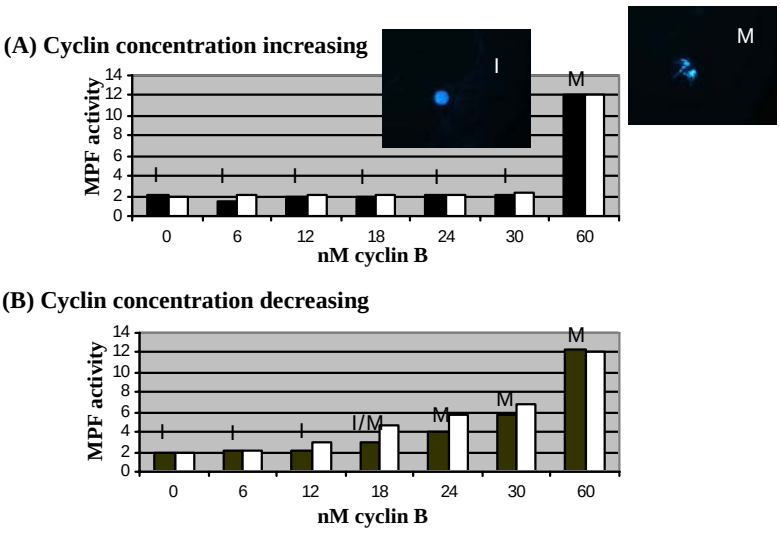

Figure 4.9. Bistability of MPF activation in frog cell extracts. We measured MPF activity in extracts supplemented with increasing and decreasing amounts of cyclin B. (A) With increasing cyclin B concentration, we reproduced the MPF activation threshold first observed by Solomon [SOL90]. (B) With decreasing cyclin B concentration, we confirmed several properties of the signal-response curve (Fig. 8B) predicted by Novak & Tyson [NOV93]: the cyclin threshold for MPF inactivation is about three times lower than the cyclin threshold for MPF activation, the control system is bistable for cyclin concentrations between the thresholds, and MPF activity on the upper branch of the S-shaped curve is roughly proportional to cyclin concentration.

Just above the activation threshold, the control system exhibits 'critical slowing down'
In his original paper on the cyclin threshold for MPF activation, Solomon reported that the time lag from cyclin addition to MPF activation is 10-20 min for all cyclin concentrations above threshold. However, the Novak-Tyson model predicts that the time lag should correlate inversely with cyclin level at concentrations marginally above the activation threshold. To resolve this discrepancy, we made careful measurements of sperm morphology and MPF activity at 15 min intervals during the activation process, for cyclin concentrations close to the MPF-activation threshold (Fig. 10). Quite clearly (Fig. 10a and d), the lag time increases as the cyclin concentration gets closer to the threshold value, exactly as predicted. An appreciable lag time is seen only for cyclin concentrations within 20 nM above threshold, which explains why the effect was not noticed by Solomon [SOL90]. MPF activity measurements (Fig. 10b) have been fit quite well by numerical simulations of the Novak-Tyson model (Fig. 10c).

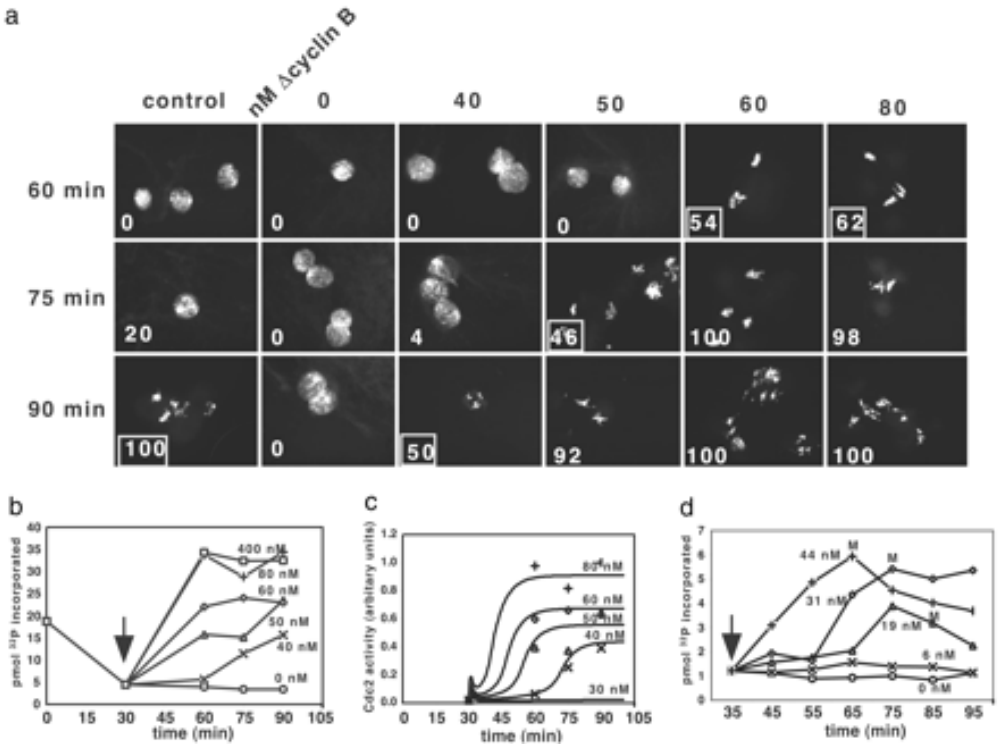

Figure 4.10. Cdc2 activation exhibits a critical slowing down near the MPF activation threshold. Extracts were supplemented with cycloheximide at 0 min and Δcyclin B at 30 min (interphase). Control extract lacking cycloheximide entered mitosis at 90 min. Samples were collected every 15 min for microscopic analysis of nuclear morphology (*a*) and histone H1 kinase activity (*b*). In *a*, at each time is indicated the percent of nuclei that had undergone nuclear envelope breakdown and chromatin condensation. The extract was qualitatively scored as entering mitosis (boxed numbers) when >40% of the nuclei had condensed chromatin and no nuclear envelope. (*c*) Experimental data (symbols) from *b* are displayed alongside simulations of the Novak-Tyson model (curves). (*d*) Histone H1 kinase activity measured in an extract collected every 10 min with varying concentrations of Δcyclin B added at 35 min. M = time when nuclear morphology first indicated mitosis. Arrows denote addition of Δcyclin B in *b* and *d*. The preparation of Δcyclin B used in *d* was more active than the others, resulting in a lower activation threshold.

Slowing down is a general property of dynamical systems close to saddle-node bifurcation points (the turning points at T_i and T_a in Fig. 8B). Hence, slowing down is another signature of the hysteresis loop that underlies transitions into and out of mitosis.

The unreplicated-DNA checkpoint raises the MPF-activation threshold

High concentrations of unreplicated DNA block cell-cycle progression in most eukaryotic cells, including frog cell extracts. Novak and Tyson suggested that unreplicated DNA acts by raising the cyclin threshold, and hence a high level of cyclin may override the block to mitosis induced by unreplicated DNA. To test this prediction, extracts were supplemented with 1,200 sperm nuclei per µl and set off toward mitosis I in the presence or absence of cycloheximide and aphidicolin (an inhibitor of DNA synthesis). Δcyclin B was added to these extracts at 40 min (interphase). The aphidicolin-treated extract remained in interphase for the duration of the experiment (140 min) even in the absence of cycloheximide (Fig. 11). As in Fig. 9, the activation threshold was 40 nM in cycloheximide-treated extracts without aphidicolin. In the presence of aphidicolin, the activation threshold was between 80-100 nM Δcyclin B, confirming the predicted effect of unreplicated DNA on the hysteresis loop.

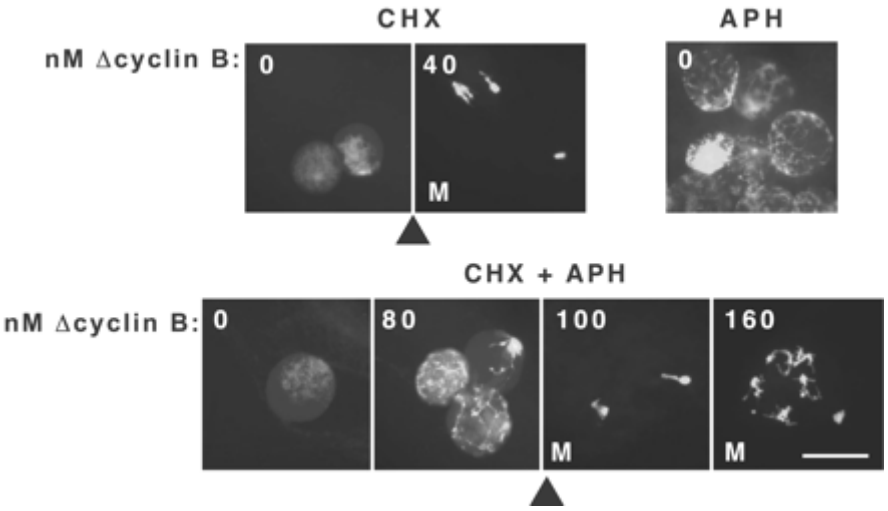

Figure 4.11. The cyclin threshold for Cdc2 activation is raised by unreplicated DNA. Extracts containing 1,200 nuclei per µl were supplemented at 0 min with cycloheximide, aphidicolin, or both (CHX + APH). ΔCyclin B was added at 40 min (interphase). Photographs of sperm nuclei were taken under fluorescence microscopy at 140 min. Extracts are labeled M when >90% nuclei on a slide appear mitotic. Triangle denotes threshold concentration of cyclin. (Scale bar = 50 µm.)

Further Experimental Studies of the Unreplicated-DNA Checkpoint in Frog Cell Extracts
I. Auckland & J.C. Sible
Unpublished

We decided to pursue in more detail the effects of unreplicated DNA on the transition into mitosis in frog cell extracts. The experimental group set out to measure these effects under a variety of conditions. The modeling group set out to update and improve the 1993 Novak-Tyson model, in support of the experiments. And the software group set out to create parameter estimation algorithms that would fit the models to the data. Our efforts in these directions are described in separate chapters of this report. The entire project has not yet been brought to a satisfactory conclusion.

DNA can be replicated over a range of nuclear concentrations in cell-free egg extracts
In order to generate quantitative experimental data regarding DNA replication checkpoints, we had first to establish an appropriate range of concentrations of sperm nuclei. At lower concentrations (800 nuclei/μl), aphidicolin-treated extracts enter mitosis about 30 min after control extracts (Sha and Sible, unpublished data). To establish a working maximum concentration of nuclei, we varied nuclear concentration from 550 to 4400/μl in extracts without aphidicolin (Fig. 12). Extracts with 2200 nuclei/μl or less entered mitosis within 120 minutes, suggesting that DNA was replicated in these extracts. However, extracts containing concentrations of 2750 nuclei/μl and above did not enter mitosis, even after 210 minutes. In our experience, extracts lose integrity after approximately 200 minutes, and we are unable to determine unambiguously the cell cycle state by nuclear morphology. Therefore, the maximum concentration of nuclei we will use for most experiments will be about 2000/μl. For experiments in which we wish to create a strong block to replication, we need to use ≥1200 nuclei/μl and aphidicolin. These extracts remain blocked in interphase for >140 min (Fig. 13).

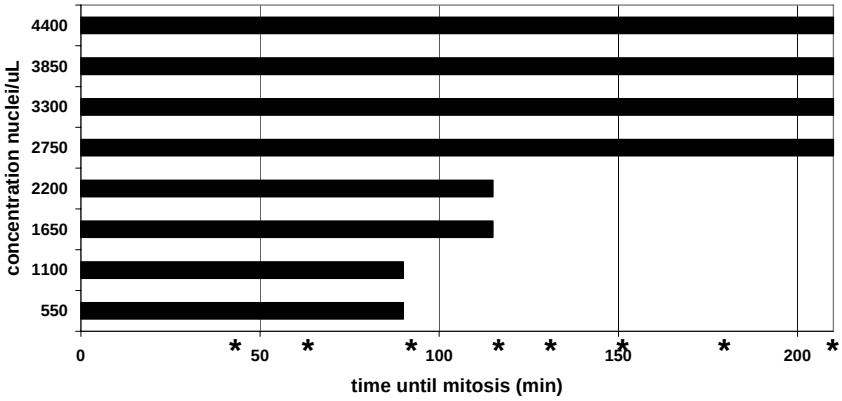

Figure 4.12. The effect of nuclear concentration on time into mitosis in extracts. A frog cell extract was prepared and aliquots were supplemented with sperm nuclei at the indicated final concentrations. At t = 0, extracts were activated (released from M-phase arrest) by addition of $CaCl_2$ to a concentration of 0.4 mM. At the times indicted by asterisks (*), aliquots of extracts were stained with DAPI and observed by fluorescence and phase-contrast microscopy. Extracts were scored as in mitosis when nuclear envelope breakdown (NEB) was >90%

DNA replication checkpoints function by enlarging the hysteresis loop

In addition to establishing appropriate experimental bounds on nuclear concentration, the experiments shown in Fig. 12 establish a quantitative relationship between nuclear concentration and the timing of entry into mitosis, both in the absence and presence of aphidicolin. We predict that the lengthening of the lag time into mitosis by increasing concentrations of sperm nuclei is due to enlarging the hysteresis loop, increasing the cyclin threshold for entry into mitosis, both in the absence and presence of aphidicolin. Since this assumption is central to our model of DNA replication checkpoints, we performed preliminary experiments to test its validity.

In the first set of experiments, we measured the lag time until mitosis in extracts with two different nuclear concentrations. These extracts were supplemented with 0.4 mM $CaCl_2$ (to release from M-phase arrest), 100 μg/ml cycloheximide (to block translation of endogenous cyclin), 1100 or 2200 sperm nuclei/μl, and varied concentrations of recombinant, nondegradable cyclin B (Δcyclin B). As shown in the representative experiment in Fig. 13, nuclear concentration altered time until mitosis at intermediate concentrations of Δcyclin B. No differences between extracts containing 1100 and 2200 nuclei/μl were observed at 17.5 and 84 nM Δcyclin B, which were, respectively, well below and above the threshold concentrations for entry into mitosis, as measured previously. In contrast, with 35 nM Δcyclin B, extracts with 1100 nuclei/μl entered mitosis by 160 minutes, whereas extracts with 2200 nuclei/μl did not enter mitosis even after 210 minutes. With 42 nM Δcyclin B, extracts with both concentrations of nuclei entered mitosis, but with different lag times. These results are consistent with our prediction that increasing concentrations of DNA enlarge the hysteresis loop, even in the absence of aphidicolin. Furthermore, these types of experiments provide quantitative data that can be compared with simulations of our mathematical model to aid in parameter estimation.

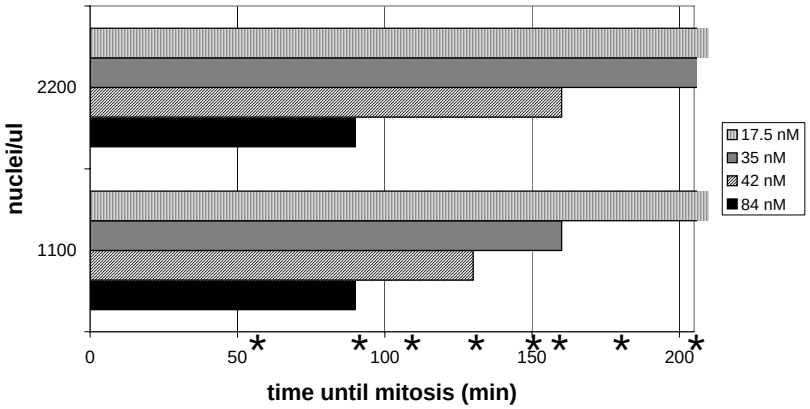

Figure 4.13. Effect of nuclear concentration on lag times into mitosis at different concentrations of Δcyclin B. A cell extract was prepared and supplemented with sperm nuclei at the indicated concentrations. Extracts were activated (released from M-phase arrest) by addition of $CaCl_2$ to a concentration of 0.4 mM. Extracts were supplemented with 100 μg/ml cycloheximide then aliquoted and supplemented with the concentrations of Δcyclin B indicated in the legend. At the time indicated by asterisks (*), aliquots of extracts were stained with DAPI and observed by fluorescence and phase microscopy. Extracts were scored as in mitosis when NEB was >90%.

The second set of experiments was performed essentially the same way except that 100 μg/ml aphidicolin was added to block DNA replication. The concentrations of Δcyclin B were higher in these experiments, based on our previous studies of cyclin thresholds in aphidicolin-treated

extracts (Sha et al., 2003). As shown in Fig. 14, aphidicolin raised the threshold concentration of Δcyclin B required to trigger mitosis at both concentrations of nuclei. At the lower concentration of nuclei (1100/μl), the threshold was between 70 and 105 nM, and at the higher concentration (2200/μl), the threshold was between 105 and 140 nM. In this experiment, extracts were not monitored at early time points to determine differences in lag time into mitosis. We predict that at concentrations of Δcyclin B above [Cdk1], which is present at constant levels, extracts will behave identically, since Cdk1 will become limiting. Based on Fig. 3 and data not shown, [Cdk1] is between 105 and 200 nM.

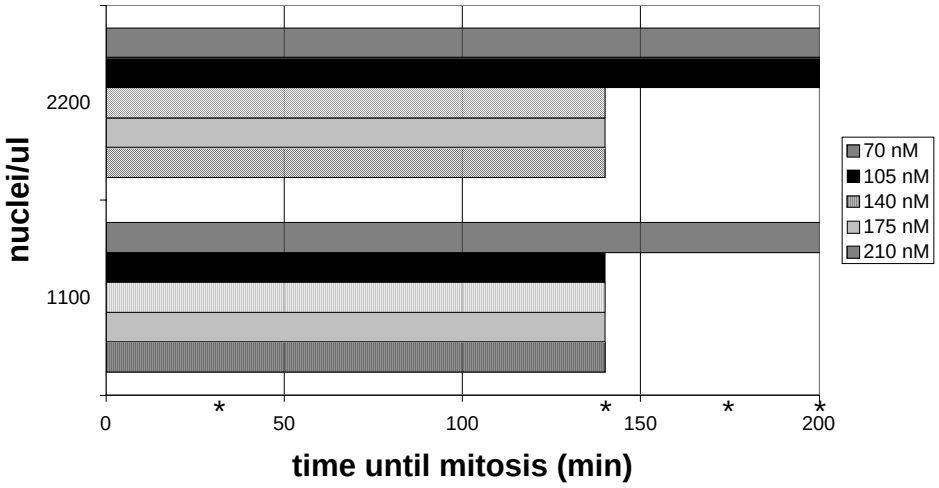

Figure 4.14. Effect of nuclear concentration on cyclin thresholds in aphidicolin-treated extracts. A cell extract was prepared and supplemented with sperm nuclei at the indicated final concentrations. Extracts were activated by addition of $CaCl_2$, supplemented with 100 μg/ml cycloheximide and 100 μg/ml aphidicolin, then aliquoted and supplemented with the concentrations of Δcyclin B indicated in the legend. At the times indicated by asterisks (*), aliquots of extracts were stained with DAPI and observed by fluorescence and phase-contrast microscopy. Extracts were scored as in mitosis when NEB was >90%.

5.0 Details of Key Accomplishments in Software Development

5.1 Jig Cell

JigCell is a suite of software components intended to provide a problem-solving environment for bottom-up modeling of molecular regulatory networks (see Fig. 2.1). To support the most tedious and error-prone steps of the modeling cycle, JigCell provides three major facilities. The Model Builder assists the user to translate a wiring diagram into a correct and consistent set of differential-algebraic-discrete equations. The kinetic constants in the model, which are, for the most part, unknown at this stage are given names instead of numerical values. The Run Manager associates a particular experimental protocol with (1) a model (mathematical equations), (2) a specific set of parameter values and initial conditions, and (3) specifications for numerical simulation of the equations. The Run Manager tracks instructions for deriving the specific parameter values from a "basal" parameter set, so that the modeler can easily explore the dynamics of a model by twiddling the basal parameter values. The Comparator contains experimental data, a pointer to the appropriate row in a run file for simulating this data, output from the simulation, instructions for transforming simulation results into predictions in the same format as the experimental data, and a facility for quantifying the goodness-of-fit of the simulated to observed data and flagging outliers.

In order to explain the features of our software, we will refer regularly to a simple, representative example of a protein interaction network: the control of cyclin-dependent kinase (Cdk) activity in frog cells illustrated in Fig. 5.1.

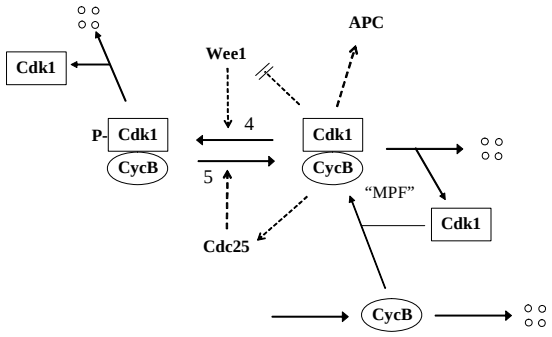

Figure 5.1. Activation of M-phase promoting factor (MPF) in frog cells [NOV93]. Mitosis is initiated by cyclin-dependent kinase (Cdk1) in association with cyclin B (CycB). In frog eggs, CycB is synthesized steadily (reaction 1) and degraded periodically (reaction 2; catalyzed by the anaphase promoting complex, APC). CycB combines rapidly with Cdk1 subunits (reaction 3) to form active MPF. MPF is inactivated by phosphorylation (reaction 4; catalyzed by Wee1) and re-activated by dephosphorylation (reaction 5; catalyzed by Cdc25). Three feedback signals control this network: MPF activates Cdc25 (positive feedback), MPF inactivates Wee1 (mutual antagonism), and MPF activates the APC (negative feedback).

5.1.1 The JigCell Model Builder

Developers: Marc Vass, Ranjit Randhawa

http://jigcell.biol.vt.edu/JCMB.html

Regulatory network models attempt to deduce the physiological properties of a cell from wiring diagrams of its control systems. These wiring diagrams are graphs where vertices represent the concentrations of the interacting macromolecules, and edges represent chemical reactions. Edges are directed from reactants toward products. Edges may also be annotated with the name(s) of species (catalysts, e.g., enzymes) that affect the rate of the chemical reaction without taking part in the reactions. Chemical reactions cause the concentrations of the chemical species (C_i) to change in time according to the differential equations

$$\frac{dC_i}{dt} = \sum_{r=1}^{R} b_{ij} v_j, \quad i = 1, \ldots, N \tag{5.1}$$

where R is the number of reactions, v_j is the velocity of the jth reaction, and b_{ij} is the stoichiometric coefficient of species i in reaction j ($b_{ij} < 0$ for substrates, $b_{ij} > 0$ for products, $b_{ij} = 0$ if species i does not take part in reaction j). A "Model Builder" is a user-interface for specifying reaction networks and creating the differential equations that govern the dynamics of a network. A model builder should provide the user with both guidance and flexibility in entering reactions and rate laws, it should check for common errors, it should enforce constraints such as conservation of mass and detailed balance of reversible reaction loops, and it should support features like compartments, flags, discontinuous events (like cell division), etc.

There are four classes of model builders. Virtual Cell, JDesigner and Cell Designer provide graphical user interfaces, i.e., a drawing board on which the user can construct a wiring diagram like Fig. 1. To enter rate laws, one generally clicks on the reaction edge to open a dialog box. Diagramming tools like these are intuitively appealing, but they can become very clumsy for representing large reaction networks, unless very strict diagramming rules are enforced (but then the diagram loses its intuitive appeal). Wizard interfaces, like Gepasi and Copasi, guide the user through the modeling process by a series of dialog boxes. Wizards are familiar interfaces for guiding users through a complex, highly-structured and well-defined task that is essential but infrequent, like loading software on a computer or preparing tax forms. But wizard interfaces can be tiresomely slow for expert users who are carrying out a task with some frequency (daily or weekly). Script-based interfaces, like SCAMP (for reaction networks) or WinPP (for reaction equations), are fast and flexible, and often preferred by experts who are used to programming languages. But they are not suitable for novices. The JigCell Model Builder (JCMB) (Vass et al., 2006) uses a spreadsheet interface, with each row specifying a particular reaction or auxiliary information needed for the model (user-supplied rate laws, flags, discontinuous events, etc.). A spreadsheet is a familiar paradigm for entering and manipulating information, with the advantage that a great deal of information can be displayed on each screen.

The JCMB User's Manual is available on the web at:
http://jigcell.biol.vt.edu/jigcell/docs/Model%20Builder/JCMBDoc.html

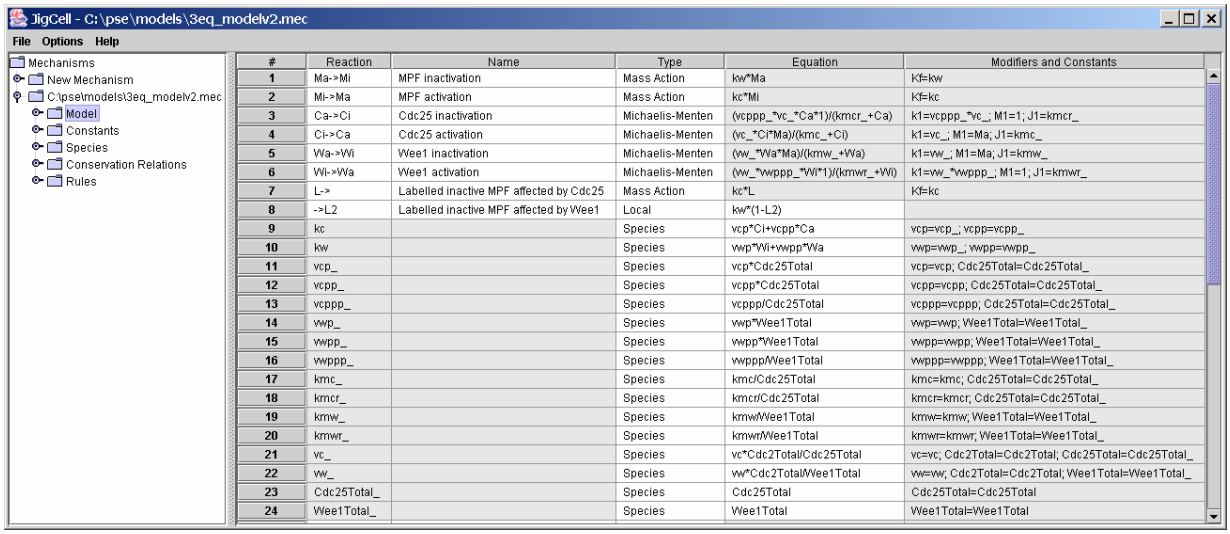

#	Reaction	Name	Type	Equation	Modifiers and Constants
1	Ma->Mi	MPF inactivation	Mass Action	kw*Ma	Kf=kw
2	Mi->Ma	MPF activation	Mass Action	kc*Mi	Kf=kc
3	Ca->Ci	Cdc25 inactivation	Michaelis-Menten	(vcppp_*vc_*Ca*1)/(kmcr_+Ca)	k1=vcppp_*vc_; M1=1; J1=kmcr_
4	Ci->Ca	Cdc25 activation	Michaelis-Menten	(vc_*Ci*Ma)/(kmc_+Ci)	k1=vc_; M1=Ma; J1=kmc_
5	Wa->Wi	Wee1 inactivation	Michaelis-Menten	(vw_*Wa*Ma)/(kmw_+Wa)	k1=vw_; M1=Ma; J1=kmw_
6	Wi->Wa	Wee1 activation	Michaelis-Menten	(vw_*vwppp_*Wi*1)/(kmwr_+Wi)	k1=vw_*vwppp_; M1=1; J1=kmwr_
7	L->	Labelled inactive MPF affected by Cdc25	Mass Action	kc*L	Kf=kc
8	->L2	Labelled inactive MPF affected by Wee1	Local	kw*(1-L2)	
9	kc		Species	vcp*Ci+vcpp*Ca	vcp=vcp_; vcpp=vcpp_
10	kw		Species	vwp*Wi+vwpp*Wa	vwp=vwp_; vwpp=vwpp_
11	vcp_		Species	vcp*Cdc25Total	vcp=vcp; Cdc25Total=Cdc25Total_
12	vcpp_		Species	vcpp*Cdc25Total	vcpp=vcpp; Cdc25Total=Cdc25Total_
13	vcppp_		Species	vcppp/Cdc25Total	vcppp=vcppp; Cdc25Total=Cdc25Total_
14	vwp_		Species	vwp*Wee1Total	vwp=vwp; Wee1Total=Wee1Total_
15	vwpp_		Species	vwpp*Wee1Total	vwpp=vwpp; Wee1Total=Wee1Total_
16	vwppp_		Species	vwppp/Wee1Total	vwppp=vwppp; Wee1Total=Wee1Total_
17	kmc_		Species	kmc/Cdc25Total	kmc=kmc; Cdc25Total=Cdc25Total_
18	kmcr_		Species	kmcr/Cdc25Total	kmcr=kmcr; Cdc25Total=Cdc25Total_
19	kmw_		Species	kmw/Wee1Total	kmw=kmw; Wee1Total=Wee1Total_
20	kmwr_		Species	kmwr/Wee1Total	kmwr=kmwr; Wee1Total=Wee1Total_
21	vc_		Species	vc*Cdc2Total/Cdc25Total	vc=vc; Cdc2Total=Cdc2Total; Cdc25Total=Cdc25Total_
22	vw_		Species	vw*Cdc2Total/Wee1Total	vw=vw; Cdc2Total=Cdc2Total; Wee1Total=Wee1Total_
23	Cdc25Total_		Species	Cdc25Total	Cdc25Total=Cdc25Total
24	Wee1Total_		Species	Wee1Total	Wee1Total=Wee1Total

Figure 5.2. The frog cell model (Fig. 1) in the JigCell Model Builder

A typical JCMB spreadsheet is illustrated in Fig. 5.2. A *reaction row*, e.g., row 1, has the format Reactant(s) -> Products(s). The stoichiometry of the reaction is specified by writing an integer directly in front of a species name or by separating the stoichiometric coefficient from the name by an asterisk. The "type" column specifies the rate law to be applied to this reaction, maybe a standard rate law (like mass action or Michaelis Menten) or a user-supplied rate law (defined elsewhere) or a "local" rate law (defined in the next column and applicable only to this reaction). The rate law is displayed in the next column, subject to additional information supplied in the last column. The last column supplies specific names for all the generic rate constants used in the rate law, and identifies any modifiers (enzymes, transcription factors, etc.) with specific species in the model. (A modifier may be a constant concentration.)

A *rate law* row defines a user-supplied rate law that can be used elsewhere in the spreadsheet to specify the rates of certain reactions. A *function row* specifies an algebraic function that takes a list of arguments and returns a value. A *species equation* row specifies an equation for computing a chemical species that does not appear as a substrate or product in any of the reactions.

The JCMB automatically generates some other spreadsheets providing the user with necessary information. The *Constants Spreadsheet* shows the user all rate constants and other parameters (e.g., constant species, conserved sums) in the model. These constants may be assigned numerical values here (default values), but that is not required. The *Species Spreadsheet* lists all reactants and products, and allows the user to specify initial conditions for a simulation, if desired.

The JCMB is a model editor. It can start from scratch, or it can take an SBML file as input, in which case it populates the spreadsheet from the data in the file. The user changes the model and outputs the new or modified model as an SBML file. In addition, JigCell provides capabilities for outputting a mathematical description of the model (differential equations) as FORTRAN or as an '.ode' file for use by WinPP and XPP. The ode file is more readable than FORTRAN.

5.1.2 The JigCell Run Manager

Developers: Marc Vass, Ranjit Randhawa

http://jigcell.biol.vt.edu/JCRM.html

A model of a complex macromolecular regulatory system (a gene-protein interaction network) will be used to understand a large variety of experimental results. We need a tool to keep track of all the simulations involved in fitting the model to the data. For example, when modeling the yeast cell cycle, we must simulate the phenotypes of 10's or 100's of mutant strains. This involves a simulation run for each strain, where each simulation run differs from others in a small number of parameters. The JigCell Run manager (JCRM) is a tool that allows users to express a hierarchy of simulation runs that define the minor differences between runs. That is, one run might be identical to a base run, except for changes to a few parameters or initial conditions. Hierarchies can be built up, whereby a given simulation inherits the differences from the basal run and from one or more other runs. In this way, the modeler specifies the inheritance rules once and for all, and then the basal parameter specifications can be changed at will. The JCRM automatically adjusts all simulation runs to the current basal specifications.

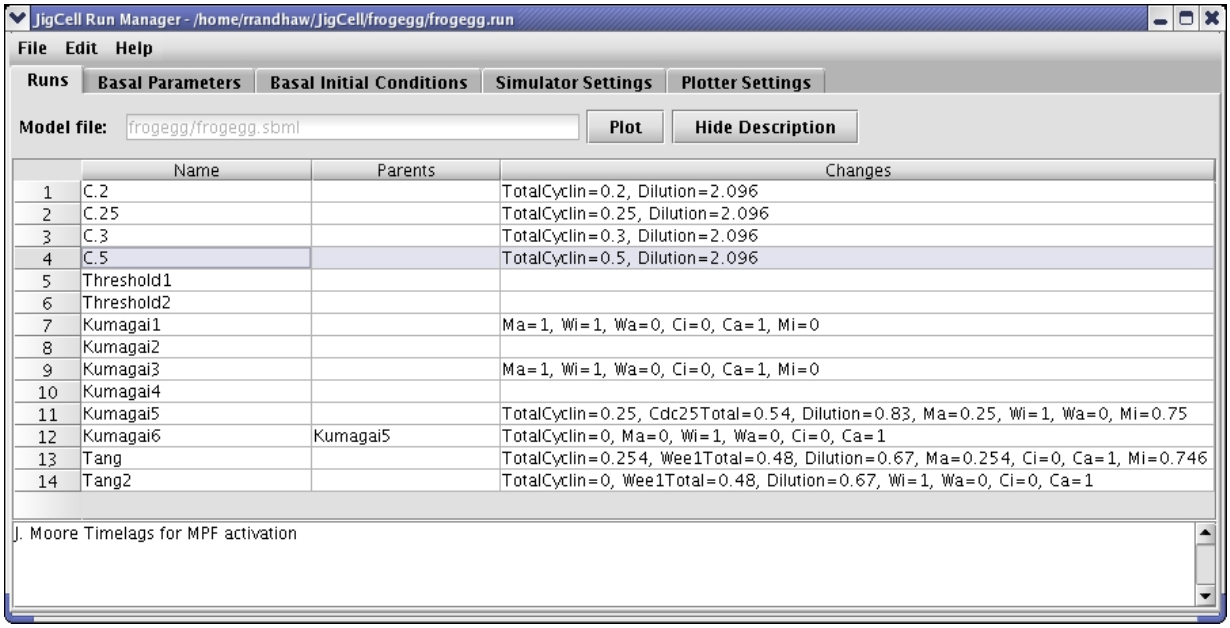

	Name	Parents	Changes
1	C.2		TotalCyclin=0.2, Dilution=2.096
2	C.25		TotalCyclin=0.25, Dilution=2.096
3	C.3		TotalCyclin=0.3, Dilution=2.096
4	C.5		TotalCyclin=0.5, Dilution=2.096
5	Threshold1		
6	Threshold2		
7	Kumagai1		Ma=1, Wi=1, Wa=0, Ci=0, Ca=1, Mi=0
8	Kumagai2		
9	Kumagai3		Ma=1, Wi=1, Wa=0, Ci=0, Ca=1, Mi=0
10	Kumagai4		
11	Kumagai5		TotalCyclin=0.25, Cdc25Total=0.54, Dilution=0.83, Ma=0.25, Wi=1, Wa=0, Mi=0.75
12	Kumagai6	Kumagai5	TotalCyclin=0, Ma=0, Wi=1, Wa=0, Ci=0, Ca=1
13	Tang		TotalCyclin=0.254, Wee1Total=0.48, Dilution=0.67, Ma=0.254, Ci=0, Ca=1, Mi=0.746
14	Tang2		TotalCyclin=0, Wee1Total=0.48, Dilution=0.67, Wi=1, Wa=0, Ci=0, Ca=1

Figure 5.3. The Run Manager Spreadsheet for the frog cell model.

JCRM manages the description and execution of ensembles of simulation runs using a tabbed spreadsheet interface (Fig. 5.3). There are 5 tabs in the JCRM for Runs, Basal Parameters, Basal Initial Conditions, Simulator Settings and Plotter Settings. In the Runs tab the spreadsheet interface specifies how to simulate a certain experiment and contains 3 columns. The name column specifies the name of a run (or experiment). The parents column describes the hierarchy of a particular run. The changes column presents a list of changes to the basal parameters, basal initial conditions, simulator settings and plotter settings that have been made for a particular run. The changes are made using the changes editor (Fig. 5.4), which opens when the user clicks on the changes cell for a particular run. The changes for a particular run override the changes inherited by any parents and propagate to its children. The colors reflect where the changes are

made, blue for changes made in the current run (locally) or green for changes inherited from a parent (or older ancestor).

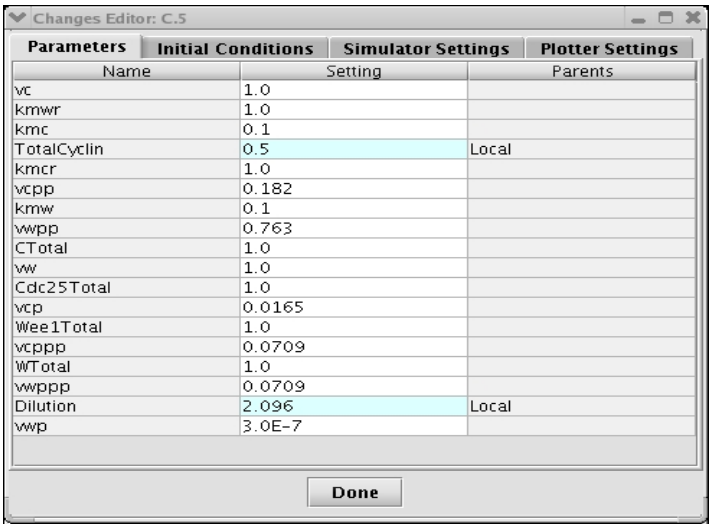

Name	Setting	Parents
vc	1.0	
kmwr	1.0	
kmc	0.1	
TotalCyclin	0.5	Local
kmcr	1.0	
vcpp	0.182	
kmw	0.1	
vwpp	0.763	
CTotal	1.0	
vw	1.0	
Cdc25Total	1.0	
vcp	0.0165	
Wee1Total	1.0	
vcppp	0.0709	
WTotal	1.0	
vwppp	0.0709	
Dilution	2.096	Local
vwp	3.0E-7	

Figure 5.4. The Changes Editor of JigCell Run Manager.

Figure 5.3 shows a Run Manager spreadsheet for simulating some experiments done on frog cell extracts to characterize the activation of MPF. Each row is a separate experiment. For example, rows 1-4 describe four experiments done by Jonathon Moore on MPF activation in extracts prepared with different amounts of non-degradable cyclin B (20, 25, 30 and 50 nM). The parameter sets are all derived from the same basal set (whatever the basal parameter values happen to be): the only difference being that the parameters/initial conditions “TotalCyclin” and “Dilution” are set appropriately in each row. The plot button on the Runs tab invokes an immediate simulation of any row and plots the results. This feature is handy in checking that all the information for simulating this particular experiment has been correctly entered.

The Basal Parameters and Basal Initial Conditions tabs permit the user to view and make changes to the basal settings for all runs.

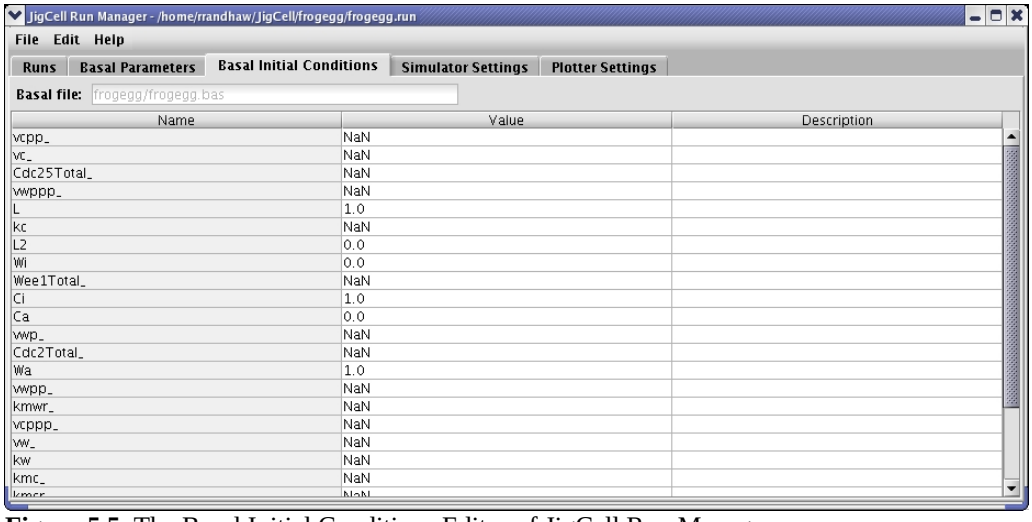

Name	Value	Description
vcpp_	NaN	
vc_	NaN	
Cdc25Total_	NaN	
vwppp_	NaN	
L	1.0	
kc	NaN	
L2	0.0	
Wi	0.0	
Wee1Total_	NaN	
Ci	1.0	
Ca	0.0	
vwp_	NaN	
Cdc2Total_	NaN	
Wa	1.0	
vwpp_	NaN	
kmwr_	NaN	
vcppp_	NaN	
vw_	NaN	
kw	NaN	
kmc_	NaN	

Figure 5.5. The Basal Initial Conditions Editor of JigCell Run Manager.

The Simulator Settings tab specifies the simulator to be used and numerical values for the simulator's parameters: total time of integration, method to use, tolerances, output interval, etc. In Fig. 5.6 the simulator package is XPP. The other main simulator provided is LSODAR, for solving stiff differential equations. Other simulators can be added easily. For example, Gillespie's Stochastic Simulation Algorithm could be provided, or access given to the capabilities of the BioNetS package for stochastic simulation (a part of DARPA's BioSPICE).

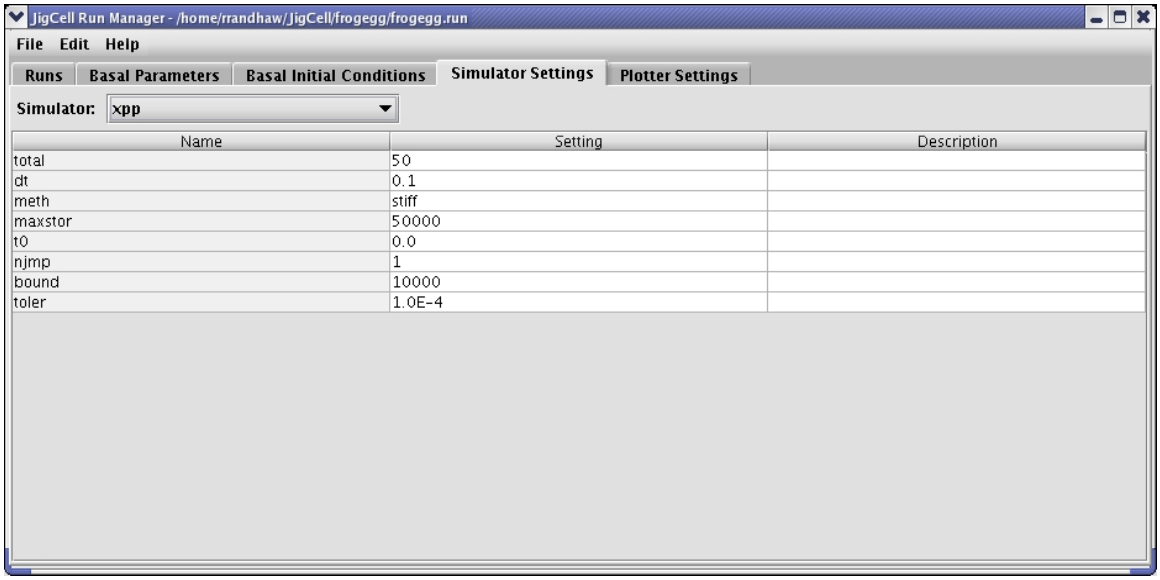

Figure 5.6. The Simulator Settings tab of JigCell Run Manager.

On the Plotter Settings tab (Fig. 5.7) the user can specify the variables to be plotted and customize the plot by selecting colors, mark styles, whether to connect points, etc. Alternatively the user may simply use the default settings, after selecting what variable to plot.

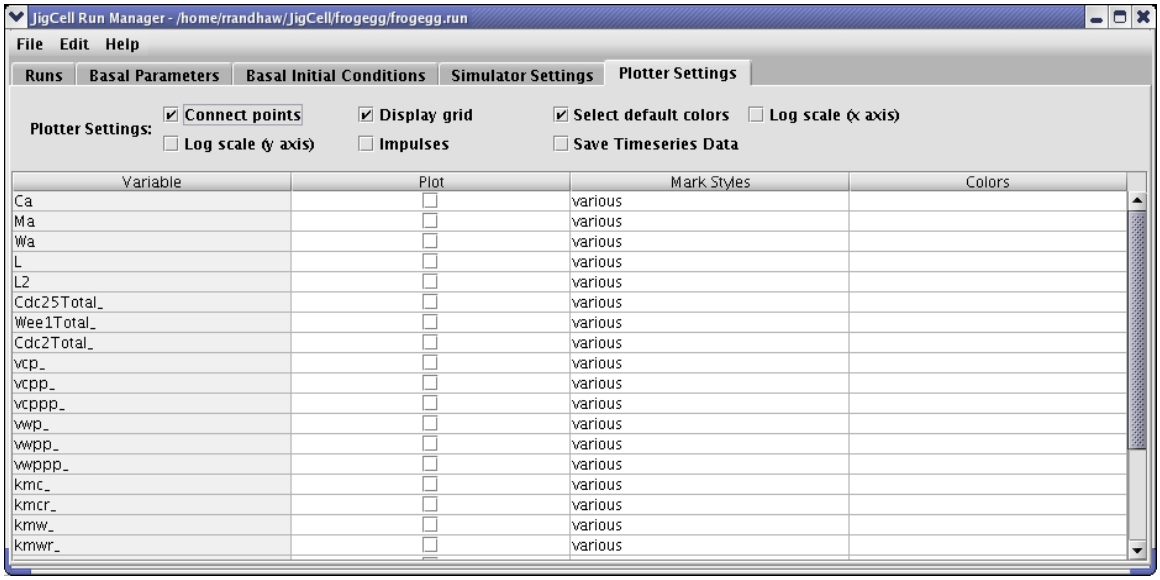

Figure 5.7. The Plotter Settings tab of JigCell Run Manager.

The Run Manager provides a sophisticated mechanism for keeping track of logical relationships among simulations done on a single model to fit a variety of experiments. Suppose we wanted to describe the simulation of a series of yeast cell mutants. The first row of the Run Manager might describe how to simulate wild-type cells, using a basal parameter set. The second row might describe the simulation of a Cln2-deletion mutant using exactly the same information as in row 1, except that the rate constant for synthesis of Cln2 (given the name "kscln2" in the Model Builder) is singled out and given the value 0. Suppose row three describes a mutant cell with two copies of the wild-type Cln2 gene. In this case, kscln2 must be singled out and multiplied by 2. Now, if the modeler decides that his/her first guess of a numerical value for kscln2 is inopportune, it is a simple matter to change the value of kscln2 in the basal parameter set, and this change will be propagated automatically by the Run Manager to all simulations of mutants involving changes in expression of Cln2. By organizing information in this way, the Run Manager allows the modeler easily to explore the parameter space of a model over a complicated set of simulations.

The JigCell Run Manager is unique among the many software programs intended to support molecular systems biology. Downloads and documentation for the Run Manager are available from the JigCell web site.

5.1.3 The JigCell Comparator

Developer: Nicholas Allen

http://jigcell.biol.vt.edu/compare.html

The Comparator is a tool for quantitative comparison of experimental data to model simulations. Source code, documentation, and a 'walk through' are provided on the JigCell web site.

The Comparator is organized as a series of spreadsheets, accessed from tabs on the header bar. In Fig. 5.8, the first spreadsheet, for entering experimental data, is selected. The data is recorded as a "lists of lists". Elements of these lists may real numbers, integers, Boolean variables, or character strings. For instance, in Fig. 5.8, the list ((2, 0.75), (4, 0.51), (8, 0.21)) represents a time series of measurements of relative activity of MPF in a frog cell extract (75% of maximal activity after 2 min, etc.). The data was extracted from Fig. 4b of Kumagai & Dunphy [KUM95]. This format is very flexible for recording biochemical and genetic observations. For example, the list (true, 1.8) might answer the questions "is the mutant viable?" and "if so, how much large is it at division compared to wild-type cells?" The list (false, "anaphase") might answer the questions "is the mutant viable?" and "if not, at what phase in the cell cycle is it arrested?"

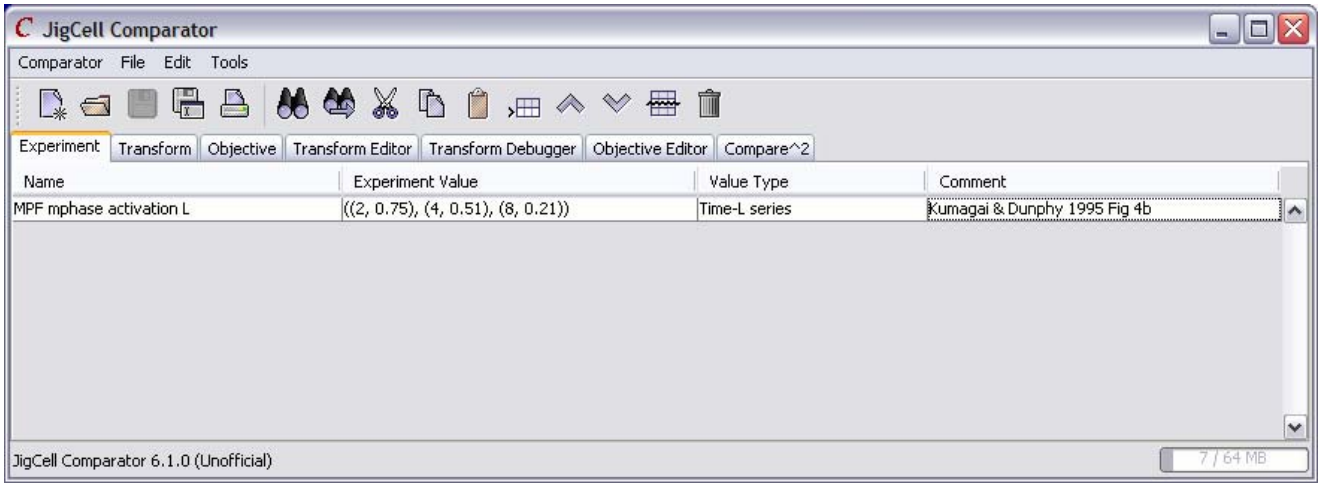

Figure 5.8. The Jig Cell Comparator: Experimental data spreadsheet.

The second tab (Fig. 5.9) associates experimental data with a simulation. The first two columns repeat info from the Experiment tab. Column 3 contains instructions on how to simulate this experiment. It points to a row of a run file created by the Run Manager. The simulator specified there is invoked to return time series of all the variables in the model, in the form of a table whose columns are: t, x1(t), x2(t), … The simulator output is then passed through a program, called a "Transform", that converts simulator output into the same format as the experimental data: say (false, "anaphase") or, as in Fig. 5.9, a time series of MPF activity.

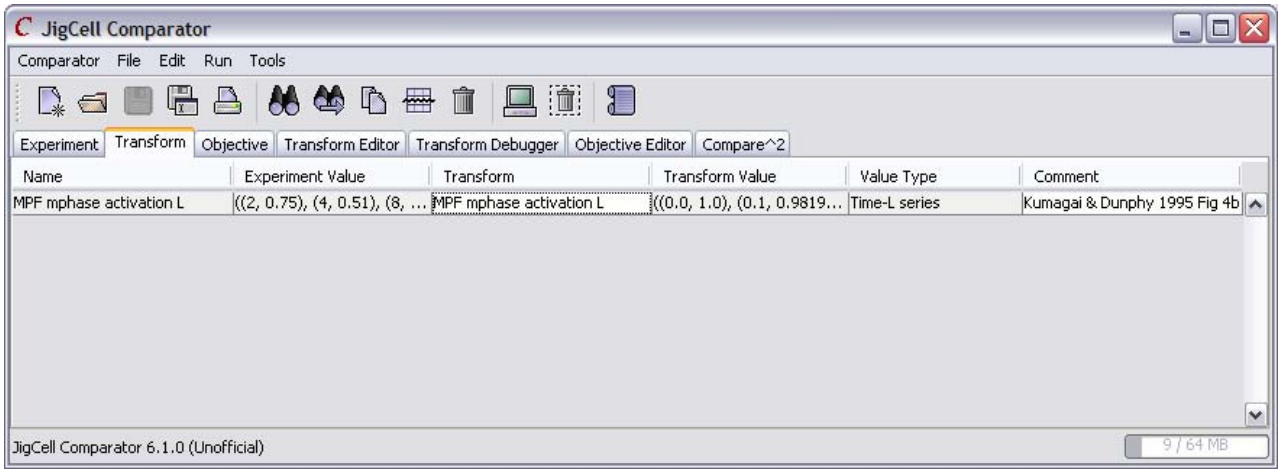

Figure 5.9. The JigCell Comparator: Transform spreadsheet.

The third tab describes how to compute a numerical value representing the goodness-of-fit of the simulation to the data, and specifies a threshold for this number, beyond which the fit is considered unacceptable. For example, in Fig. 5.10, column 4 specifies that the experimental data in column 2 is to be compared to the simulated time course in column 3 by a weighted orthogonal sum of squares (WOSS = sum of squares of the shortest distance (in a weighted-orthogonal sense) from each data point to the simulated curve). Column 5 is the result of this calculation. It is compared, according to Column 6 to a user-specified threshold. If the comparison is unacceptable, this comparison is highlighted in color so that the modeler can see at

a glance where the model (equations plus parameter values) is having problems. In this case, the fit of the model to the data (Fig. 5.11) is excellent.

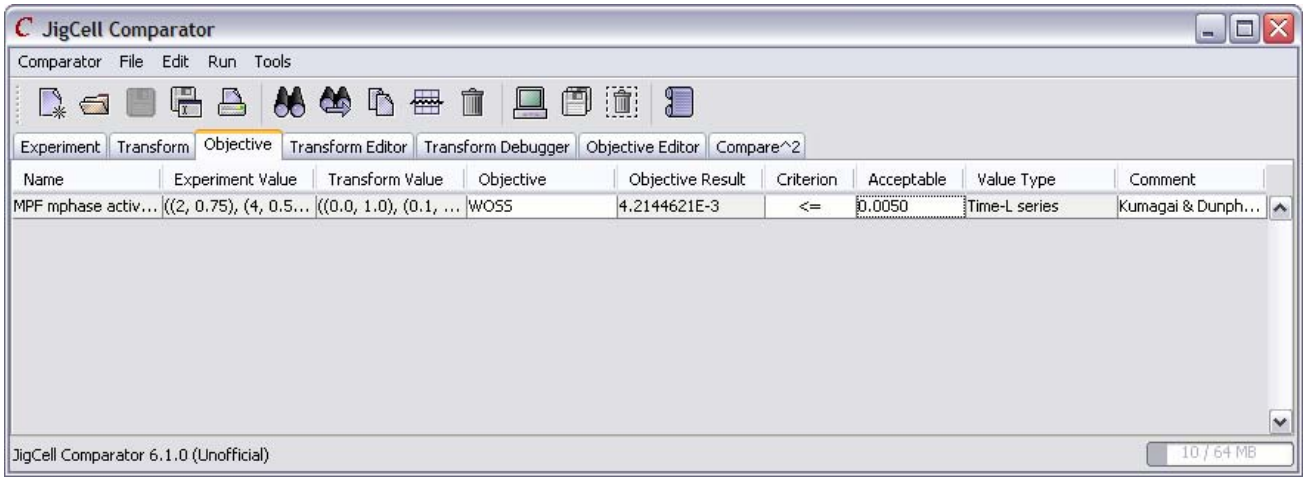

Figure 5.10. The JigCell Comparator: Objective spreadsheet.

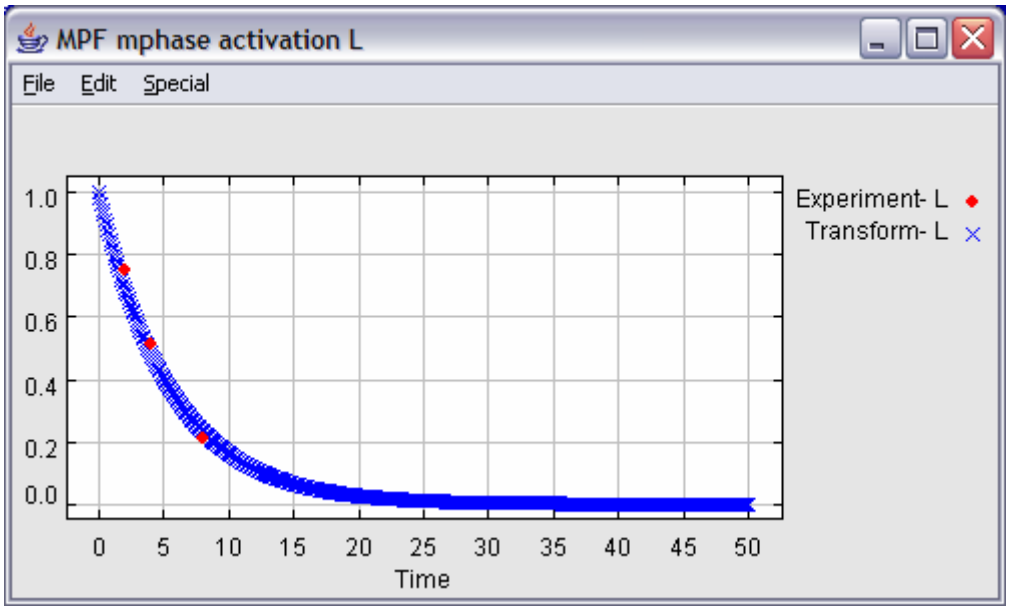

Figure 5.11. The JigCell Comparator: sample fit of model (X) to data points (o)

The most difficult part of process is writing the computer program that transforms simulation output into the format of the experimental data. For time series data, the Transform is trivial, but for yeast mutant phenotypes, the Transform is very complicated. For qualitative observations, like 'Mutant X is blocked in anaphase', it is also difficult to compute a sensible numerical value for the Objective Function. These issues examined in detail in Allen et al. (2006): "Computer evaluation of network dynamics models with application to cell cycle control in budding yeast."

Summary

JigCell is designed to support the modeling cycle outlined in Fig. 2.1. The model builder assists the user in defining a chemical reaction network and writing the differential equations that describe the network's dynamics. In our philosophy, the model's equations are treated separately from the parameter values. The model equations give names but not numerical values to the rate constants and other parameters needed to define the reaction rates. The numerical values of these constants (collectively called "parameters") are recorded in a separate file, called the "basal" parameter file. There are also basal files for initial conditions and simulator parameters. The Run Manager manages a collection of simulations on a model (an SBML file from the ModelBuilder) together with its basal files. Each row of a run file is a simulation of the model for specific values of the parameters and initial conditions; values that are derived from the basal sets. The Run Manager keeps track of the logical relationships among the parameters and initial conditions. By organizing the simulations in this way, the Run Manager allows for easy exploration of the model's parameter space, the inner loop of the modeling cycle (Fig. 2.1), which is the most common and tedious part of the process. By changing the numerical value of a suspect parameter in the basal set, the modeler can now see how the change propagates through the entire model and affects simulations of all the data to be modeled. The Comparator highlights the discrepancies between the data and the new parameter set. The parameter change may indeed fix the problem for which it was intended, but may introduce new and unexpected discrepancies between the model and the experimental data. The Compare-Square capability of the Comparator helps the user to compare two different parameter sets.

By automating the comparison process, the Comparator takes all the drudgery out of the parameter-twiddling stage of model exploration, when the modeler is testing his/her intuition about the dynamic properties of a wiring diagram. It also provides the groundwork for the next stage: automatic parameter estimation. The computer can now score a fit of the model to the data and explore parameter space automatically for (possibly multiple) regions of good fit. Parameter optimization can be performed by local gradient-following algorithms or by global search algorithms. We are developing such tools, as described in the next section, but they are not yet integrated into JigCell.

5.2 Parameter Estimation

In 1993, Novak and Tyson presented a model of MPF activation in frog cell extracts (see Fig. 1). In order to show that the solutions of their equations were consistent with the known properties of DNA synthesis and nuclear division in intact eggs and extracts, Novak and Tyson had to estimate numerical values of the ~dozen kinetic constants appearing in their equations. Although there were, at the time, direct experimental measurements of only one of these constants, Novak and Tyson were able to predict rate constants for the crucial phosphorylation and dephosphorylation reactions simply by fitting their model to basic qualitative facts about the control system. A few years later, Kumagai and Dunphy [KUM95] and Lee et al. [LEE94] observed the rates of these reactions on recombinant proteins in egg extracts, obtaining values in close agreement with theoretical predictions, as shown by Marlovits et al. [MAR98]. This model and data set provide the standard illustration of JigCell software, as described in the previous section. They were also used as our first test case for automatic parameter estimation: to find an optimal fit of the Novak-Tyson model to the data summarized in Marlovits et al.

The experiments under consideration are quite diverse: some time courses of individual components, thresholds for MPF activation and inactivation, and some ‘time lag’ measurements. They come from different laboratories, under subtly different conditions, using different recombinant proteins. The “weight” given to each measurement is often a subjective decision. Measurements are rarely repeated enough times to generate reliable statistics, and measurement errors in the independent variable are often comparable to errors in the dependent variable. In cases like this, which are common in systems biology, we propose to use the public domain software package ODRPACK, which minimizes the weighted sum of orthogonal distances between the experimental data and the predictions of the model (Zwolak et al., 2005a). To minimize this "error function" ODRPACK uses the Levenberg-Marquardt method. ODRPACK needs an initial set of parameter values, for which we used the Marlovits’ estimates. The model equations were integrated by LSODAR, a public domain software package that efficiently solves stiff and non-stiff systems of ordinary differential equations.

From the Marlovits’ initial guess, ODRPACK quickly converged to an optimal set of parameter values that are not too different from the Marlovits’ values, although the value of the objective function dropped eight-fold.

Next, we searched for a globally optimal solution to the same parameter estimation problem (Zwolak et al., 2005b), using a public domain software package VTDIRECT. The DIRECT algorithm (JON93] divides a p-dimensional box in parameter space into smaller boxes and then systematically subdivides the boxes in search of regions of parameter space where the error function values are small. The algorithm is deterministic, globally convergent, and (in a certain sense) computationally efficient. DIRECT calls a user-supplied error function (the one calculated by ODRPACK) to evaluate points in the search space. Only function evaluations are used; the algorithm does not require estimates of the derivatives of the error function. DIRECT subdivides boxes according to a prescription that balances further exploration of boxes with the lowest values of the error function (i.e., the most promising regions of parameter space so far) against further exploration of the largest boxes remaining (i.e., regions of parameter space that have not

been much explored so far). A simple example of how DIRECT explores a two-dimensional parameter space is provided in Fig. 5.12.

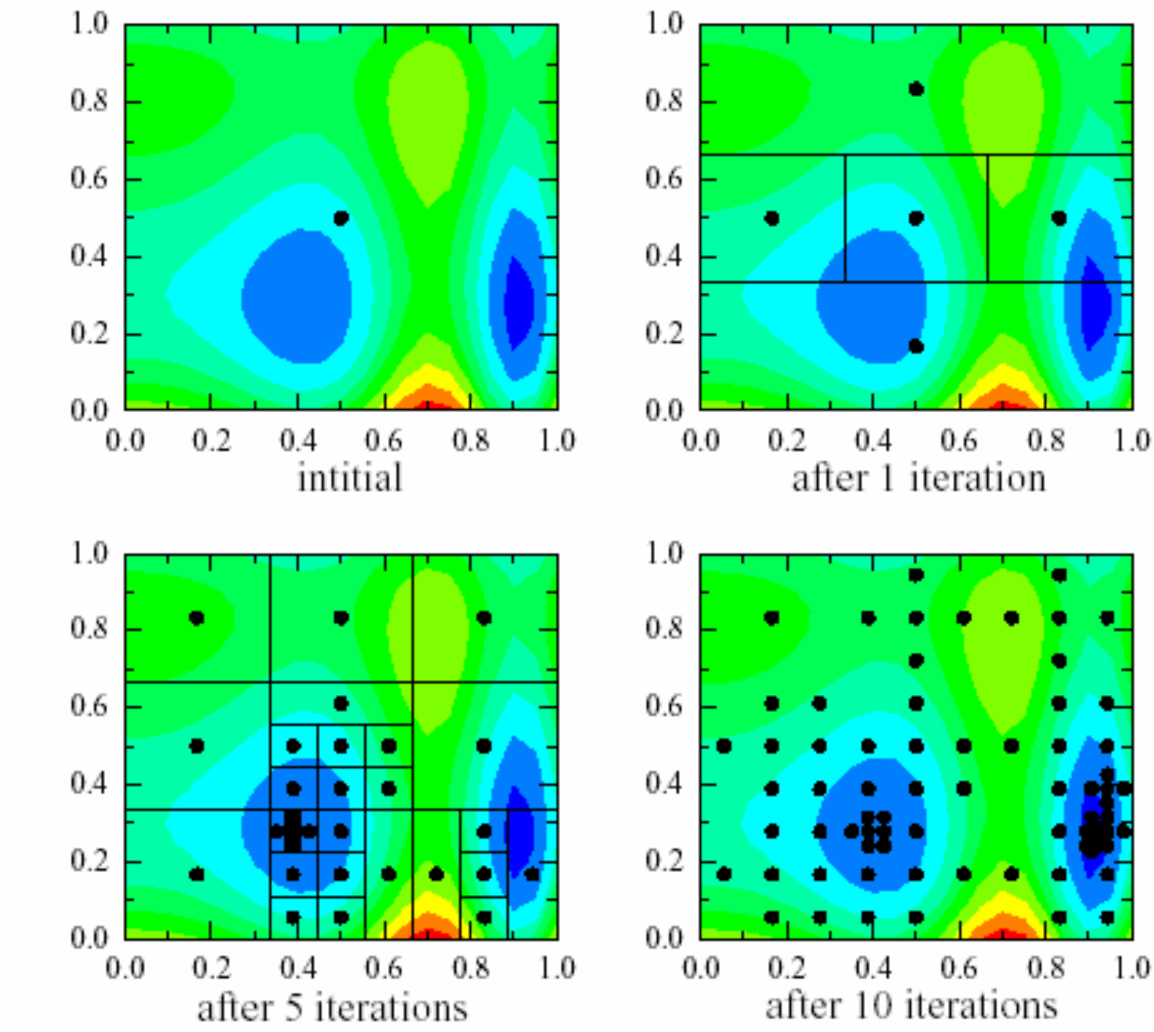

Figure 5.12. A pictorial example of rectangle divisions made by VTDIRECT for a simple two-parameter problem. VTDIRECT detects the local minimum after only 5 iterations and has refocused its efforts on the global minimum after 10 iterations.

VTDIRECT is run for a certain fixed number of error function evaluations and returns the best point found so far plus some other "promising" points sufficiently distant from the best point. We then use ODRPACK to find the locally optimal parameter set(s) close to these points returned by VTDIRECT.

The results of this procedure were interesting. The global search found a second region of parameter space where the fit was just as good as the local search (ODRPACK alone) from the Marlovits' initial guess. The second solution implied that one of the rate laws in the model was incorrectly chosen to be Michaelis-Menten, when a simpler mass-action rate law would do just as well. The simpler model has one fewer parameter to estimate. Otherwise, all other parameter values were quite comparable to the original Marlovits' estimates. For each estimated parameter

ODRPACK gives error-bounds, which are computed from the covariance matrix of the error function at the minimum. For the frog cell model, the error bounds are quite close for all parameters, except for two Michaelis constants. This exercise confirms the reasoning used by Marlovits et al. [MAR98], demonstrates that the data constrain the model parameters tightly, and identifies an accurate, global solution to the parameter estimation problem.

With this success in hand, we decided to tackle global parameter estimation for the budding-yeast cell-cycle model (Panning et al., 2007). This problem is considerably more difficult because: (1) the budding yeast model ~10 times more complex than the frog cell model, (2) the budding yeast data set is ~10 times more extensive, and (3) the budding yeast data is more qualitative than the frog cell extract data. The molecular mechanism of cell cycle control in budding yeast was explored primarily by genetic experiments, with outcomes like "Mutant X is viable, with an extended G1 period and average cell size about twice as large as wild-type cells," or "Mutant Y is inviable, arrested in early S phase with an elongated bud." From observations like these, we build an error function (Allen et al., 2006) that varies discontinuously with parameter changes. For example, the model may predict cell viability for a specific parameter value, $p_{56} < p_{56}^{o}$, and inviability for $p_{56} > p_{56}^{o}$. If the observation is "viable," then this contribution to the error function will show no change, at first, with increasing p_{56}. But, when p_{56} increases through p_{56}^{o}, then the error function will undergo an abrupt increase, as the false prediction is penalized. Hence, derivatives of the error function with respect to the parameters are uninformative, and we cannot use efficient gradient-based search algorithms, like Levenberg-Marquardt. For this problem, we can still use VTDIRECT for global searching, but we replace ODRPACK by a local optimization algorithm, MADS (Mesh-Adaptive Direct Search), that does not require gradients of the error function.

We used a version of the budding yeast model with 36 nonlinear ordinary differential equations requiring 143 parameter estimates. The model was optimized against a data set consisting of phenotypes of 115 different mutants. For each mutation, the model must be simulated, the output transformed, and the predicted phenotype compared to observations to compute a contribution to the error function for this mutant. The 115 specific contributions are summed up to give an error for that specific set of parameter values. It takes approximately 17 seconds to do this evaluation on a 2.3 GHz Power PC G5 processor. At this rate, to explore 1.5 million points in parameter space would take about a year on a PC. Using parallel implementations of DIRECT and MADS (pVTDIRECT and NOMAD), we carried out the optimization on System X, a cluster of 1100 dual-processor Mac G5 nodes at Virginia Tech.

pVTDIRECT was initialized on a box in 143-dimensional parameter space, with the center of the box placed at the parameter values estimated by Chen et al. (2004). Because DIRECT does its first error function evaluation at the center point, it immediately gets a good score (470), which is the score to beat. (A random point in the box will have a score ~2000.) pVTDIRECT ran for 473 iterations, using 1024 processors and making 1.5 million error function evaluations, and returned a point in parameter space at which the error function = 212. Following up on this point using NOMAD produced no further improvement.

A selection of other 'promising' points from DIRECT's search were passed to MADS for refinement, and MADS found final error function values in the range (190, 240). It seems

impossible to get a better score with the Chen et al. (2004) model. Typically, of the 115 mutants in the data set, there are 7-10 whose phenotypes are incorrectly predicted by the model. Another few mutants are on the knife's edge, meaning that, if the optimal parameter values are randomly perturbed by +/- 0.5%, the model fails to predict correctly the phenotypes of a few additional mutants.

Our results indicate that the DIRECT/MADS combination can be used effectively to search globally for an optimal parameter point in a high dimensional parameter space, for a realistic model of a molecular regulatory system constrained by real experimental data that is a mixture of qualitative and quantitative observations.

Parameter Estimation Toolkit

Developer: Jason Zwolak
http://mpf.biol.vt.edu/pet/

PET provides a graphical user interface for defining and running simulations of an SBML model. Runs are managed in hierarchical manner, similar to the JigCell Run Manager, and both programs use the same format for run files. PET also provides facilities for automatic parameter estimation by fitting the model to time course data. PET is intended to run under Windows, Mac OS X, and Unix. PET uses Perl and Gtk+ to achieve cross platform support. PET has been tested and is known to work correctly under Windows and Linux. PET is freely downloadable from the web site above, along with a tutorial on its use.

PET is driven through a set of wizards reached by tabs from the main screen. After loading an SBML model and a basal parameter set, PET provides a wizard (the 'Edit Basals' tab) for editing and managing alternative basal sets. The next tab ('Edit Simulations' in Fig. 5.13) allows the user to define the changes to basal sets (parameter values and initial conditions) that are necessary to simulate a particular experiment. As in the JigCell Run Manager, these changes can be expressed as algebraic functions of parameter names. These functions are evaluated at run-time, using the current basal values, whatever they may be.

On the next tab ('Edit Data') one enters time-series data for a particular species, chosen from a list of dependent variables in the model. PET can fit a collection of experimental data sets with a series of simulation runs defined for a single model.

Next one opens the 'Estimator Settings' tab, which is divided into three parts (Fig. 5.14). In the left-hand panel, each row corresponds to a parameter. Checking a box in the "Fixed" column specifies that that parameter's value is to remain fixed throughout parameter estimation. Min, Max and Initial specify the desired lower bound, upper bound, and initial value of a parameter to be estimated. In the middle column is displayed the experimental time course to be fitted. The user can supply weights for each data point. In the right-hand panel one chooses the optimization algorithm to be used and changes, if necessary, the tolerances and other constants that control the optimization procedure.

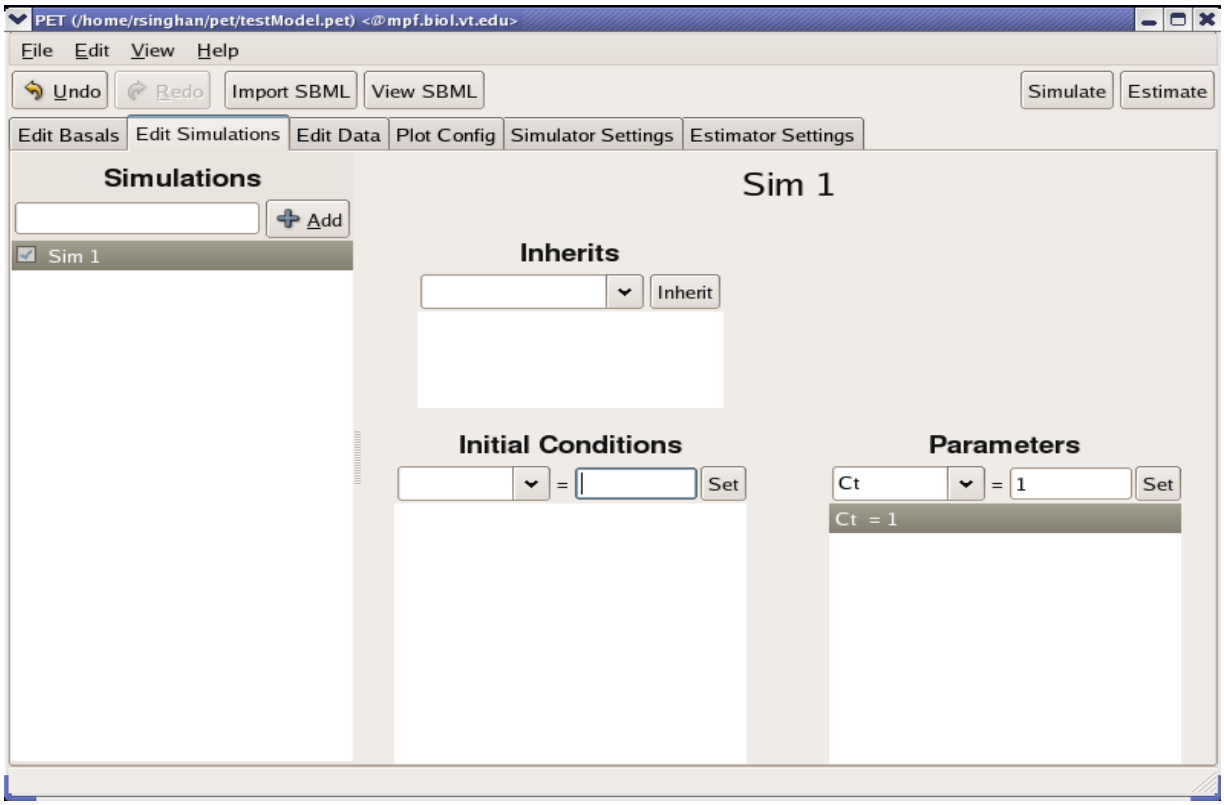

Figure 5.13. The ‘Edit Simulations’ tab in PET.

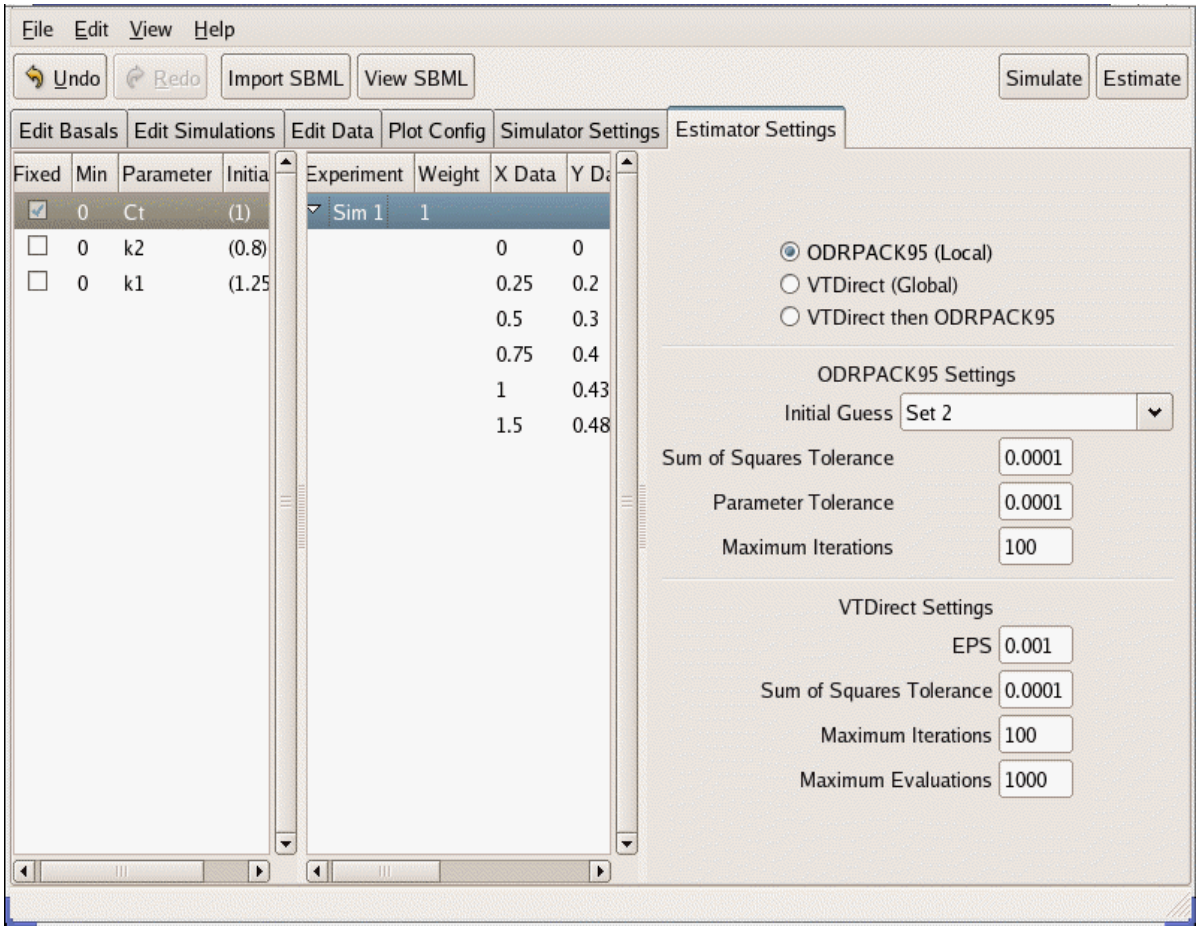

Figure 5.14. The 'Estimator Settings' tab in PET.

Now the user is ready to click the 'Estimate' button. The estimated parameter values are stored in a new 'basal' parameter set called 'Estimated'. With these new values of the parameters, the user can simulate the model and display the results, to see how good the fit is.

PET is a work in progress. Improvements to be made include a richer variety of optimization algorithms, and the ability to fit data types other than time courses.

Param Batch

Developer: Jason Zwolak
http://mpf.biol.vt.edu/software/homegrown/param_batch/

This program provides a batch system for simulating ODE systems with varying parameters on each simulation. The result of a Param Batch run is a PDF or PS file containing plots of all the simulations. Hand "twiddling" of parameters is also supported by PET. Parameter twiddling is a very useful tool for modelers in the initial stage of exploration of a model.

5.3 Bifurcation Analysis

Oscill8

Developer: Emery D. Conrad
http://sourceforge.net/projects/oscill8

Bifurcation theory is an important tool for making connections between macromolecular reaction networks (expressed as systems of nonlinear ordinary differential equations) and cell physiology (the responses of a cell to specific stimuli). Bifurcation theory describes the qualitative features of a dynamical system. A bifurcation point is a combination of parameter values where the solution of a system on nonlinear ODEs undergoes a dramatic change of character. For example, a steady state disappears and the control system jumps to a different steady state (saddle-node bifurcation), or a steady state loses stability and gives way to stable oscillations (a Hopf bifurcation). These bifurcations can often be associated with physiological responses of cells. For example, saddle-node bifurcations might be decision points, where the cell abandons the original steady state (decision 1) and adopts a new steady state (decision 2). Past a Hopf bifurcation, the cell leaves the resting state (steady state) and begins to signal periodically (oscillations), as do, for example, insulin-secreting pancreatic cells in response to blood glucose level.

There are several powerful software programs for bifurcation analysis of systems of nonlinear ODEs. One of the best is AUTO http://sourceforge.net/projects/auto2000/, written by E. Doedel. AUTO is very reliable, but it has some drawbacks. First of all, it is difficult for novices to use. XPPAUT provides a nice front-end to AUTO, integrated with the other analysis features of XPP; but XPP is a pretty sophisticated tool, not designed for systems biologists. Secondly, neither AUTO nor XPPAUT have any capability to record the history of a modeler's exploration of parameter space. Third, modelers desire some tools for searching parameter space automatically for desired bifurcations. Overcoming these drawbacks was the goal of Oscill8.

Oscill8 consists of two distinct pieces that communicate via TCP/IP. o8core, written in C++ is the core of numerical algorithms, controlled by a command-line interface. oscill8, written in C#, is a graphical interface that runs on Windows XP. Linux and MacOS X. By separating the two components, the core programs can be run remotely using powerful computing resources while the GUI runs on a local machine as a controlling client.

The GUI, oscill8, provides many services, including: (a) batched generation of one- and two-parameter bifurcation diagrams, (b) a parameter twiddler, which allows a modeler to explore parameter space quickly and flexibly, (c) a random-walk search feature that explores the bifurcations of a model locally in parameter space, and (d) a search procedure that optimizes parameter values for a desired one-parameter bifurcation diagram.

The last of these features, the optimization of a bifurcation structure, is an entirely novel product of the DARPA BioSPICE project at Virginia Tech. We define a *bifurcation structure*, $S = \{B_1, B_2, \ldots, B_N\}$, as the sequence of bifurcation points, $B_i = (\alpha_i, \beta_i, \tau_i)$, encountered along a steady state curve on a one-parameter bifurcation diagram. Here, α = parameter value, β = state variable values, and τ = bifurcation type (saddle-node, Hopf, etc.). The relative positions of these bifurcation points with respect to one another partitions parameter space into regions of qualitatively different dynamical behavior. When two bifurcation diagrams have the same bifurcation structure, we say they are compatible; otherwise, they are incompatible. We measure the distance between two compatible structures, S and S', by

$$\Phi(S,S') = \sum_{j=1}^{N}\left[\left(\frac{\alpha_j}{|\alpha|} - \alpha_j'\right)^2 + \sum_{k=1}^{n}\left(\frac{\beta_{j,k}}{|\beta_k|} - \beta_{j,k}'\right)^2\right] \qquad (5.2)$$

If Oscill8 has found a bifurcation structure S that is compatible with the desired structure S', then the program seeks to minimize the distance function $\Phi(S,S')$. In order to find a compatible structure, given a starting structure that is incompatible, Oscill8 uses an evolutionary algorithm to search the parameter space. The user must give Oscill8 some help in the form of a sequence of bifurcation structures, $S_1, S_2, \ldots S_M$, that are likely to lead in small steps from the starting structure S to the desired structure S'. The evolutionary algorithm currently implemented in Oscill8 seems to be effective, but there is room here for a great deal of research into good-better-best ways to explore parameter space in search of particular bifurcation structures.

Why is this feature so important? Remember, the goal of computational cell biology is to forge mathematical links between macromolecular reaction networks and cell physiology. The chain of reasoning is

ReactionNetwork↔DifferentialEquations↔VectorField↔BifurcationStructure↔CellPhysiology

Working backwards from cell physiology, we may have a good guess of the bifurcation structure we desire. Working backward from differential equations, we may suspect that a certain reaction network can create that bifurcation structure. But, in general, we do not know where in parameter space the desired bifurcation structure might live (if anywhere). The bifurcation-search facility of Oscill8 has been designed to guide the computer through parameter space in search of a desired bifurcation structure. If the algorithm is successful, then (bingo!) we have hit the jackpot. If it is

unsuccessful, then we have some confidence that the desired bifurcation structure is indeed impossible given the hypothetical reaction network. In that case, we can make a new hypothesis and search again.

5.4 Modularity, Composition and Fusion

Developer: Ranjit Randhawa

Most large network models, like the budding yeast model or the generic cell cycle model described in Chapter 3, are built from smaller modules. Currently this process of composing small models into ever larger (more comprehensive and more accurate) models is done by hand by professional modelers. All current model building tools and their intercommunication language (SBML-Level 2) are designed for monolithic models. The tools and the language do not support notions like submodels, fusion of submodels, dissociation of submodels, etc. The goal of this part of Virginia Tech's BioSPICE project is to define these notions and provide software support for the procedures (Shaffer et al., 2006; Randhawa et al., 2007).

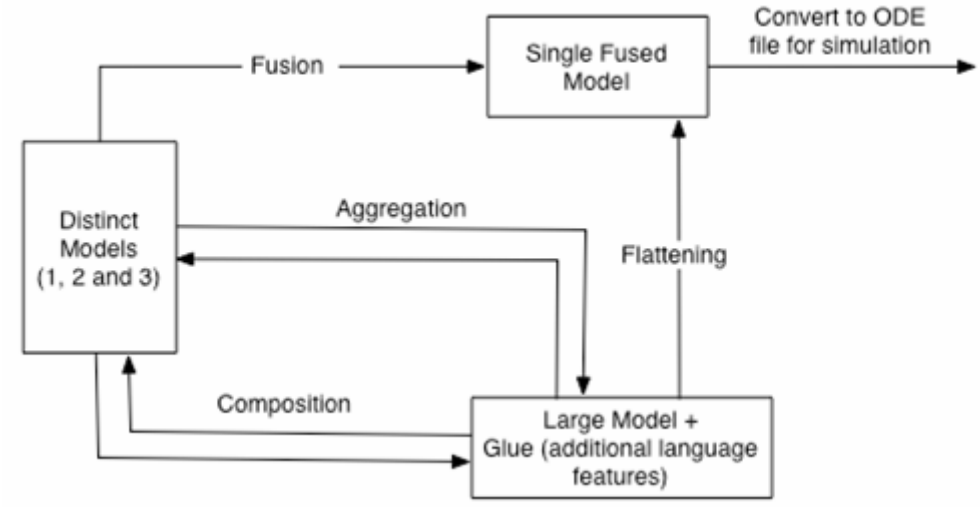

Figure 5.15. Model fusion, composition, aggregation and flattening.

The process of combining two or more submodels into a larger, more comprehensive model can be thought of in several different ways (Fig. 5.15). 'Fusion' is an iterative and irreversible process of combining distinct submodels into a single unified model, containing all the relevant information of the original collection without any redundancies. A Fusion tool takes two or more SBML-Level2 models as input and guides the user through the steps of identifying and resolving any inconsistencies among the models. A wizard interface seems most appropriate for this tool. The output of model fusion is a single, unified SBML-Level2 model. From this output file it would be impossible to reconstruct the input files.

What we call 'Composition' is a reversible form of fusion. A Composition tool looks exactly like a Fusion tool, but the submodels retain their identity, and the tool keeps a record of all the

changes that must be made in order to fuse the submodels together. The output of a Composition tool would be SBML-Level3 (not yet defined), which would be a list of submodels (each one is a perfectly valid Level2 SBML model) followed by new SBML syntax that describes the 'glue' for sticking the submodels together. Clearly, the submodels are easily identified and stripped out of the SBML-Level3 file, if desired. We envision a Flattening tool that takes a composed SBML-Level3 model, applies the glue, and welds the submodels together into a single Level2 fused model, suitable for use by analysis and simulation tools that require SBML-Level2 models.

'Aggregation,' in our minds, is a constrained case of composition. An Aggregation tool packages up a submodel (SBML-Level2) into a 'module' with specific 'input' and 'output' ports. (The module would be an SBML-Level3 object, because the notion of input and output ports needs to be formalized in the Level3 specification.) The Aggregation tool then takes modules and hooks them together, an output of one module being connected to the input port of another module. A graphical interface seems most appropriate for this tool.

The Model Fusion tool is operational and is downloaded as an integral part of the JigCell Suite. The Model Composition tool has been under development since the end of the BioSPICE project. It will be finished in early 2007 and added to the JigCell Suite. Modularization and Aggregation are still being defined and preliminary tools are being developed under support from NIH.

6.0 Literature Cited

[ALT87] W. Alt & J.J. Tyson (1987). A stochastic model of cell division (with application to fission yeast), *Math. Biosci.* 84:159-187.

[AUD06] C. Audet & J.E. Dennis, Jr. (2006). Mesh Adaptive Direct Search Algorithms for constrained optimization, *SIAM Journal on Optimization*, 17:188-217.

[BOG89] P.T. Boggs, R.H. Byrd, J. Rogers Donaldson & R.B. Schnabel (1989). ODRPACK -- Software for Weighted Orthogonal Distance Regression, *ACM Transactions on Mathematical Software* 15:348-364.

[CAL01] A. Calzada, M. Sacristan, E. Sanchez & A. Bueno (2001). Cdc6 cooperates with Sic1 and Hct1 to inactivate mitotic cyclin-dependent kinase, *Nature* 412:355-358.

[CHE00] K.C. Chen et al. (2000). Kinetic analysis of a molecular model of the budding yeast cell cycle, *Molec. Biol. Cell* 11:369-391.

[CRO02] F.R. Cross, V. Archanbault, M. Miller & M. Klovstad (2002). Testing a mathematical model of the yeast cell cycle, *Molec. Biol. Cell* 13:52-70.

[DOE86] E.J. Doedel & J.P. Kernévez (1986). AUTO: Software for continuation problems in ordinary differential equations with applications, Technical report, Applied Mathematics, California Institute of Technology.

[EDG94] B.A. Edgar, D.A. Lehman & P.H. O'Farrell (1994). Transcriptional regulation of string (cdc25): a link between developmental programming and the cell cycle, *Development* 120:3131-3143.

[EDG96] B.A. Edgar & S.A. Datar (1996). Zygotic degradation of two maternal Cdc25 mRNAs terminates Drosophila's early cell cycle program, *Genes & Devel.* 10:1966-1977.

[GHA03] S. Ghaemmaghami et al. (2003). Global analysis of protein expression in yeast, *Nature* 425:737-741.

[GIL76] D.T. Gillespie (1976). A general method for numerically simulating the stochastic time evolution of coupled chemical reactions, *J. Comput. Physics* 22:403-434.

[GOL91] A. Goldbeter (1995). A model for circadian oscillations in the Drosophila period protein, *Proc. Roy. Soc. London Ser. B* 261:319-324.

[HAN00] D. Hanahan & R.A. Weinberg (2000). The hallmarks of cancer, *Cell* 100:57-70.

[HAR89] L.H. Hartwell & T.A. Weinert (1989). Checkpoints: controls that ensure the order of cell cycle events, *Science* 246:629-634.

[HAR96] R.S. Hartley, R.E. Hempel & J.L. Maller (1996). In vivo regulation of the early embryonic cell cycle in Xenopus, *Devel. Biol.* 173:408-419.

[HAR97] R.S. Hartley, J.C. Sible, A.L. Lewellyn & J.L. Maller (1997). A role for cyclin E/Cdk2 in the timing of the midblastula transition in Xenopus embryos, *Devel. Biol.* 188:312-321.

[HOL98] F.C. Hostege et al. (1998). Dissecting the regulatory circuitry of a eukaryotic genome, *Cell* 95:717-728.

[HOL04] J. Holtzendorff et al. (2004). Oscillating global regulators control the genetic circuit driving a bacterial cell cycle, *Science* 304:983-987.

[JOH76] G.C. Johnston, J.R. Pringle & L.H. Hartwell (1976). Coordination of growth with cell division in the yeast Saccharomyces cerevisiae, *Exp. Cell Res.* 105:79-98.

[JON93] D.R. Jones, C.D. Perttunen & B.E. Stuckman (1993). Lipschitzian optimization without the Lipschitz constant, *J. Optim. Theory* 79:157-181.

[KON71] R.J. Konopka & S. Benzer (1971). Clock mutants of Drosophila melanogaster, *Proc. Natl. Acad. Sci. U.S.A.* 68:2112-2116.

[KUM95] A. Kumagai & W.G. Dunphy (1995). Control of the Cdc2/Cyclin B complex in Xenopus egg extracts arrested at a G2/M checkpoint with DNA synthesis inhibitors, *Molec. Biol. Cell* 6:199-213.

[KUZ98] Y.A. Kuznesov (1998). Elements of Applied Bifurcation Theory, 2nd Ed., Springer Verlag.

[LAR85] O. Larsson, A. Zetterberg & W. Engstrom (1985). Consequences of parental exposure to serum–free medium for progeny cell division, *J. Cell Sci.* 75:259-268.

[LAU00] M.T. Laub et al. (2000). Global analysis of the genetic network controlling a bacterial cell cycle, *Science* 290:2144-2148.

[LEE94] T.H. Lee, C. Turck & M.W. Kirschner (1994). Inhibition of cdc2 activation by INH/PP2A, *Molec. Biol. Cell* 5:323-338

[LEW00] D. Lew, Cell-cycle checkpoints ensure coordination between nuclear and cytoplasmic events in Saccharomyces cerevisiae, *Curr. Opin. Genet. Devel.* 10:47-53.

[MAR98] G. Marlovits, C.J. Tyson, B. Novak & J.J. Tyson (1998). Modeling M-phase control in Xenopus oocyte extracts: the surveillance mechanism for unreplicated DNA, *Biophys. Chem.* 72:169-184.

[MEN98] M.D. Mendenhall & A.E. Hodge (1998). Regulation of Cdc28 cyclin-dependent protein kinase activity during the cell cycle of the yeast Saccharomyces cerevisiae. *Microbiol. Molec. Biol. Rev.* 62:1191-1243.

[MIL01] M.E. Miller & F.R. Cross (2001). Mechanisms controlling subcellular localization of the G1 cyclins Cln2p and Cln3p in budding yeast, *Molec. Cell. Biol.* 21:6292-6311.

[NAS96] K. Nasmyth (1996). At the heart of the budding yeast cell cycle, *Trends in Genetics* 12:405-412.

[NOV93] B. Novak & J.J. Tyson (1993). Numerical analysis of a comprehensive model of M-phase control in Xenopus oocyte extracts and intact embryos, *J. Cell Sci.* 106:1153-1168.

[NUR75] P. Nurse (1975). Genetic control of cell size at cell division in yeast, *Nature* 256:547-551.

[NUR76] P. Nurse, P. Thuriaux & K. Nasmyth (1976). Genetic control of the cell division cycle in fission yeast, *Molec. Gen. Genetics* 146:167-178.

[NUR90] P. Nurse (1990). Universal control mechanism regulating onset of M-phase, *Nature* 344:503-508.

[PAR89] A.B. Pardee (1989). G1 events and regulation of cell proliferation, *Science* 246:603-608.

[POM03] J.R Pomerening, E.D. Sontag & J.E. Ferrell, Jr. (2003). Building a cell cycle oscillator: hysteresis and bistability in the activation of Cdc2, N*ature Cell Biology* 5:346-351.

[POM05] J.R. Pomerening, S.Y. Kim & J.E. Ferrell, Jr. (2005). Systems-level dissection of the cell-cycle oscillator: bypassing positive feedback produces damped oscillations, *Cell* 122:565-578.

[RAF02] J.W. Raff, K. Jeffers & J.Y. Huang (2002). The roles of Fzy/Cdc20 and Fzr/Cdh1 in regulating the destruction of cyclin B in space and time, *J. Cell Biol.* 157:1139-1149.

[RUO97] P. Ruoff, L. Rensing, R. Kommedal & S. Mohsenzadeh (1997). Modeling temperature compensation in chemical and biological oscillators, *Chronobiol Internat.* 14:499-510.

[SIA96] R.A.L. Sia, H.A. Herald & D.J. Lew (1996). Cdc28 tyrosine phosphorylation and the morphogenesis checkpoint in budding yeast, *Molec. Biol. Cell* 7:1657-1666.

[SIA98] R.A.L. Sia, H.A. Herald & D.J. Lew (1998). Control of Swe1p degradation by the morphogenesis checkpoint, *EMBO J.* 17:6678-6688.

[SOL90] M.J. Solomon, M. Glotzer, T. Lee, M. Philippe & M. Kirschner (1990). Cyclin activation of p34Cdc2, *Cell* 63:1013-1024.

[STE04] R. Steuer (2004). Effects of stochasticity in models fo the cell cycle: from quantized cycle times to noise-induced oscillations, *J. Theor. Biol.* 228:293-301.

[SU98] T.T. Su et al. (1998). Exit from mitosis in Drosophila syncytial embryos requires proteolysis and cyclin degradation, and is associated with localized phosphorylation, *Genes & Devel.* 12:1495-1503

[SVE00] A. Sveiczer, A. Csikasz-nagy, B. Gyorffy, J.J. Tyson & B. Novak (2000). Modeling the fission yeast cell cycle: quantized cycle times in *wee1$^-$ cdc25Δ* mutant cells, *Proc. Natl. Acad. Sci. U.S.A.* 97:7865-7870.

[TYS89] J.J. Tyson (1989). Effects of asymmetric division on a stochastic model of the cell division cycle, *Math. Biosci.* 96:165-184.

[TYS99] J.J. Tyson, C.I. Hong, C.D. Thron & B. Novak (1999). A simple model of circadian rhythms based on dimerization and proteolysis of PER and TIM, *Biophys. J.* 77:2411-2417.

[TYS01] J.J. Tyson & B. Novak (2001). Regulation of the eukaryotic cell cycle: molecular antagonism, hysteresis and irreversible transitions, *J. Theor. Biol.* 210:249-263.

[ZET85] A. Zetterberg & O. Larsson (1985). Kinetic analysis of regulatory events in G1 leading to proliferation or quiescence of Swiss 3T3 cells, *Proc. Natl. Acad. Sci. U.S.A.* 82:5365-5369.

[ZET95] A. Zetterberg & O. Larsson (1995). Cell cycle progression and growth in mammalian cells: kinetic aspects of transition events. In Cell Cycle Control (edit by C. Hutchison & D. Glover, Oxford Univ Press).

7.0 Publications Resulting from this Project

2001

Tyson, J.J. K.Chen & B. Novak (2001). "Network Dynamics and Cell Physiology," Nature Rev. Molec. Cell Biol. 2:908-916.

Watson, L. T. & C. A. Baker (2001). "A fully-distributed parallel global search algorithm," *Engrg. Comput*. 18:155-169.

Zwolak, J.W., J.J. Tyson & L.T. Watson (2001) "Estimating Rate Constants in Cell Cycle Models," in *Proceedings of the High Performance Computing Symposium 2001* (A. Tentner, ed., Soc. Modeling & Simulation Internat., San Diego CA) pp. 53-57.

2002

Billups, S. C. & L. T. Watson (2002). "A probability-one homotopy algorithm for nonsmooth equations and mixed complementarity problems," *SIAM J. Optim*. 12:606-626.

He, J., L. T. Watson, N. Ramakrishnan, C. A. Shaffer, A. Verstak, J. Jiang, K. Bae, & W. H. Tranter (2002). "Dynamic data structures for a direct search algorithm," *Comput. Optim. Appl.* 23:5-25.

Novak, B., J.C. Sible & J.J. Tyson (2002). "Checkpoints in the Cell Cycle," in *Encyclopedia of Life Sciences*, Macmillan Reference Ltd., London. http://www.els.net/

Ramakrishnan, N., L.T. Watson, D.G. Kafura, C.J. Ribbens & C.A. Shaffer (2002). "Programming environments for multidisciplinary grid communities," in *Concurrency and Computation: Practice and Experience*, Vol. 14, No. 13-14, pp. 1241-1273.

Tyson, J.J., A. Csikasz-Nagy & B. Novak (2002). "The dynamics of cell cycle regulation," *BioEssays* 24:1095-1109.

Vass, M. & P. Schoenhoff (2002a). "Error detection support in a cellular modeling end-user programming environment," in *Proc. HCC'02 IEEE Symposium on Empirical Studies of Programmers*, IEEE Press.

Vass, M., J.M. Carroll & C.A. Shaffer (2002b). "Supporting Creativity in Problem Solving Environments," in *Creativity and Cognition 4* .

Watson, L. T. (2002). "Probability-one homotopies in computational science," *J. Comput. Appl. Math.* 140:785-807.

Zwolak, J. W., J. J. Tyson & L. T. Watson (2002). "Parameter estimation in a cell cycle model for frog egg extracts," in *Proc. High Performance Computing Symposium 2002* (A. Tentner, Ed., Soc. Modeling and Simulation Internat., San Diego, CA) pp. 67-74.

2003

Allen, N., L. Calzone, K.C. Chen, A. Ciliberto, N. Ramakrishnan, C.A. Shaffer, J.C. Sible, J.J. Tyson, M. Vass, L.T. Watson & J. Zwolak (2003a). "Modeling regulatory networks at Virginia Tech," *Omics* 7:285-299.

Allen, N.A., C.A. Shaffer, M.T. Vass, N. Ramakrishnan & L.T. Watson (2003b). "Improving the development process for eukaryotic cell cycle models with a modeling support environment," *Simulation* 79:674-688.

Archambault, V., C.X. Li, A.J. Tackett, R. Waesch, B.T. Chait, M.P. Rout & F.R. Cross (2003). "Genetic and biochemical evaluation of the importance of Cdc6 in regulating mitotic exit," *Mol. Biol. Cell* 14: 4592-4604.

Ciliberto, A., B. Novak & J.J. Tyson (2003a). “Mathematical model of the morphogenesis checkpoint in budding yeast,” *J. Cell Biol.* 163:1243-1254.
Ciliberto, A., M.J. Petrus, J.J. Tyson & J.C. Sible (2003b). “A kinetic model of the cyclin E/Cdk2 developmental timer in *Xenoupus laevis* embryos,” *Biophys. Chem.* 104:573-589.
Cross, F.R. (2003). “Two redundant oscillatory mechanisms in the yeast cell cycle,” *Devel. Cell* 4:741-752.
Sha, W., J. Moore, K. Chen, A.D. Lassaletta, C.S. Yi, J.J. Tyson & J.C. Sible (2003). “Hysteresis drives cell-cycle transitions in *Xenopus laevis* egg extracts,” *Proc. Natn. Acad. Sci. USA* 100:975-980.
Tyson, J.J., K.C. Chen & B. Novak (2003). “Sniffers, buzzers, toggles and blinkers: dynamics of regulatory and signaling pathways in the cell,” *Curr. Opin. Cell Biol.* 15:1-11.
Verstak, A., N. Ramakrishnan, L. T. Watson, J. He, C. A. Shaffer, K. K. Bae, J. Jiang, W. H. Tranter, & T. S. Rappaport (2003). “BSML: a binding schema markup language for data interchange in problem solving environments,” *Sci. Programming* 11:199-224.
Zwolak, J.W., J.J. Tyson, and L.T. Watson (2003) “Finding All Steady State Solutions of Chemical Kinetic Models,” in *Proc. High Performance Computing Symposium* 2003 (I. Banicescu, ed., Soc. for Modeling and Simulation Internat., San Diego, CA) pp. 47-53.

2004

Battogtokh, D. & J.J. Tyson (2004a). “Bifurcation analysis of a model of the budding yeast cell cycle,” *Chaos* 14:653-661.
Battogtokh, D. & J.J. Tyson (2004b). “Turbulence near cyclic fold bifurcations in birhythmic media,” *Phys. Rev. E* 70:026212.
Chen, K.C., L. Calzone, A. Csikasz-Nagy, F.R. Cross, B. Novak & J.J. Tyson (2004). “Integrative analysis of cell cycle control in budding yeast,” *Mol. Biol. Cell* 15:3841-3862.
Novak, B. & J.J. Tyson (2004). “A model for restriction point control of the mammalian cell cycle,” *J. Theor. Biol.* 230:563-579.
Sveiczer, A., J.J. Tyson & B. Novak (2004). “Modeling the fission yeast cell cycle,” *Brief. Funct. Genomics & Proteomics* 2:298-307.
Thornton, B.R., K.C. Chen, F.R. Cross, J.J. Tyson & D.P. Toczyski (2004). “Cycling without the cyclosome: modeling a yeast strain lacking the APC,” *Cell Cycle* 3:629-633.
Vass, M.T., N.A. Allen, C.A. Shaffer, N. Ramakrishnan, L.T. Watson & J.J. Tyson (2004)."The JigCell Model Builder and Run Manager," *Bioinformatics* 20:3680-3681.
Zwolak, J.W., J.J. Tyson & L.T. Watson (2004). “Finding all steady state solutions of chemical kinetic models,” *Nonlinear Analysis: Real World Applications* 5:801-814.

2005

Ciliberto, A., B. Novak & J.J. Tyson (2005a). “Steady states and oscillations in the p53/Mdm2 network,” *Cell Cycle* 4:488-493.
Ciliberto, A., A. Lukacs, A. Toth, J.J. Tyson & B. Novak (2005b). “Rewiring exit from mitosis,” *Cell Cycle* 4:1107-1112.
Cross, F.R., L. Schroeder, M. Kruse & K.C. Chen (2005). “Quantitative characterization of a mitotic cyclin threshold regulating exit from mitosis,” *Mol. Biol. Cell* 16:2129-2138.

Novak, B., K. Chen & J.J. Tyson (2005) “Systems biology of the yeast cell cycle engine,” in *Systems Biology* (L. Alberghina & H. Westerhoff, Eds., Springer-Verlag, Heidelberg & New York).

Zwolak, J.W., J.J. Tyson & L.T. Watson (2005a). “Parameter estimation for a mathematical model of the cell cycle in frog eggs,” *J. Comput. Biol.* 12:48-63.

Zwolak, J.W., J.J. Tyson & L.T. Watson (2005b). “Globally optimized parameters for a model of mitotic control in frog egg extracts,” *IEE Proc. Sys. Biol.* 152:81-92.

2006

Allen, N.A., K.C. Chen, C.A. Shaffer, J.J. Tyson & L.T.Watson (2006). “Computer evaluation of network dynamics models with application to cell cycle control in budding yeast,” *IEE Proc. Syst. Biol.* 153:13-21.

Battogtokh, D. & J.J. Tyson (2006a). “Periodic forcing of a mathematical model of the eukaryotic cell cycle,” *Phys. Rev. E* 73:011910.

Battogtokh, D. & J.J. Tyson (2006b). “Synchronization of eukaryotic cells by periodic forcing,” *Phys. Rev. Lett.* 96:148102.

Brazhnik, P. & J.J. Tyson (2006), “Convergent evolution of cell cycle control networks in bacteria and yeast,” *Cell Cycle* 5:522-529.

Conrad, E.D. & J.J. Tyson (2006), “Modeling molecular interaction networks with nonlinear ordinary differential equations,” in *Systems Modeling in Cellular Biology* (Z. Szallasi, V. Periwal & J. Stelling, Eds., MIT Press, Cambridge MA) pp. 97-123.

Csikasz-Nagy, A., D. Battogtokh, B. Novak & J.J. Tyson (2006), “Analysis of a generic model of eukaryotic cell cycle regulation,” *Biophys. J.* 90:4361-4379.

Sauro, H.M., A.M. Uhrmacher, D. Harel, M. Hucka, M. Kwiatokowski, P. Mendes, C.A. Shaffer, L. Stromback & J.J. Tyson (2006). “Challenges of Modeling and Simulation in Systems Biology,” in *Proceedings 2006 Winter Simulation Conference* (edit. by L.F. Perrone et al., Monterey CA) pp. 1720-1730.

Shaffer, C.A., R. Randhawa & J.J. Tyson (2006) “The role of composition and aggregation in modeling macromolecular regulatory networks,” in *Proceedings 2006 Winter Simulation Conference* (edit. by L.F. Perrone et al., Monterey CA) pp. 1628-1635.

Tyson, J.J. (2006). “Another turn for p53,” *Molec. Syst. Biol.* 4100060.

Vass, M., C. A. Shaffer, N. Ramakrishnan, L. T. Watson, and J. J. Tyson (2006). “The JigCell Model Builder: an error-reducing editor for creating regulatory network models,” *IEEE Trans. Comput. Biol. Bioinformatics* 3:155-164

2007

Calzone, L., D. Thieffry, J.J. Tyson & B. Novak (2007), “Dynamical modeling of syncytial mitotic cycles in *Drosophila* embryos,” *Mol. Syst. Biol.* (under revision).

Ciliberto, A., F. Capuani & J.J. Tyson (2007). “Modeling networks of coupled enzymatic reactions using the total quasi-steady state approximation,” *PLoS Comput. Biol.* (in press).

Conrad, E.D. & J.J. Tyson (2007). “Oscill8: tools and techniques for bifurcation analysis and parameter optimization of biological models,” (in preparation).

Csikasz-Nagy, A., B. Novak & J.J. Tyson (2007). “Reverse engineering models of cell cycle regulation,” in Cellular Oscillatory Mechanisms (N. Monk & M. Maroto, eds., Landes Bioscience, in press).

Csikasz-Nagy, A., B. Gyorffy, O. Kapuy, J.J. Tyson & B. Novak (2007) "Modeling the septation initiation network (SIN) in fission yeast cells," *Curr. Genet.* (in press).

Hong, C.I., E.D. Conrad, B. Novak & J.J. Tyson (2007) "A proposal for robust temperature compensation of circadian rhythms." *Proc. Natl. Acad. Sci.* (in press).

Li, S., P. Brazhnik, B. Sobral & J.J. Tyson (2007). "Molecular regulation of DNA synthesis and cell division cycle in Caulobacter crescentus: a quantitative study of stalked cell cycles," *PLoS Comput. Biol.* (submitted).

Novak, B., J.J. Tyson, B. Gyorffy & A. Csikasz-Nagy (2007) "Irreversible transitions in the cell cycle are consequences of systems-level feedback," *Nature Cell Biology* (in press).

Panning, T.D., L.T. Watson, N.A. Allen, K.C. Chen, C.A. Shaffer & J.J. Tyson (2007a) "Deterministic parallel global parameter estimation for a model of the budding yeast cell cycle," *J. Global Optim.* (in press).

Panning, T.D., L.T. Watson, C.A. Shaffer & J.J. Tyson (2007b). "A mathematical programming formulation for the budding yeast cell cycle," (submitted).

Randhawa, R., C.A. Shaffer & J.J. Tyson (2007). "Fusing and composing macromolecular regulatory network models," To appear in Proceedings of the 2007 High Performance Computing Symposium (Norfolk, VA).

Sabouri-Ghomi, M., A. Ciliberto, B. Novak & J.J. Tyson (2007) "Antagonism and bistability in protein interaction networks," *J. Theor. Biol.* (submitted).

Sible, J.C. & J.J. Tyson (2007) "Application of mathematical modeling to cell cycle questions," *Methods* 41:238-247.

Tyson, J.J. (2007). "Bringing cartoons to life," *Nature* (in press).

Zhang, T., P. Brazhnik & J.J. Tyson (2007) "Exploring mechanisms of the DNA-damage response: p53 pulses and their possible relevance to apoptosis," *Cell Cycle* 6:85-94.

8.0 List of Abbreviations

AU	Arbitrary Units
Cdk	Cyclin-dependent kinase
CKI	Cyclin-dependent Kinase Inhibitor
DIRECT	DIViding RECTangles
HB	Hopf Bifurcation
JCMB	JigCell Model Builder
JCRM	JigCell Run Manager
MADS	Mesh Adaptive Direct Search
MPF	M-phase Promoting Factor
NEB	Nuclear Envelope Breakdown
ODE	Ordinary Differential Equation
ODRPACK	Orthogonal Distance Regression software PACKage
PET	Parameter Estimation Toolkit
PDE	Partial Differential Equation
PSE	Problem Solving Environment
SBML	Systems Biology Markup Language
SN	Saddle Node bifurcation
SNIPER	Saddle-Node Infinite-PERiod bifurcation
SPICE	Simulation Program for Intra-Cellular Evaluation